APPENDICES

APPENDIX A

Combustion Synthesis Experiments

A.1 Glass L-junction for combining precursor streams

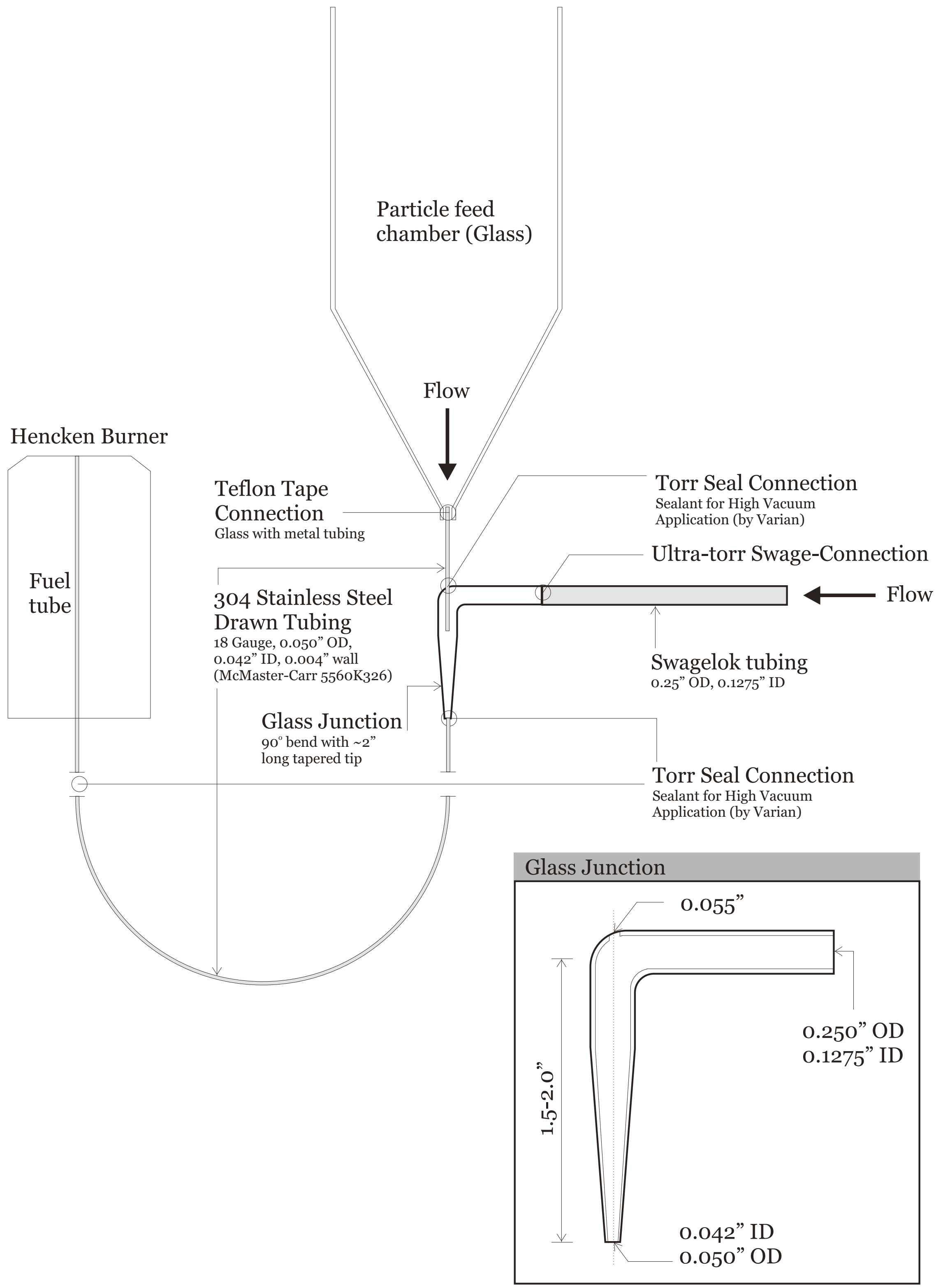

A.2 Rotameter Calibrations

Ar dilution
Manufacturer: OMEGA
Tube Model No. R-6-15-B
Metered Gas: (Vol. Basis)
7.5% O2, 92.5% Ar

Scale (mm)	Omega Ar (lpm)	Calibrated (lpm)
34	9.54	10.109
35	9.84	10.427
36	10.15	10.755
37	10.45	11.073
38	10.76	11.401
39	11.07	11.730
40	11.37	12.048
41	11.68	12.376
42	11.99	12.705
43	12.30	13.033
44	12.61	13.362
45	12.92	13.690
46	13.24	14.029
47	13.56	14.368
48	13.88	14.707
49	14.21	15.057
50	14.53	15.396
51	14.86	15.746
52	15.19	16.095
53	15.52	16.445
54	15.85	16.795
55	16.18	17.144
56	16.51	17.494
57	16.84	17.844
58	17.17	18.193
59	17.51	18.554
60	17.84	18.903
61	18.18	19.264
62	18.53	19.635
63	18.87	19.995
64	19.21	20.355
65	19.55	20.715
66	19.89	21.076
67	20.23	21.436
68	20.57	21.796
69	20.91	22.156
70	21.26	22.527
71	21.60	22.888
72	21.95	23.258
73	22.30	23.629
74	22.65	24.000
75	23.01	24.382
76	23.37	24.763
77	23.73	25.145
78	24.11	25.547
79	24.48	25.939
80	24.87	26.352
81	25.25	26.755
82	25.64	27.168
83	26.03	27.582
84	26.43	28.005
85	26.82	28.419
86	27.21	28.832
87	27.61	29.256
88	28.00	29.669
89	28.38	30.072

Hydrogen
Manufacturer: OMEGA
Tube Model: N082-03st
Metered Gas: Hydrogen

Scale (mm)	Calibrated (lpm)
30	0.999
35	1.222
40	1.442
45	1.660
50	1.874
55	2.086
60	2.294
65	2.500
70	2.703
75	2.903
80	3.100
85	3.294
90	3.485
95	3.673
100	3.858
105	4.041
110	4.220
115	4.397
120	4.570
125	4.741
130	4.909
135	5.073
140	5.235
145	5.394
150	5.550

TMT/Argon
Manufacturer: OMEGA
Model No. FL-5311C
Metered Gas: Argon

Omega Calibration

Scale [mm]	Argon Flow [mL/min]
2	7.066
4	9.364
6	11.748
8	14.132
10	16.516
12	19.240
14	22.219
16	25.539
18	29.370
20	33.797
22	38.735
24	44.183
26	50.228
28	56.698
30	63.508
32	70.744
34	78.321
36	86.323
38	94.751
40	103.520
42	112.714
44	122.419
46	132.550
48	143.021
50	154.003
52	165.325
54	176.903
56	188.651
58	200.570
60	212.488
62	224.321
64	236.070
66	247.562

Lab Calibration

upscale [mm]	Vol [mL]	Time [s]	Flow Rate [mL/min]
10	20	60.84	19.72
18	40	69.36	34.60
29.5	40	39.49	60.77
40.5	60	33.89	106.23
50	80	32.06	149.72
60	100	27.59	217.47

Lab Calibration

downscale [mm]	Vol [mL]	Time [s]	Flow Rate [mL/min]
60	100	28.10	213.52
50	100	36.33	165.15
40	100	58.53	102.51
30	100	89.58	66.98
20	100	170.02	35.29
10	100	319.89	18.76

PFS/Argon
Manufacturer: OMEGA
Model No.
Metered Gas: Argon

Scale [mm]	Flow Rate [mL/min]
20	260.42
30	521.20
40	788.88
50	1021.59
60	1300.12
70	1551.11
80	1814.48
90	2075.70
100	2315.24
110	2551.67
120	2778.93
130	3048.78
140	3308.12

A.3 Summary of experiments

The following table presents a summary of combustion synthesis experiments relevant to the synthesis studies and to the gas sensing studies presented in the dissertation. The table also provides information about the samples collected using bulk and TEM sampling. Refer to the grid sampling tables following. Experiments conducted before the ones presented here are documented in Tiffany Miller's thesis.

Summary of experiments conducted using the combustion synthesis facility

Ref.	Date	Description	Gas flows (rotameter scale, mm) or [lpm] H_2 (70)	O_2 [1.47]	$Ar_{dilu.}$ (55)	Ar_{TMT} (30)	Ar_{PFS} (20)	Solid precursor Au-	Pd-	Cu-	Al-	Shroud	Chimney	Samples Bulk height/time/mass [cm]/[min]/[mg]	TEM box:grid/height [cm]
A	6/1/05	Re-fire	•	•	•	(25)	(30)	•				•		27/-/-	
B	6/3/05	Re-fire	•	[1.48]	•	(25)	•	•				•		27/20/-	050520:A3,A4/18.5
C	6/3/05	Re-fire	•	•	•	(25)	•	•				•			050520: A5,A6/18.5, A7/10
D	6/4/05	Nickel Acetate	•	•	•	(25)	•					•		27/25/-	050520:A8,A9,A10,B1,B2/18.5
E	6/11/05	Re-fire	•	•	•	•	•	•				•	•	50/12/306	050520: B5/18.5, B6/37
F	6/11/05	Re-fire	•	•	•	•	•	•				•	•	50/-/-	050520:B7,B8,B9/37
G	6/12/05	Height Study	•	•	•	•	•	•						27/14/-	050520: B10/0.5, C1/1, C2/2, C3/5, C4/9, C5/13, C6,C7/18.5
H	6/20/05	MACS	(65)	[1.48]	•	•	•						•	50/-/-	050520: C8/37, C9/16.5, C10/10
I	7/6/05	MACS	(55)	[1.46]	•	•	•					•	•	50/-/21	
J	7/13/05	TNBT at 100 ^oC	•	•	(50)	(40)	•					•	•	40/-/3	050520:D2,D3/10
K	7/14/05	PIV	•	•	(50)	•	•				•	•			
L	7/22/05	2 Solid Reactants No TMT	•	[1.48]	•		•				•	•		27/11/-	050520: D6/25, D7,D8/15
M	7/22/05	Re-fire	•	[1.48]	•	•	•	•				•	•	50/12/-	
N	7/23/05	Decomposed Gold Acetate	•	•	•	•	•	•				•	•	50/8/-	050520:D9,D10/37
O	8/15/05	Yen-Hung's Study	•	[1.44]	•	•	•					•			050520:E2,E3/27
P	8/18/05	MACS with Pt	(55)	•	•	•	•					•		50/10/-	050520:E4/16.5
Q	8/18/05	MACS with Pt	(55)	•	•	•	•					•	•	50/10/-	050520:E5/37
R	10/23/05	MACS with Au	(55)	[1.44]	•	•	•	•				•	•	50/10/-	050520:E9,E10/37
S	10/23/05	MACS with Al	(55)	[1.44]	•	•	•				•	•	•	50/-/-	050722:A1,A2/37
T	10/28/05	MACS with Al	(55)	[1.46]	•	•	•				•	•	•		
U	10/28/05	MACS	(55)	[1.46]	•	•	•					•	•	50/12.5/-	
V	11/2/05	Methane-Unassisted	•	[1.48]	•	•	•						•	50/15/-	050722:A3/37
W	11/5/05	MACS Height Study	(55)	[1.46]	•	•	•					•	•		050722: A6/1, A7/2, A8/5, A9/9, A10/13, B3/20, B4/25
X	11/8/05	MACS Height Study	(55)	[1.48]	•	•	•					•	•		050722: B5/5, B6/9, B7/20, B8/25
Y	5/22/07	Gas Sensors Rerun	•	•	•	•	•					•		27/30/4	
Z	5/22/07	Gas Sensors Rerun	•	•	•	•	•					•	•	37/25/98	
ZA	5/24/07	Gas Sensors Rerun	•	•	(50)	•	•					•	•	37/25/168	
ZB	5/25/07	Gas Sensors Rerun	•	•	(50)	•	•					•	•	37/30/112	
ZC	5/31/07	Gas Sensors Rerun	•	•	(50)	•	•					•	•	37/30/82	
ZD	6/20/07	Gas Sensors Rerun	•	•	(50)	•	•					•	•	37/16/180	
ZE	6/21/07	Nanorod Sensor	(55)	•	•	•	•					•	•	37/20/309	
ZF	7/12/07	Au Doped Sensor	•	[1.48]	(50)	•	•	•				•	•	37/30/455	
ZG	8/1/07	Pd Doped Sensor	•	[1.48]	(50)	•	(25)		•			•	•	37/20/528	
ZH	10/16/07	Gas Sensors	•	•	(50)	•	•					•	•	37/15/-	
ZI	10/17/07	Gas Sensors Rerun	•	•	(50)	•	•					•	•	37/11/350	
ZJ	11/21/07	Gas Sensors	•	[1.45]	(50)	•	(25)					•	•	37/15/393	

A.4 TEM grid index

TEM Grid Box: 050520

Grid	Expt. Ref.	Description	Date	Location [cm]
A1		Colloidal Au		
A2		Colloidal Au		
A3	B	Re-fire	6/3/05	18.5
A4	B	Re-fire	6/3/05	18.5
A5	C	Re-fire	6/3/05	18.5
A6	C	Re-fire	6/3/05	18.5
A7	C	Re-fire	6/3/05	10
A8	D	Nickel Acetate	6/4/05	18.5
A9	D	Nickel Acetate	6/4/05	18.5
B1	D	Nickel Acetate	6/4/05	18.5
B2	D	Nickel Acetate	6/4/05	18.5
B3		Colloidal Au	6/11/05	
B4		Colloidal Au	6/11/05	
B5	E	Re-fire	6/11/05	18.5
B6	E	Re-fire	6/11/05	37
B7	F	Re-fire	6/11/05	37
B8	F	Re-fire	6/11/05	37
B9	F	Re-fire	6/11/05	37
B10	G	Height Study	6/12/05	0.5
C1	G	Height Study	6/12/05	1
C2	G	Height Study	6/12/05	2
C3	G	Height Study	6/12/05	5
C4	G	Height Study	6/12/05	9
C5	G	Height Study	6/12/05	13
C6	G	Height Study	6/12/05	18.5
C7	G	Height Study	6/12/05	18.5
C8	H	MACS	6/20/05	37
C9	H	MACS	6/20/05	16.5
C10	H	MACS	6/20/05	10
D1			7/6/05	
D2	J	TNBT at 100 ^{o}C	7/13/05	10
D3	J	TNBT at 100 ^{o}C	7/13/05	10
D5		Colloidal Au	7/20/05	
D6	L	2 Solid Reactants No TMT	7/22/05	25
D7	L	2 Solid Reactants No TMT	7/22/05	15
D8	L	2 Solid Reactants No TMT	7/22/05	15
D9	N	Decomposed Gold Acetate	7/23/05	37
D10	N	Decomposed Gold Acetate	7/23/05	37
E2	O	Yen-Hung's Study	8/15/05	27
E3	O	Yen-Hung's Study	8/15/05	27
E4	P	MACS with Pt	8/18/05	16.5
E5	Q	MACS with Pt	8/18/05	37
E6		MACS with Pt	10/23/05	37
E7		MACS with Pt	10/23/05	37
E8		MACS with Pt	10/23/05	37
E9	R	MACS with Pt	10/23/05	37
E10	R	MACS with Pt	10/23/05	37

TEM Grid Box: 050722

Grid	Expt. Ref.	Description	Date	Location [cm]
A1	S	MACS with Al	10/23/05	37
A2	S	MACS with Al	10/23/05	37
A3	V	Methane-Unassisted	11/2/05	37
A6	W	MACS Height Study Rerun 11/5/05	11/5/05	1
A7	W	MACS Height Study Rerun 11/5/05	11/5/05	2
A8	W	MACS Height Study Rerun 11/5/05	11/5/05	5
A9	W	MACS Height Study Rerun 11/5/05	11/5/05	9
A10	W	MACS Height Study Rerun 11/5/05	11/5/05	13
B3	W	MACS Height Study Rerun 11/5/05	11/5/05	20
B4	W	MACS Height Study Rerun 11/5/05	11/5/05	25
B5	X	MACS Height Study Rerun 11/5/05	11/8/05	5
B6	X	MACS Height Study Rerun 11/5/05	11/8/05	9
B7	X	MACS Height Study Rerun 11/5/05	11/8/05	20
B8	X	MACS Height Study Rerun 11/5/05	11/8/05	25

TEM Grid Box: 060601

Grid	Expt. Ref.	Description	Date	Location [cm]
C2		Toluene PMMA SnO2 Au	6/21/06	
D1		MSP Deposition	6/28/06	
D2		Explosive Gold Acetate	6/29/06	

TEM Grid Box: 060929

Grid	Expt. Ref.	Description	Date	Location [cm]
A8		AuAc Decomposition	1/27/07	1 mm
A9		AuAc Decomposition	1/27/07	1 mm
B1		AuAc Decomposition		
B2		AuAc Decomposition		
B7		AuAc Decomposition		4 mm
B10		AuAc Decomposition		4 mm
C4		AuAc Decomposition	2/24/07	1 mm
C5		AuAc Decomposition	2/24/07	1 mm
C8		AuAc Decomposition		1 mm
C10		AuAc Decomposition		1 mm
D1		Sputtered Au on Glass	2/8/07	
D9		AuAc Decomposition		2 mm
D10		AuAc Decomposition		2 mm
E1		Dispersion SnO2	12/11/07	
E2		Dispersion SnO2 Au	12/11/07	
E4		Dispersion SnO2 Pd	12/11/07	
E8		AuAc Decomposition		1 mm
E10		AuAc Decomposition		1 mm

A.5 Sampling piston residence time study

Sampling time for a range of controller time setting

Controller time (s)	0.50	0.75	1.00	0.40	0.30	0.30
Pressure (psi)	100	100	100	100	100	100
Travel						
start (us)	3233301	2161090	25949741	8549914	1244432	2949970
end (us)	3494409	2422198	26216405	8811023	1494429	3205523
trav. Time (s)	0.2611	0.2611	0.2667	0.2611	0.2500	0.2556
Residence						
start (us)	3494409	2422198	26216405	8811023	1494429	3205523
end (us)	3711074	2888860	26938620	8922133	1494429	3216634
res. Time (s)	0.2167	0.4667	0.7222	0.1111	0.0000	0.0111
Total time (s)	0.478	0.728	0.989	0.372	0.250	0.267

Sampling time for controller time setting of 0.30 seconds

Controller (s)	0.30	0.30	0.30	0.30	0.30	0.30	0.30	0.30	average
Pressure (psi)	100	100	100	100	100	100	100	100	
Travel									
start (us)	846645	2266610	3869903	5566527	7126488	8583118	10059748	11726373	
end (us)	1093306	2516603	4126563	5823187	7379815	8836445	10313075	11983033	
trav. Time (s)	0.2467	0.2500	0.2567	0.2567	0.2533	0.2533	0.2533	0.2567	0.2533 ± 0.0036
Residence									
start (us)	1093306	2516603	4126563	5823187	7379815	8836445	10313075	11983033	
end (us)	1096639	2539936	4146563	5836520	7396481	8856445	10329741	11996366	
res. Time (s)	0.0033	0.0233	0.0200	0.0133	0.0167	0.0200	0.0167	0.0133	0.0158 ± 0.0061
Total time (s)	0.250	0.273	0.277	0.270	0.270	0.273	0.270	0.270	0.269 ± 0.008

Sampling time for controller time setting of 0.40 seconds

Controller (s)	0.40	0.40	0.40	0.40	0.40	0.40	0.40	0.40	average
Pressure (psi)	100	100	100	100	100	100	100	100	
Travel									
start (us)	909977	2489938	4189895	5696524	7489813	9133105	10819729	12629684	
end (us)	1166637	2743265	4443222	5949851	7743140	9386432	11076390	12883011	
trav. Time (s)	0.2567	0.2533	0.2533	0.2533	0.2533	0.2533	0.2567	0.2533	0.2542 ± 0.0015
Residence									
start (us)	1166637	2743265	4443222	5949851	7743140	9386432	11076390	12883011	
end (us)	1273301	2866595	4566552	6076515	7869803	9509762	11203053	13009675	
res. Time (s)	0.1067	0.1233	0.1233	0.1267	0.1267	0.1233	0.1267	0.1267	0.1229 ± 0.0068
Total time (s)	0.363	0.377	0.377	0.380	0.380	0.377	0.383	0.380	0.377 ± 0.006

APPENDIX B

Gas sensor study

B.1 Summary of experiments

A study of sensor performance with a range of binders for undoped SnO_2 sensors

Sensor	Binder Description	Date	Run	Sensitivity		Time Response		Response Description
				$S = \frac{R_a}{R_g}$	Average	τ (sec)	Average	
I	Hydroxypropyl Cellulose in Isopropyl Alcohol. Sonicated	05/03	1	4.72	4.34 ± 0.4	34.88	14.4 ± 11.8	Higher ambient response after CO exposure. Secondary response during CO exposure.
		05/03	2	3.80		7.32		
		05/07	1	4.73		13.57		
		05/07	2	4.16		7.62		
		05/07	3	4.31		7.87		
J	Ethyl Cellulose in α-terpineol	05/09	1	3.22	3.05 ± 0.24	2.44	4.2 ± 1.5	Similar but worse than Sensor I except time response
		05/09	2	2.78		5.13		
		05/09	3	3.16		5.00		
K	Tetraethylorthosilicate (TEOS) with HCl, Water and Ethanol	05/10	1	3.16	2.97 ± 0.15	27.27	35.0 ± 5.9	Almost ideal response curves. Slight drift towards higher resistance.
		05/10	2	2.97		35.29		
		05/10		2.80		41.67		
		05/10	3	2.96		35.93		

Sensor performance summary. Dates range from June 6th, 2007 to April 16th, 2008

Sensor	Description	Date	Run	$S = \frac{R_a}{R_g}$	Averages	$S = \frac{R_a - R_g}{R_a}$ (%)	Averages (%)	time (sec)	Averages (sec)
L	SnO_2	6-Jun	1	11.92		91.61		9	
			2	12.25		91.80		10	
			3	14.94	13.04 ± 1.660	93.31	92.24 ± 0.932	9	9.54 ± 0.8
L	SnO_2	7-Jun	1	16.75		94.03		10	
			2	19.44		94.85		11	
			3	17.58	17.92 ± 1.377	94.31	94.40 ± 0.417	10	10.44 ± 0.2
M	SnO_2	8-Jun	1	15.82		93.60		16	
			2	13.90		92.81		14	
			3	16.49	15.40 ± 1.342	93.90	93.44 ± 0.563	16	15.33 ± 1.3
M	SnO_2 @ 333C	9-Jun	1	20.83		95.20		12	
			2	17.77	19.30 ± 2.160	94.37	94.79 ± 0.587	13	12.40 ± 0.8
M	SnO_2 @ 333C	11-Jun	1	19.51		94.88		13	
			2	20.12		95.00		12	
			3	18.28	19.30 ± 0.940	94.53	94.80 ± 0.244	12	12.38 ± 0.6
M	SnO_2 @ 454C	13-Jun	1	14.30		93.01		8	
			2	10.50		90.47		9	
			3	10.81	11.87 ± 2.109	90.75	91.41 ± 1.393	8	8.00 ± 0.5
M	SnO_2 @ 375C	14-Jun	1	19.18		94.79		9	
			2	20.04		95.00		8	
			3	19.00	19.41 ± 0.553	94.74	94.84 ± 0.138	10	8.75 ± 0.9
M	SnO_2 @ 336C	19-Jun	1	10.34		90.33		12	
			2	9.05		88.95		15	
			3	9.34	9.58 ± 0.674	89.30	89.53 ± 0.717	15	14.10 ± 1.5
N	SnO_2	22-Jun	1	6.10		83.62		11	
			2	6.49		84.59		13	
			3	5.57	6.05 ± 0.464	82.03	83.41 ± 1.292	15	13.10 ± 1.8
N	SnO_2	25-Jun	1	8.41		88.11		13	
			2	7.12		86.96		15	
			3	8.95	8.16 ± 0.939	88.83	87.97 ± 0.943	13	13.67 ± 1.2
P	Nanorods	9-Jul	1	8.50		88.24		10	
			2	7.53		86.73		12	
			3	7.45	7.83 ± 0.585	86.58	87.18 ± 0.918	12	10.97 ± 0.9
P	Nanorods	10-Jul	1	8.87		88.73		10	
			2	9.28		89.22		11	
			3	8.35	8.83 ± 0.466	88.00	88.65 ± 0.614	10	10.20 ± 0.4
Q	Nanorods	12-Jul	1	8.58		88.35		10	
			2	6.85		85.41		13	
			3	6.63	7.35 ± 1.072	84.91	86.22 ± 1.859	13	11.97 ± 1.9
Q	Nanorods	13-Jul	1	9.02		88.90		11	
			2	7.52		86.71		13	
			3	7.34	7.96 ± 0.921	86.38	87.33 ± 1.370	12	12.03 ± 0.9
R	Au-doped	18-Jul	1	6.18		83.82		8	
			2	4.70		78.73		11	
			3	4.21	5.03 ± 1.027	76.23	79.59 ± 3.868	12	10.59 ± 2.3
R	Au-doped	19-Jul	1	9.54		89.52		7	
			2	8.09		87.64		9	
			3	6.40	8.01 ± 1.573	84.37	87.18 ± 2.606	9	8.08 ± 1.0
S	Au-doped	22-Jul	1	6.91		85.54		16	
			2	4.30		76.77		21	
			3	6.63	5.95 ± 1.431	84.92	82.41 ± 4.894	19	18.44 ± 2.5
S	Au-doped	24-Jul	1	9.77		89.77		15	
			2	7.51		86.69		22	
			3	6.45	7.91 ± 1.696	84.50	86.99 ± 2.647	20	18.99 ± 4.0

Continued: Sensor performance summary.

Sensor	Description	Date	Run	$S = \frac{R_a}{R_g}$	Averages	$S = \frac{R_a - R_g}{R_a}$ (%)	Averages	time (sec)	Averages
U	Pd-doped	4-Aug	1	15.97		94.00		8	
			2	10.06		90.00		8	
			3	8.10	11.38 ± 4.097	88.00	90.67 ± 3.055	10	8.89 ± 1.1
U	Pd-doped	6-Aug	1	33.09		96.98		2	
			2	12.84		92.00		8	
			3	9.05	18.33 ± 12.926	88.90	92.63 ± 4.076	10	6.48 ± 4.4
U	Pd-doped	7-Aug	1	14.50		93.00		7	
			2	9.44		89.00		10	
			3	9.74	11.23 ± 2.839	89.74	90.58 ± 2.128	8	7.97 ± 1.5
V	Alfa.A SnO_2	8-Aug	1	2.59		61.39		23	
			2	2.49		59.87		32	
			3	2.42	2.50 ± 0.086	58.65	59.97 ± 1.373	31	28.83 ± 4.9
V	Alfa.A SnO_2	9-Aug	1	3.24		69.15		25	
			2	2.67		62.58		31	
			3	2.39	2.77 ± 0.432	58.21	63.31 ± 5.507	38	31.03 ± 6.3
W	Au-doped	17-Oct	1	1.3		20		22	
			2	1.2		13		40	
			3	1.1	1.17 ± 0.076	9	13.90 ± 5.444	79	47.16 ± 29.0
Y	Au-doped	23-Oct	1	4.8		79		15	
			2	4.5		77		23	
			3	4.3	4.50 ± 0.250	77	77.50 ± 1.323	25	20.82 ± 5.4
Y	Au-doped	25-Oct	1	4.5		78		27	
			2	4.6		78		25	
			3	4.6	4.56 ± 0.030	78	78.00 ± 0.000	28	26.77 ± 2.0
Z	SnO_2	15-Nov	1	1.7		40		21	
			2	1.6		38		43	
			3	1.6	1.63 ± 0.029	38	38.67 ± 1.155	43	35.78 ± 12.6
ZA	SnO_2	17-Nov	1	1.9		46		41	
			2	2.0		49		46	
			3	2.2	2.00 ± 0.167	54	49.67 ± 4.041	47	44.67 ± 3.2
ZB	SnO_2	19-Nov	1	2.1		52		23	
			2	2.1		53		35	
			3	2.2	2.14 ± 0.059	55	53.33 ± 1.528	35	31.00 ± 6.9
ZC	SnO_2 std	21-Nov	1	2.0		49		19	
			2	1.5		34		29	
			3	1.4	1.63 ± 0.302	29	37.33 ± 10.408	41	29.67 ± 11.0
ZC	SnO_2+binder	25-Nov	1	4.1		76		31	
			2	4.1		76		36	
			3	3.9	4.05 ± 0.095	75	75.67 ± 0.577	33	33.17 ± 2.8
ZF	SnO_2 std	29-Nov	1	1.55		35		26	
			2	1.44		31		53	
			3	1.43	1.47 ± 0.07	30	32.00 ± 2.65	49	42.67 ± 14.6
ZF	SnO_2 binder	30-Nov	1	3.07		67		31	
			2	2.5		60		48	
			3	2.5	2.69 ± 0.33	61	62.67 ± 3.79	46	41.67 ± 9.3
ZG	SnO_2-dispers	3-Dec	1						
			2	1.49		13		15	
			3	1.25	1.37 ± 0.17	20	16.50 ± 4.95	47	31.00 ± 22.6
ZH	SnO_2-dispers	4-Dec	1	3.38		69		23	
			2	3.67		72		29	
			3	4.09	3.71 ± 0.36	76	72.33 ± 3.51	27	26.33 ± 3.1
ZH	SnO_2-disp-bind	4-Dec	1	1.64		38		27	
			2	1.35		26		70	
			3	1.32	1.44 ± 0.18	25	29.67 ± 7.23	49	48.67 ± 21.5

Continued: Sensor performance summary.

Sensor	Description	Date	Run	$S = \frac{R_a}{R_g}$	Averages	$S = \frac{R_a - R_g}{R_a}$ (%)	Averages	time (sec)	Averages
ZI	SnO_2 std	5-Dec	1	1.66		40		40	
			2	1.44		30		30	
			3	1.44	1.51 ± 0.13	31	33.67 ± 5.51	31	33.67 ± 5.5
ZJ	SnO_2-Au disp	8-Dec	1	1.084		8		72	
			2	1.083		7.7		75	
			3	1.084	1.08 ± 0.00	7.7	7.80 ± 0.17	75	74.00 ± 1.7
ZK	SnO_2-Au disp	9-Dec	1	1.01		1		47	
			2	1.01		0.9		79	
			3	1.01	1.01 ± 0.00	0.9	0.93 ± 0.06	90	72.00 ± 22.3
ZL	SnO_2-disp	10-Dec	1	3.8		73		24	
			2	4.12		76		32	
			3	4.33	4.08 ± 0.27	77	75.33 ± 2.08	27	27.67 ± 4.0
ZQ	Au-SnO_2 & SnO_2	23-Jan	1	1.043		4		33	
	(1:10 disp.)		2	1.053		5		50	
			3		1.05 ± 0.01		4.50 ± 0.71		41.50 ± 12.0
ZS	Coll. Au:SnO_2	4-Feb	1	2.4		58		15	
	(1:10 disp.)		2	1.86		46		21	
	2 Layer		3		2.13 ± 0.38		52.00 ± 8.49		18.00 ± 4.2
ZS	Coll. Au:SnO_2	7-Feb	1	2.38		58		15	
	(1:10 disp.)		2	2.43		59		20	
	5 Layer		3		2.41 ± 0.04		58.50 ± 0.71		17.50 ± 3.5
ZR	SnO_2 disp	28-Jan	1	3.06		67		24	
	1 Layer		2	2.69		63		32	
			3	2.76	2.84 ± 0.20	64	64.67 ± 2.08	28	28.00 ± 4.0
ZR	SnO_2 disp	30-Jan	1	4.31		77		22	
	2 Layer		2	3.86		74		28	
			3	3.96	4.04 ± 0.24	75	75.33 ± 1.53	30	26.67 ± 4.2
ZR	SnO_2 disp	13-Feb	1	11.7		91		14	
	3 Layer		2	7.8		87		17	
			3	7	8.83 ± 2.51	86	88.00 ± 2.65	17	16.00 ± 1.7
ZR	SnO_2 disp	18-Feb	1	5.8		83		17	
	4 Layer		2	3.7		72		21	
			3	3.45	4.32 ± 1.29	71	75.33 ± 6.66	19	19.00 ± 2.0
ZR	SnO_2 disp	20-Feb	1	6.4		84		15	
	5 Layer		2	3.3		70		26	
			3	3.7	4.47 ± 1.69	73	75.67 ± 7.37	24	21.50 ± 5.4
ZT	SnO_2:sputAu	9-Feb	1	7.1		86		15	
			2	4.87		80		24	
			3	4.8	5.59 ± 1.31	79	81.67 ± 3.79	21	20.00 ± 4.6
ZT	SnO_2:sputAu	11-Feb	1	7.6		87		18	
			2	6		83		23	
			3	5.8	6.47 ± 0.99	83	84.33 ± 2.31	23	21.33 ± 2.9
ZU	SnO_2:sputAu	15-Feb	1	7.86		87		16	
			2	5.53		82		20	
			3	5.39	6.26 ± 1.39	82	83.67 ± 2.89	20	18.67 ± 2.3
ZV	SnO_2 disp	22-Feb	1	4.78		79		20	
	5 layer		2	3.13		68		29	
	5 hr sinter		3	3.26	3.72 ± 0.92	69	72.00 ± 6.08	29	26.00 ± 5.2
ZW	SnO_2 disp	26-Feb	1	3.88		74		17	
	3 Layers		2	3.14		68		23	
	3 hr sinter		3	3.04	3.35 ± 0.46	67	69.67 ± 3.79	25	21.67 ± 4.16

Continued: Sensor performance summary.

Sensor	Description	Date	Run	$S=\frac{R_a}{R_g}$	Averages	$S=\frac{R_a-R_g}{R_a}$ (%)	Averages	time (sec)	Averages
ZX	SnO_2 disp	29-Feb	1	3.5		71		21	
	1 Layer		2	3.1		67		27	
			3	3.1	3.23 ± 0.23	68	68.67 ± 2.08	30	26.00 ± 4.58
ZX	SnO_2 disp	25-Mar	1	6.25		84		19	
	2 Layer		2	5.03		80		23	
			3	4.93	5.40 ± 0.73	80	81.33 ± 2.31	25	22.33 ± 3.06
ZX	SnO_2 disp	29-Mar	1	6.2		84		16	
	3 Layer		2	4.3		77		18	
			3	4.1	4.87 ± 1.16	76	79.00 ± 4.36	20	18.00 ± 2.00
ZX	SnO_2 disp	2-Apr	1	5.68		82		18	
	4 Layer		2	3.64		73		26	
			3	3.4	4.24 ± 1.25	70	75.00 ± 6.24	25	23.00 ± 4.36
ZX	SnO_2 disp	7-Apr	1	6.34		84		13	
	5 Layer		2	3.95		75		19	
			3	3.5	4.60 ± 1.53	72	77.00 ± 6.24	22	18.00 ± 4.58
ZY	SnO2 disp	15-Apr	1	6.51		85		14.5	
	Au-Pd sputtered		2	4.72		79		20	
			3	4.03	5.09 ± 1.28	75	79.67 ± 5.03	20	18.17 ± 3.18
ZZ	SnO2:Al2O3 disp	16-Apr	1	2.13		53		26	
			2	1.77		43		31	
			3	1.6	1.83 ± 0.27	35	43.67 ± 9.02	35	30.67 ± 4.51

B.2 MATLAB code for sensitivity and time response data analysis

```
% ***************************************************************************
%
% MATLAB program: sensoranalysis.m
% Evaluates the sensitivity and time response of SnO2 gas sensor when
% exposed to reducing gas such as CO
%
% Smitesh Bakrania
% Created: May 9th, 2007
% Modified: June 8th, 2007
%
% ***************************************************************************

clear

% File Reading and Data Extracting

datafile = input('CSV file (exclude .csv): ', 's'); % prompts for the file
datafile = [datafile '.csv']; % attaches the extension
data = csvread(datafile); % reads in the file

hold on
plot(data(:,4)) % plotting resistance as a function of matrix rows
grid minor
hold off

starttime = input('From data point:         '); % insert sensing start point
endtime = input('To data point:           '); % insert sensing end point

data = [data(starttime:endtime,2) data(starttime:endtime,4)]; % truncating

% SENSITIVITY

dsize = length(data)-1;

% calculating derivative
% stores all the derivatives in d1 with respect to time
for i=1:dsize
    d1(i+1,:) = (data(i,2)-data(i+1,2))/(data(i,1)-data(i+1,1));
end

% finds the minimum in the derivative (CO turned ON)
```

```
% start of the response
[c,ind1] = min(d1); % finds the min in derivative
ind1 = ind1-15; % data point 15 points before the min in derivative for S
dropstart = [data(ind1,1) data(ind1,2)]; % datapoint where the res drop begins

data = data(ind1:end,:);
d1 = d1(ind1:end);

% end of response
[c,ind2] = min(data(:,2));
dropend = [data(ind2,1) data(ind2,2)];

% calculating sensitivity
S = dropstart(2)/dropend(2);
S1 = (dropstart(2)-dropend(2))/dropstart(2);

% TIME RESPONSE

trespdata1 = data(15:ind2,:);

% relative scaling (time starts from zero and resistance ends at zero)
trespdata(:,1) = trespdata1(:,1)-trespdata1(1,1);
trespdata(:,2) = trespdata1(:,2)-trespdata1(end,2);

% calculating natural log of the resistance signal
lny = log(trespdata(:,2));

% cutoff index value for linear fitting through plotting tool
startoff = 1; % change when start point too early
cutoff = 10; % change when end point is too late, normally 17

% linear fit
p = polyfit(trespdata(startoff:cutoff,1), lny(startoff:cutoff), 1);
tau = -(1/p(1))*60;

% generates data values for the fit line
trespdata2 =  [trespdata(startoff:cutoff,1), (p(1)*trespdata(startoff:cutoff,1))+p(2)];

% display results
display(' ')
display('    Sensitivity')
disp(S)
display('Alt.Sensitivity')
disp(S1)
display('    Time Response [sec]')
disp(tau)

% Plotting Results
subplot(2,1,1);
hold on
plotyy(data(:,1),data(:,2),data(:,1),d1)
plot(trespdata1(startoff,1), trespdata1(startoff,2), ...
'o', 'color', 'red', 'linewidth', 1.2)
plot(trespdata1(cutoff,1), trespdata1(cutoff,2), ...
'o', 'color', 'magenta', 'linewidth', 1.2)
plot(dropstart(1), dropstart(2), 'o', 'color', 'green', 'linewidth', 1.4)
plot(dropend(1), dropend(2), 'o', 'color', 'green', 'linewidth', 1.4)
xlabel('time [min]'), ylabel('resistance [kOhms]')
legend('sensor response', 'time response data beginning', ...
'time response data end', 'sensitivity calcu. points')
hold off

subplot(2,1,2);
hold on
plot(trespdata(startoff:cutoff,1), lny(startoff:cutoff), 'linewidth', 1.1)
plot(trespdata2(:,1), trespdata2(:,2), 'color', 'r')
xlabel('relative time [mins]'), ylabel('natural log of resistance')
legend('linearized signal', 'linear fit')
hold off
```

APPENDIX C

Material Analysis

C.1 XRD Analysis procedure

XRD data acquisition and analysis for tin dioxide powder samples
Smitesh Bakrania, July 26, 2005

Software: DMSNT ThermoARL

Sample preparation

Lay the sample using a blade in a 1cm square pattern, thick enough to be opaque.
User Iso-propyl alcohol for adhesion and uniformity.

Data Acquisition

User the following parameters for the full scan and the 3 peak (high resolution) scan:

scan type	Scan	step	range (deg)	scan rate (deg/min)	time (min)
Full Scan	continuous	0.02	15-90	4.0	18
3peak Scan	continuous	0.02	23-41	0.5	36

For superimposing tin dioxide index pattern use 41-1445 and for gold 4-734

Data Analysis

- Once the data is acquired, use the Background Subtraction option under Analysis in the menu bar.
- Use the default options with Box Car Curve Fit with default value of 1.5 degrees for background subtraction.
- Once the background is subtracted the Peak Finder option under Analysis will be available. User the Peak Finder default options: Peak Finder using Digital Filtering of ESD 4 and Ripple Multiplier of 1.5. Make sure only the peaks you are interested in are captured. If not then play with the numbers to achieve this as best possible.
- Once this is completed, use the Profile Fit option under Analysis and see all the peaks are listed – if not you can remove the one's that are not needed. On the right hand side of the panel there are options for the fit. Use the Pearson 7 fit since it best describes the peak and click Calculate to proceed. See the curve fitting results on your plot and note the error shown on the calculation window.
- Note down the peak, the amplitude (CPS), Position (degrees) and the FWHM (degrees) for later calculation in the Scherrer formula.

C.2 MATLAB code for image analysis

```
% ************************************************************************
%
% Title:    diameter.m
% Description:  for calculating particle diameters for vertically
%               centered circles generated using corelDRAW.
% Date:     March 19th, 2005
% Edited:   August 18th, 2005
% Author:   Smitesh Bakrania
%
% ************************************************************************
clear;

% ACQUIRES INPUTS REGARDING THE FILE AND SCALE

imfile=input('The bitmap file name: ','s'); % accesses file name
imfile=[imfile,'.bmp'];                     % adds the bmp file extension
scale=input('Scale bar dimension:  ');      % access the scale bar dimension
check=input('two sets (y/n)?:  ','s');          % second set analysis

% READING THE FILE AND ACQUIRES SCALE, CENTER COLUMN AND REVERSES BINARY

a=imread(imfile);                           % reads binary bitmap image
length=size(a);                             % gives dimensions (H x L) of 'a'
height=length(1);                           % image height in pixels
length=length(2);                           % image length in pixels
scale=scale/length;                         % microns (or nm) per pixel
mid_colm=round(length/2);                   % middle column with diameters
a=a(:,mid_colm);                            % extracts the middle column
% a=im2double(a);                           % converts uint8 to a number
a=(a-1).^2;                                 % inverses the binary; 0's & 1's

% COUNTING THE DIAMETERS IN PIXELS

b=0;                                        % initializes diameter matrix
j=1;                                        % index for 'b'(particle index)
for i=1:height
    if a(i)==1                              % checks if the number is 1
        b(j)=b(j)+1;                        % add to diameter count
        if i~=height                        % checks for matrix end
            if a(i+1)==0                    % if next number is 0
                j=j+1;                      % next particle index
                b(j)=0;                     % initiates next index
            end
        end
    end
end

% SCALES THE DIAMETERS

b=b.*scale;                                 % scales pixel diameters
% removes the first diameter as it represents the thickness of scale bar
b(1)=[];

%-------------------------------------------------------------------------

if check=='y'

% ACQUIRES INPUTS REGARDING THE FILE AND SCALE

imfile=input('The bitmap file name: ','s'); % accesses file name
imfile=[imfile,'.bmp'];                     % adds the bmp file extension
scale=input('Scale bar dimension:  ');      % access the scale bar dimension

% READING THE FILE AND ACQUIRES SCALE, CENTER COLUMN AND REVERSES BINARY

a=imread(imfile);                           % reads binary bitmap image
length=size(a);                             % gives dimensions (H x L) of 'a'
height=length(1);                           % image height in pixels
length=length(2);                           % image length in pixels
scale=scale/length;                         % microns (or nm) per pixel
mid_colm=round(length/2);                   % middle column with diameters
a=a(:,mid_colm);                            % extracts the middle column
% a=im2double(a);                           % converts uint8 to a number
a=(a-1).^2;                                 % inverses the binary; 0's & 1's

% COUNTING THE DIAMETERS IN PIXELS

b1=0;                                        % initializes diameter matrix
```

```
j=1;                                        % index for 'b'(particle index)
for i=1:height
    if a(i)==1                              % checks if the number is 1
        b1(j)=b1(j)+1;                        % add to diameter count
        if i~=height                        % checks for matrix end
            if a(i+1)==0                    % if next number is 0
                j=j+1;                      % next particle index
                b1(j)=0;                     % initiates next index
            end
        end
    end
end

% SCALES THE DIAMETERS

b1=b1.*scale;                                 % scales pixel diameters
% removes the first diameter as it represents the thickness of scale bar
b1(1)=[];
b=[b b1];
end

%-------------------------------------------------------------------------

% PLOTTING

%hist(b,15);                                 % histogram with 15 bins

% mn=mean(b); sd=std(b,1);                    % mean & standard deviation

%geometric mean
[freq mid]=hist(b,15);                      % provides the frequency and midpoints
lndp=log(mid);                              % natural log of midpoints
fract=freq/sum(freq);                       % fractional population
fracts=fract/(mid(3)-mid(2));               % fractional population per nm
                                            %(divided by the interval, assumed constant)
mn=exp(sum(lndp(:).*fract(:)));             % geometric mean
mn=roundn(mn,-1);                           % rounding-off to 10^-1=0.1

%geometric standard deviation
diff=(lndp-log(mn)).^2;                     % nat. log difference
sd=exp((sum(freq(:).*diff(:))/(sum(freq)-1))^0.5); % standard dev.
sd=roundn(sd,-1);                          % rounding-off to 10^-1=0.1

%lognormal fit
maxd=max(b);
dp=0.1:0.1:maxd;       %35;
dpn=size(dp);
dpn=dpn(2);
for i=1:dpn;
    fit=exp(-(log(dp(i))-log(mn))^2/(2*(log(sd))^2))/(sqrt(2*pi)*dp(i)*log(sd));
    curve(i)=fit;
end

bar(mid, fracts);
%axis([0 35 0 0.3]);

mns=num2str(mn); sds=num2str(sd);           % to string for annotation
gtext=['mean ', mns, '; stand. dev ', sds]; % text for annotation
annotation('textbox',[0.58 0.8 0.09 0.1], ...
  'string', gtext, 'LineStyle', 'none', ...
  'FontName', 'Times New Roman'); % generates textbox
xlabel('d_p [nm]', 'FontName', 'Times New Roman');                     % labeling axis
ylabel('Fractional population [nm^-^1]','FontName', 'Times New Roman');              % labeling axis
%title('Particle Distribution plot');        % plot title
h = findobj(gca,'Type','patch');            % changing color of bars
set(h,'FaceColor','r','EdgeColor','w');     % changing color of bars

hold
plot(dp, curve, 'LineWidth', 2);

size=size(b);
size=size(2);
sizes=num2str(size);

disp('particles counted:');
disp(sizes);
disp('done');                               % displays done when done!
```

C.3 As-received gold acetate BET analysis

MICROMERITICS ANALYTICAL SERVICES The Particle Testing Authority

TriStar 3000 V6.05.01 A   Unit 1 Port 2   Serial #: 1098   Page 1

Sample: Gold(III)Acetate lot A06R004 815
Operator: MJP
Submitter: Univ. of Michigan
File: C:\...\03MARCH\06-0867.SMP

Started:	3/15/2006 10:10:46AM	Analysis Adsorptive:	N2
Completed:	3/15/2006 1:49:41PM	Analysis Bath Temp.:	77.300 K
Report Time:	3/15/2006 1:49:42PM	Sample Mass:	0.9350 g
Warm Free Space:	7.3501 cm³ Measured	Cold Free Space:	22.5621 cm³ Measured
Equilibration Interval:	10 s	Low Pressure Dose:	None
Sample Density:	1.000 g/cm³	Automatic Degas:	Yes

Sample Prep: Stage	Soak Temperature (°C)	Ramp Rate (°C/min)	Soak Time (min)
1	80	10	960

Summary Report

Surface Area

Single point surface area at P/Po = 0.306968839: 3.8090 m²/g

C.4 EMPA results on SnO_2 dispersion films

Summary of Au-doped and Pd-doped dispersion films analyzed with electron microprobe at EMAL

		Weight %					Atomic %				
Point#	Sample film	Sn	Au	O	Pd	Total	Sn	Au	O	Pd	Total
1	SnO2	79.487	-0.112	10.715		90.202	50.021	-0.043	50.021		100.043
2	SnO2	79.010	-0.070	10.651		89.661	50.013	-0.027	50.013		100.027
3	SnO2	77.340	0.239	10.426		88.005	49.953	0.093	49.953		100.000
4	SnO2	78.280	0.071	10.552		88.903	49.986	0.027	49.986		100.000
5	SnO2	78.243	0.000	10.548		88.791	50.000	0.000	50.000		100.000
6	SnO2	79.043	0.183	10.655		89.882	49.965	0.070	49.965		100.000
7	SnO2	78.719	-0.042	10.612		89.331	50.008	-0.016	50.008		100.016
8	SnO2	78.623	0.070	10.599		89.292	49.987	0.027	49.987		100.000
9	SnO2	78.725	-0.028	10.612		89.338	50.005	-0.011	50.005		100.011
10	SnO2	78.174	0.140	10.538		88.852	49.973	0.054	49.973		100.000
11	SnO2 with Au	67.682	3.799	9.124		80.604	49.168	1.663	49.168		100.000
12	SnO2 with Au	62.941	3.831	8.485		75.256	49.100	1.801	49.100		100.000
13	SnO2 with Au	62.253	2.585	8.392		73.230	49.382	1.235	49.382		100.000
14	SnO2 with Au	64.291	3.914	8.667		76.871	49.099	1.801	49.099		100.000
15	SnO2 with Au	65.003	2.822	8.763		76.587	49.354	1.291	49.354		100.000
16	SnO2 with Au	67.755	3.533	9.134		80.422	49.227	1.547	49.227		100.000
17	SnO2 with Au	70.478	3.408	9.501		83.387	49.282	1.436	49.282		100.000
18	SnO2 with Au	67.166	4.308	9.054		80.528	49.052	1.896	49.052		100.000
19	SnO2 with Au	68.257	3.226	9.201		80.684	49.298	1.404	49.298		100.000
20	SnO2 with Au	65.955	3.336	8.891		78.182	49.250	1.501	49.250		100.000
21	SnO2 with Au rim	75.247	1.735	10.144		87.125	49.655	0.690	49.655		100.000
22	SnO2 with Au rim	75.177	1.721	10.134		87.032	49.658	0.685	49.658		100.000
23	SnO2 with Au rim	76.586	1.739	10.324		88.649	49.660	0.679	49.660		100.000
24	SnO2 with Au rim	76.166	1.567	10.268		88.001	49.692	0.616	49.692		100.000
25	SnO2 with Au rim	75.547	2.158	10.184		87.890	49.573	0.853	49.573		100.000
26	SnO2 with Au rim	75.790	1.729	10.217		87.736	49.659	0.683	49.659		100.000
27	SnO2 with Au rim	76.361	1.934	10.294		88.589	49.621	0.757	49.621		100.000
28	SnO2 with Au rim	76.095	2.242	10.258		88.595	49.560	0.880	49.560		100.000
29	SnO2 with Au rim	75.951	1.855	10.238		88.044	49.635	0.731	49.635		100.000
30	SnO2 with Au rim	75.837	1.870	10.223		87.930	49.631	0.737	49.631		100.000
31	SnO2 with Pd	69.406		10.497	7.586	87.489	44.566		50.000	5.434	100.000
32	SnO2 with Pd	69.603		10.432	6.975	87.009	44.973		50.000	5.027	100.000
33	SnO2 with Pd	67.442		10.260	7.772	85.475	44.304		50.000	5.696	100.000
34	SnO2 with Pd	70.012		10.495	7.027	87.535	44.965		50.000	5.035	100.000
35	SnO2 with Pd	65.879		10.238	9.023	85.139	43.373		50.000	6.627	100.000
36	SnO2 with Pd	62.230		9.711	8.793	80.734	43.192		50.000	6.808	100.000
37	SnO2 with Pd	66.413		10.330	9.161	85.904	43.332		50.000	6.668	100.000
38	SnO2 with Pd	65.583		10.153	8.728	84.464	43.537		50.000	6.463	100.000
39	SnO2 with Pd	66.206		10.305	9.176	85.687	43.305		50.000	6.695	100.000
40	SnO2 with Pd	64.244		10.367	11.347	85.958	41.770		50.000	8.230	100.000

metal	Weight %	Atomic %
Au	3.5	1.6
Pd	8.6	6.3

C.5 TEM images

Tertiary system of SnO_2 doped with gold and aluminum

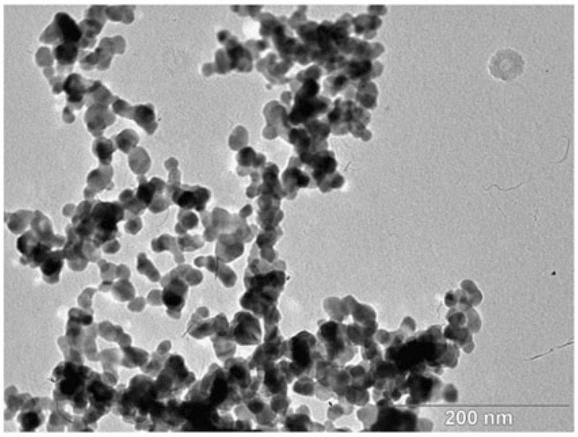

e5-1.tif

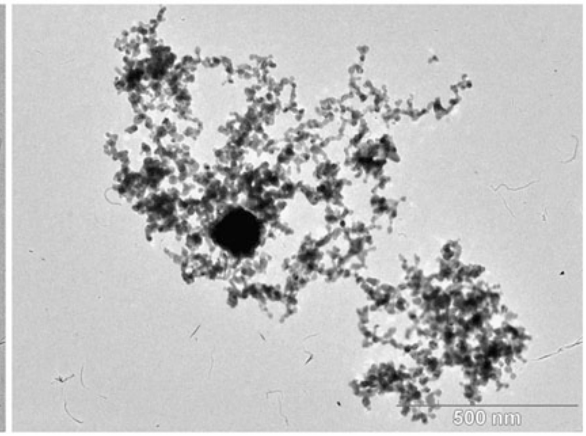

e5-10.tif

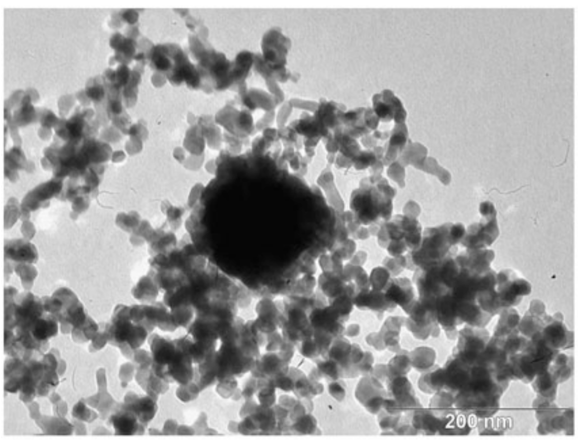

e5-11.tif

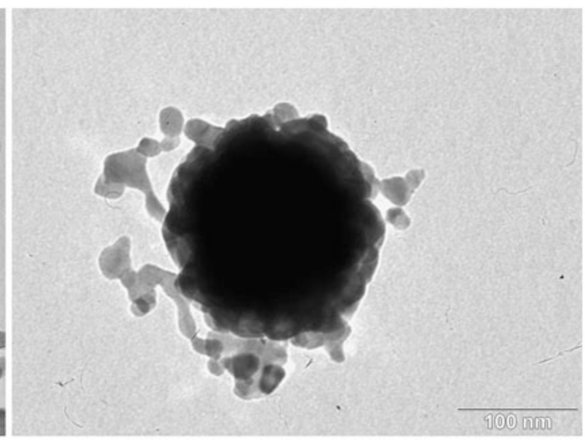

e5-12.tif

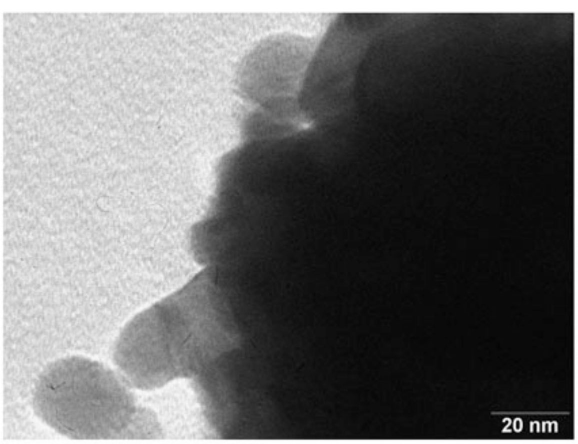

e5-13.tif

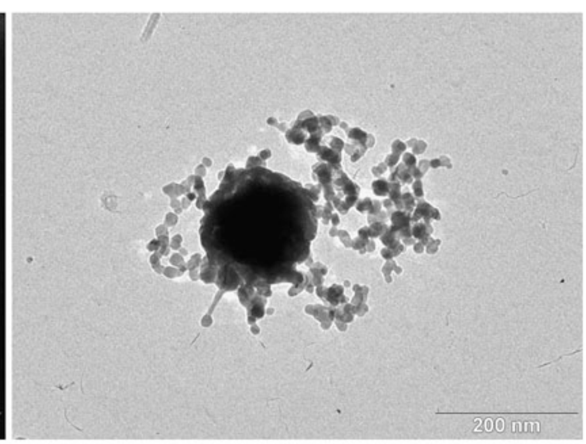

e5-14.tif

Tertiary system of SnO_2 doped with gold and aluminum

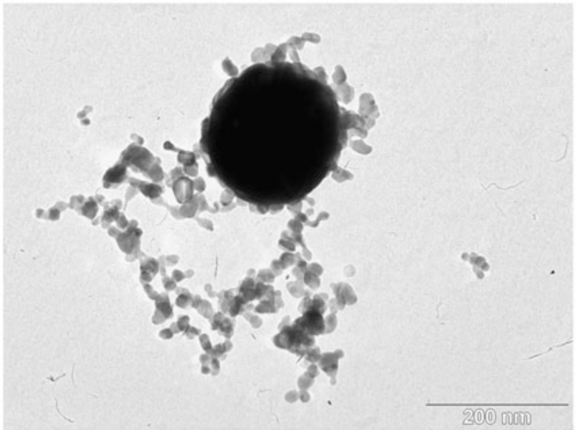

e5-15.tif

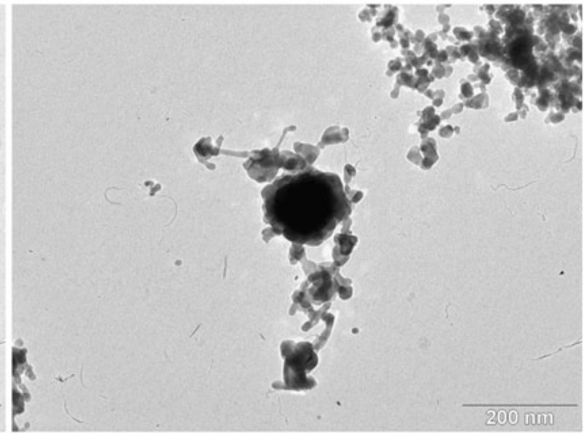

e5-16.tif

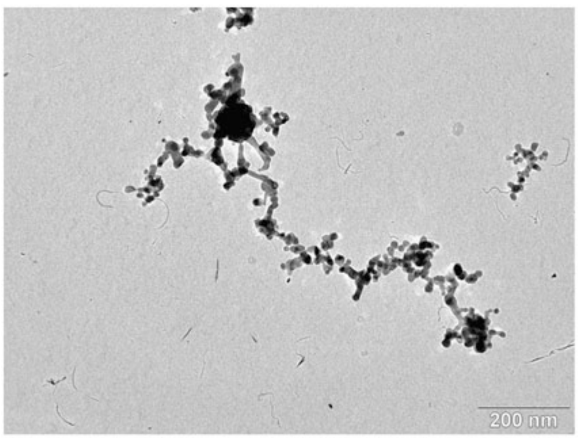

e5-17.tif

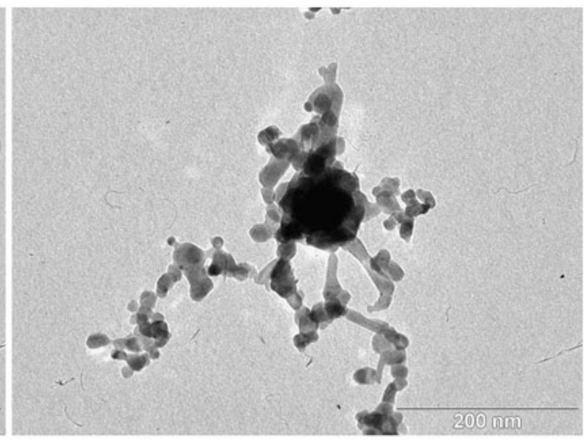

e5-18.tif

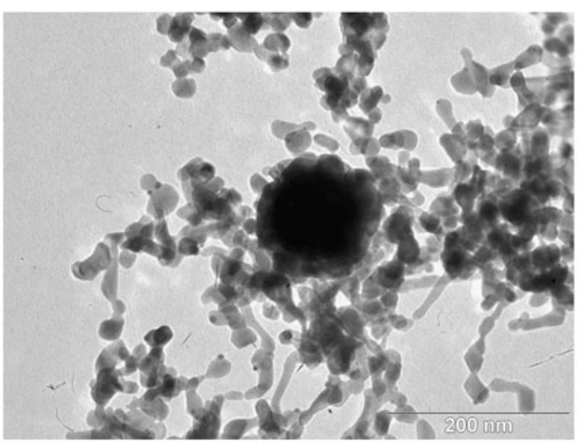

e5-19.tif

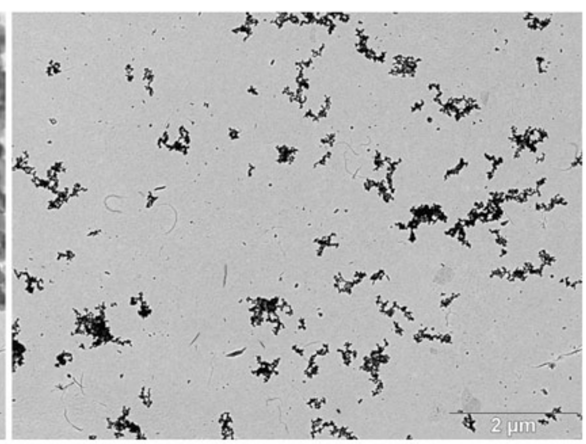

e5-2.tif

Tertiary system of SnO_2 doped with gold and aluminum

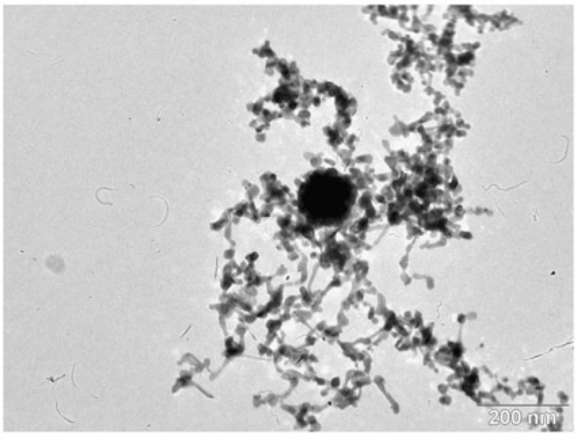

e5-20.tif

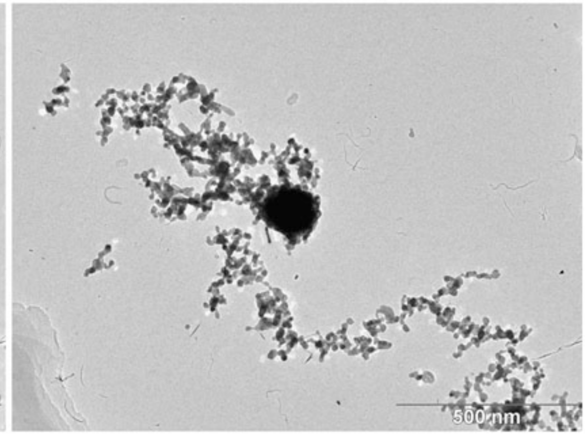

e5-21.tif

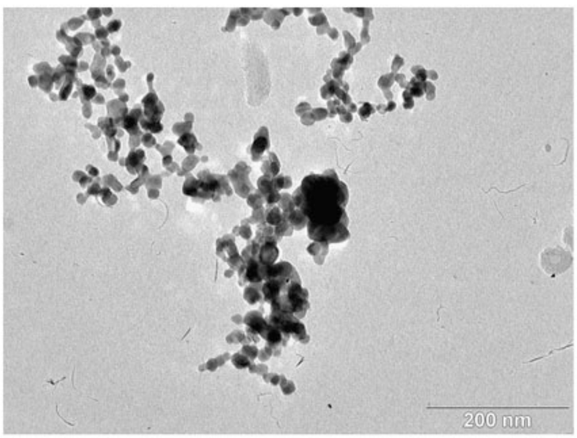

e5-22.tif

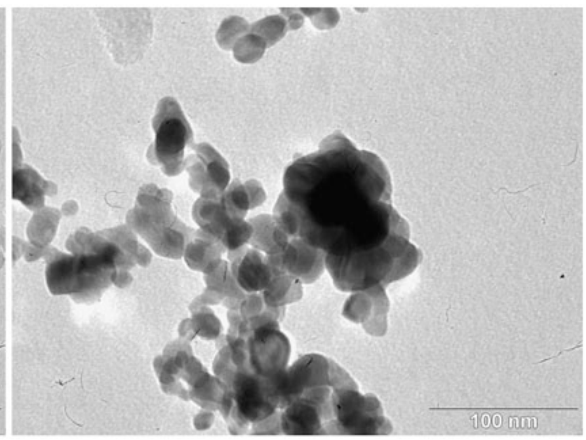

e5-23.tif

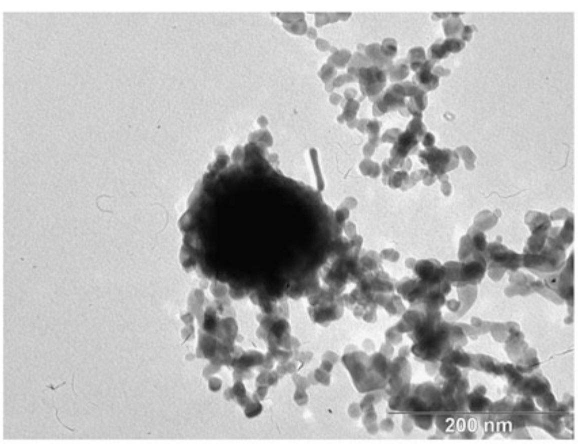

e5-24.tif

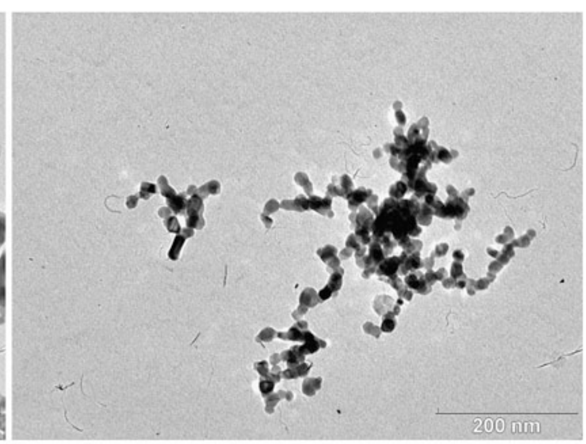

e5-25.tif

Tertiary system of SnO_2 doped with gold and aluminum

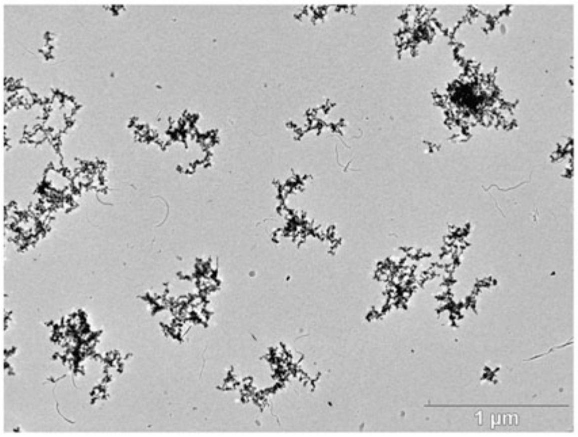

e5-26.tif

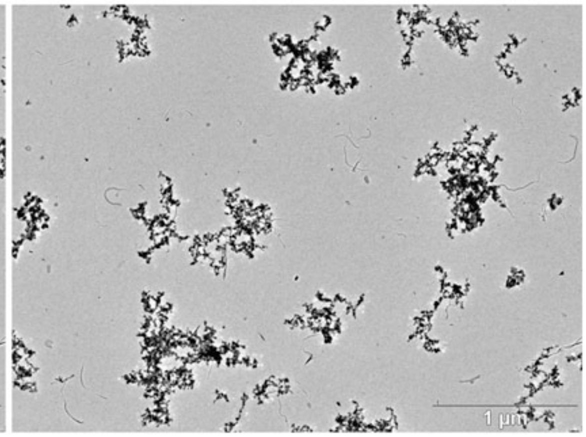

e5-27.tif

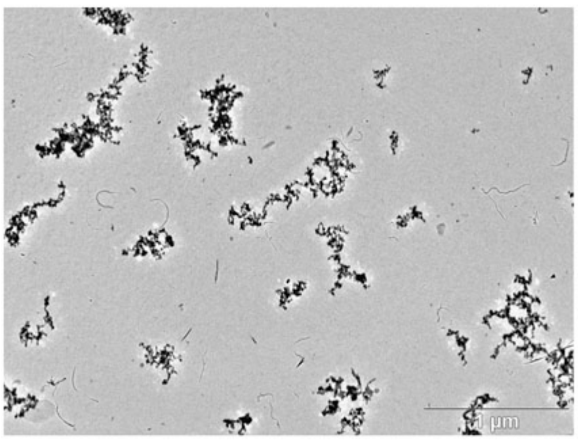

e5-28.tif

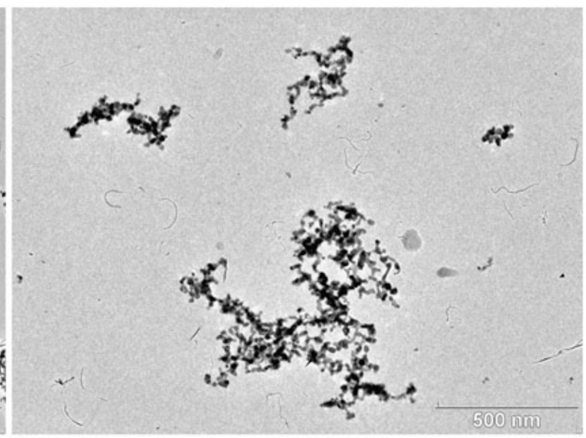

e5-29.tif

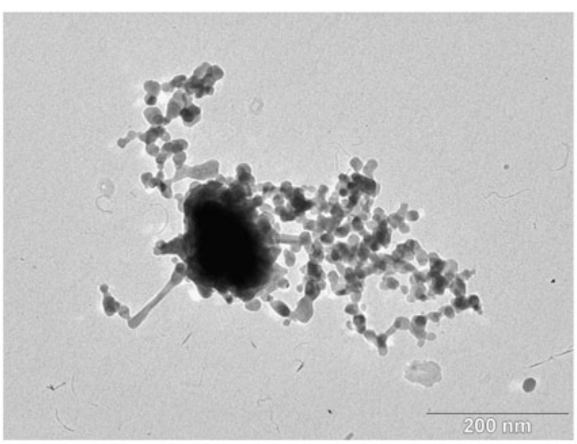

e5-3.tif

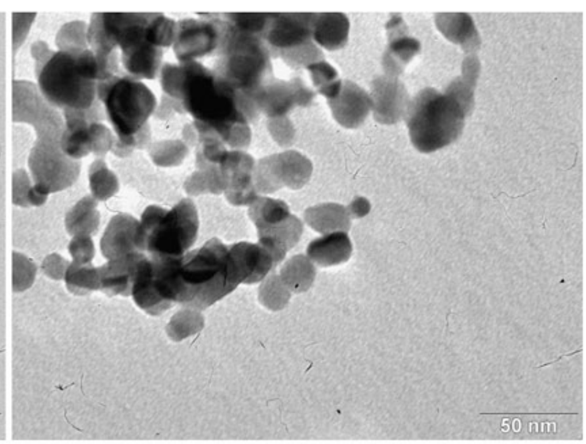

e5-30.tif

Tertiary system of SnO_2 doped with gold and aluminum

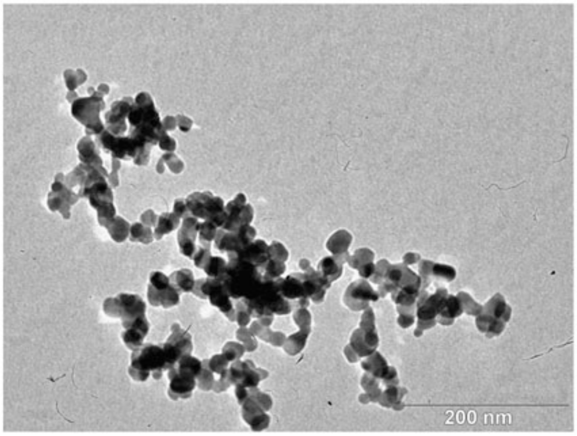

e5-31.tif

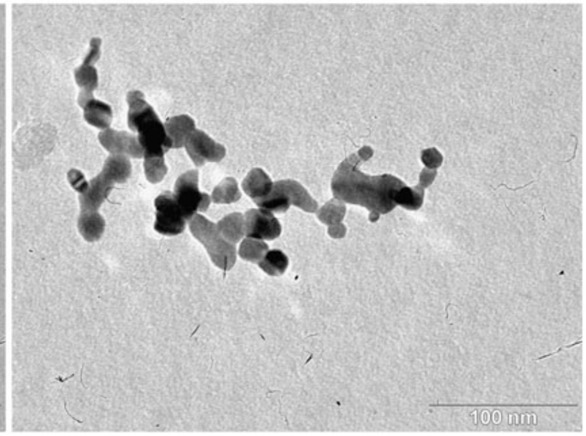

e5-32.tif

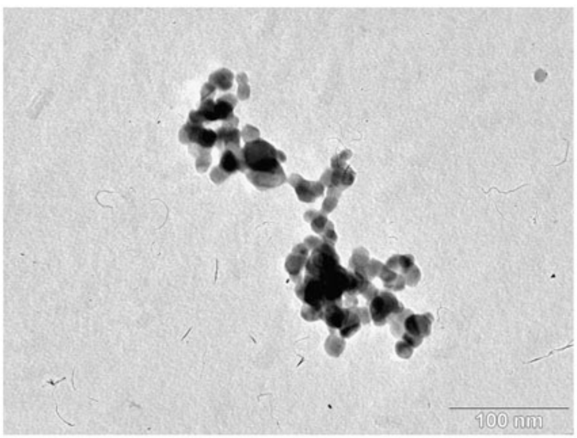

e5-33.tif

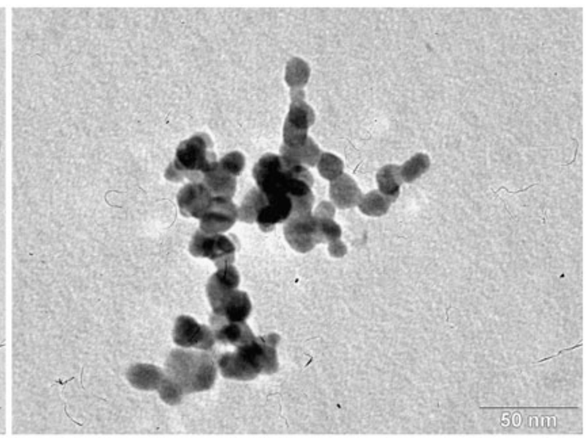

e5-34.tif

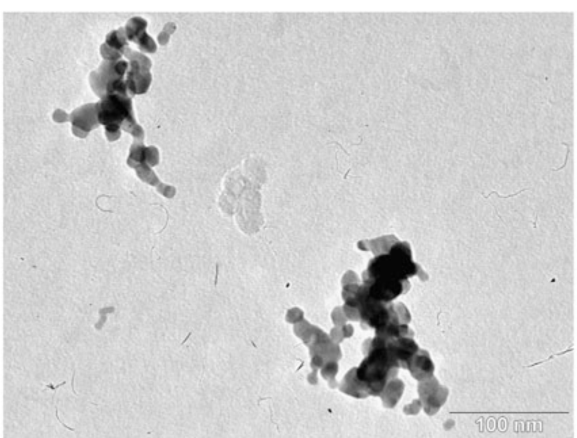

e5-35.tif

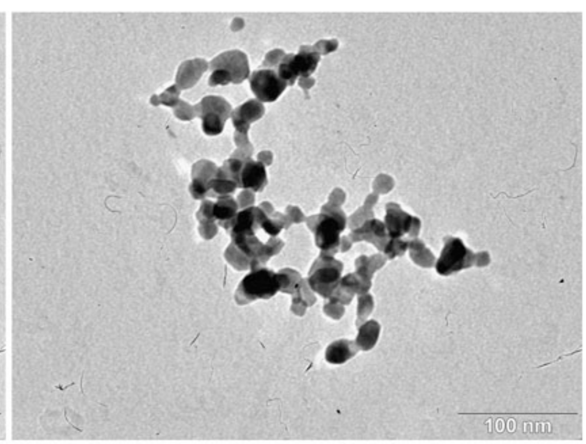

e5-36.tif

Tertiary system of SnO_2 doped with gold and aluminum

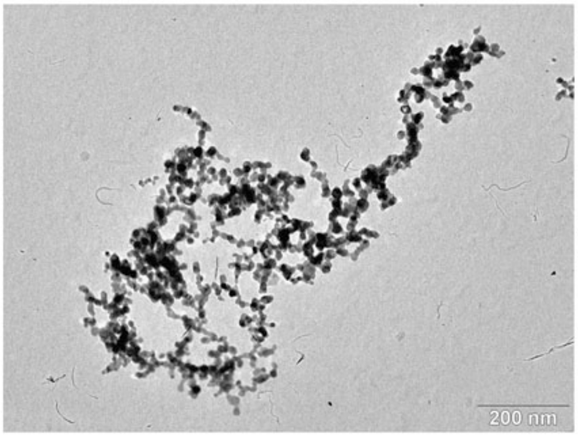

e5-37.tif

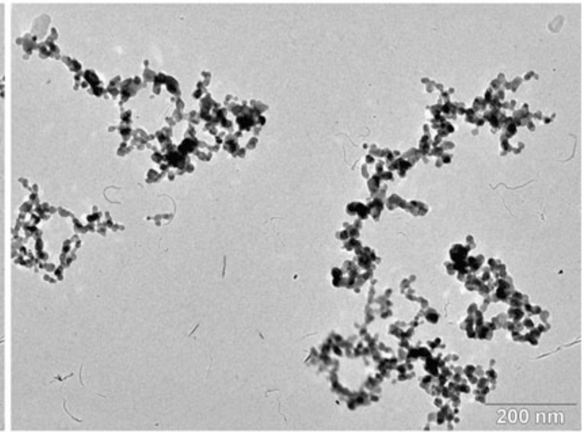

e5-38.tif

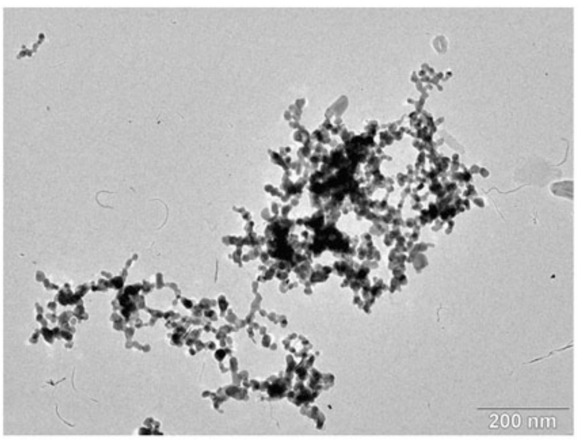

e5-39.tif

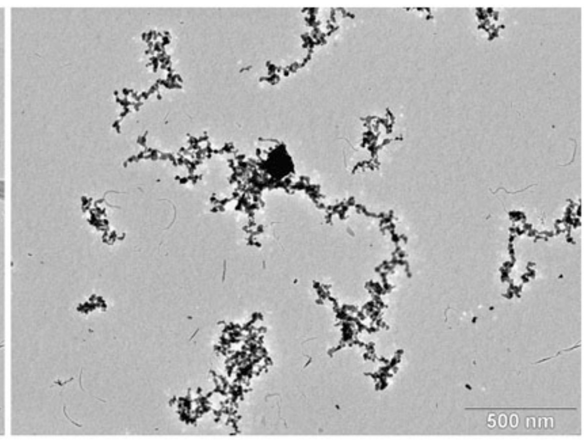

e5-4.tif

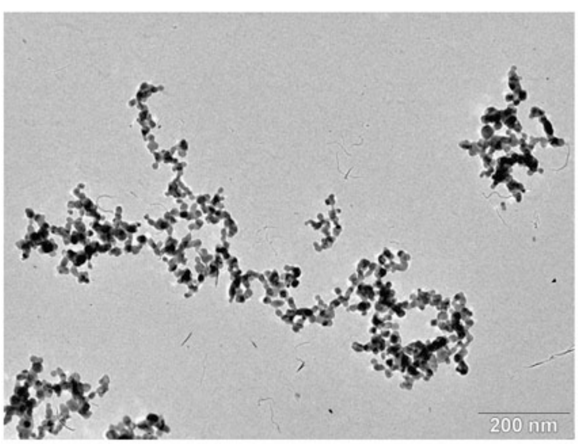

e5-40.tif

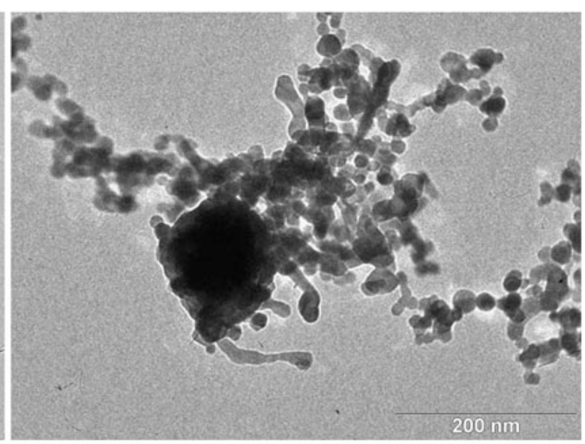

e5-5.tif

Tertiary system of SnO_2 doped with gold and aluminum

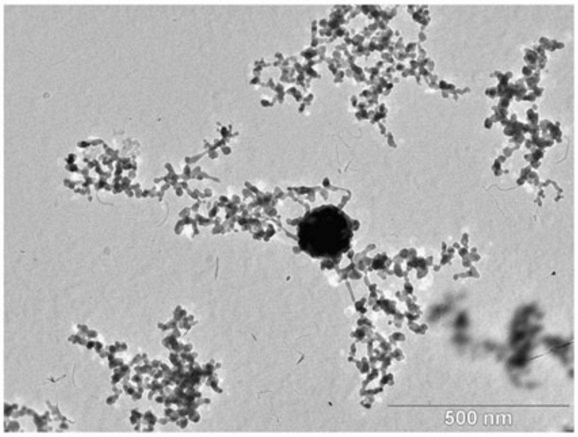

e5-6.tif

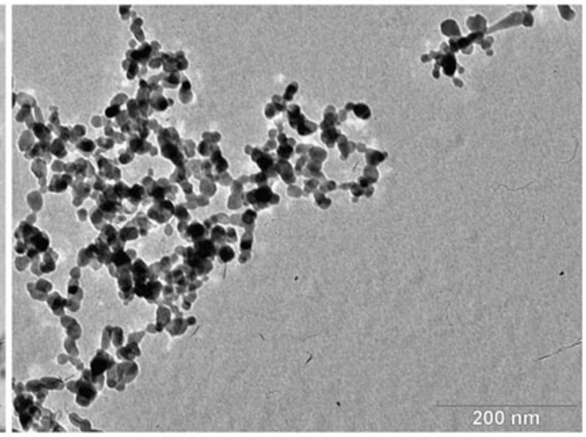

e5-7.tif

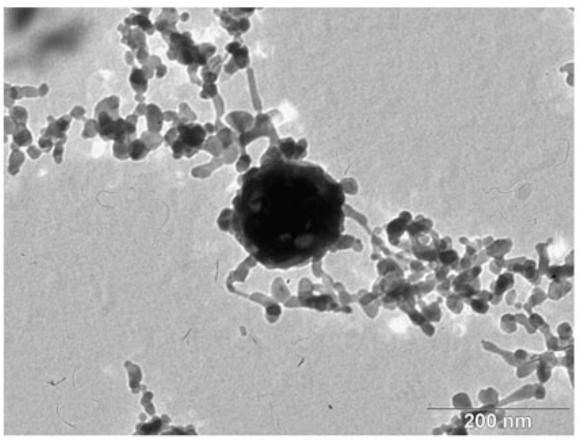

e5-8.tif

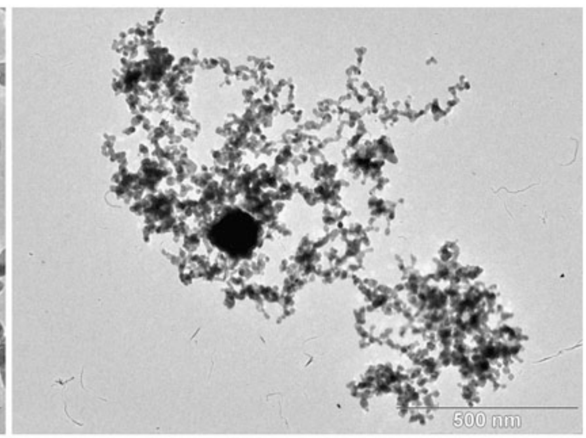

e5-9.tif

SnO_2 doped with nickel using nickel acetate

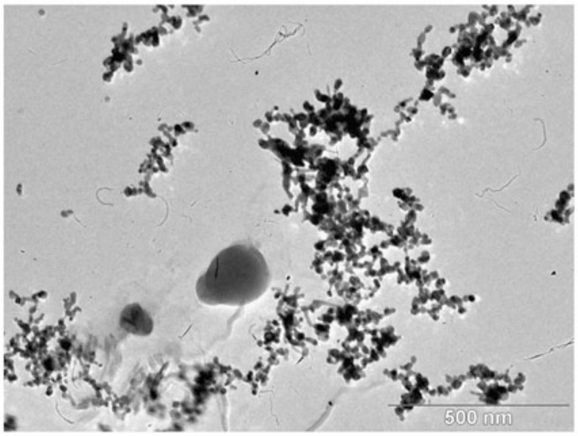

050520-a8-01-ti.tif

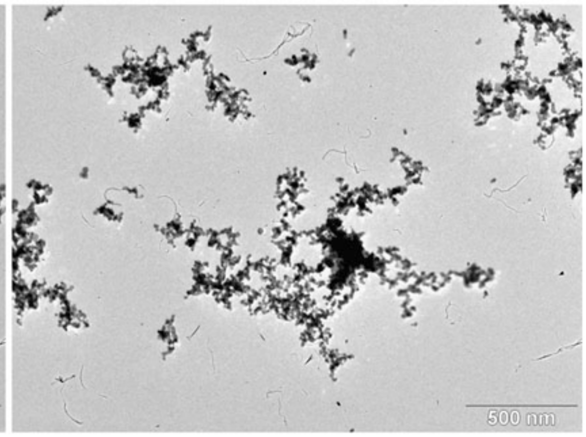

050520-a8-02-ti.tif

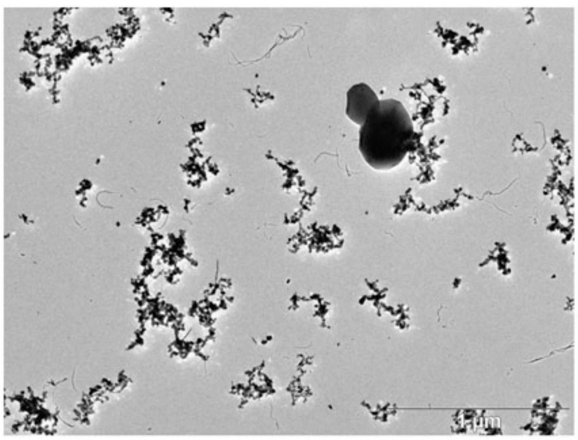

050520-a8-03-ti dp380nm.tif

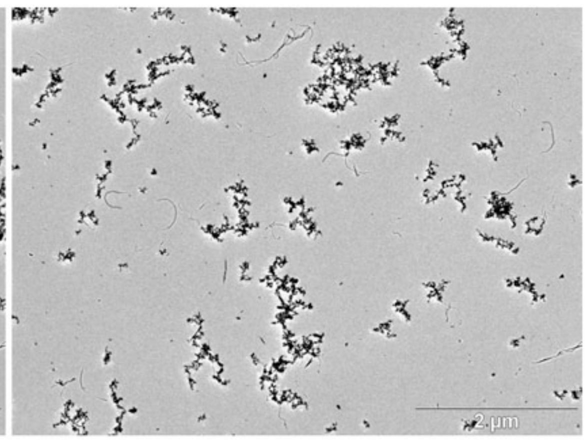

050520-a8-04.tif

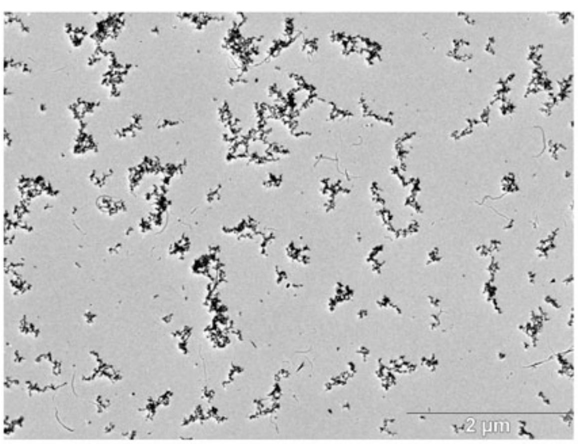

050520-a8-05.tif

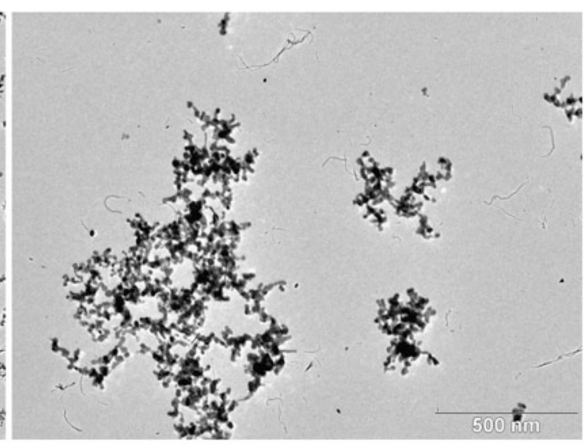

050520-a8-06.tif

SnO_2 doped with nickel using nickel acetate

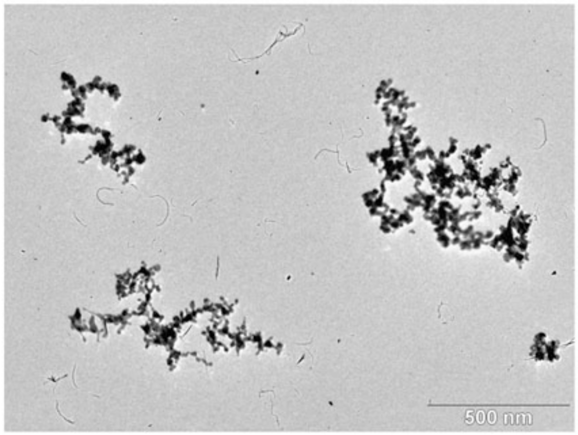

050520-a8-07.tif

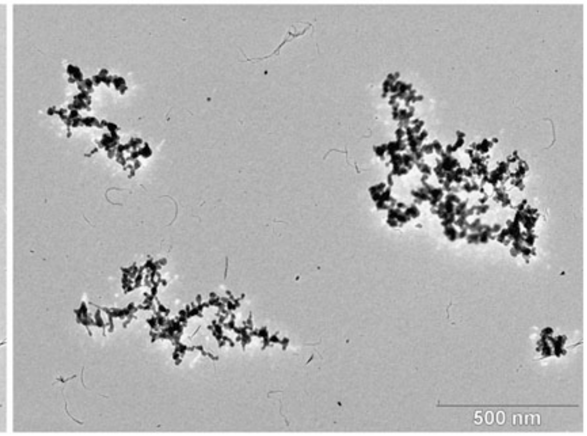

050520-a8-08.tif

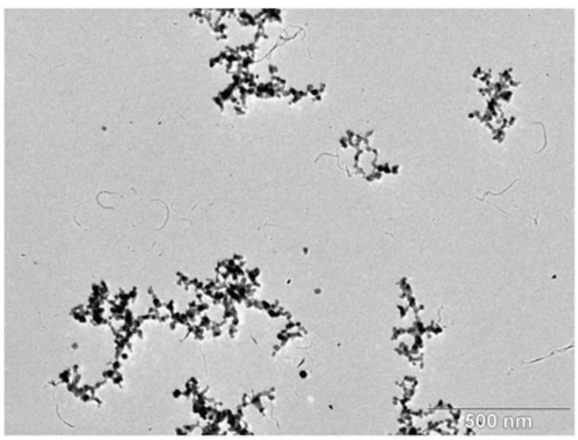

050520-a8-09.tif

SnO_2 doped with nickel using nickel acetate

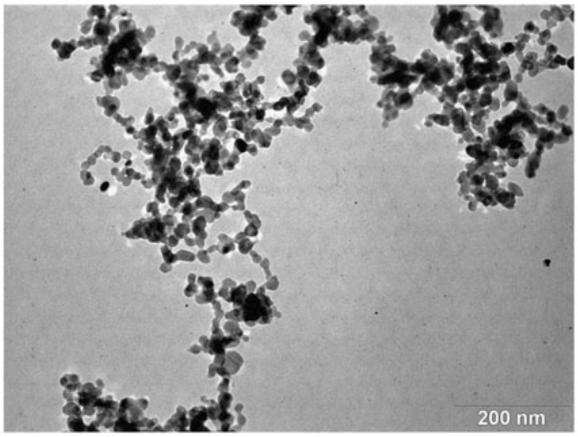

a9_1.tif

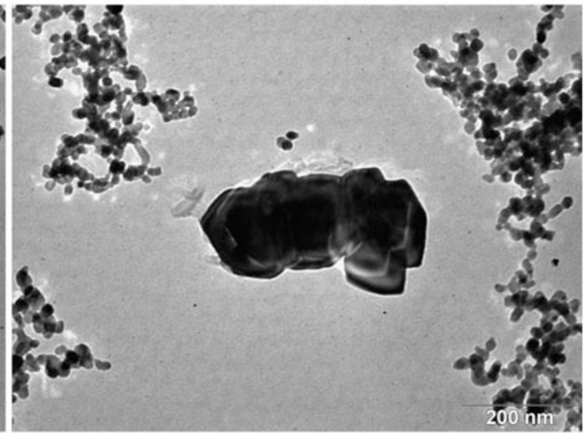

a9_2.tif

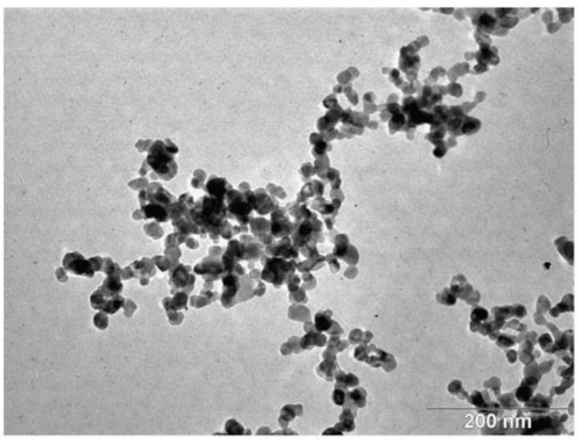

a9_3.tif

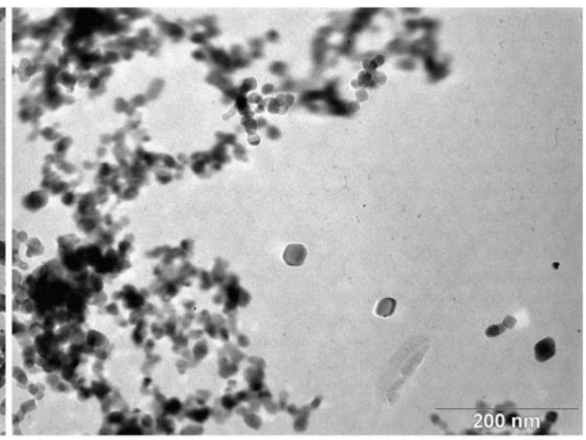

a9_4.tif

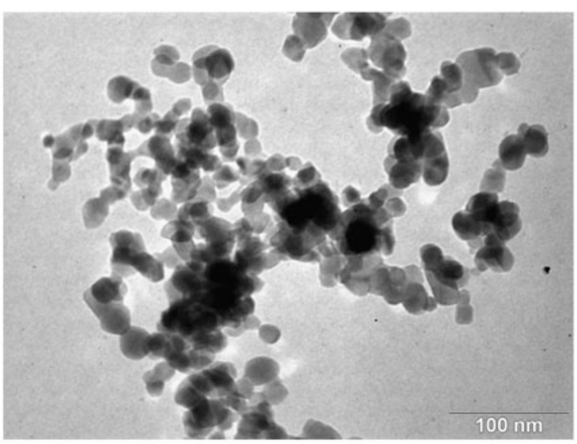

a9_5.tif

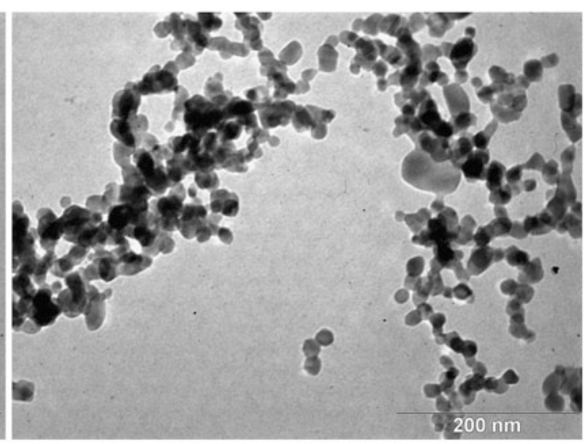

a9_6.tif

SnO_2 doped with nickel using nickel acetate

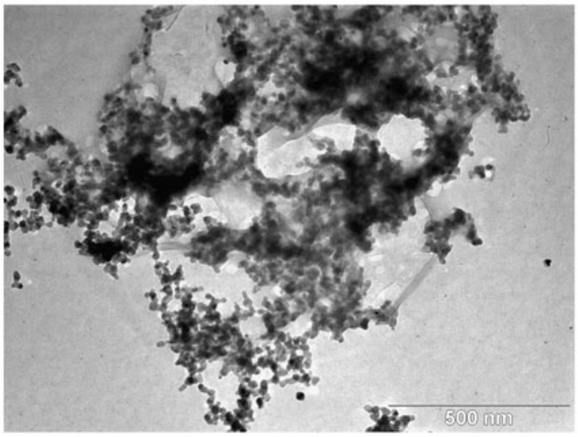

a9_7.tif

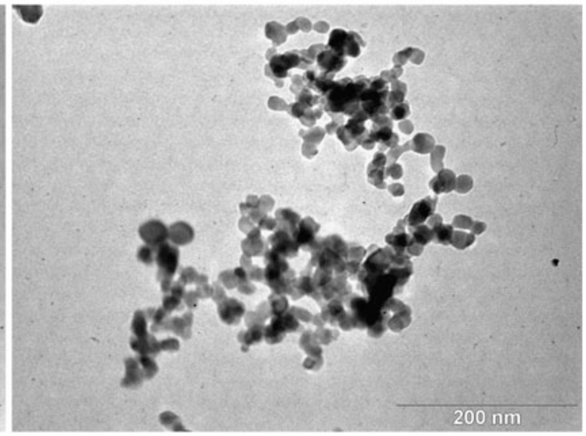

a9_8.tif

Gold-doped SnO_2 before re-fire

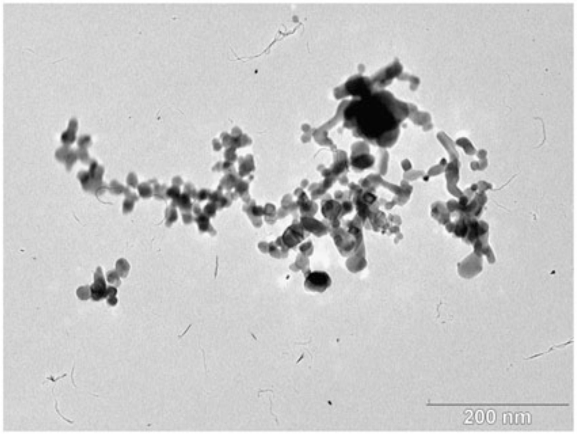

050520-a3-01.tif

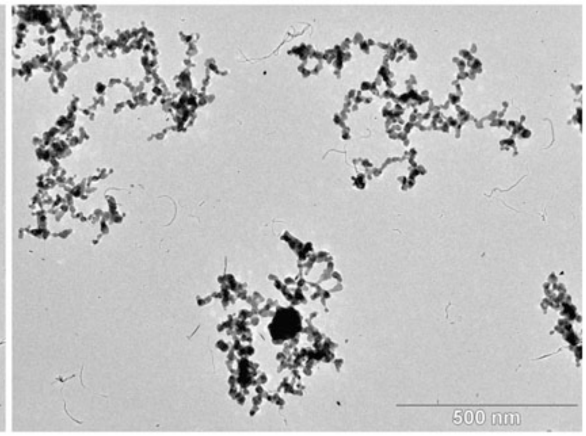

050520-a3-02.tif

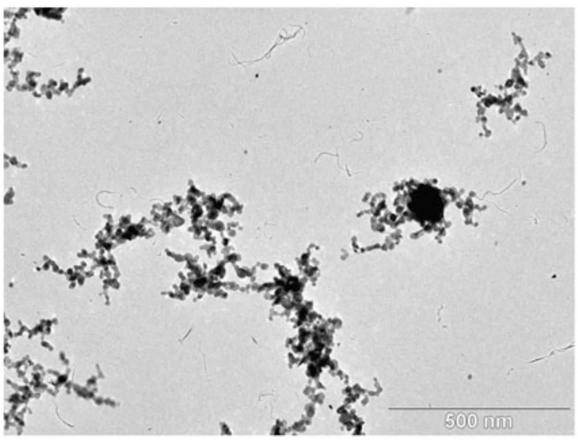

050520-a3-03.tif

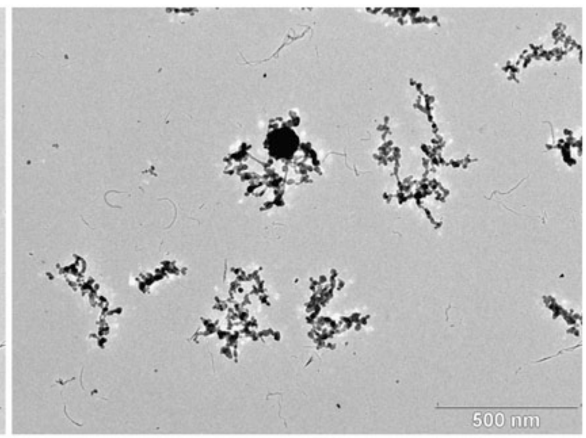

050520-a3-04.tif

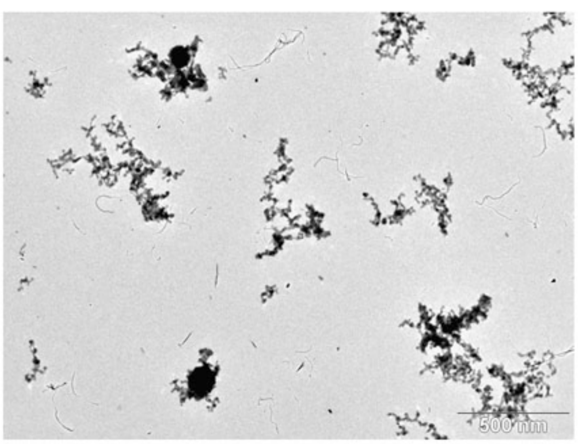

050520-a3-05.tif

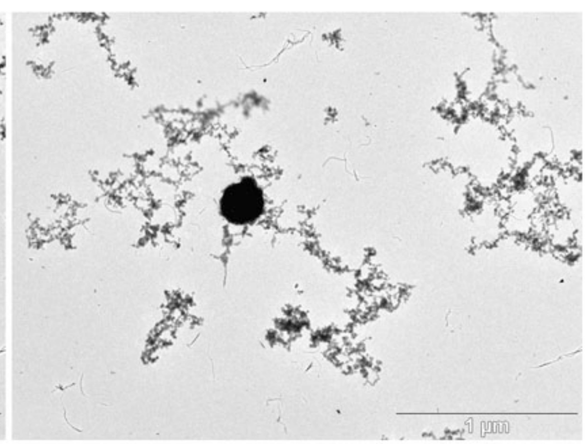

050520-a3-06.tif

Gold-doped SnO_2 before re-fire

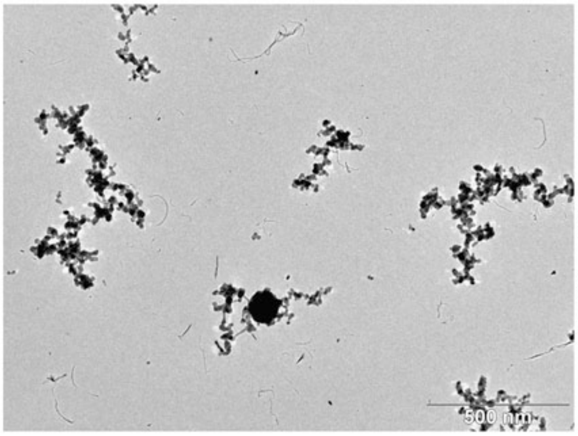

050520-a3-07.tif

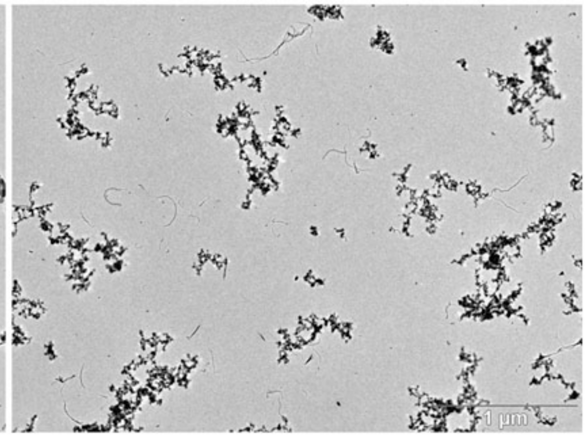

050520-a3-08.tif

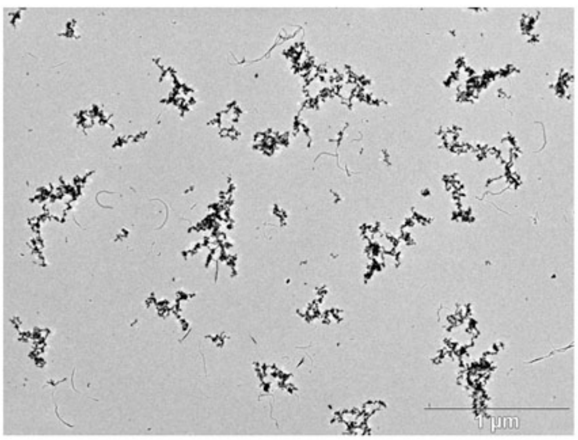

050520-a3-09.tif

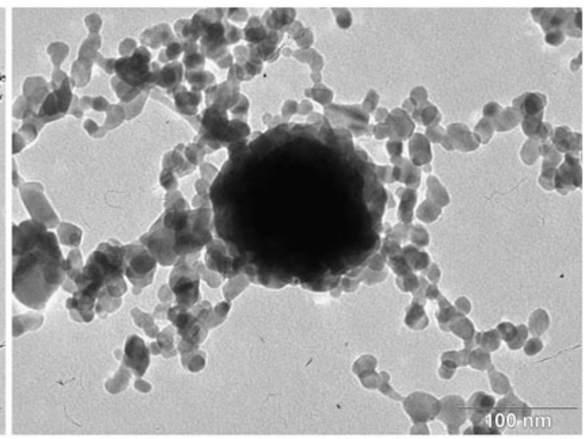

050520-a3-10.tif

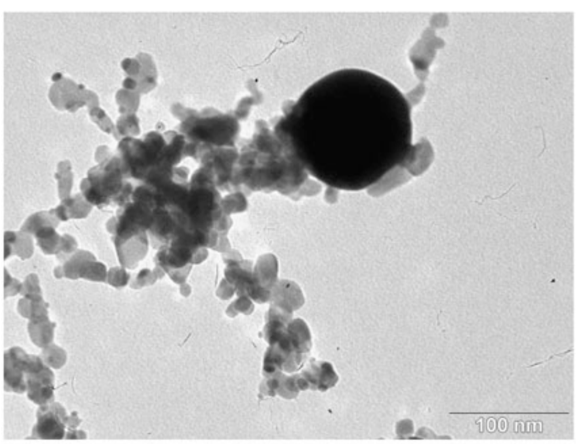

050520-a3-11.tif

Gold-doped SnO_2 before re-fire

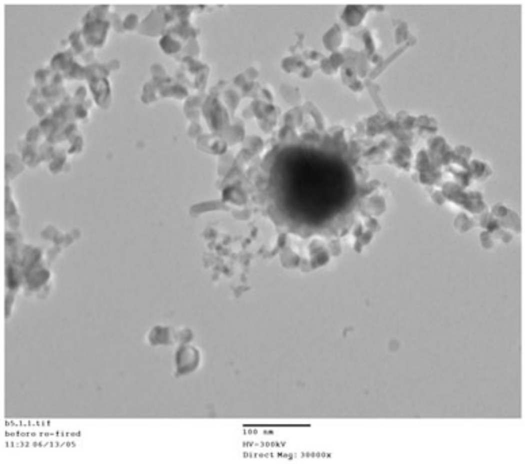

b5_1_1.tif

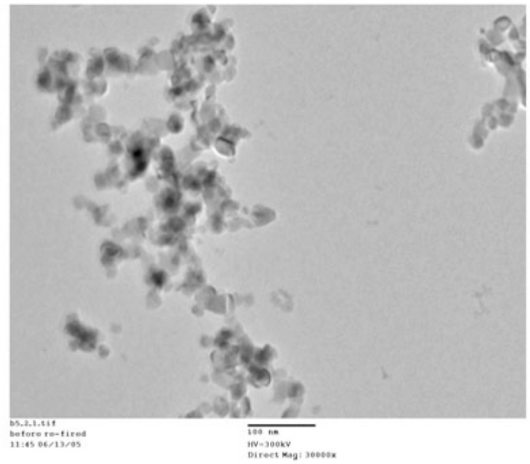

b5_2_1.tif

Gold-doped SnO_2 re-introduced as reactants

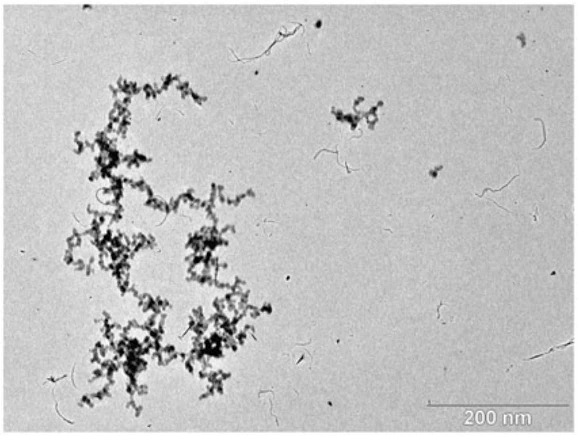

050520-a5-01.tif

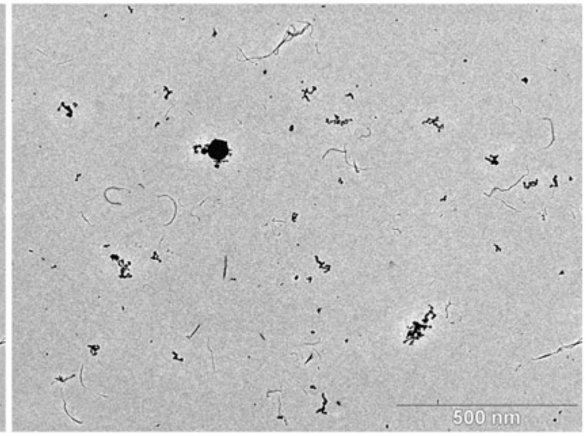

050520-a5-02.tif

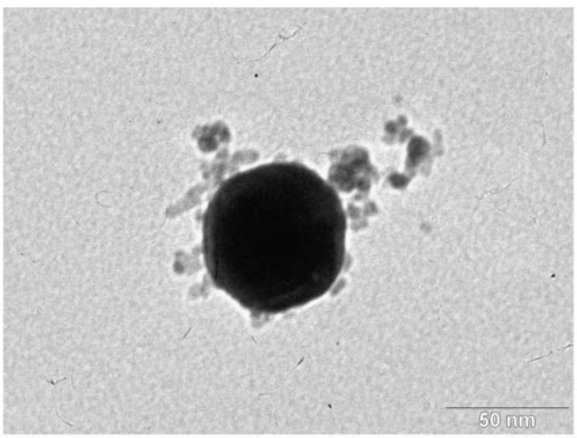

050520-a5-03.tif

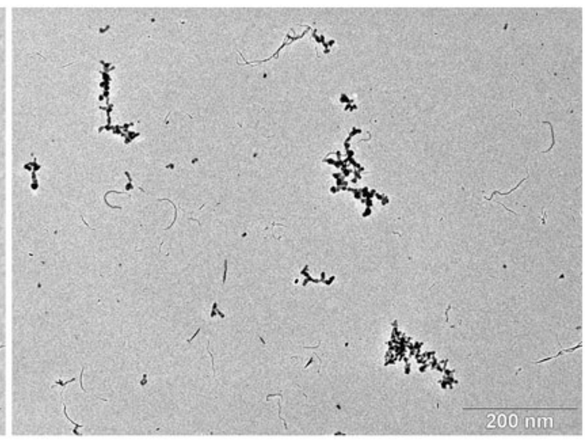

050520-a5-04.tif

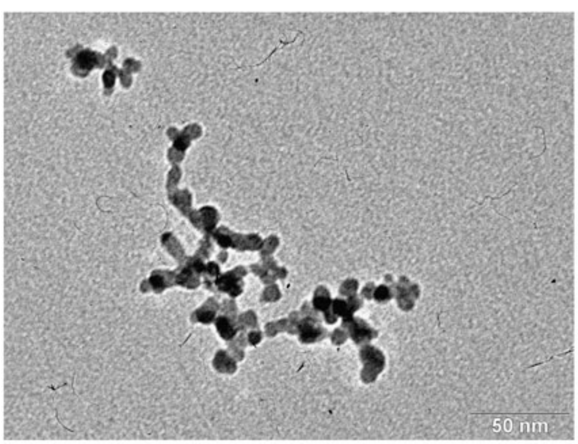

050520-a5-05.tif

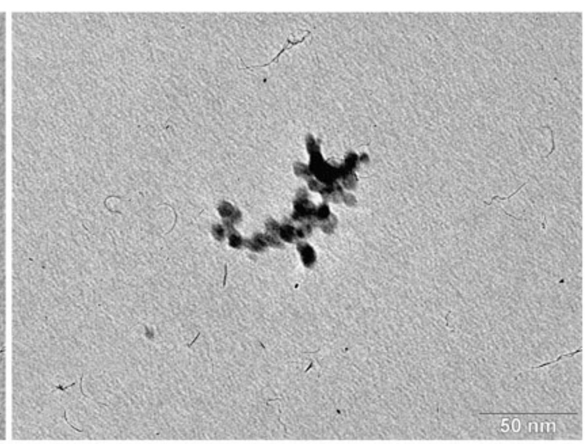

050520-a5-06.tif

Gold-doped SnO_2 re-introduced as reactants

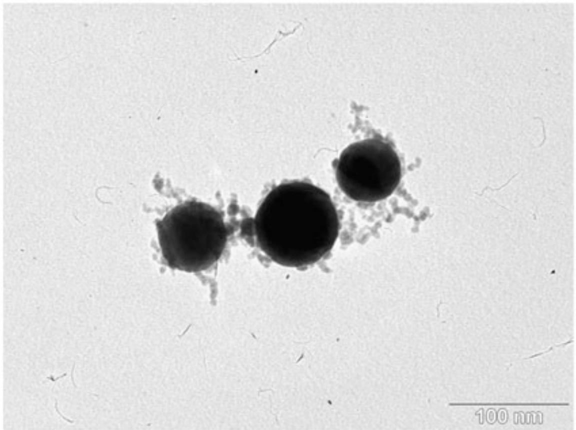

050520-a5-07.tif

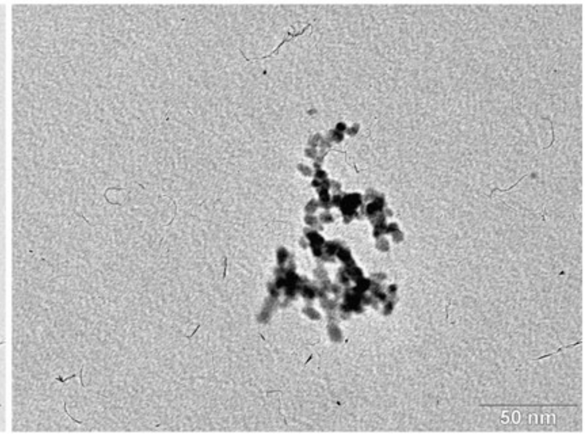

050520-a5-08.tif

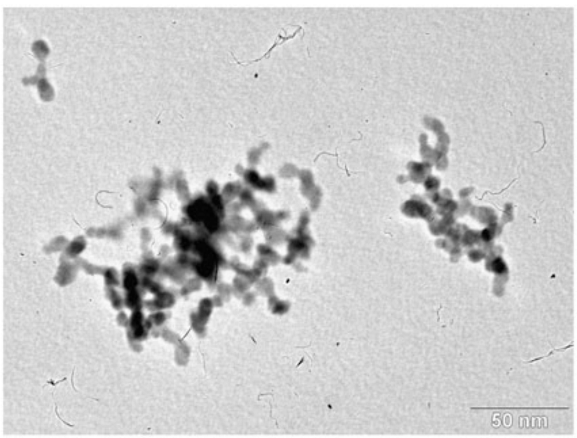

050520-a5-09.tif

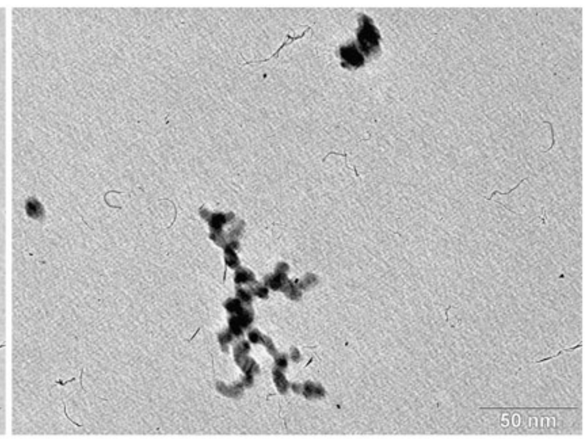

050520-a5-10.tif

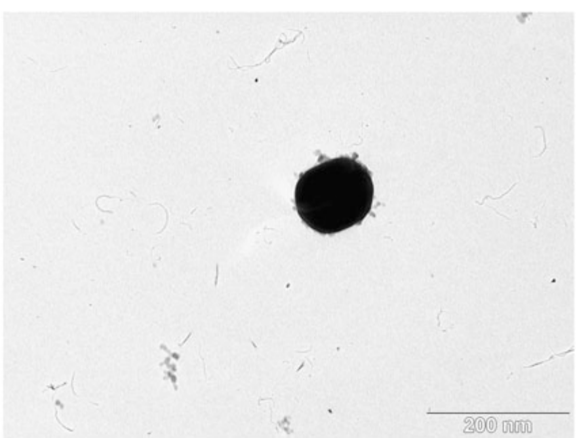

050520-a5-11.tif

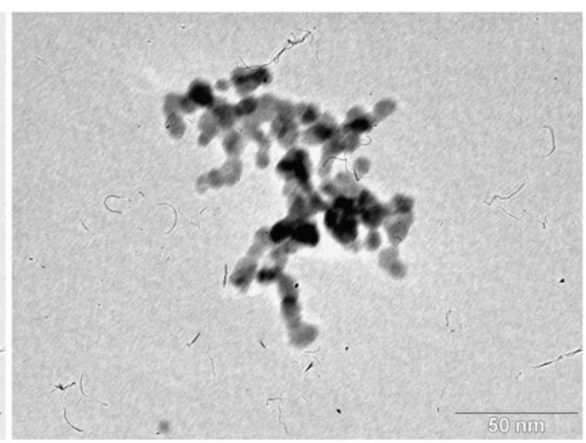

050520-a5-12.tif

Gold-doped SnO_2 re-introduced as reactants

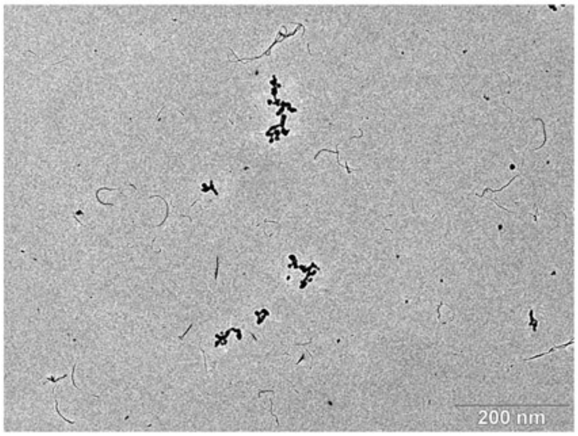

050520-a5-13.tif

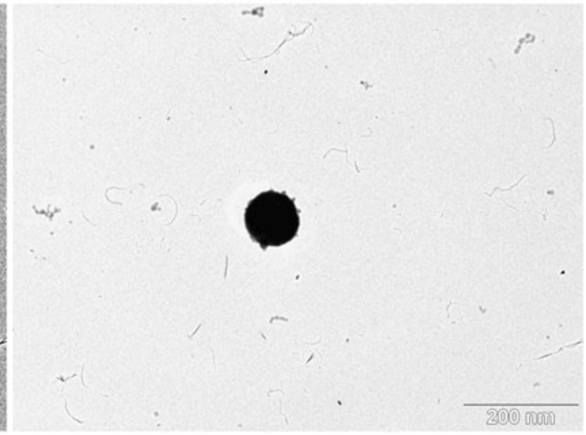

050520-a5-14.tif

Gold-doped SnO_2 re-introduced as reactants

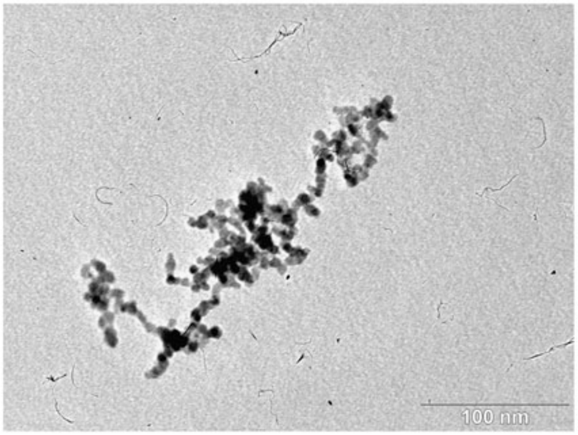

050520-a6-01.tif

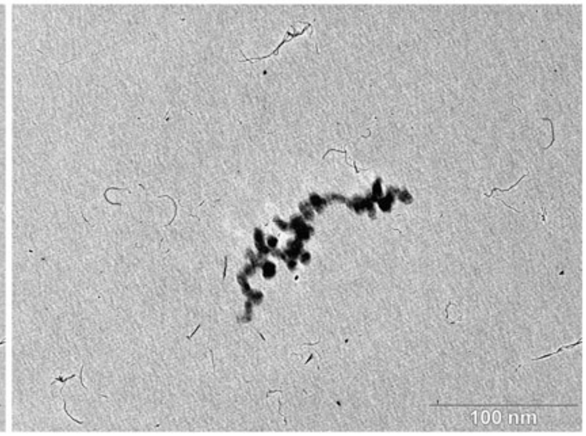

050520-a6-02.tif

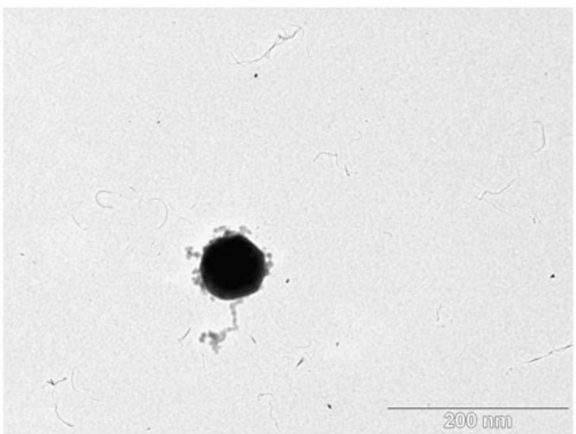

050520-a6-03.tif

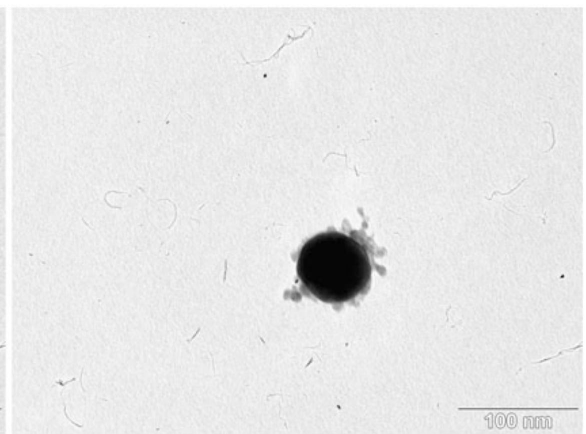

050520-a6-04.tif

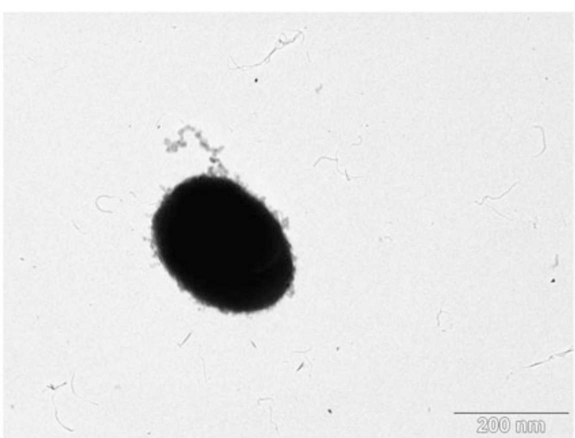

050520-a6-05.tif

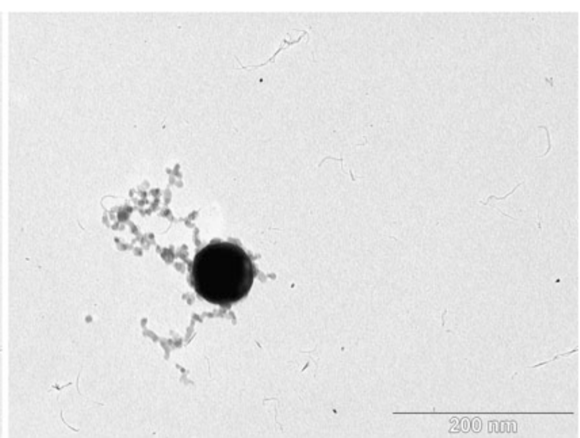

050520-a6-06.tif

Gold-doped SnO_2 re-introduced as reactants

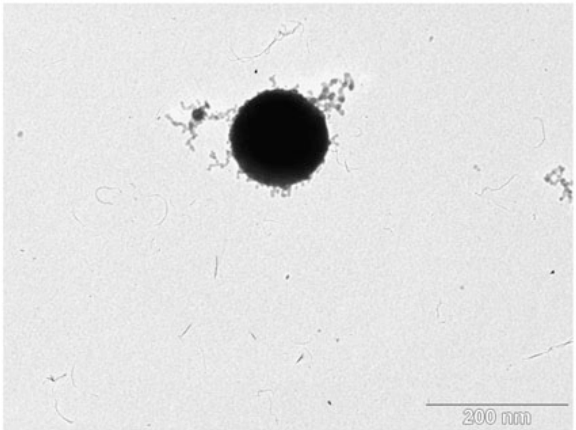

050520-a6-07.tif

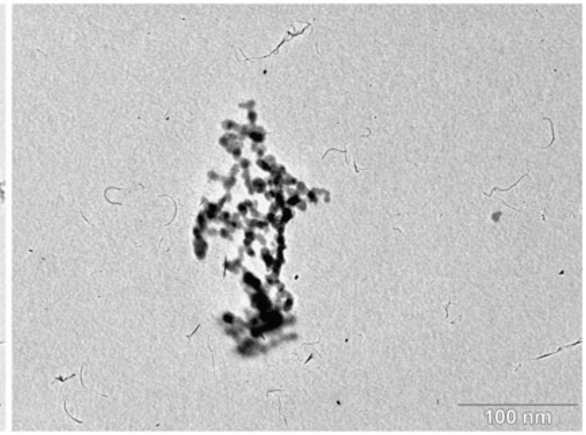

050520-a6-08.tif

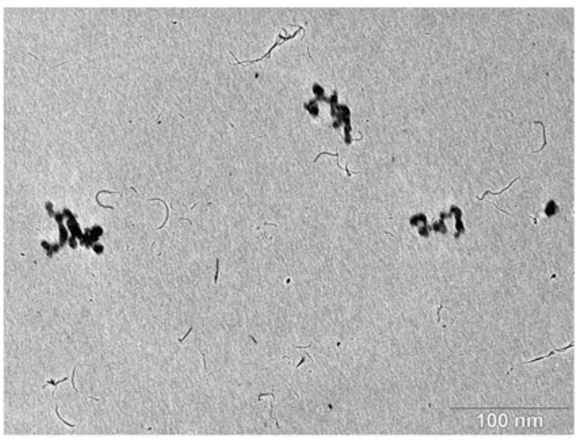

050520-a6-09.tif

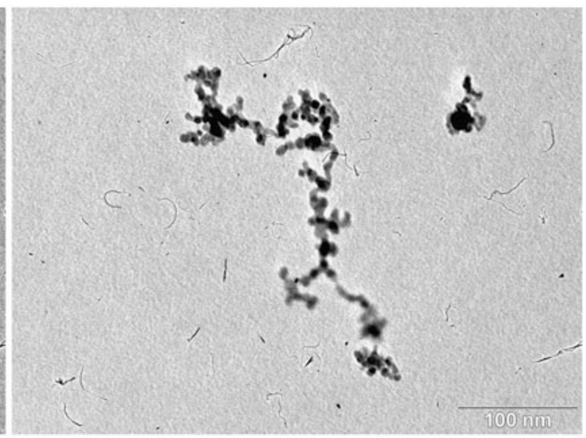

050520-a6-10.tif

Gold-doped SnO_2 re-introduced as reactants

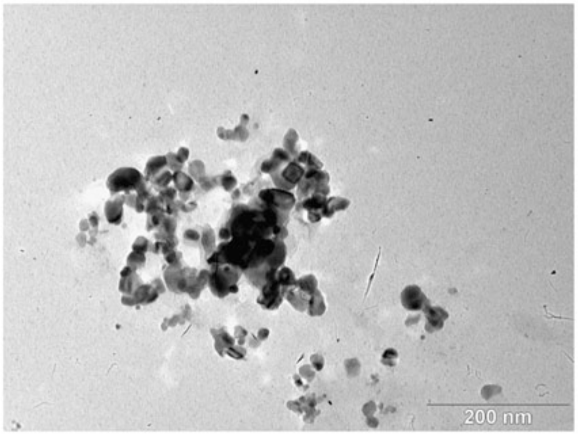

050520-b7-1.tif

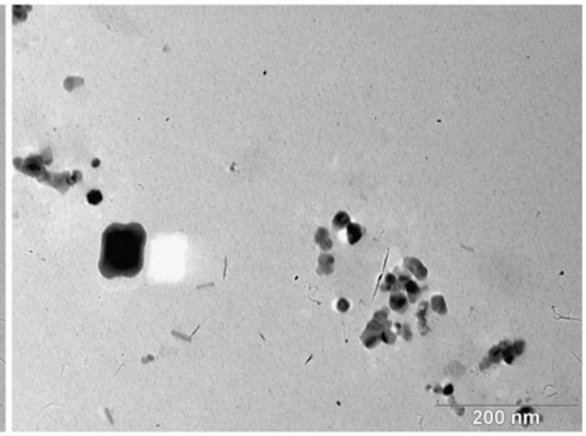

050520-b7-2.tif

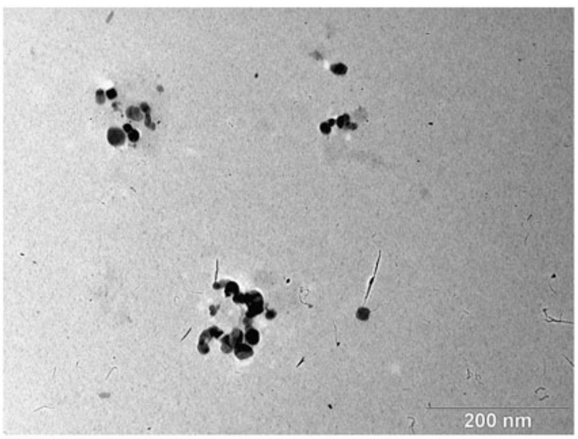

050520-b7-3.tif

SnO_2 height study - sampled at 0.5 cm

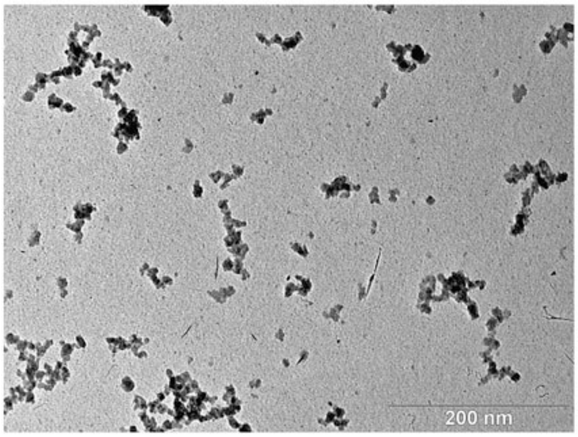

050520-b10-01.tif

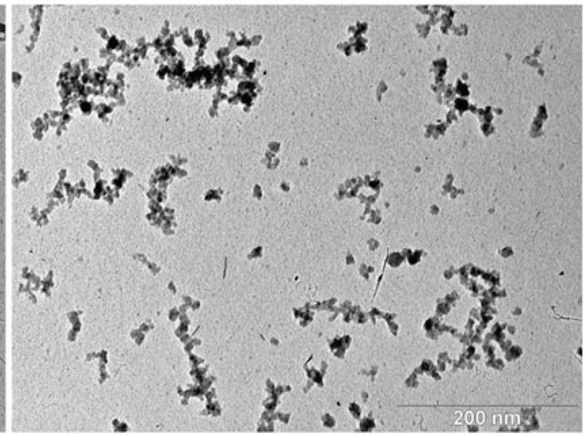

050520-b10-02.tif

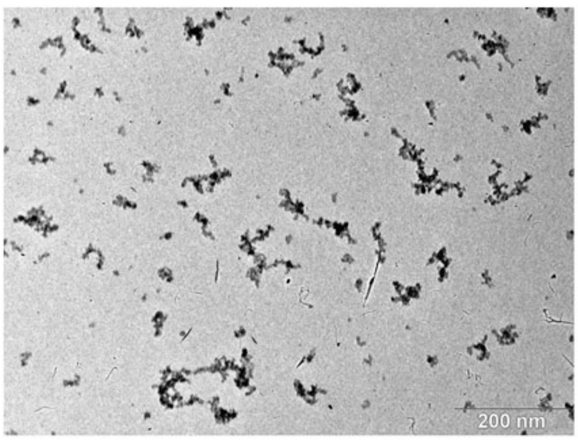

050520-b10-03.tif

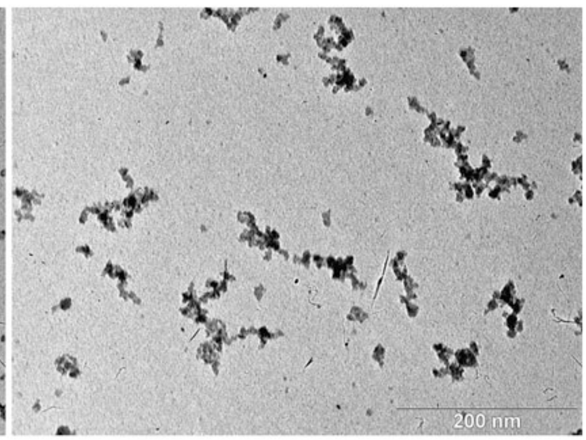

050520-b10-04.tif

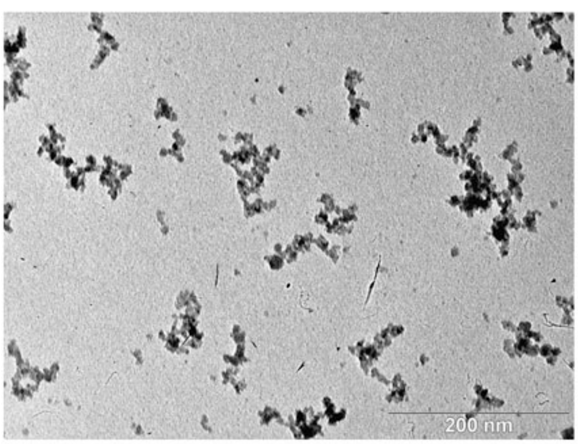

050520-b10-05.tif

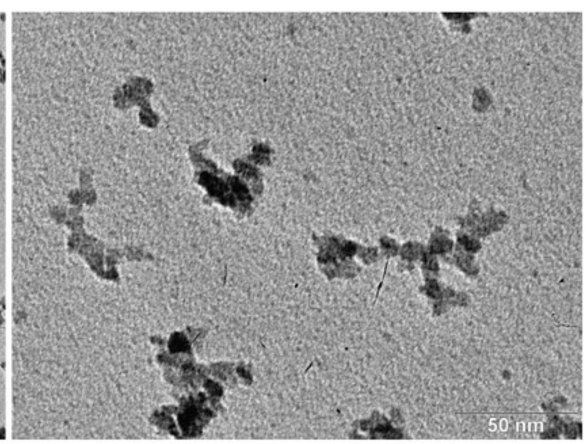

050520-b10-06.tif

SnO_2 height study - sampled at 0.5 cm

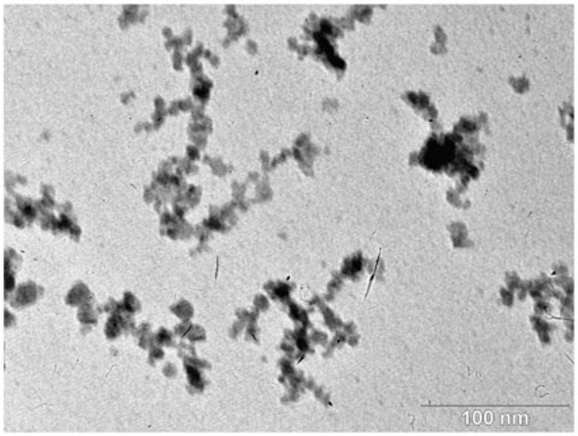

050520-b10-07.tif

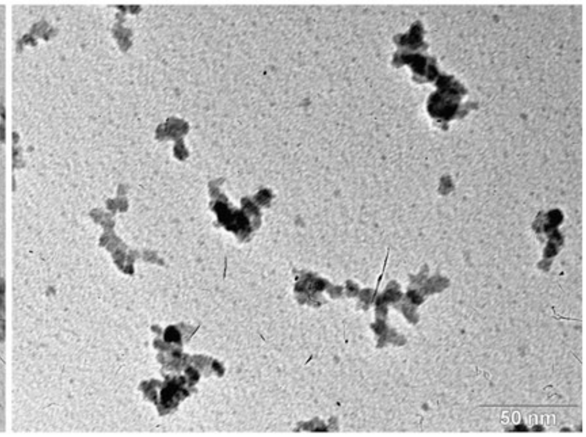

050520-b10-08.tif

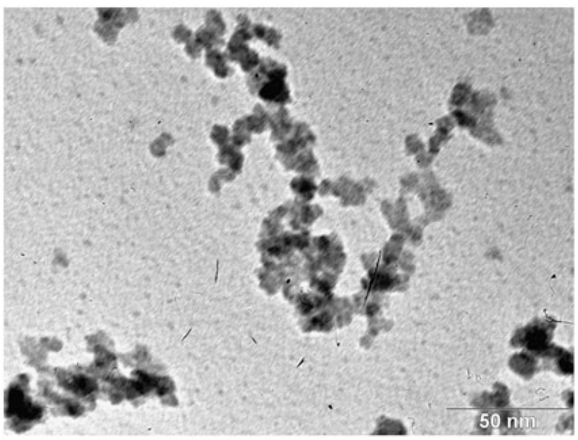

050520-b10-09.tif

SnO_2 height study - sampled at 1.0 cm

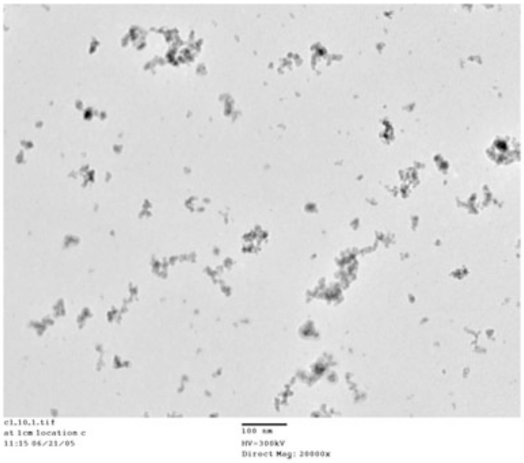

c1_10_1.tif

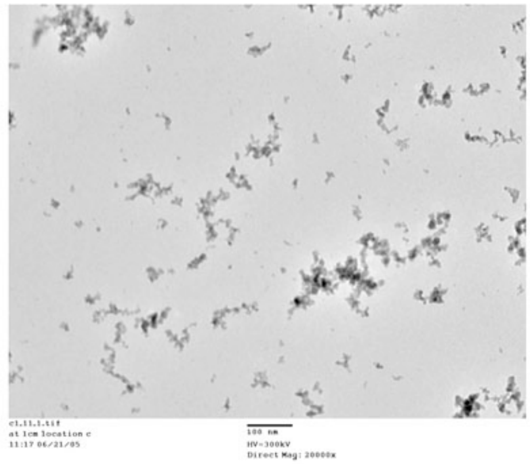

c1_11_1.tif

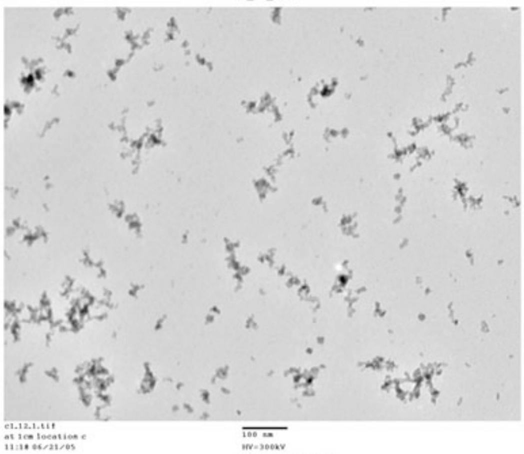

c1_12_1.tif

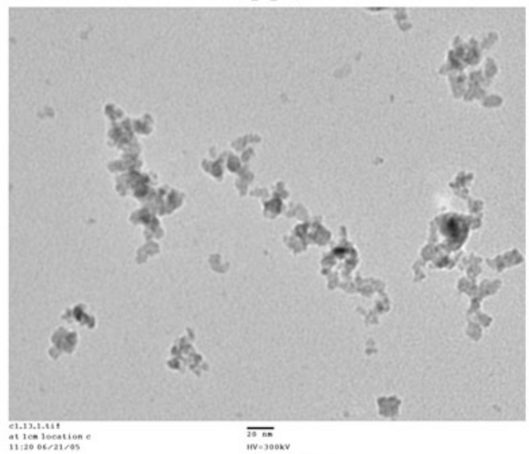

c1_13_1.tif

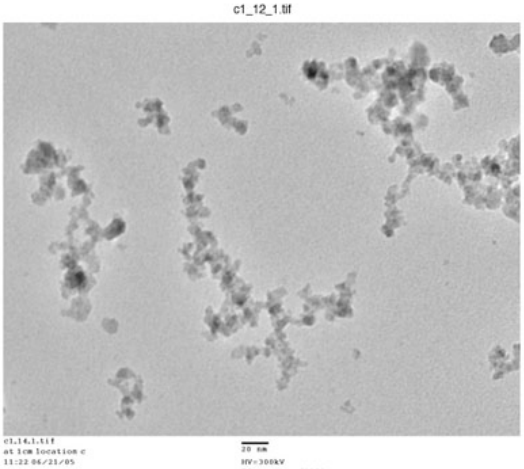

c1_14_1.tif

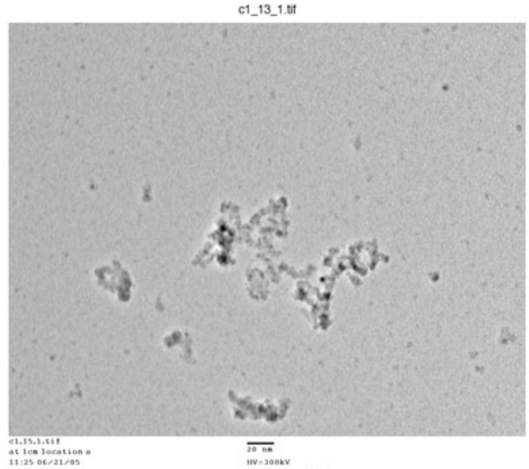

c1_15_1.tif

SnO_2 height study - sampled at 1.0 cm

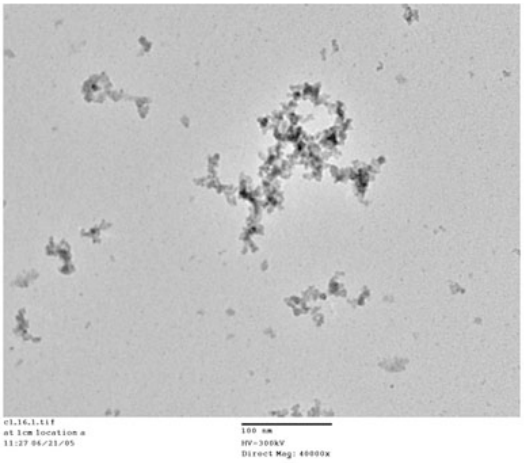

c1_16_1.tif

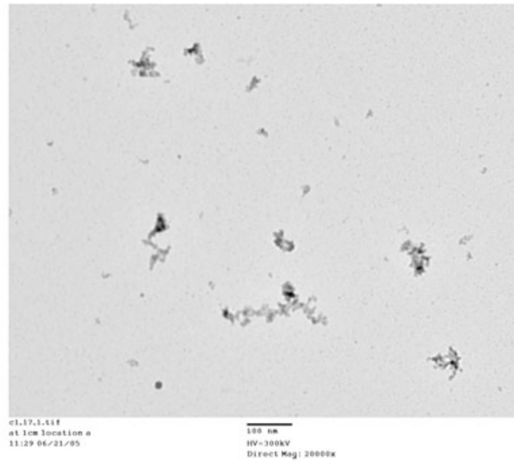

c1_17_1.tif

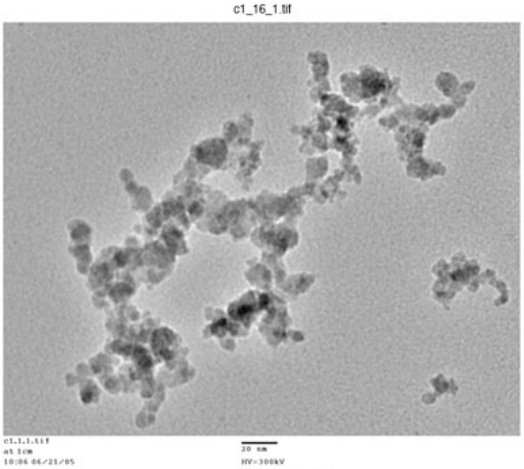

c1_1_1.tif

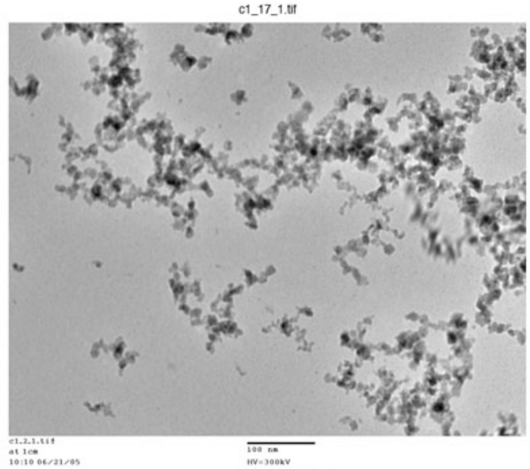

c1_2_1.tif

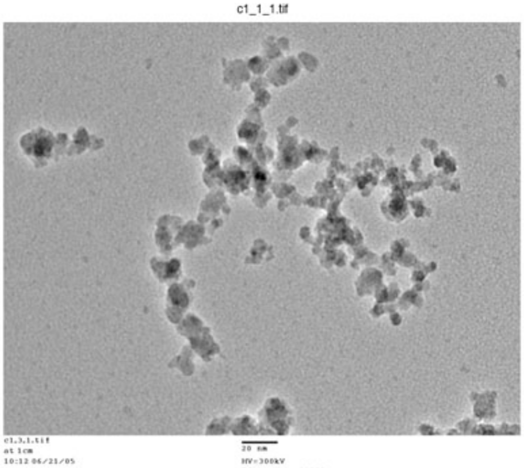

c1_3_1.tif

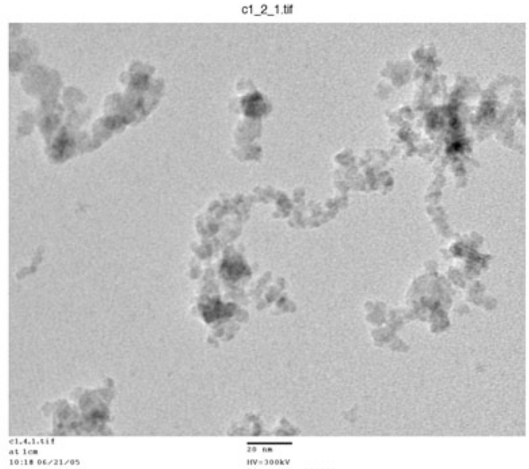

c1_4_1.tif

SnO_2 height study - sampled at 1.0 cm

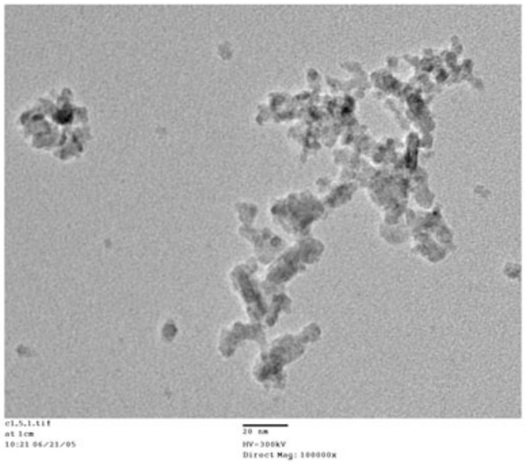

c1_5_1.tif

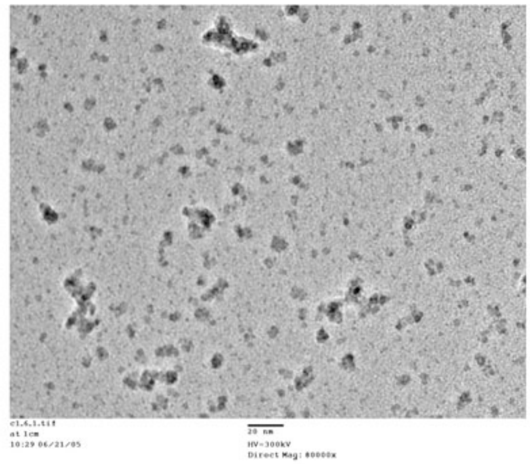

c1_6_1.tif

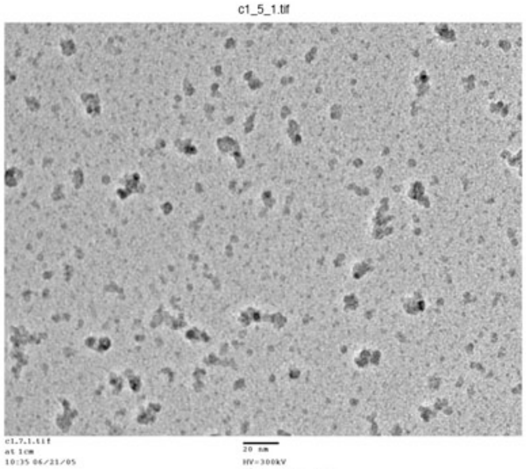

c1_7_1.tif

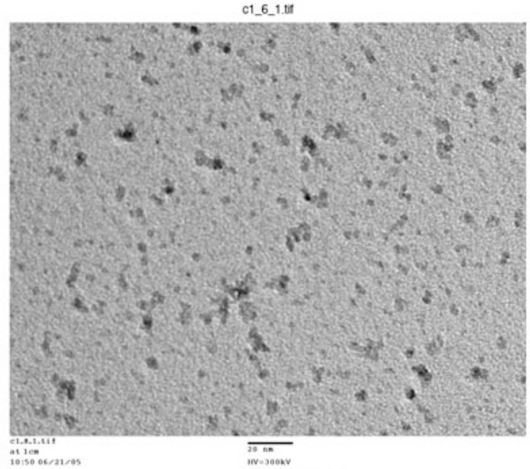

c1_8_1.tif

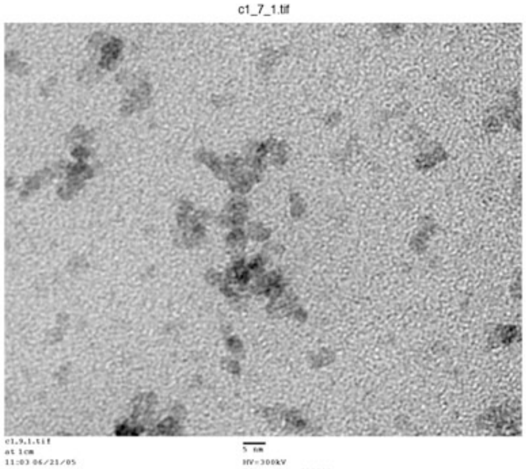

c1_9_1.tif

SnO_2 height study - sampled at 2.0 cm

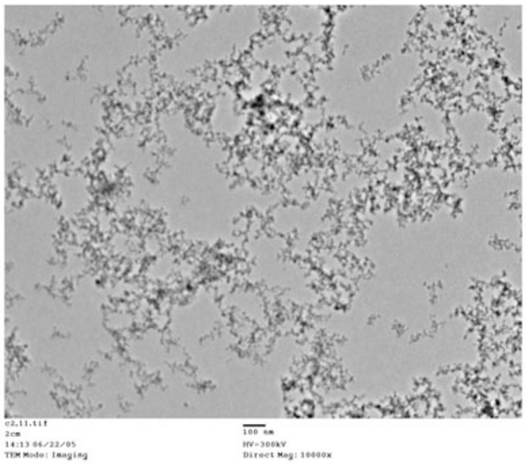

c2_11.tif

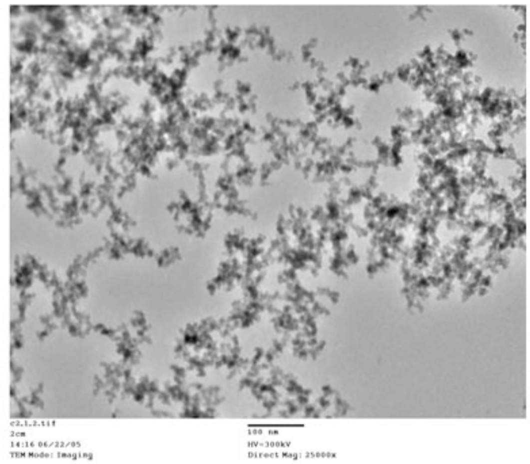

c2_1_2.tif

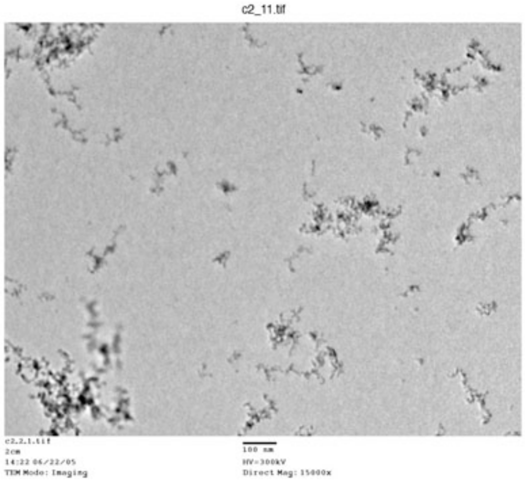

c2_2_1.tif

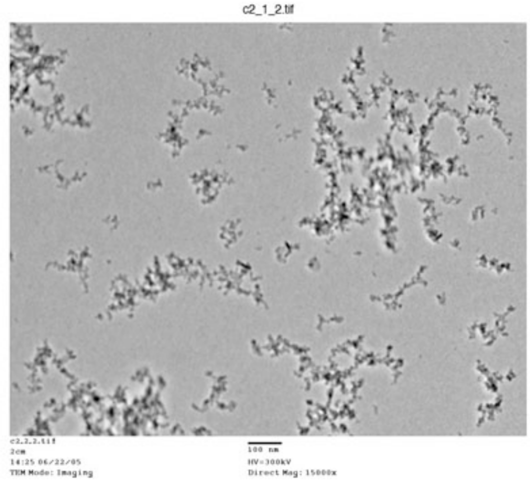

c2_2_2.tif

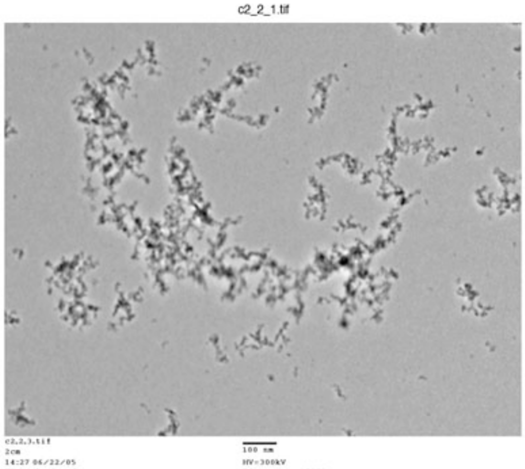

c2_2_3.tif

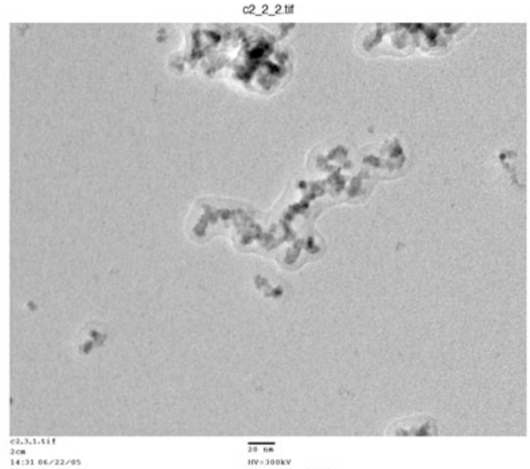

c2_3_1.tif

SnO_2 height study - sampled at 2.0 cm

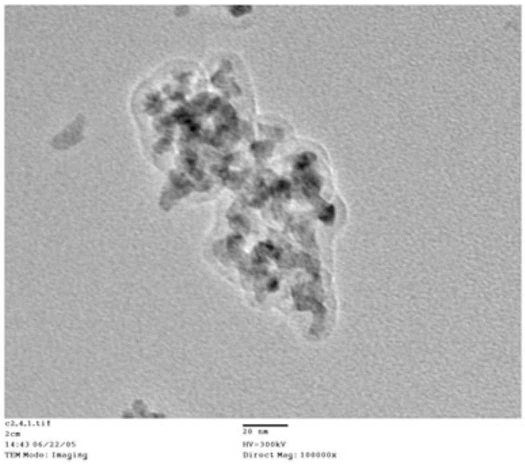

c2_4_1.tif

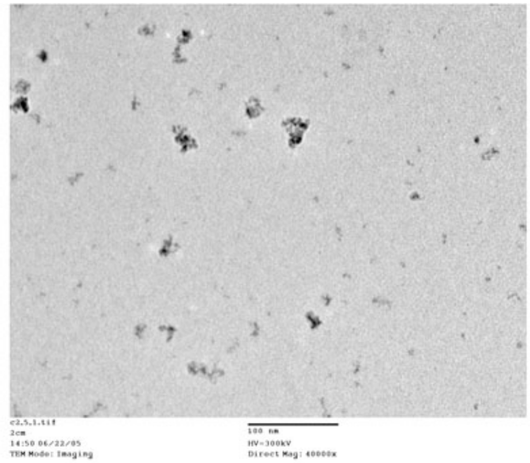

c2_5_1.tif

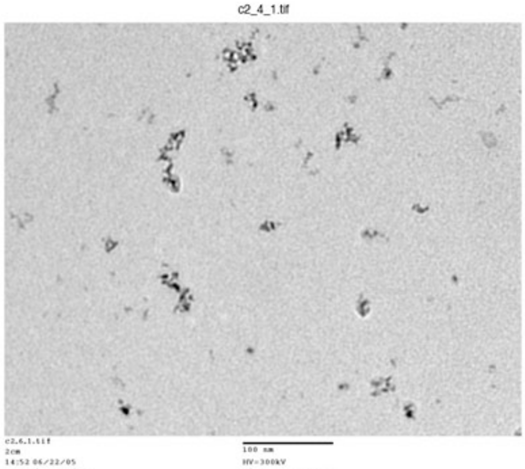

c2_6_1.tif

c2_7_1.tif

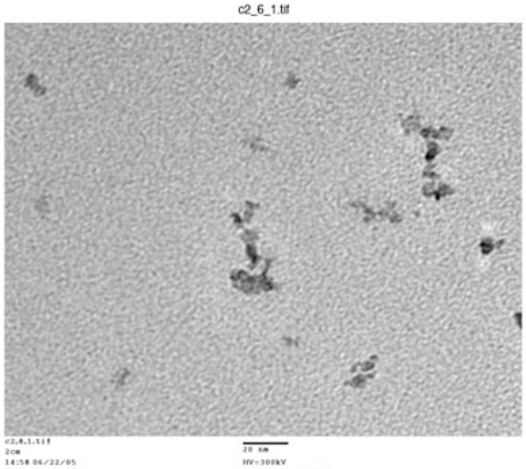

c2_8_1.tif

SnO_2 height study - sampled at 5.0 cm

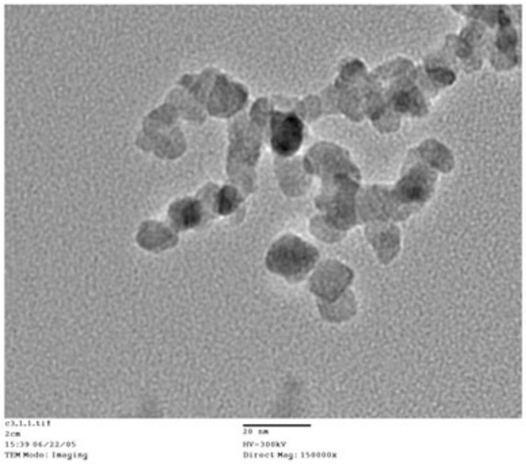

c3_1_1.tif

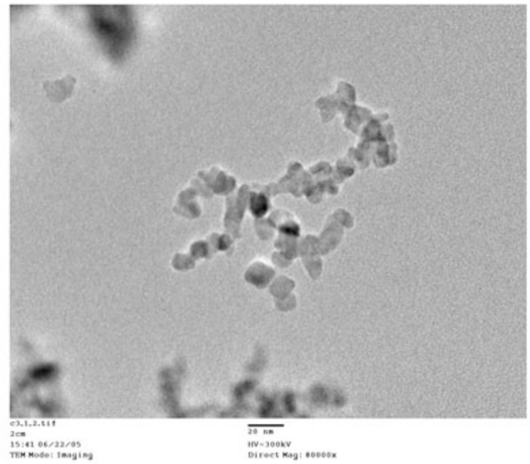

c3_1_2.tif

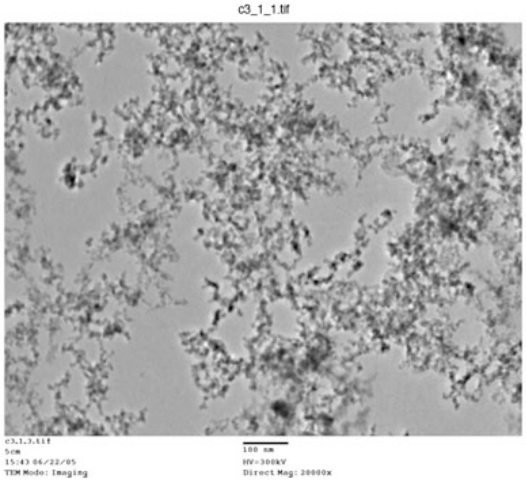

c3_1_3.tif

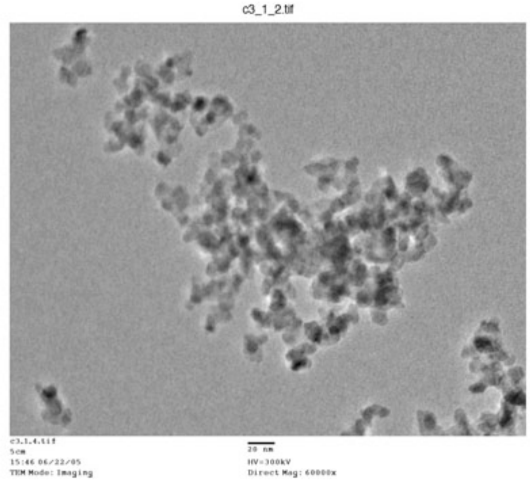

c3_1_4.tif

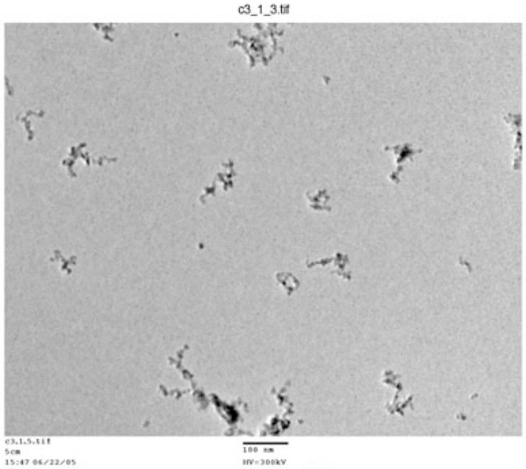

c3_1_5.tif

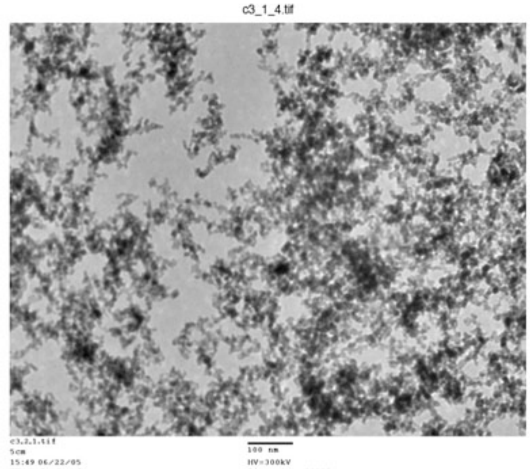

c3_2_1.tif

SnO_2 height study - sampled at 5.0 cm

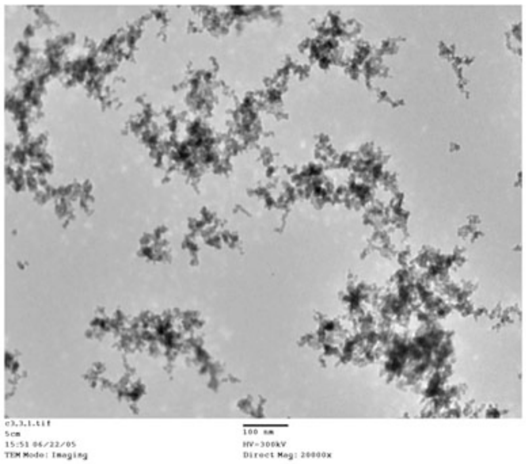

c3_3_1.tif

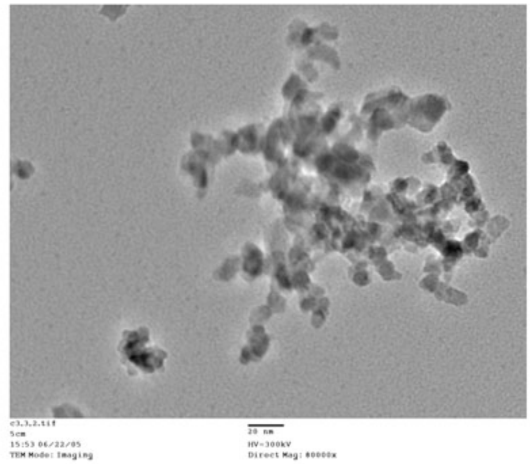

c3_3_2.tif

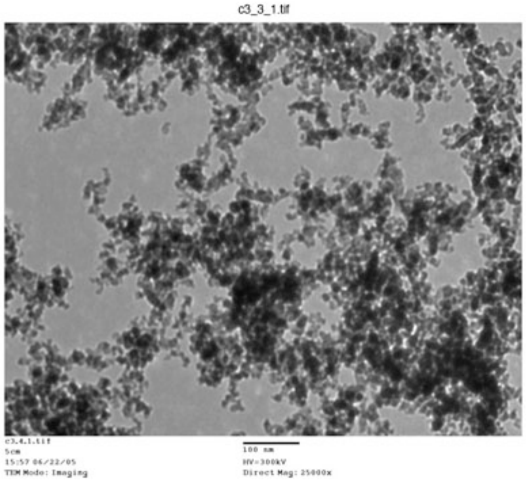

c3_4_1.tif

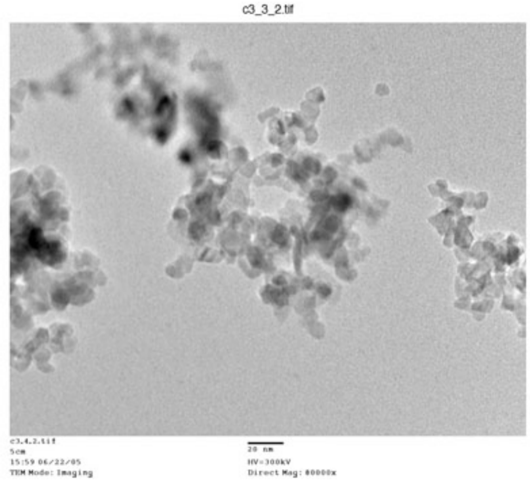

c3_4_2.tif

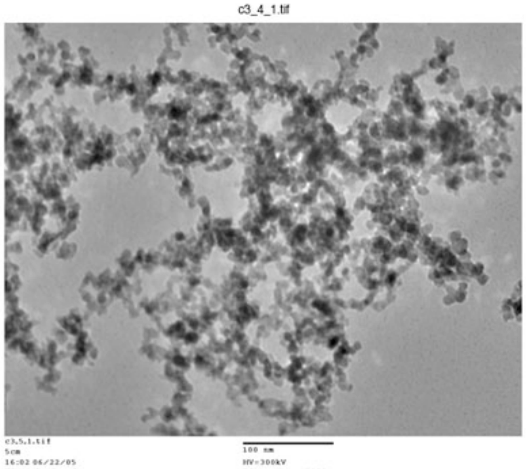

c3_5_1.tif

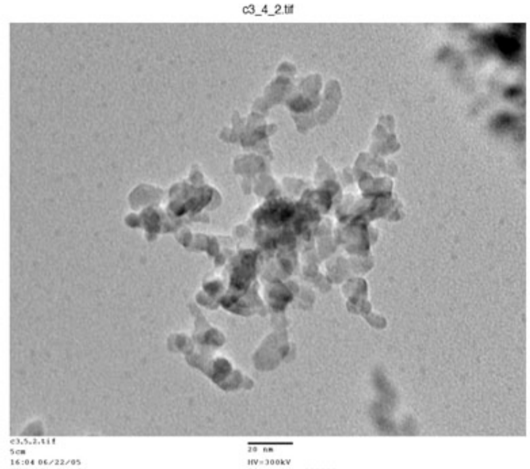

c3_5_2.tif

SnO_2 height study - sampled at 5.0 cm

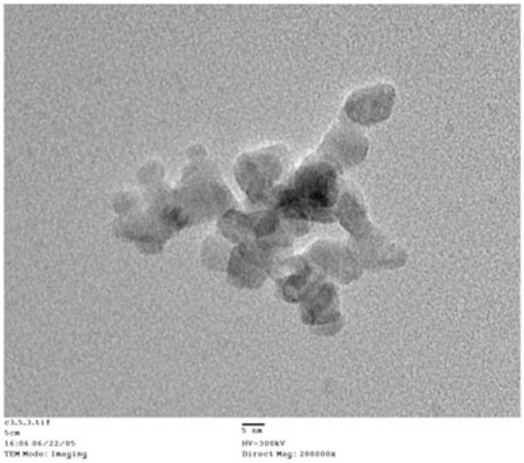

c3_5_3.tif

SnO_2 height study - sampled at 9.0 cm

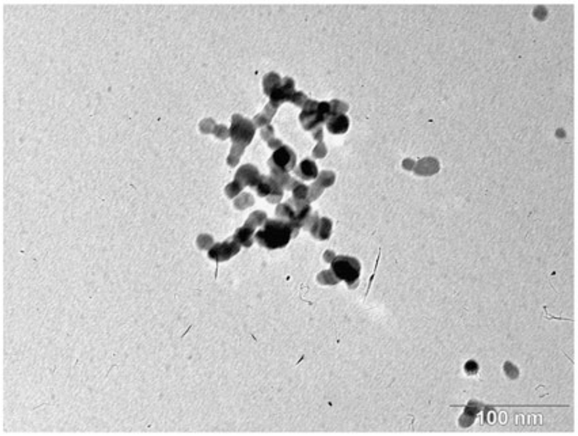

050520-c4-a-01.tif

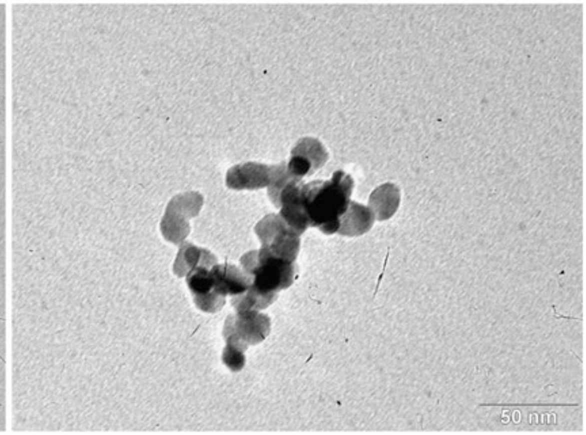

050520-c4-a-02.tif

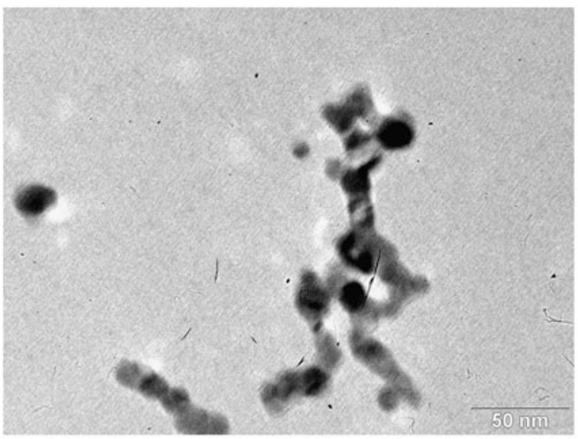

050520-c4-a-03.tif

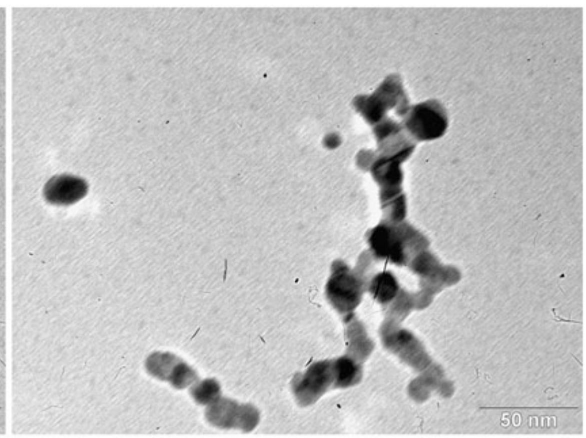

050520-c4-a-04.tif

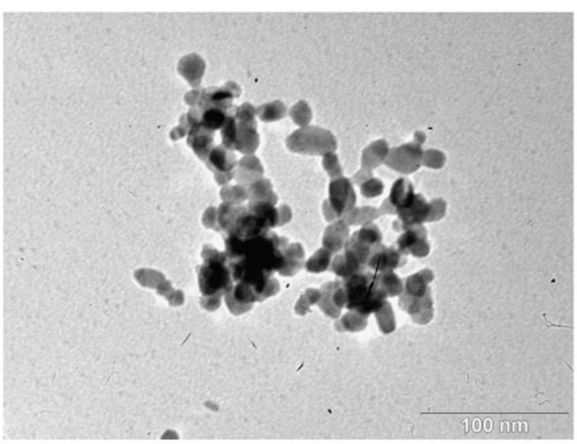

050520-c4-a-05.tif

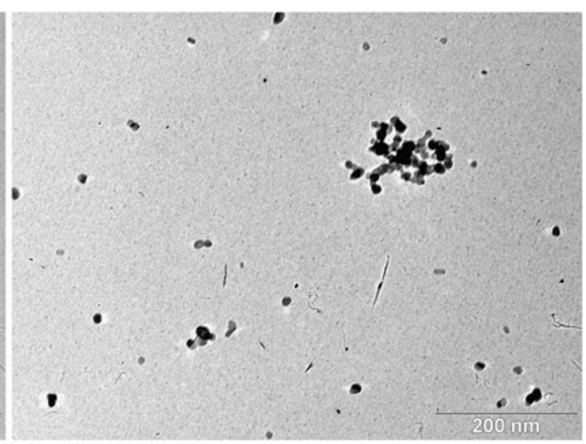

050520-c4-a-06.tif

SnO_2 height study - sampled at 9.0 cm

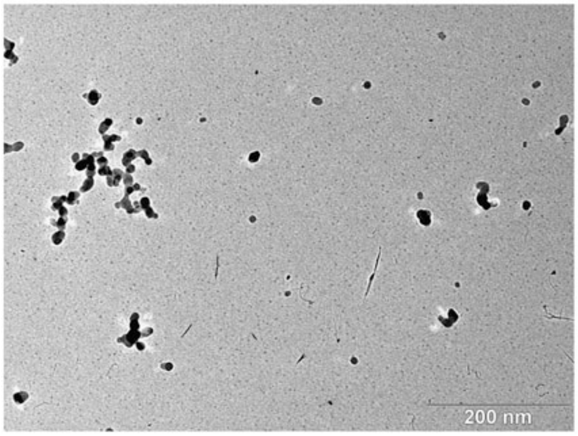

050520-c4-a-07.tif

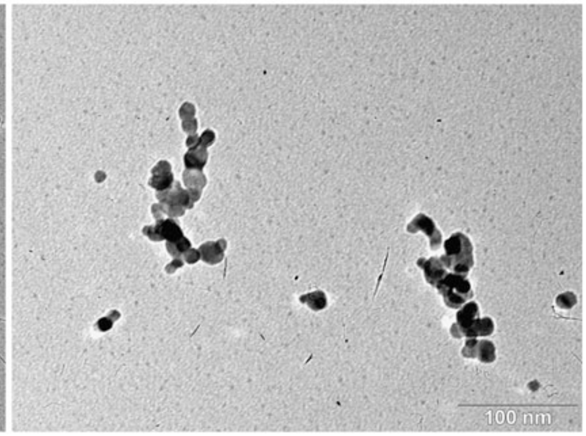

050520-c4-a-08.tif

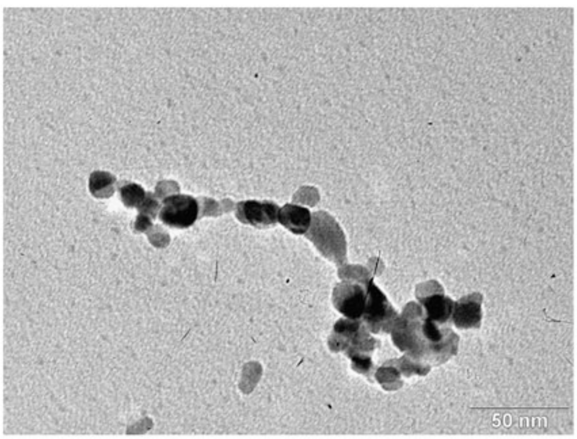

050520-c4-a-09.tif

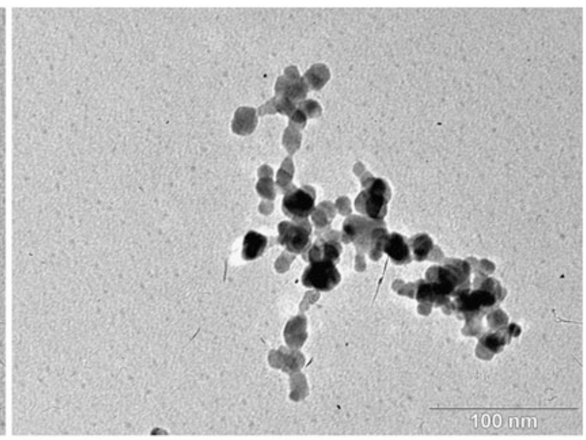

050520-c4-a-10.tif

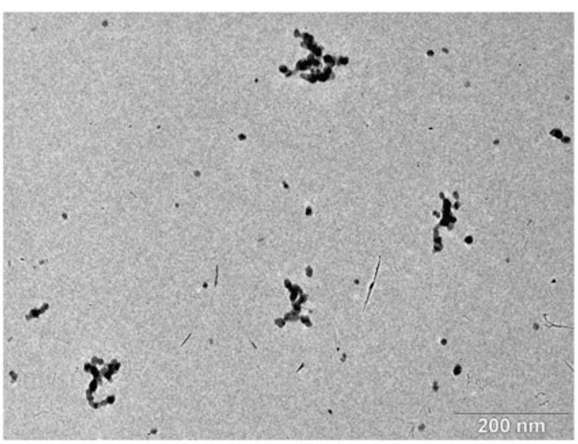

050520-c4-a-11.tif

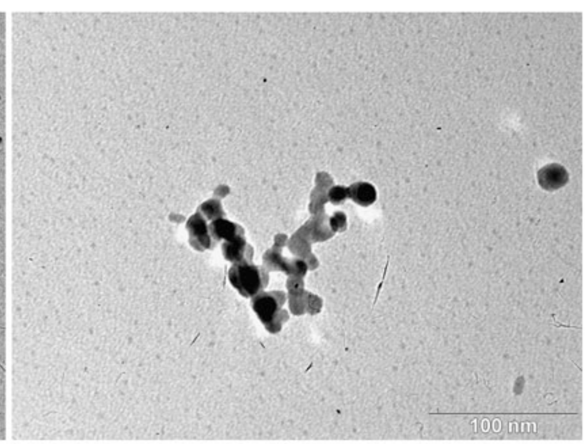

050520-c4-a-12.tif

SnO_2 height study - sampled at 9.0 cm

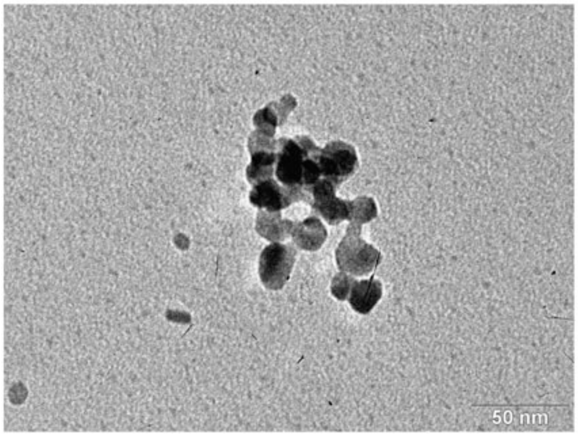

050520-c4-a-13.tif

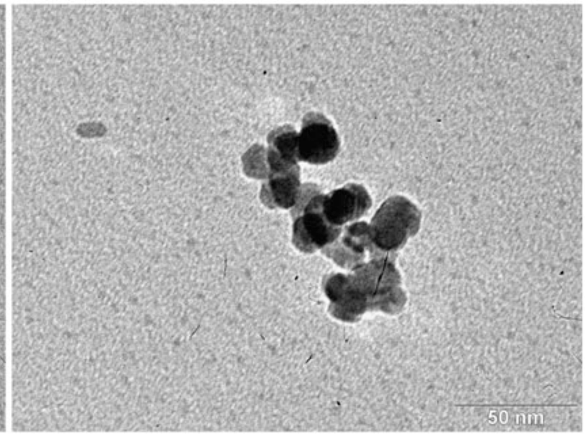

050520-c4-a-14.tif

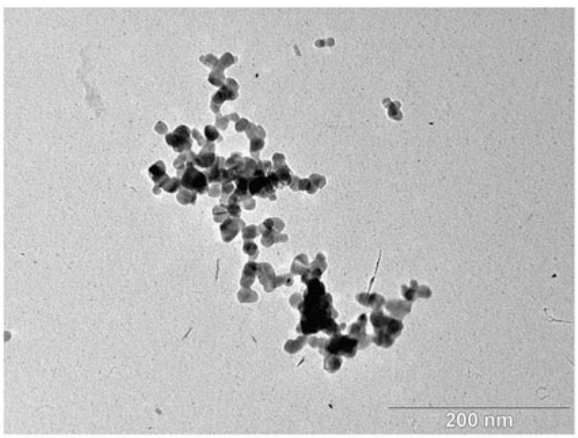

050520-c4-b-01.tif

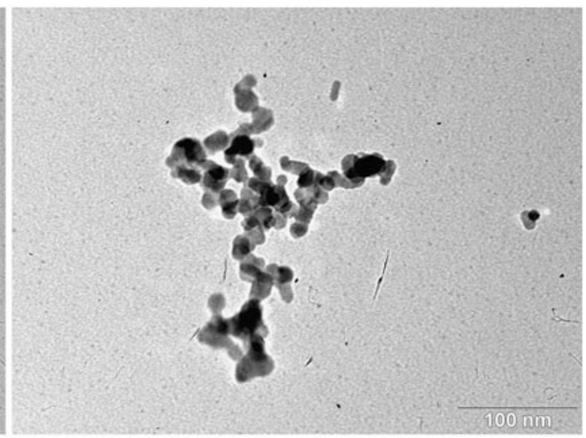

050520-c4-b-02.tif

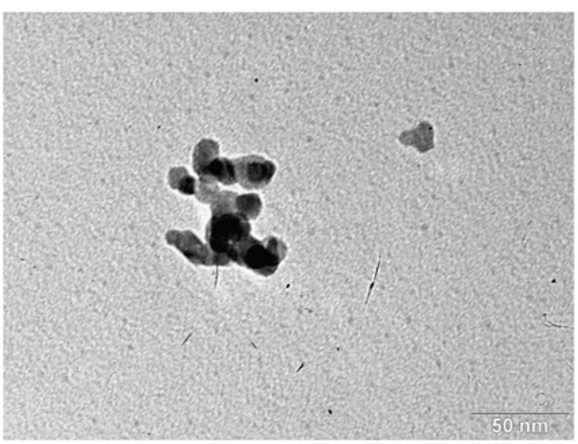

050520-c4-b-03.tif

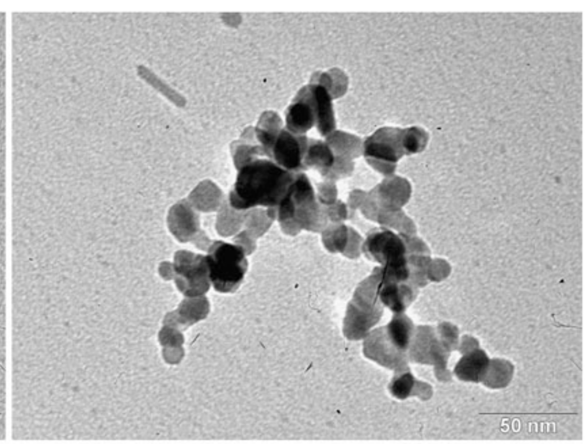

050520-c4-b-04.tif

SnO_2 height study - sampled at 9.0 cm

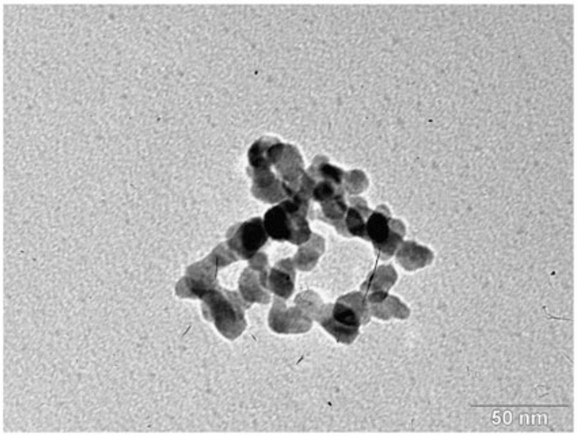

050520-c4-b-05.tif

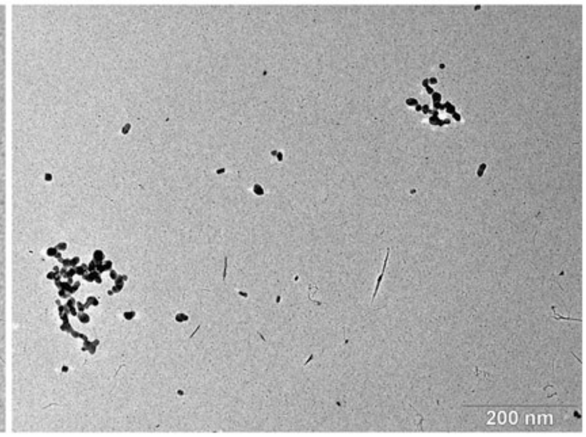

050520-c4-b-06.tif

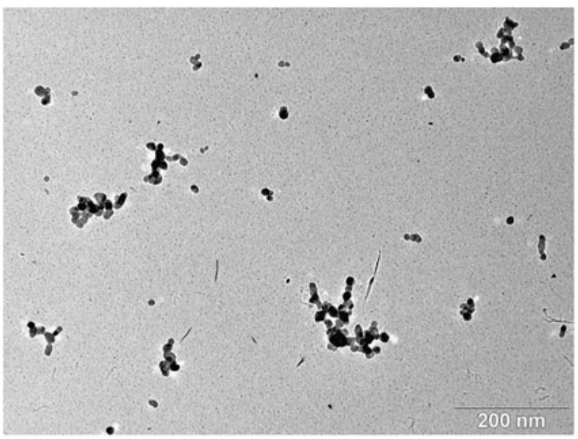

050520-c4-b-07.tif

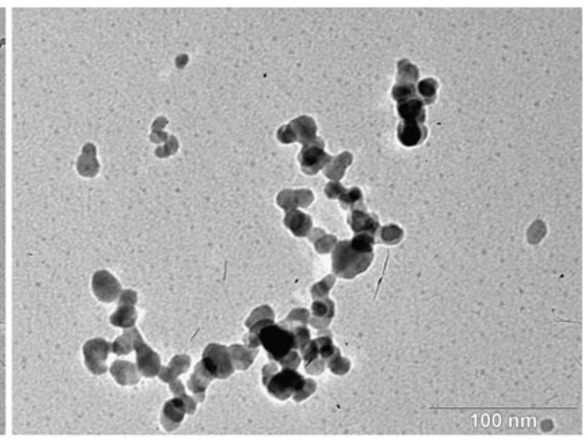

050520-c4-b-08.tif

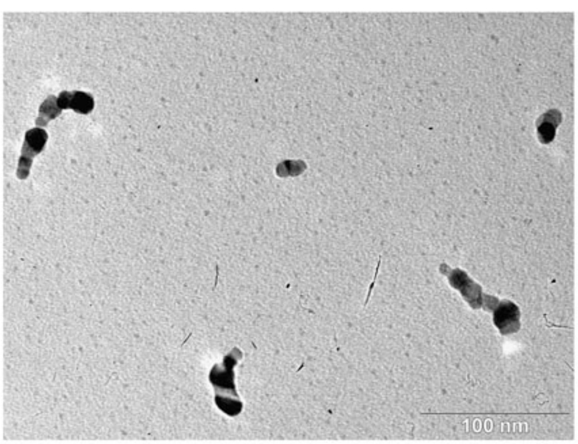

050520-c4-b-09.tif

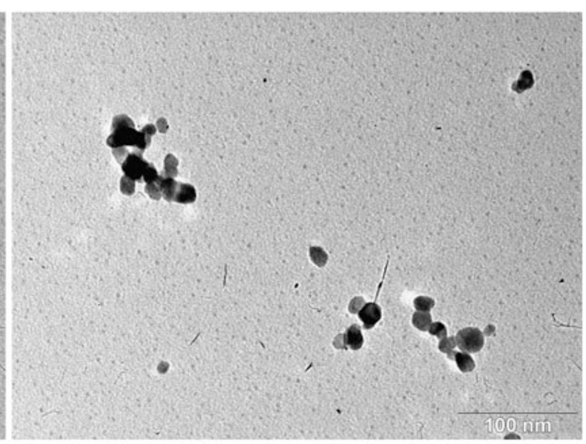

050520-c4-b-10.tif

SnO_2 height study - sampled at 9.0 cm

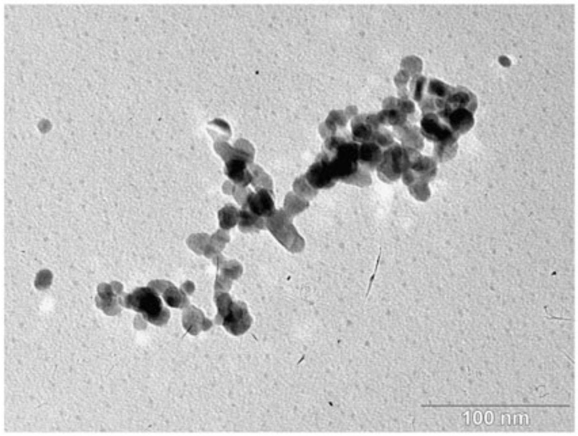

050520-c4-b-11.tif

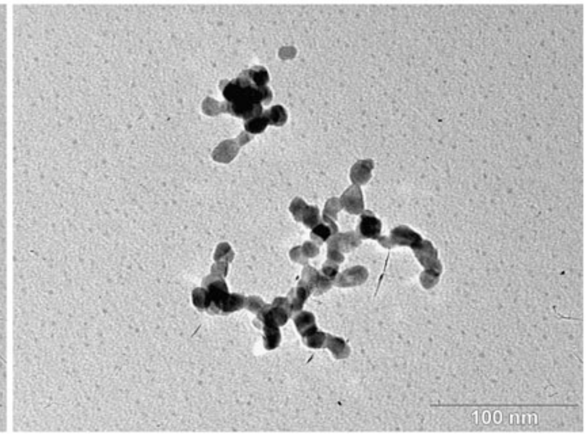

050520-c4-b-12.tif

SnO_2 height study - sampled at 13.0 cm

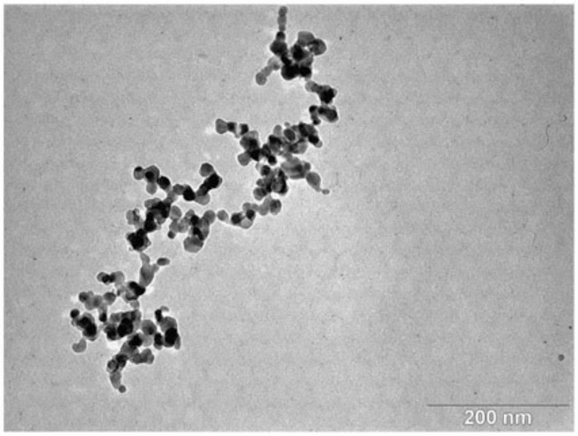

050520-c5-01.tif

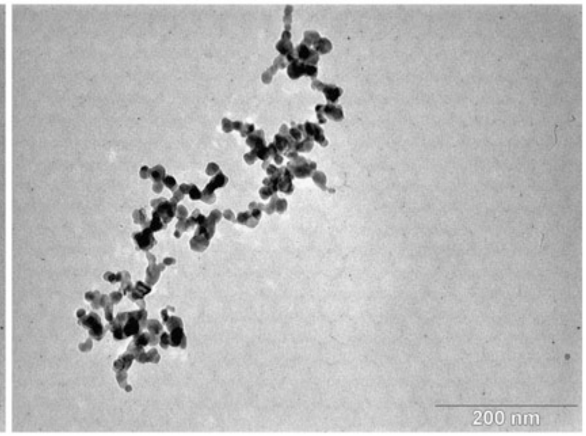

050520-c5-02.tif

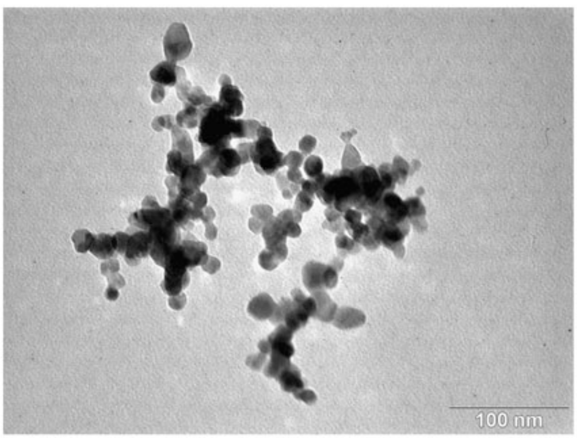

050520-c5-03.tif

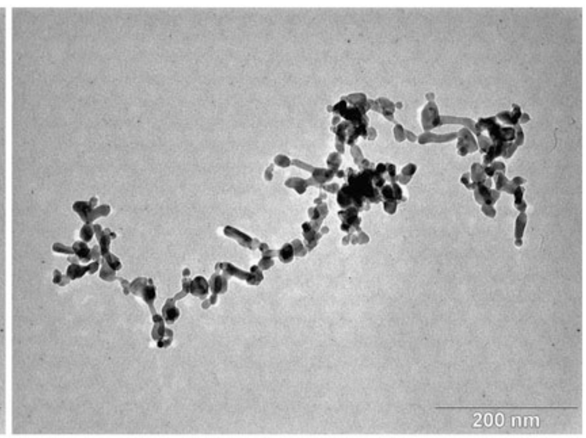

050520-c5-04.tif

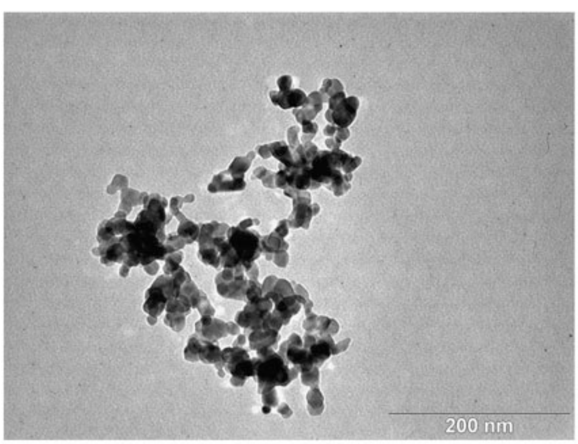

050520-c5-05.tif

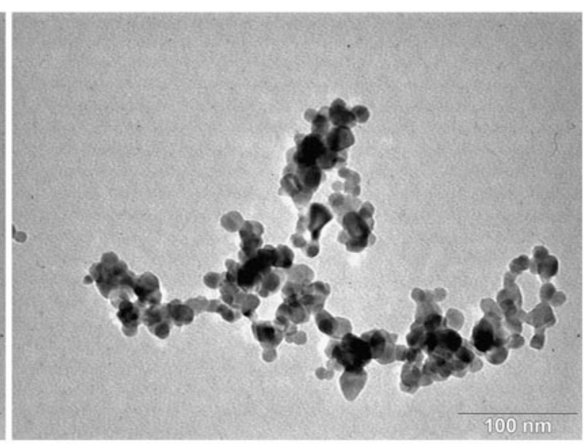

050520-c5-06.tif

SnO_2 height study - sampled at 13.0 cm

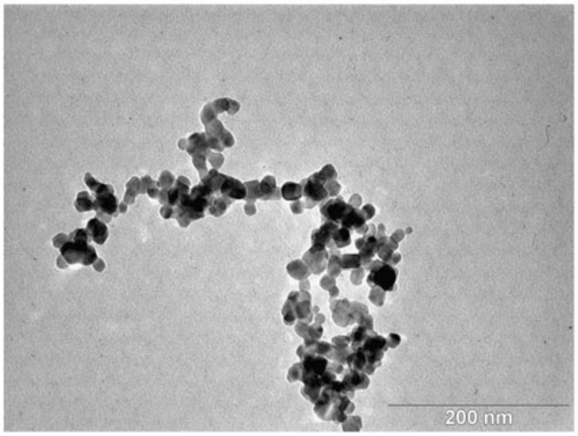

050520-c5-07.tif

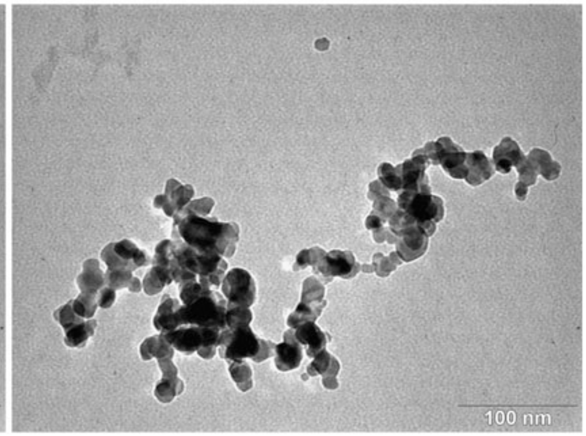

050520-c5-08.tif

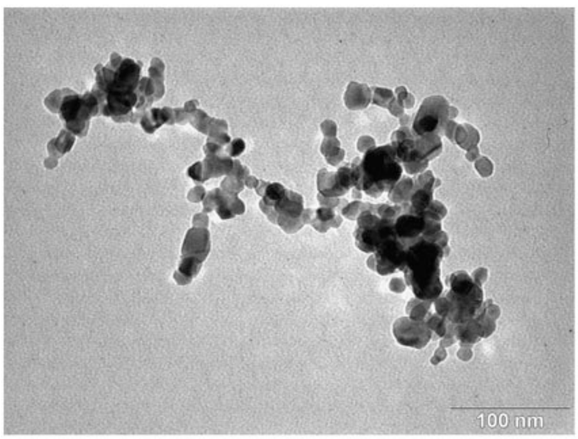

050520-c5-09.tif

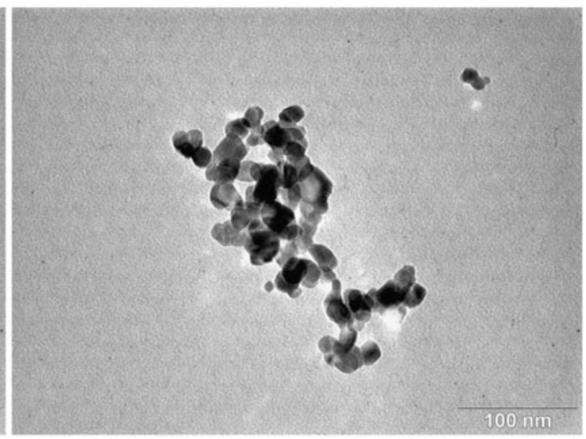

050520-c5-10.tif

SnO_2 height study - sampled at 18.5 cm

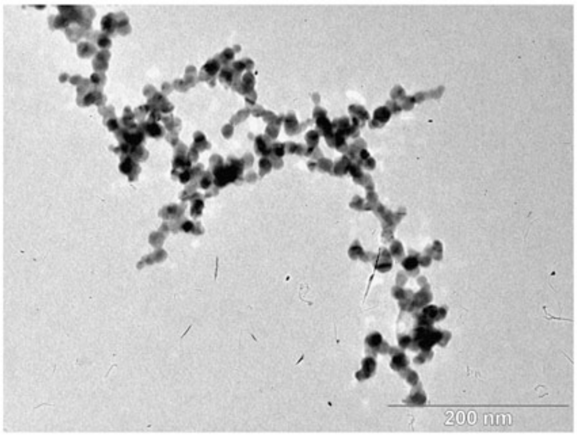

050520-c7-01.tif

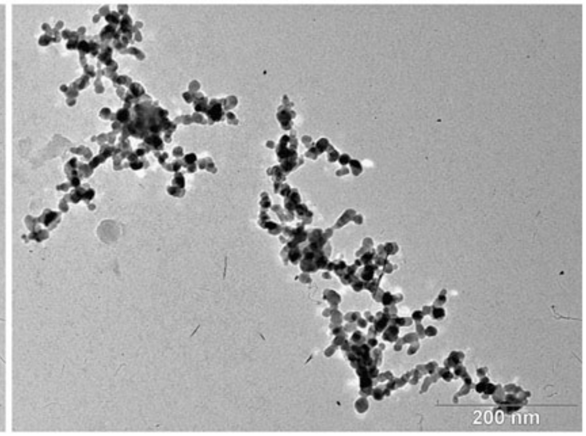

050520-c7-02.tif

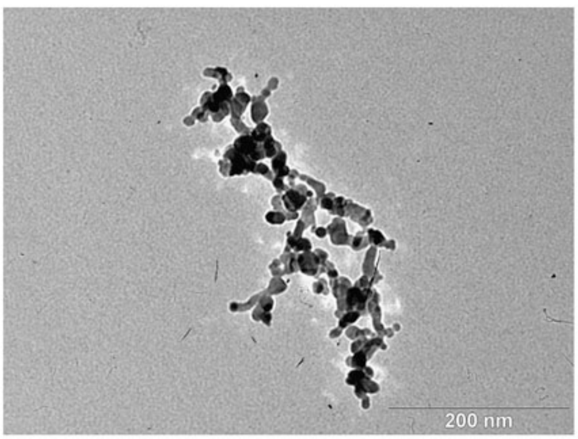

050520-c7-03.tif

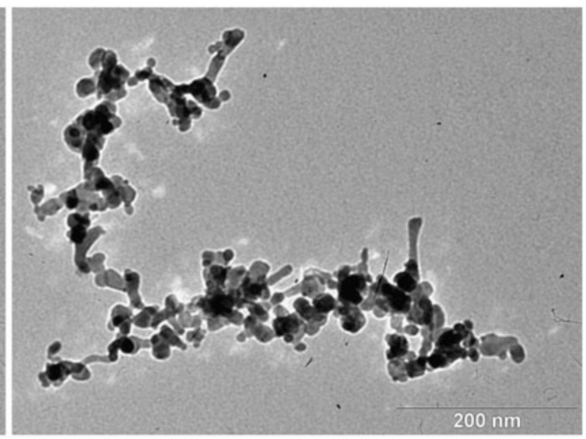

050520-c7-04.tif

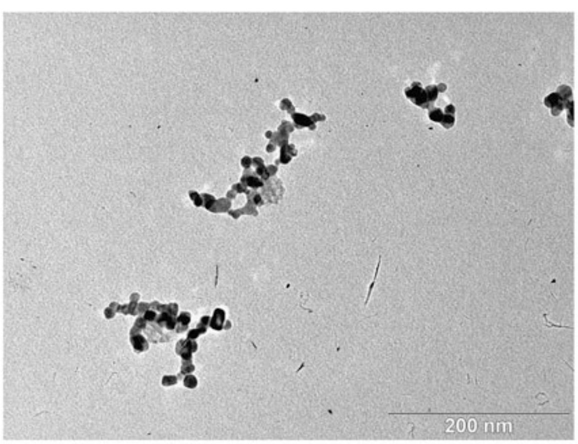

050520-c7-05.tif

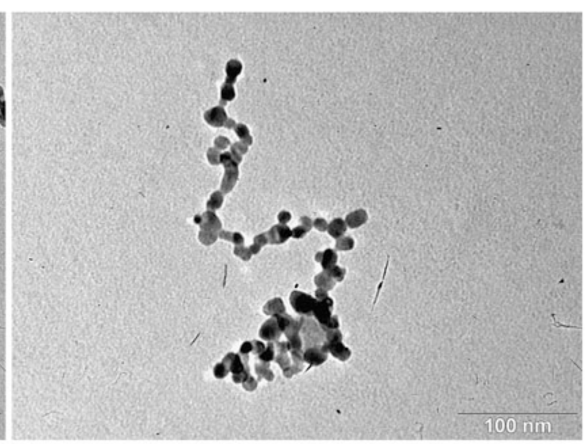

050520-c7-06.tif

SnO_2 height study - sampled at 18.5 cm

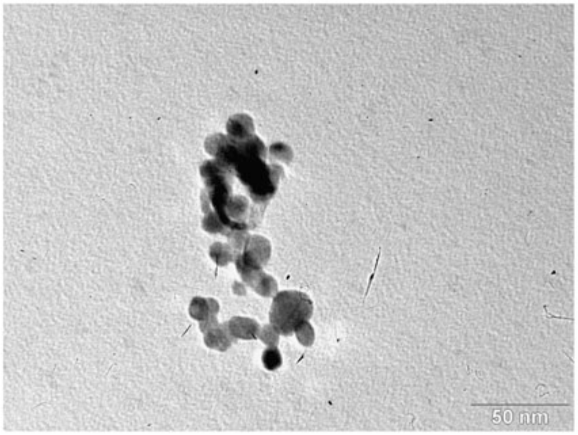

050520-c7-07.tif

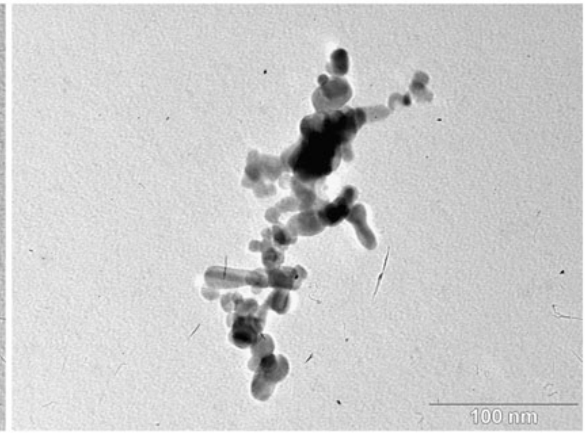

050520-c7-08.tif

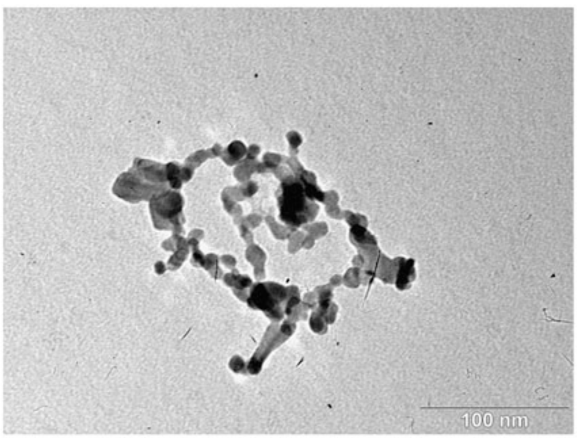

050520-c7-09.tif

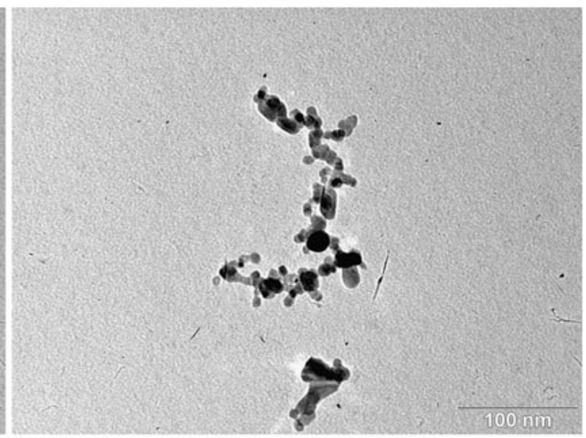

050520-c7-10.tif

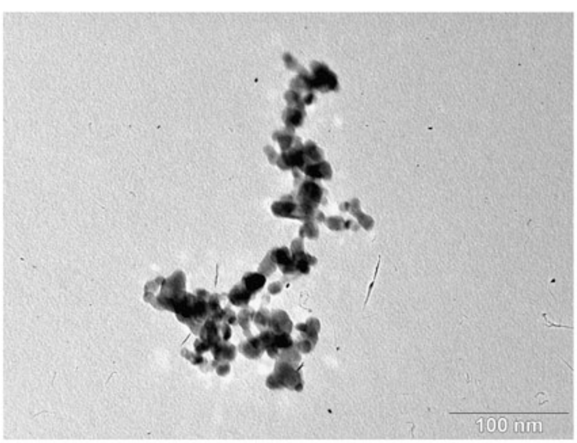

050520-c7-11.tif

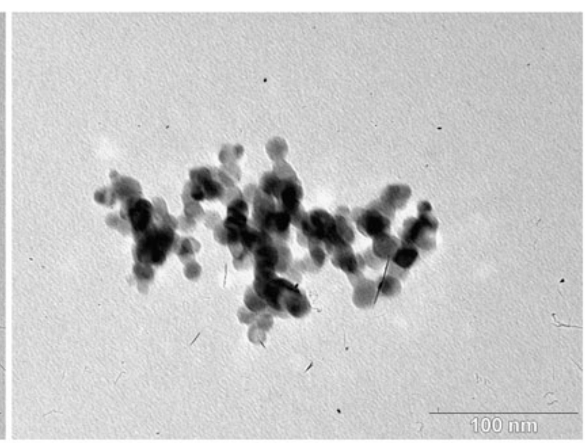

050520-c7-12.tif

SnO_2 height study - sampled at 18.5 cm

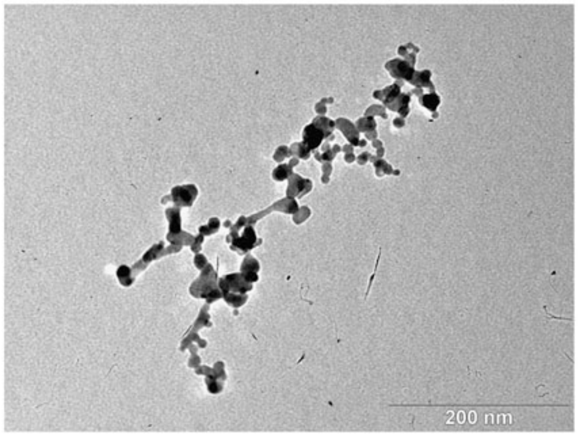

050520-c7-13.tif

Gold-doped SnO_2 - preheated gold acetate with partial decomposition

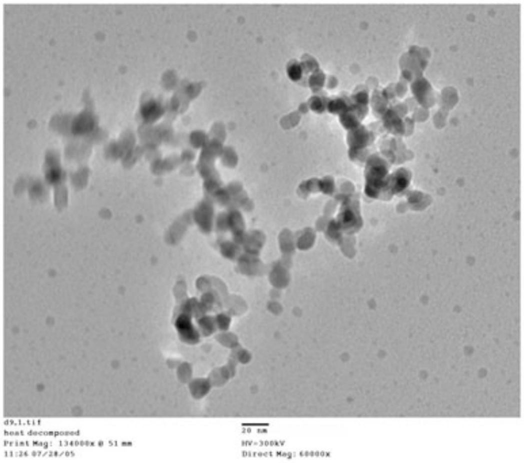

d9_1.tif

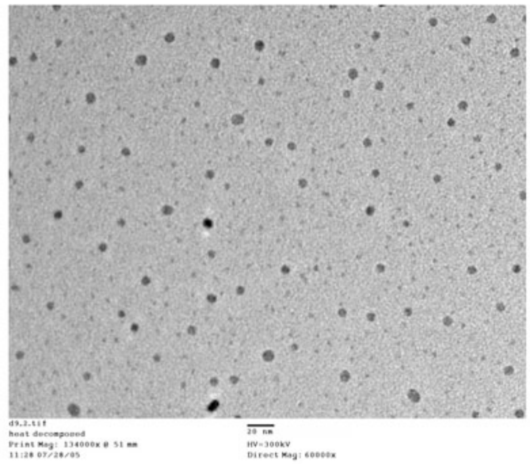

d9_2.tif

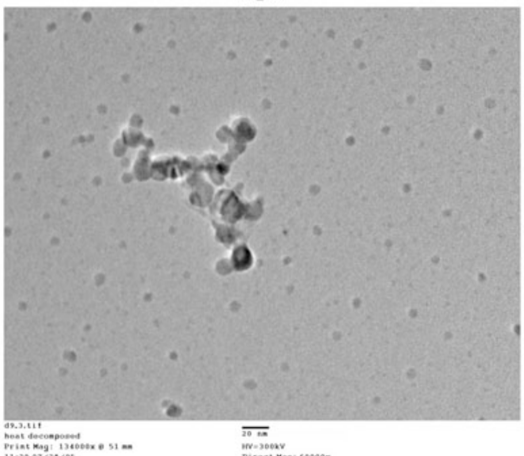

d9_3.tif

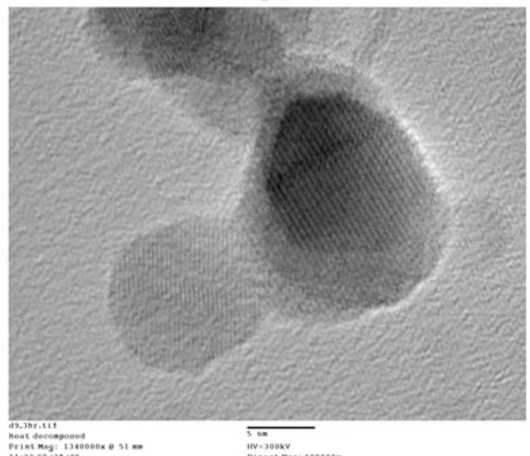

d9_3hr.tif

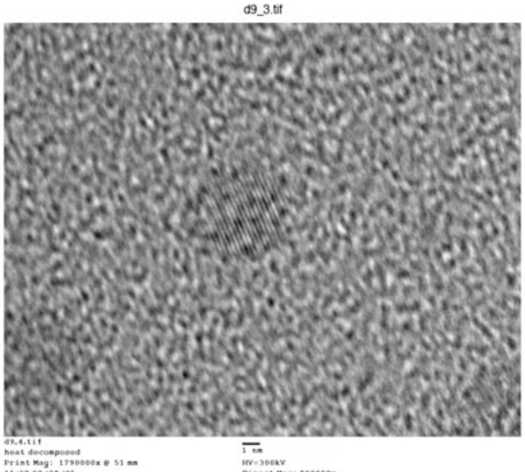

d9_4.tif

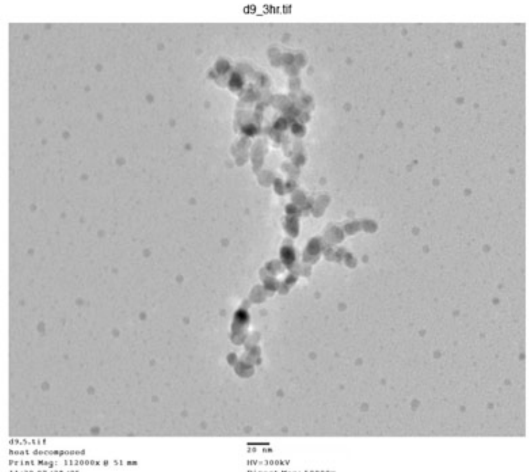

d9_5.tif

Gold-doped SnO_2 - preheated gold acetate with partial decomposition

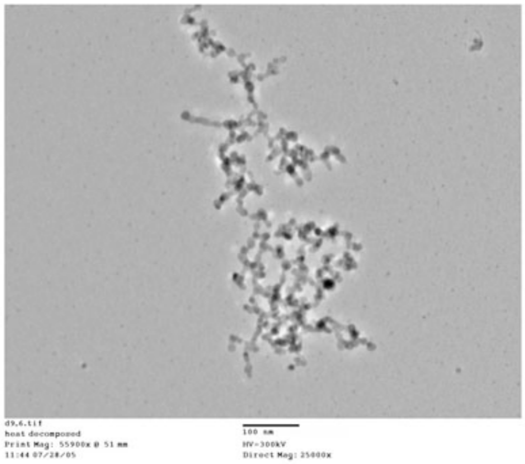

d9_6.tif

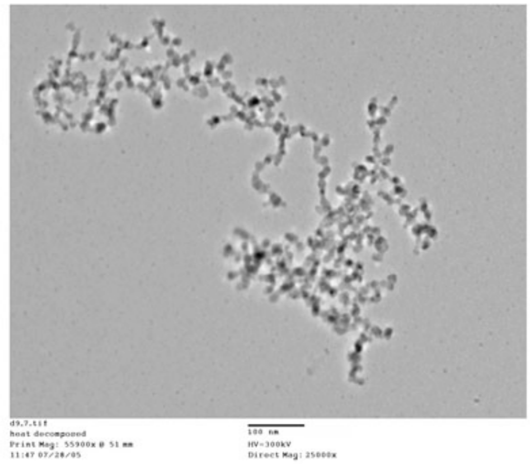

d9_7.tif

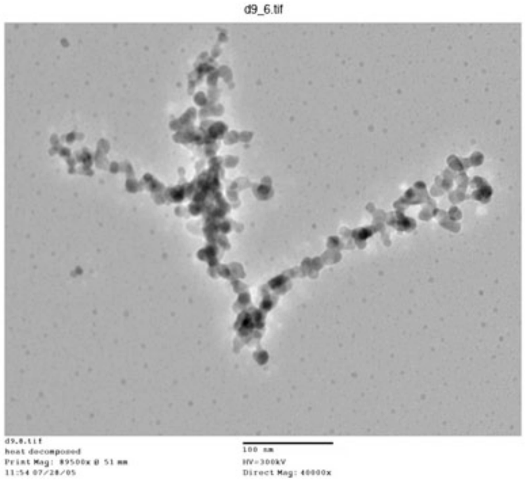

d9_8.tif

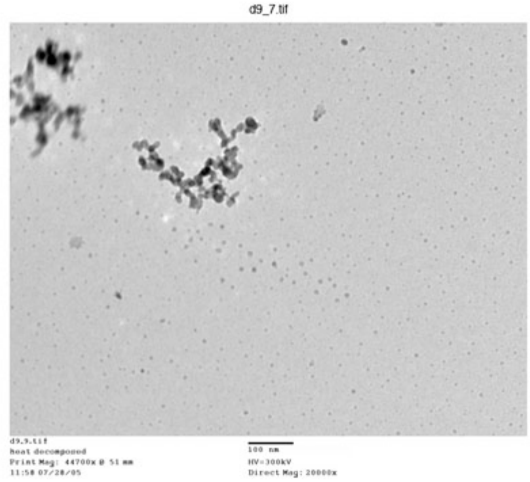

d9_9.tif

Gold-doped SnO_2 - preheated gold acetate with partial decomposition

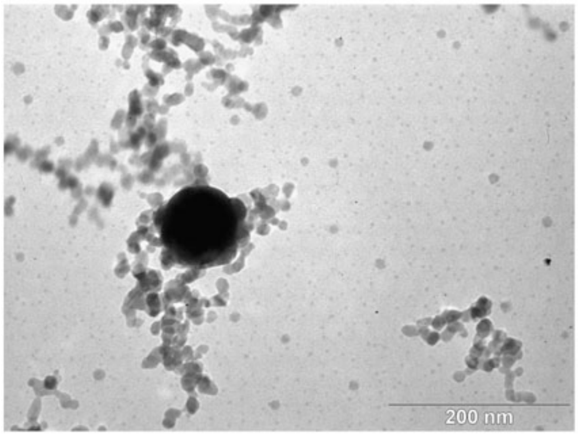

d10_1.tif

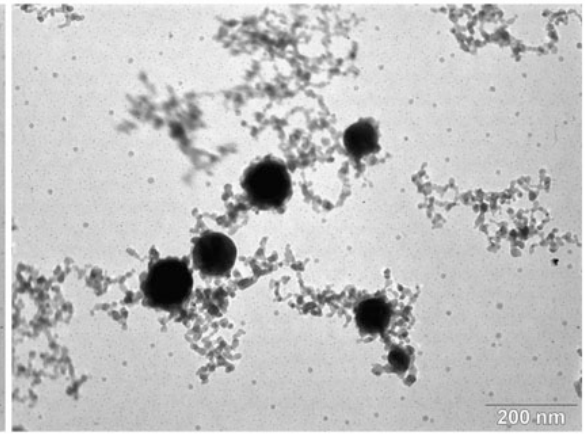

d10_2.tif

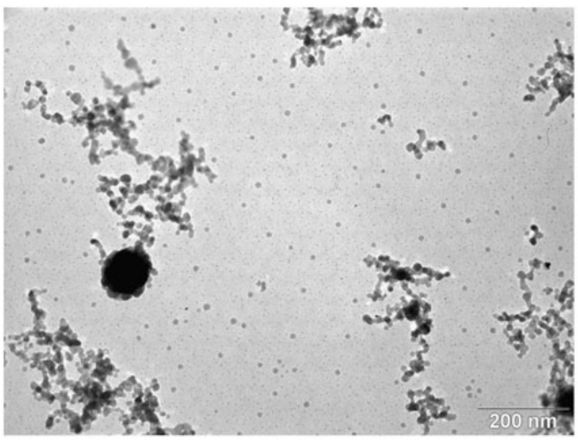

d10_3.tif

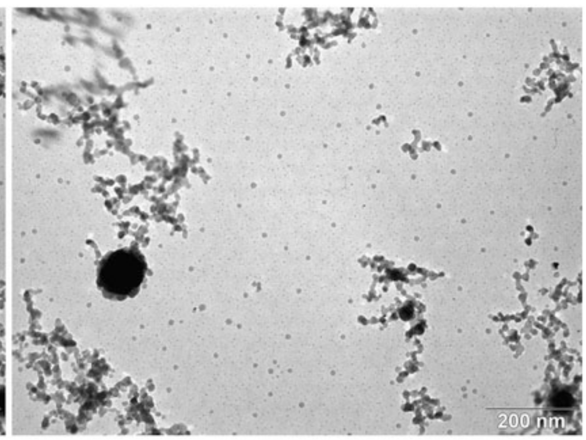

d10_4.tif

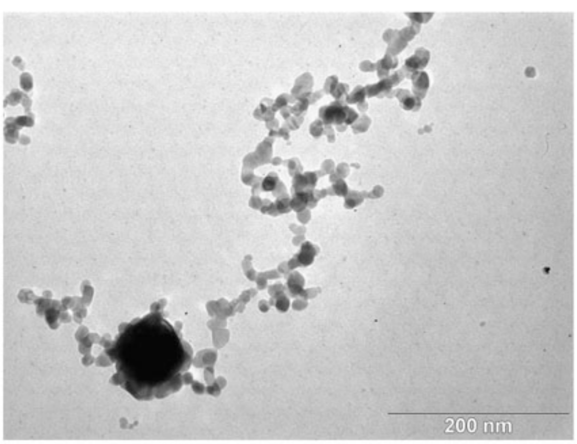

d10_5.tif

Two metal acetate precursors - gold acetate and aluminum acetate mixed

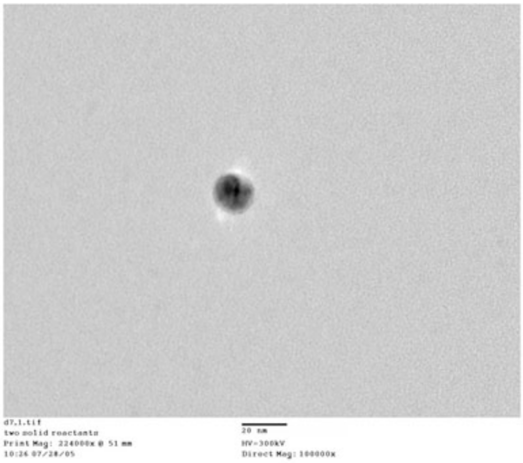

d7_1.tif

d7_2.tif

d7_3.tif

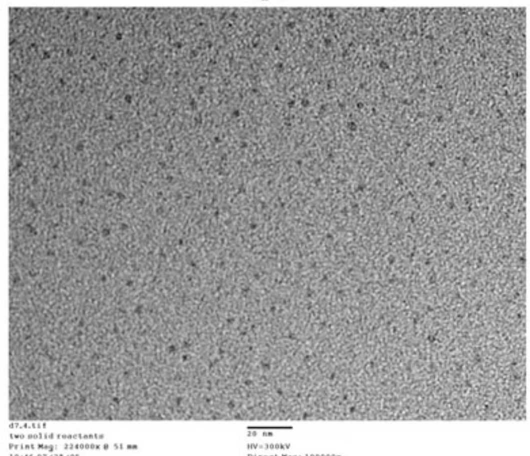

d7_4.tif

d7_5.tif

Two metal acetate precursors - gold acetate and aluminum acetate mixed

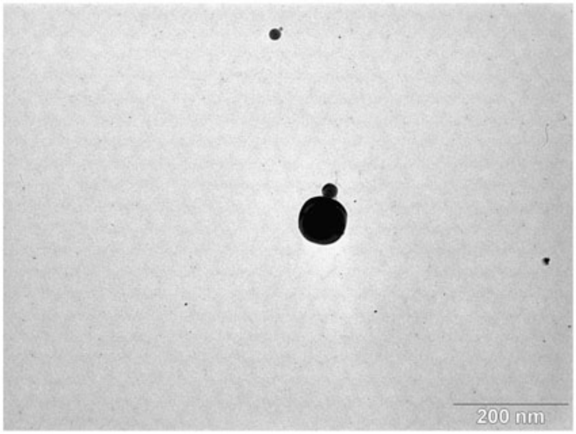

d6_1.tif

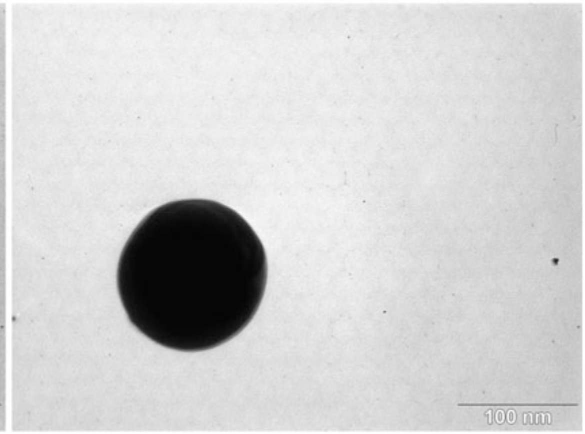

d6_2.tif

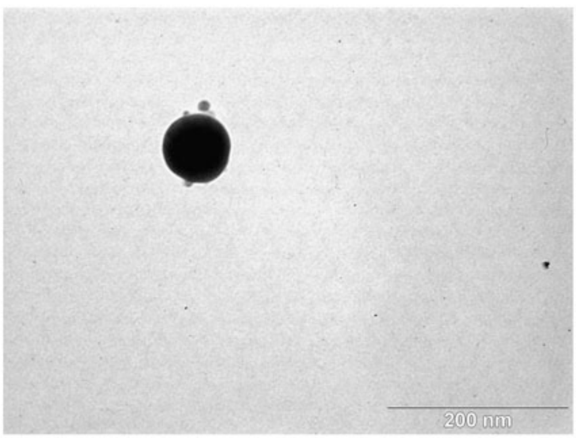

d6_3.tif

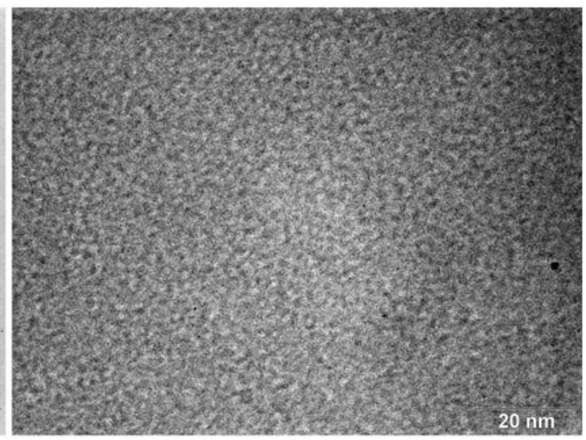

d6_4.tif

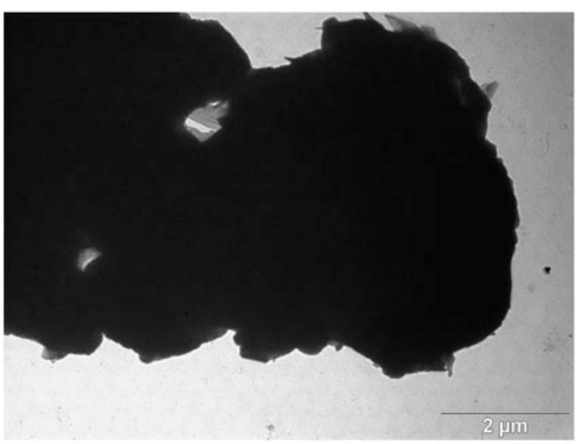

d6_5.tif

Aluminum-doped SnO_2 - identification with XEDS

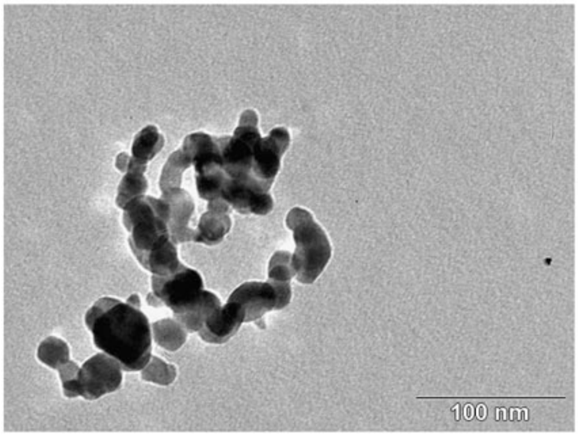

050722_a4_01.tif

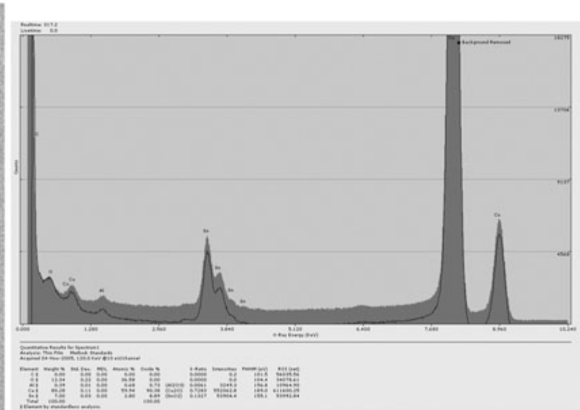

050722_a4_02 eds.bmp

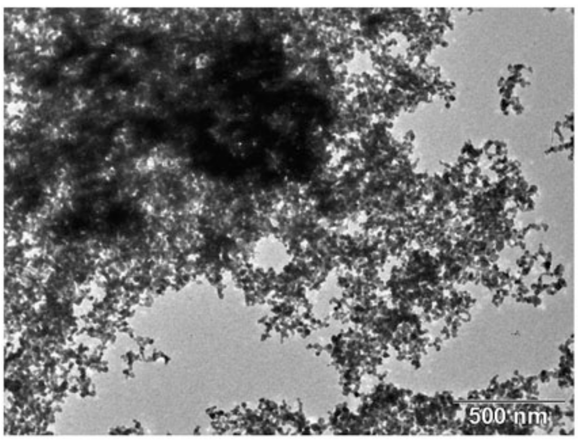

050722_a4_02.tif

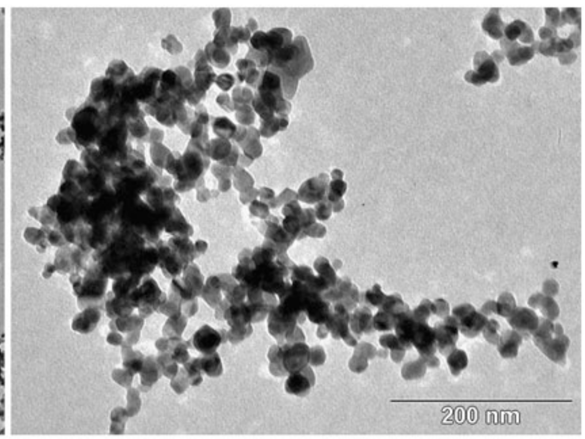

050722_a4_03.tif

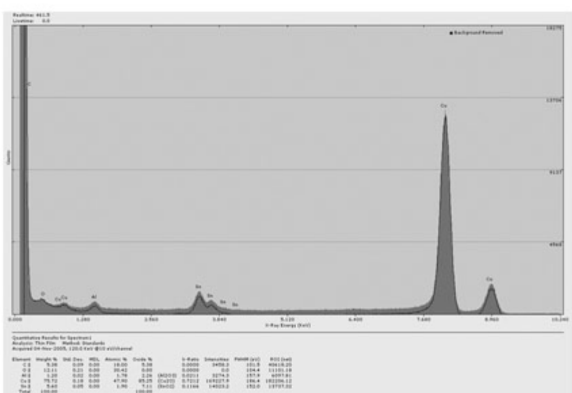

050722_a4_04 eds.bmp

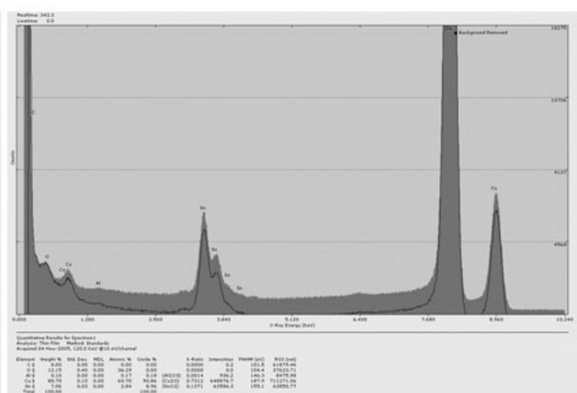

050722_a4_04 next eds.bmp

Aluminum-doped SnO_2 - identification with XEDS

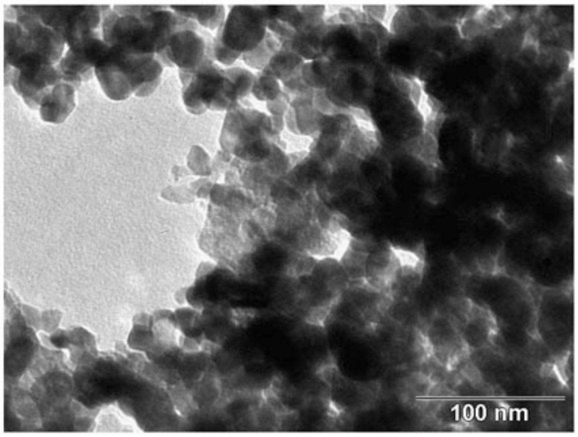

050722_a4_04.tif

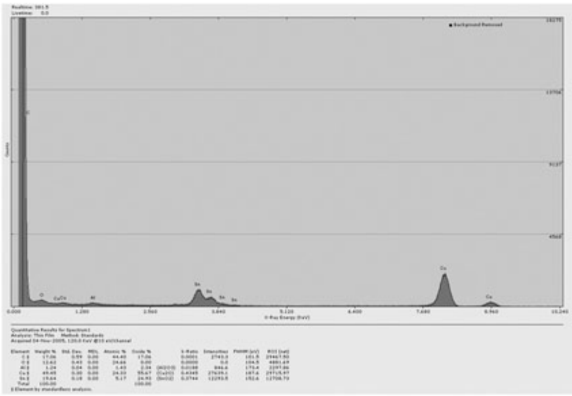

050722_a4_05 eds.bmp

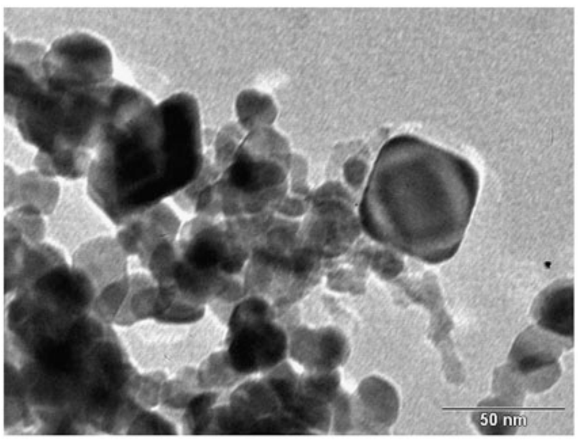

050722_a4_05.tif

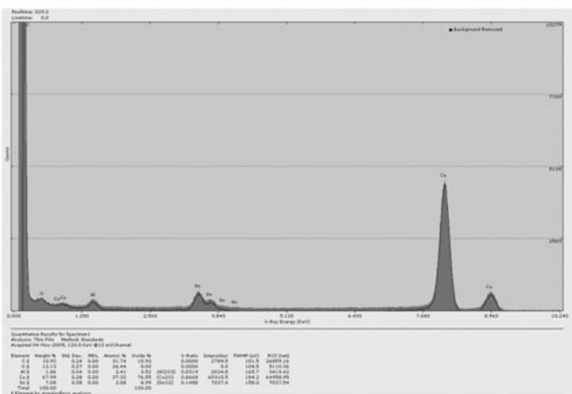

050722_a4_06 eds.bmp

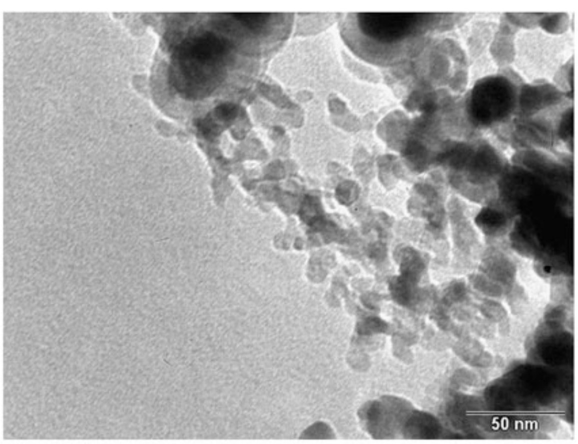

050722_a4_06.tif

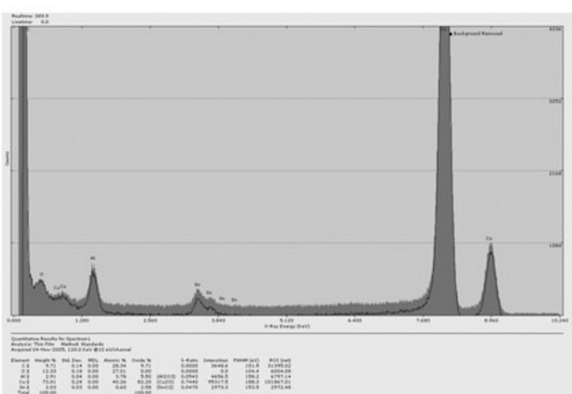

050722_a4_07 eds.bmp

Aluminum-doped SnO_2 - identification with XEDS

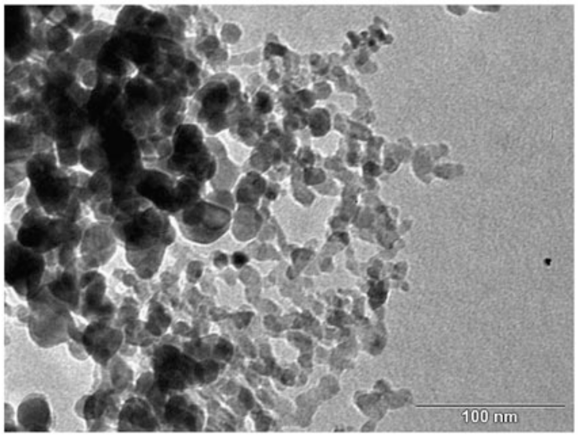

050722_a4_07.tif

undoped SnO_2

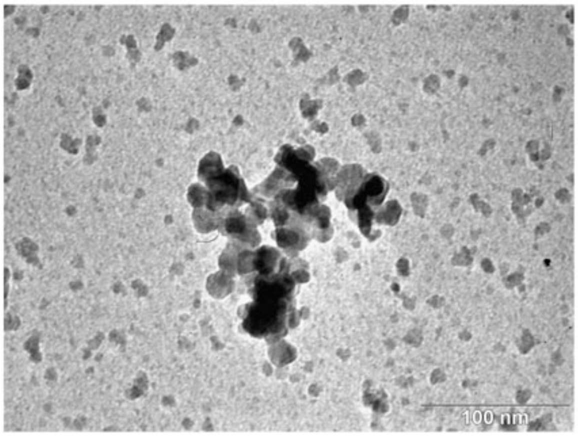

030624_b2_01.tif

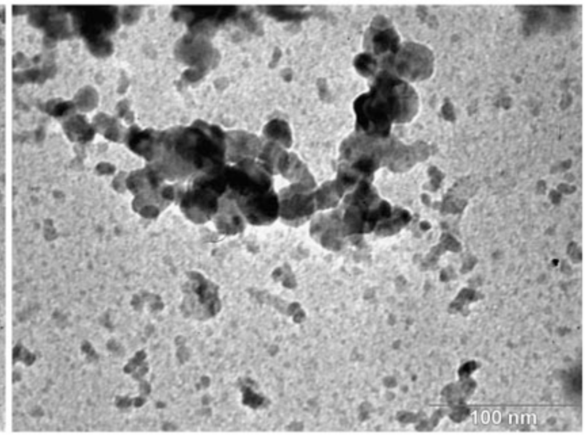

030624_b2_02.tif

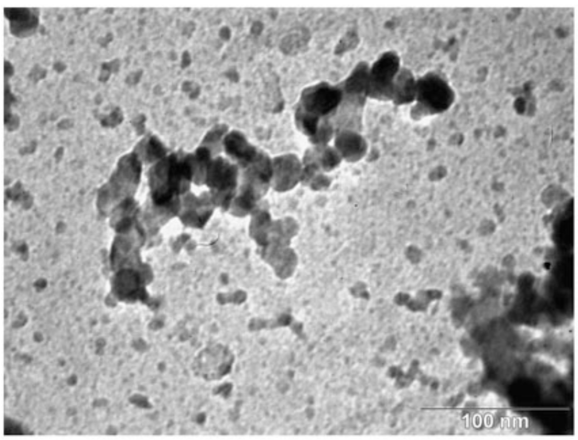

030624_b2_03.tif

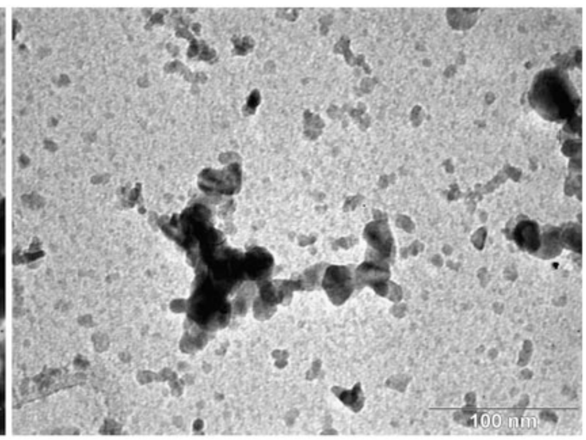

030624_b2_04.tif

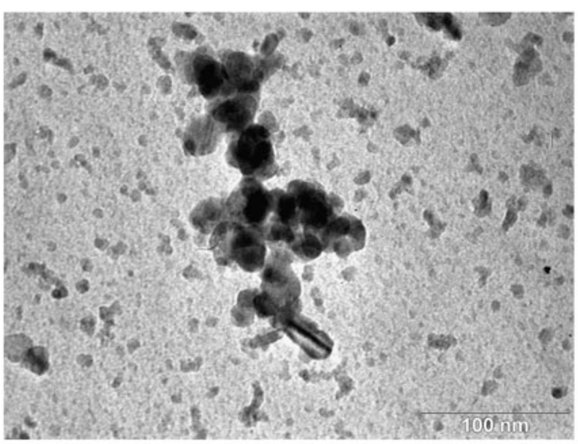

030624_b2_05.tif

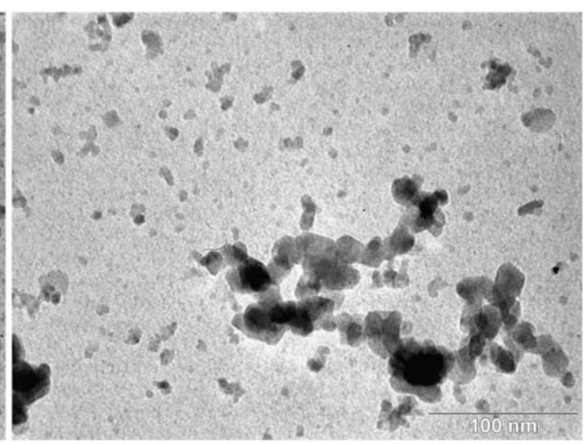

030624_b2_06.tif

undoped SnO_2

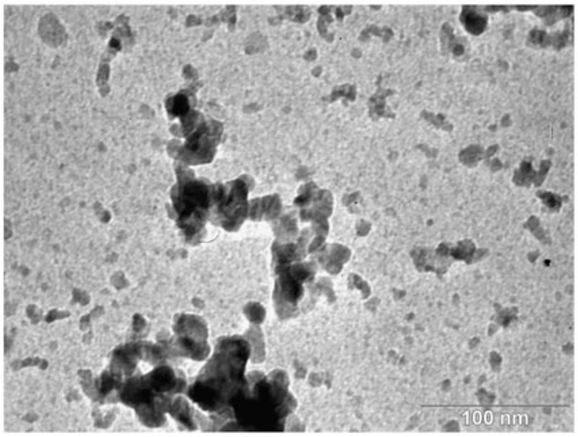

030624_b2_07.tif

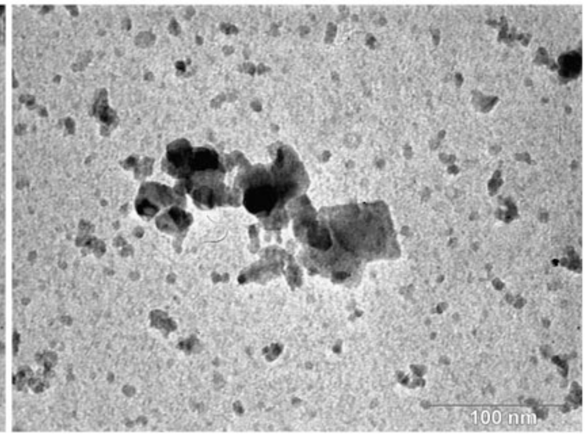

030624_b2_08.tif

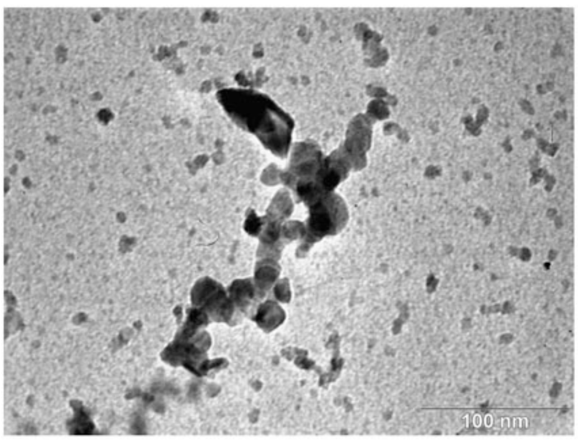

030624_b2_09.tif

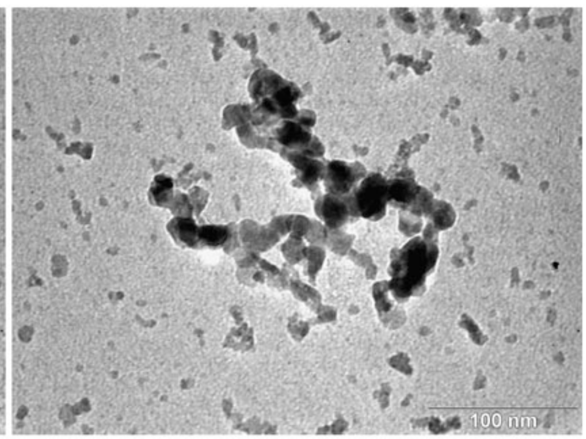

030624_b2_10.tif

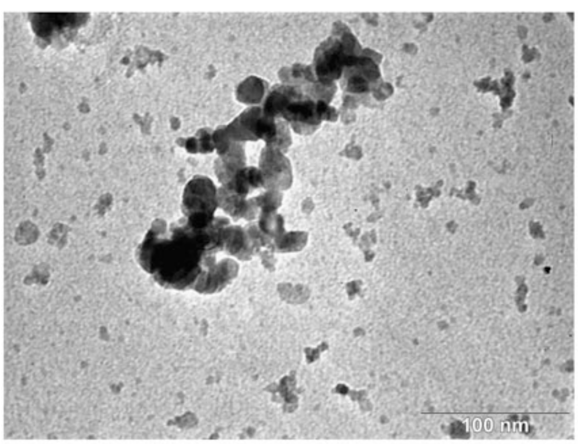

030624_b2_11.tif

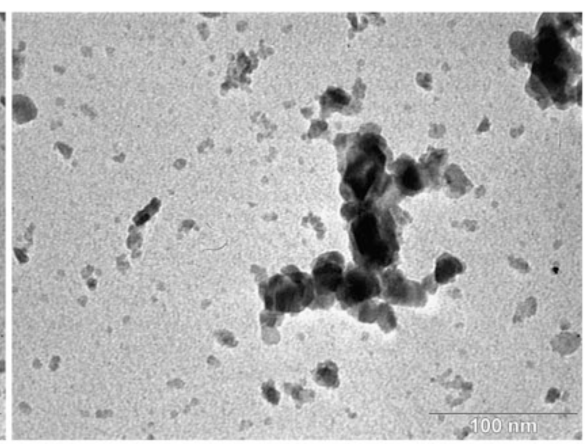

030624_b2_12.tif

undoped SnO_2 with chimney

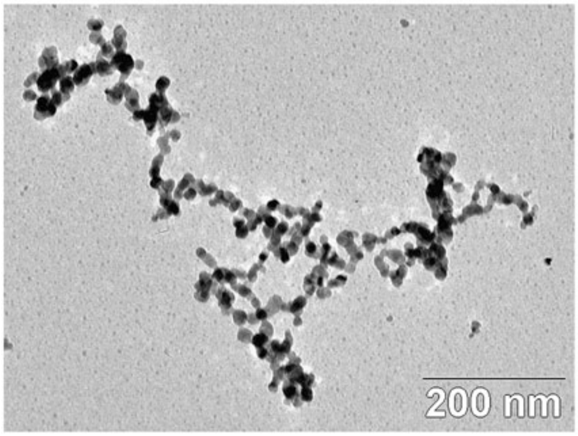

050722_a3_01.tif

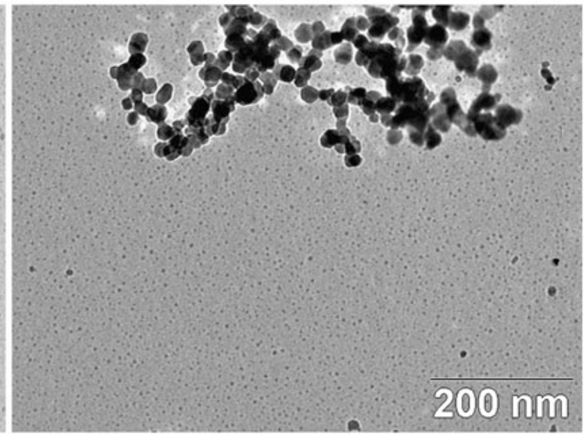

050722_a3_02.tif

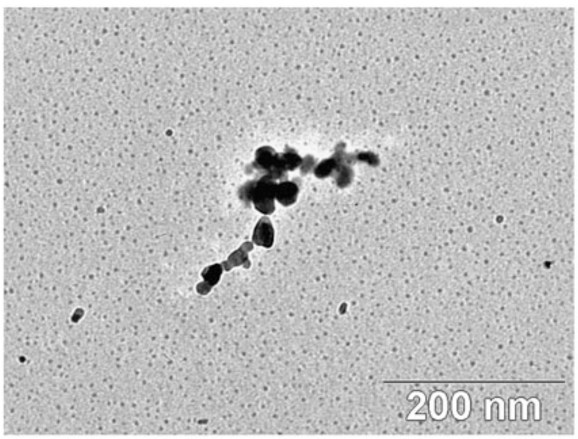

050722_a3_03.tif

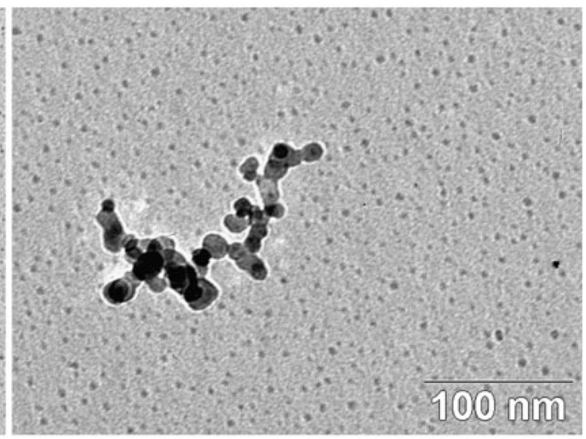

050722_a3_04.tif

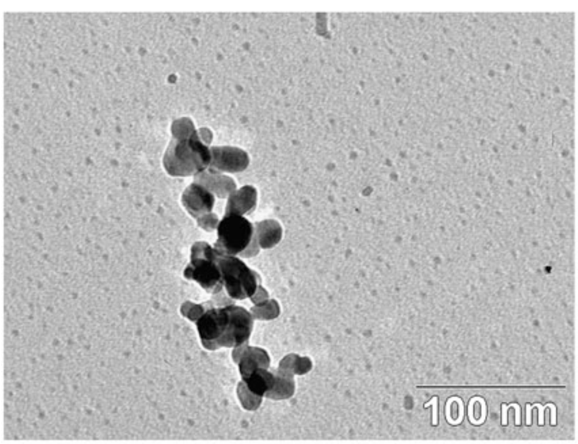

050722_a3_05.tif

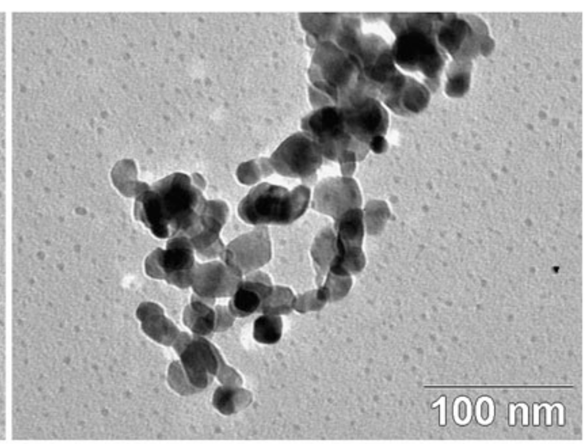

050722_a3_06.tif

undoped SnO_2 with chimney

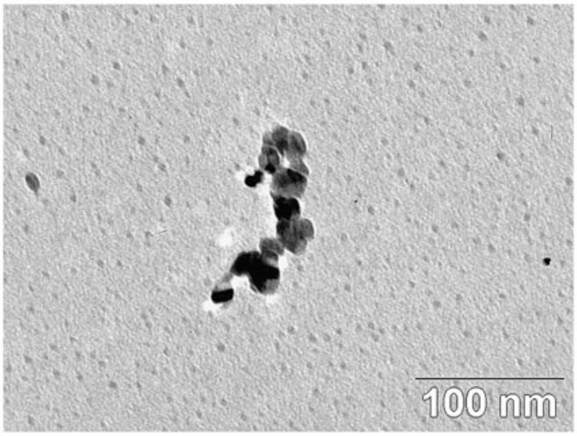

050722_a3_07.tif

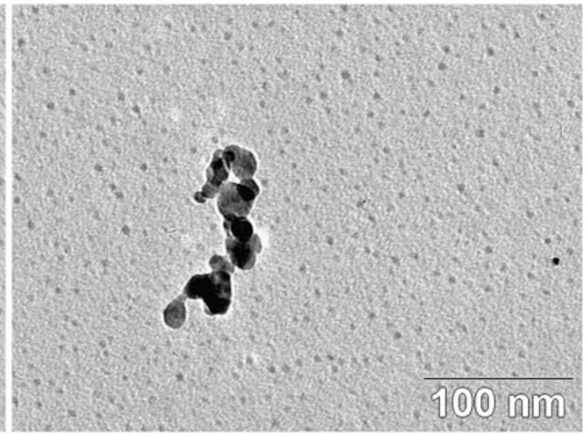

050722_a3_08.tif

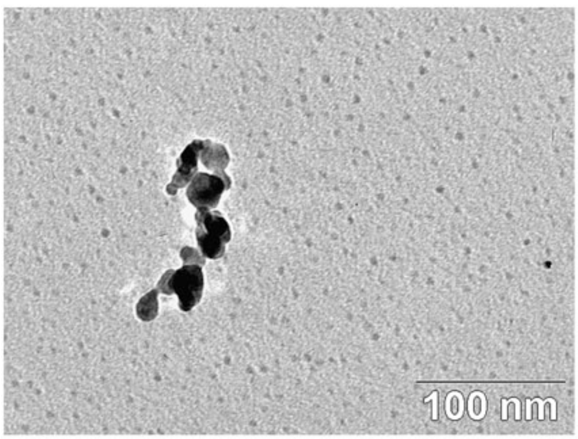

050722_a3_09.tif

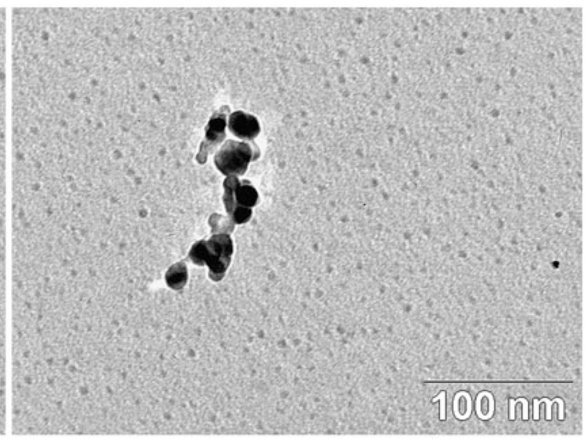

050722_a3_10.tif

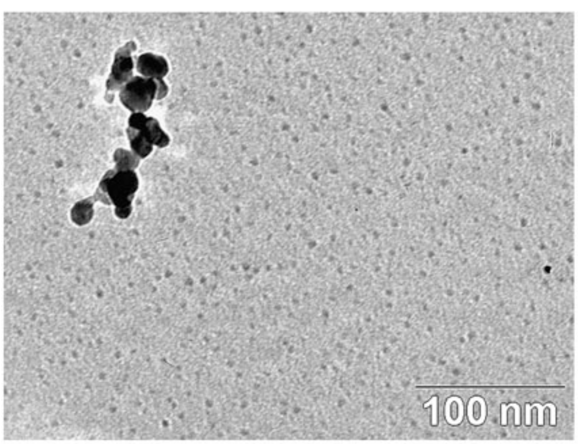

050722_a3_11.tif

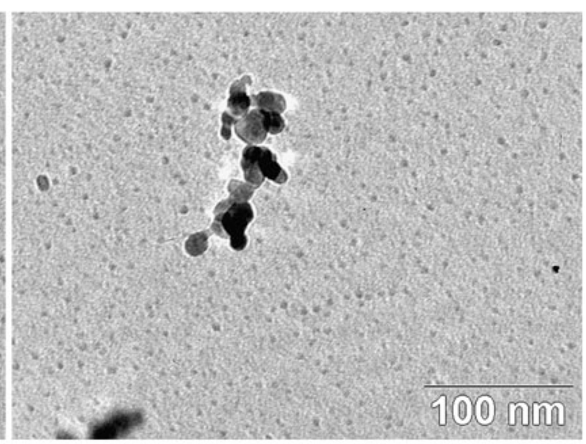

050722_a3_12.tif

undoped SnO_2 with chimney

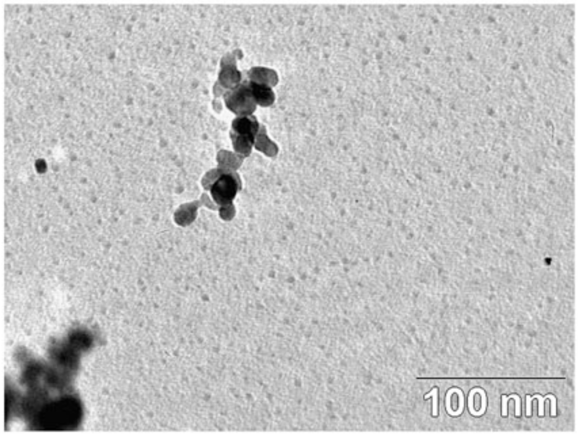

050722_a3_13.tif

undoped SnO_2 with tert-n-butyl tin precursor (heated line)

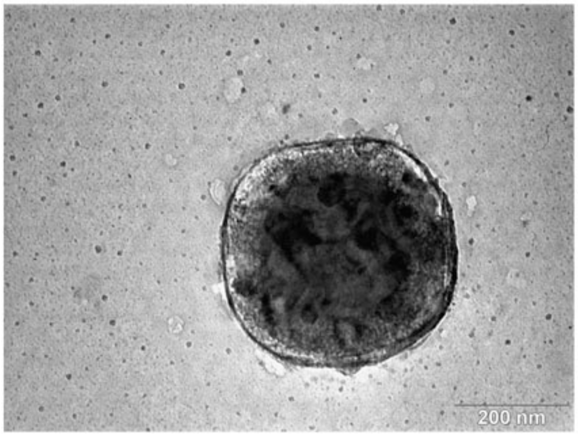

d3_01.tif

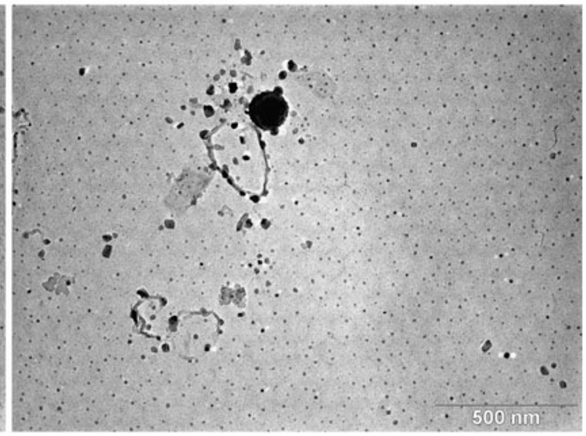

d3_02.tif

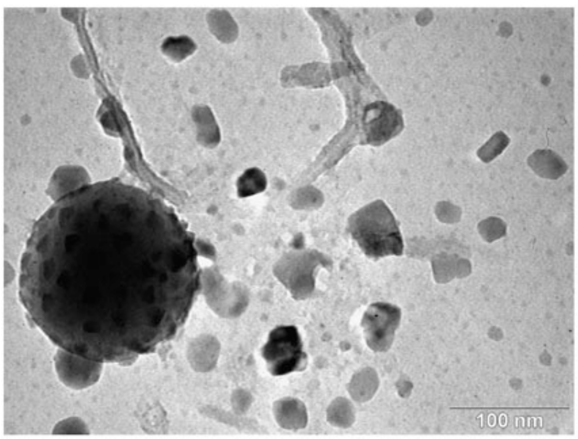

d3_03.tif

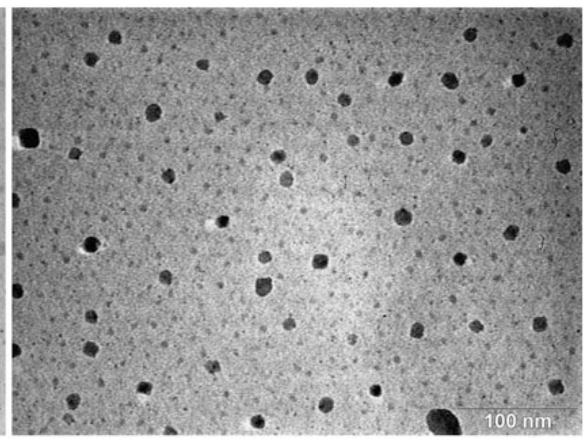

d3_04.tif

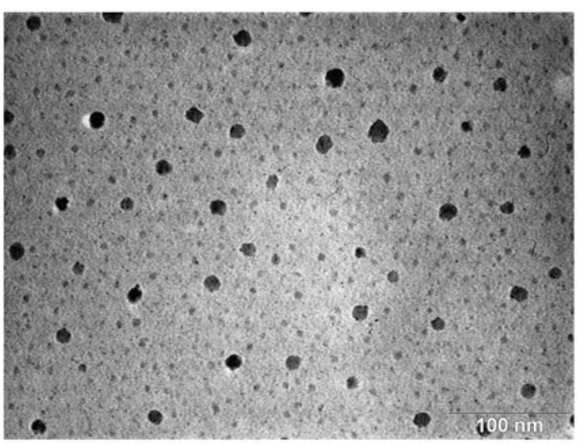

d3_05.tif

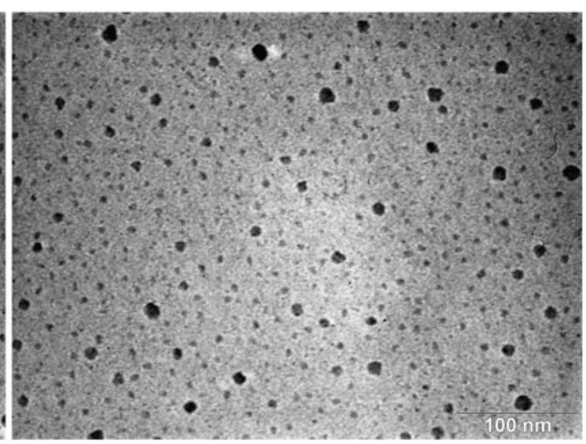

d3_06.tif

undoped SnO_2 with tert-n-butyl tin precursor (heated line)

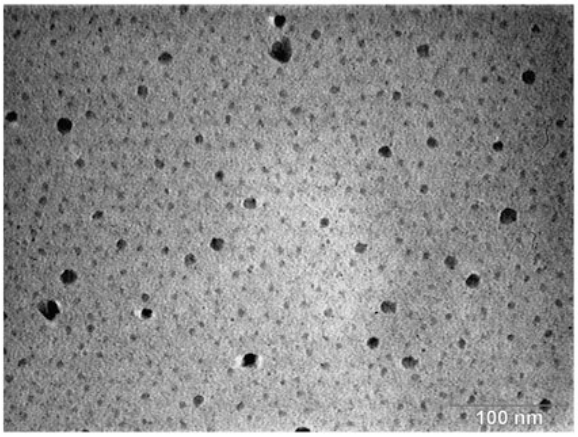

d3_07.tif

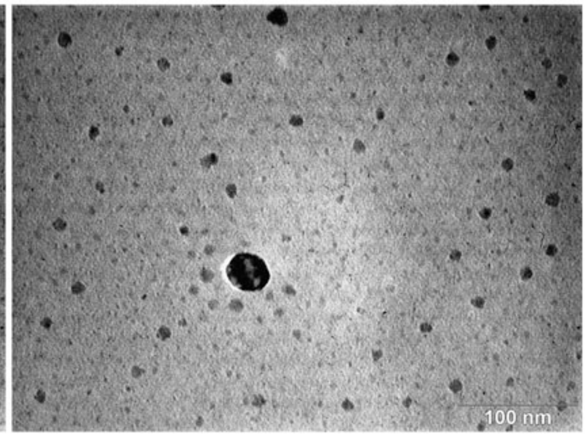

d3_08.tif

undoped SnO_2 with tert-n-butyl tin precursor (heated line)

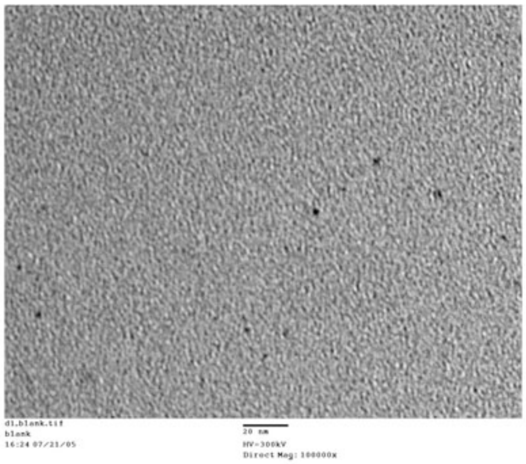

d1_blank.tif

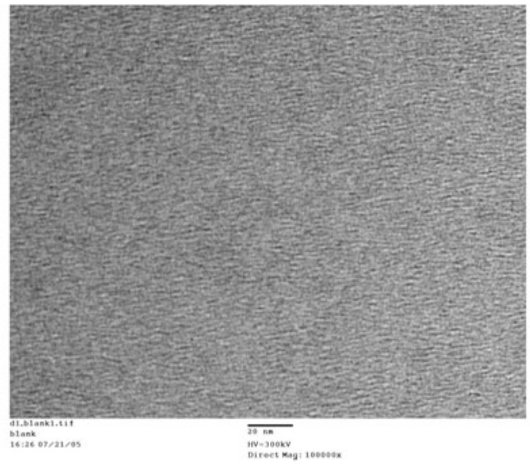

d1_blank1.tif

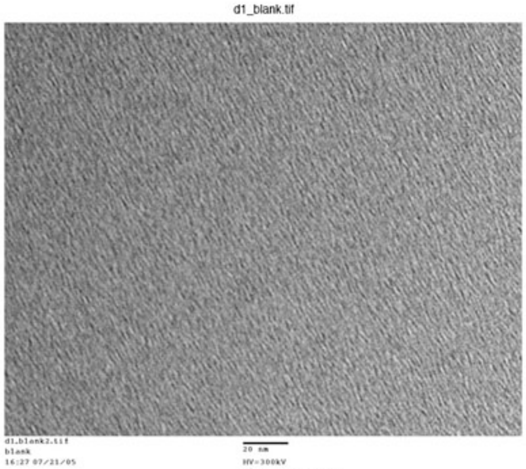

d1_blank2.tif

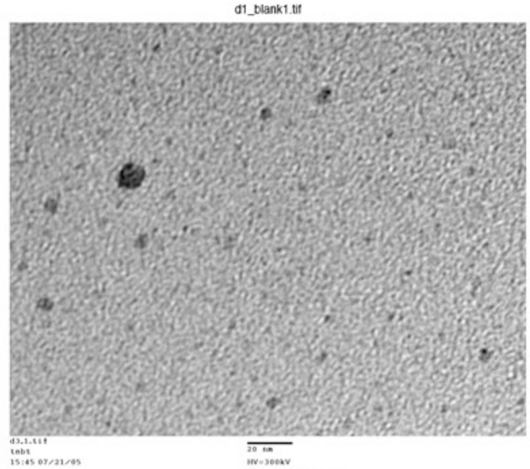

d3_1.tif

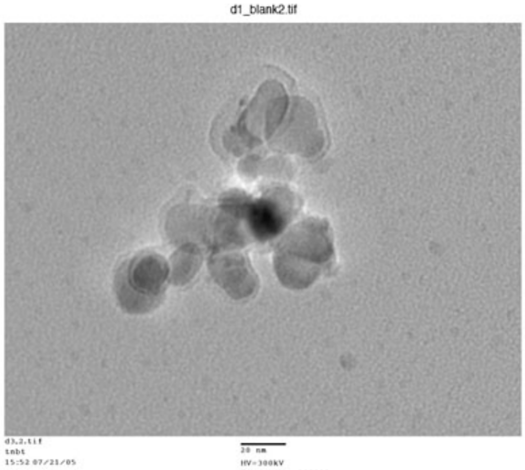

d3_2.tif

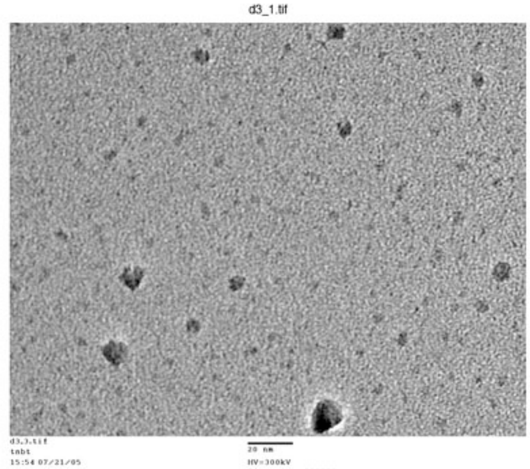

d3_3.tif

undoped SnO_2 older grids from Tiffany Miller's experiments

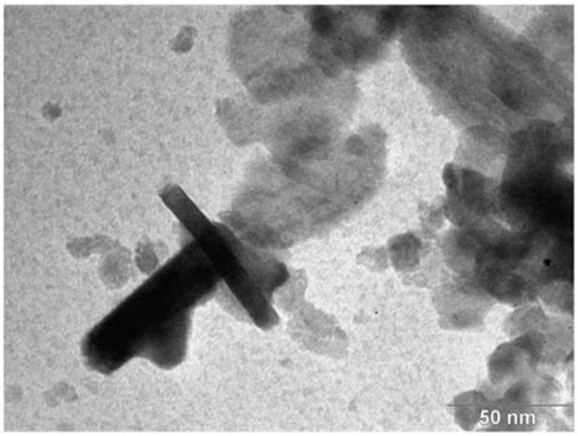

030624_b1_1.tif

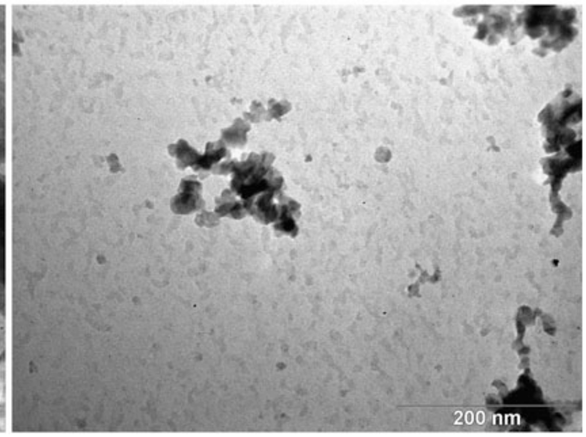

030624_b1_10.tif

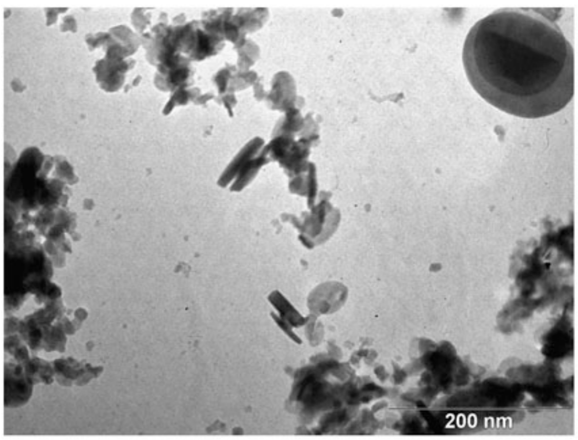

030624_b1_11.tif

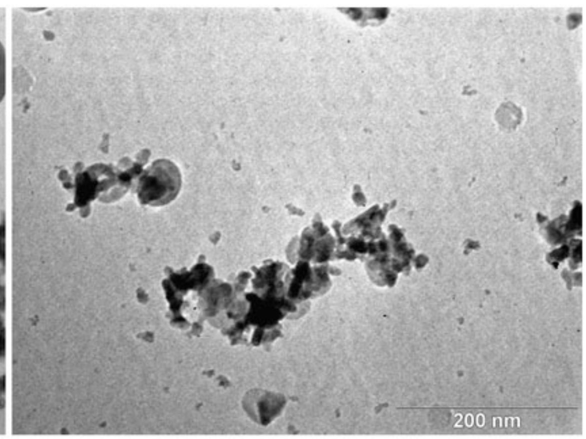

030624_b1_12.tif

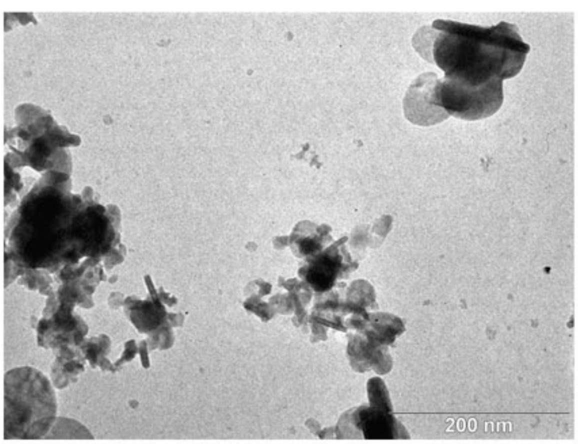

030624_b1_13.tif

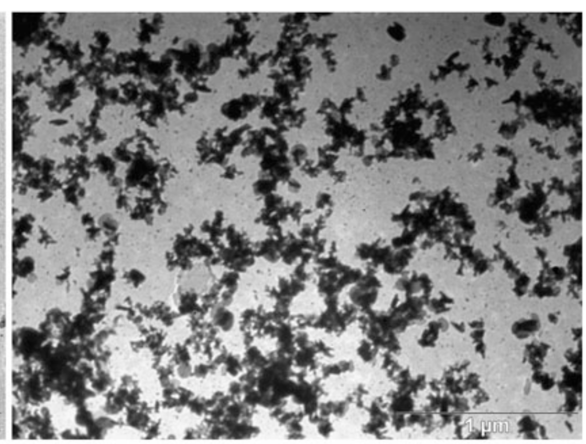

030624_b1_2.tif

undoped SnO_2 older grids from Tiffany Miller's experiments

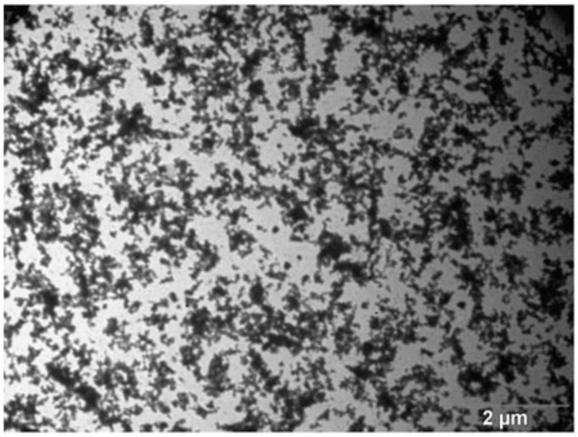

030624_b1_3.tif

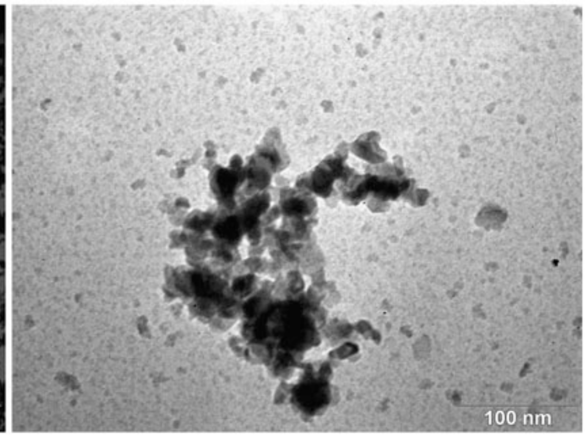

030624_b1_4.tif

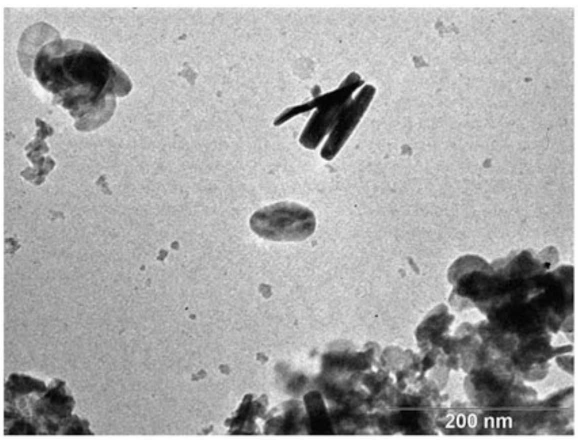

030624_b1_5.tif

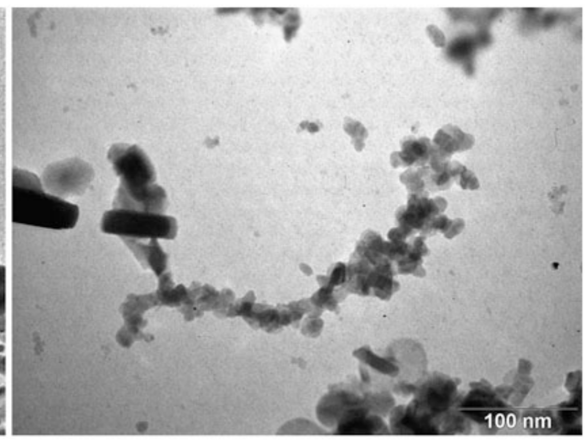

030624_b1_7.tif

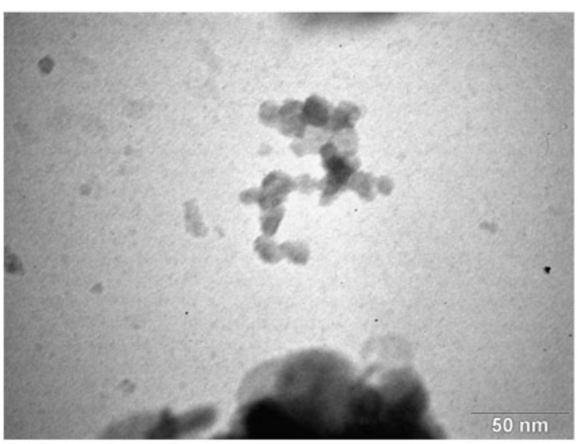

030624_b1_9.tif

undoped SnO_2 for Yen-Hung's analysis (Prof. Sastry's student)

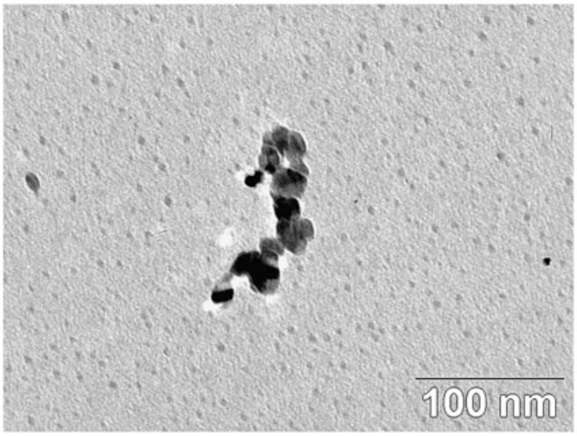

050722_a3 00deg.tif

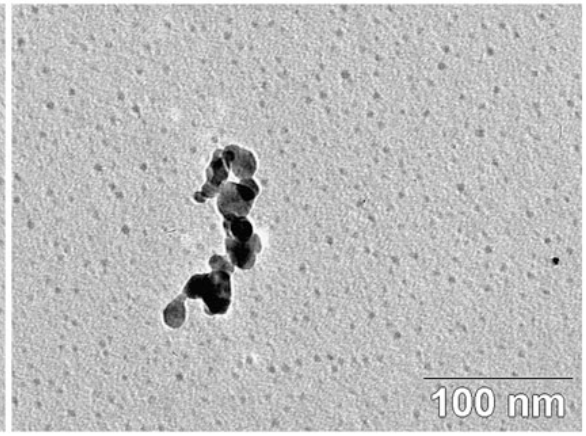

050722_a3 10deg.tif

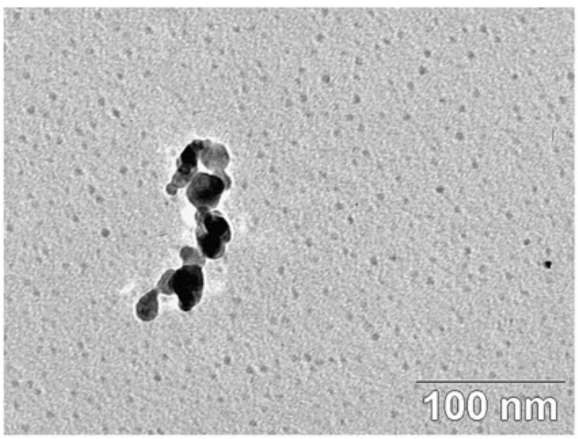

050722_a3 20deg.tif

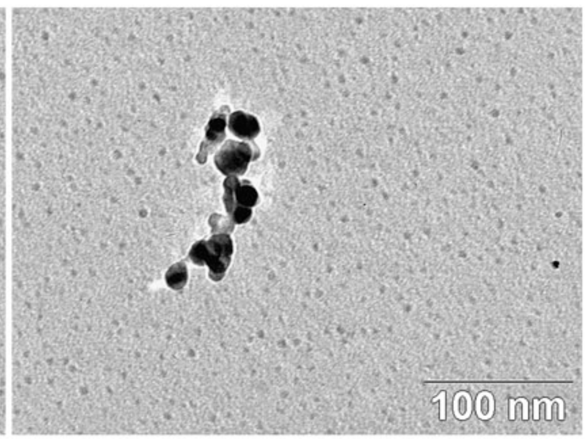

050722_a3 30deg.tif

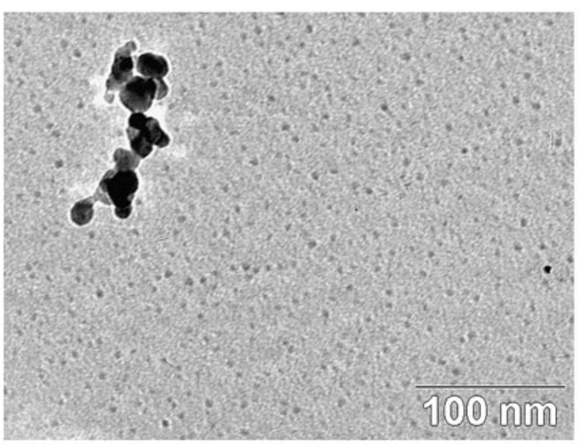

050722_a3 40deg.tif

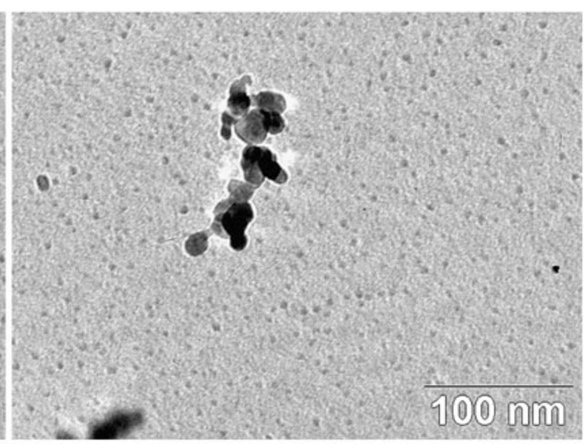

050722_a3 50deg.tif

undoped SnO_2 for Yen-Hung's analysis (Prof. Sastry's student)

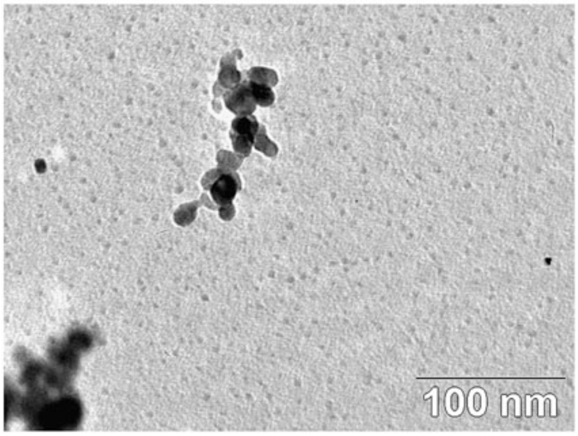

050722_a3 55deg.tif

undoped SnO_2 for Yen-Hung's analysis (Prof. Sastry's student)

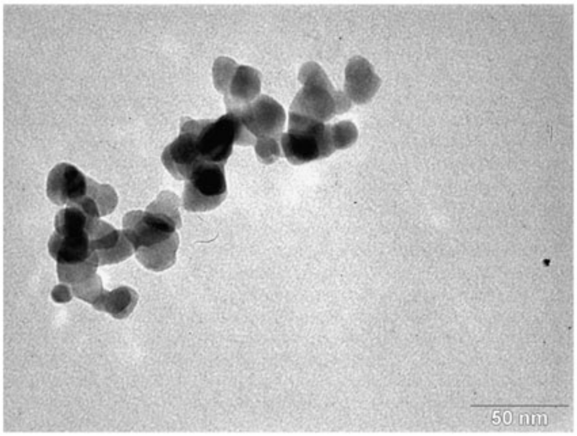

e3_01.tif

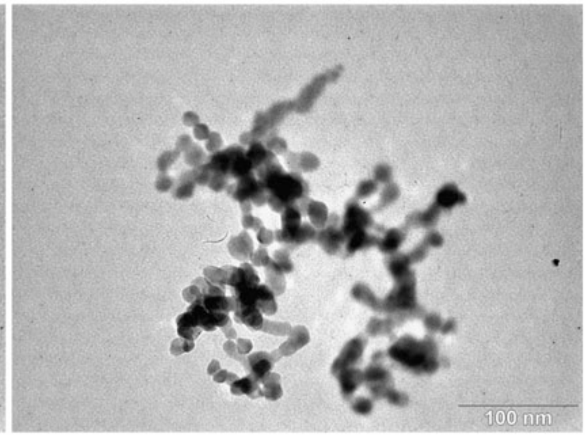

e3_02.tif

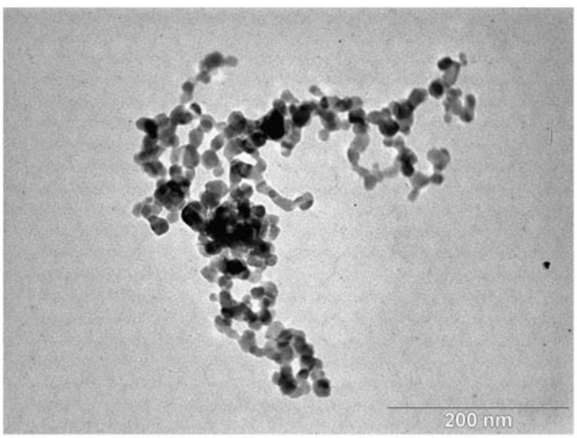

e3_03.tif

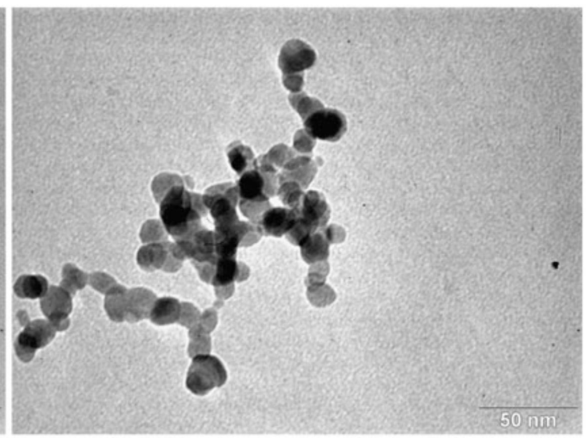

e3_04.tif

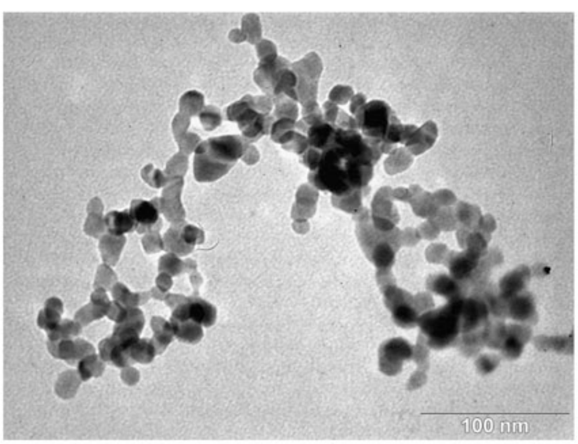

e3_05.tif

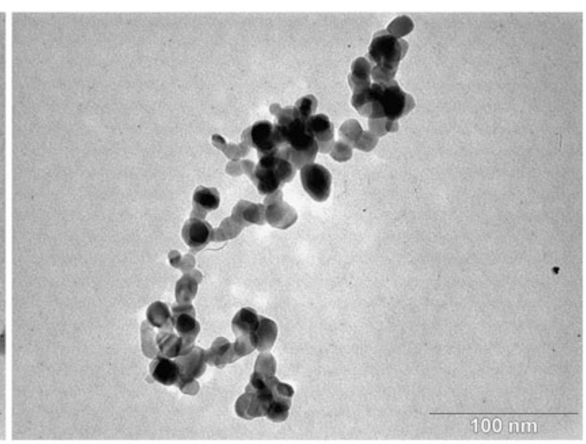

e3_06.tif

undoped SnO_2 for Yen-Hung's analysis (Prof. Sastry's student)

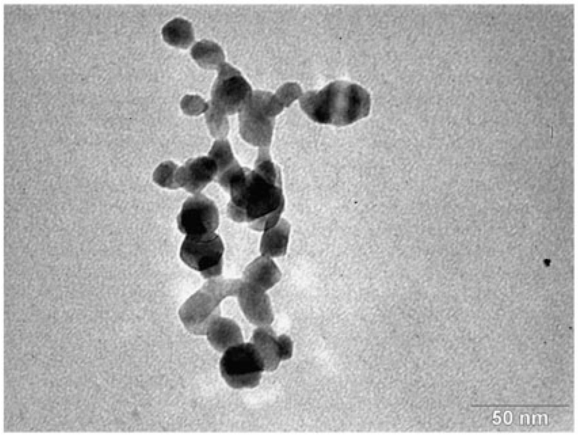

e3_07.tif

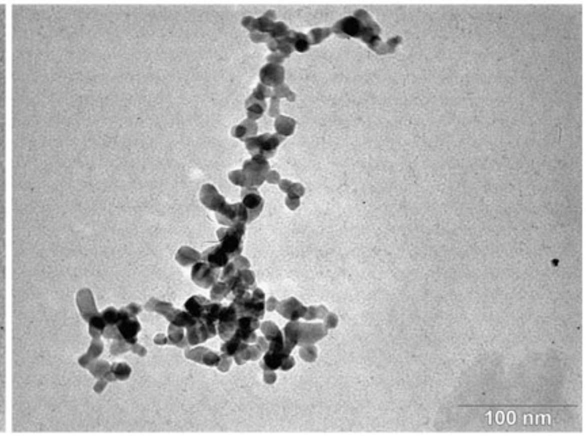

e3_08.tif

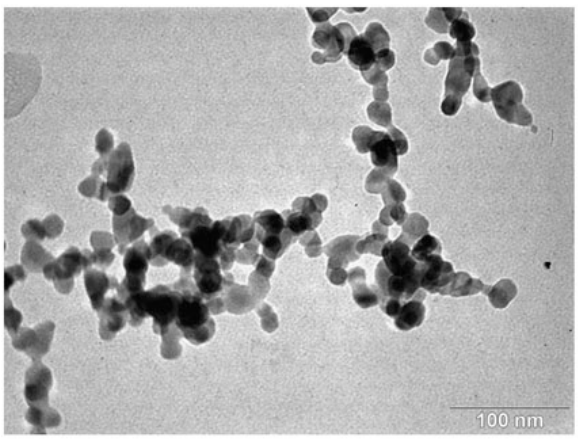

e3_09.tif

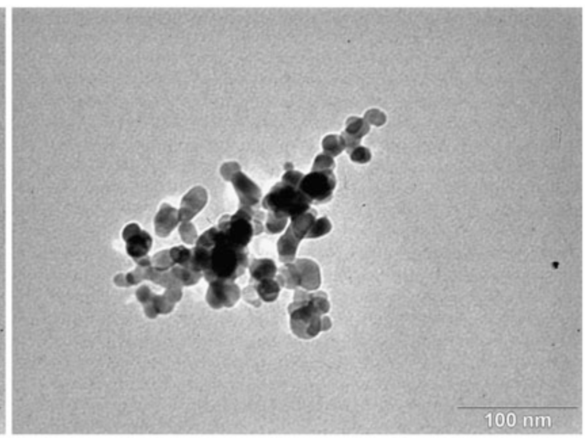

e3_10.tif

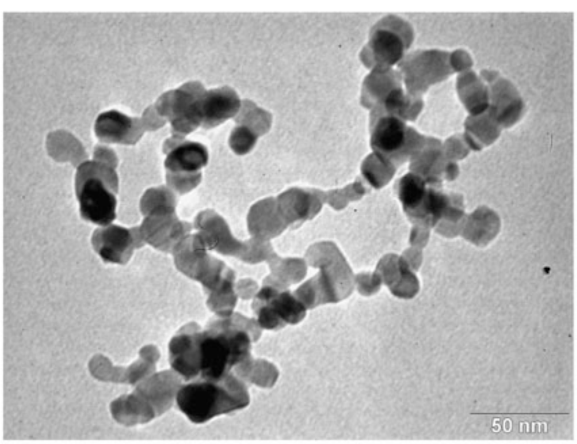

e3_11.tif

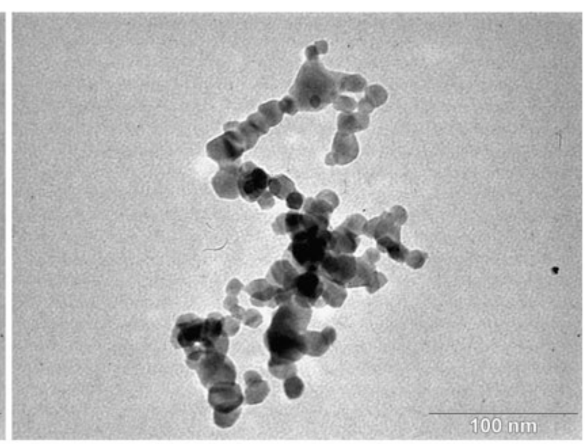

e3_12.tif

undoped SnO_2 for Yen-Hung's analysis (Prof. Sastry's student)

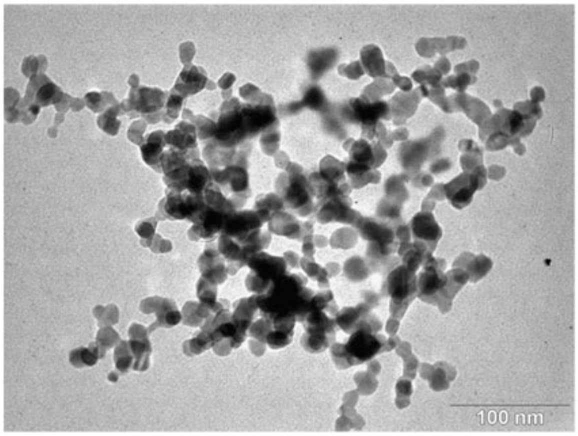

e3_13.tif

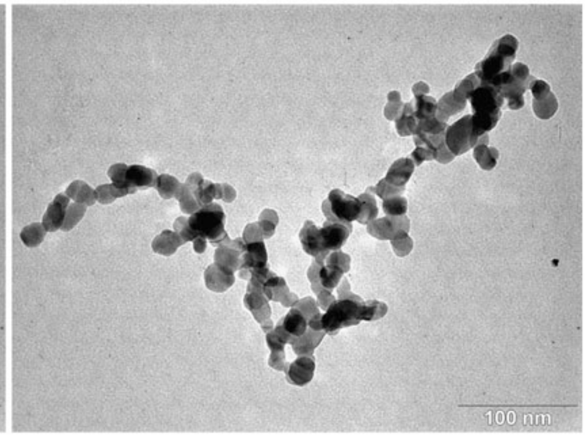

e3_14.tif

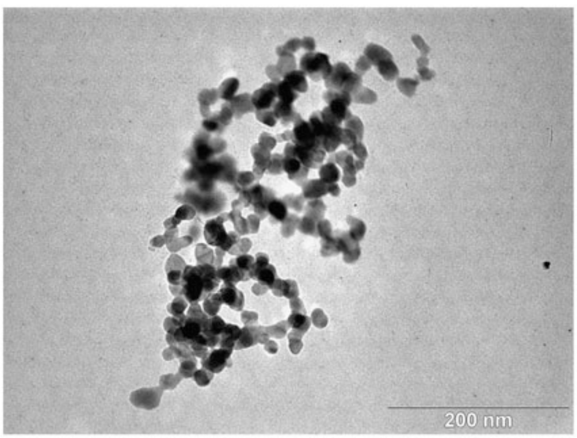

e3_15.tif

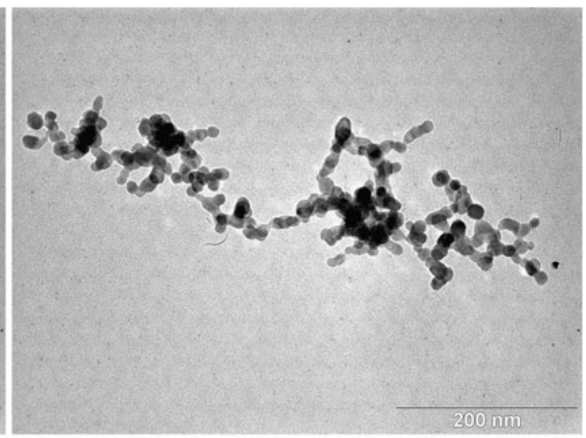

e3_16.tif

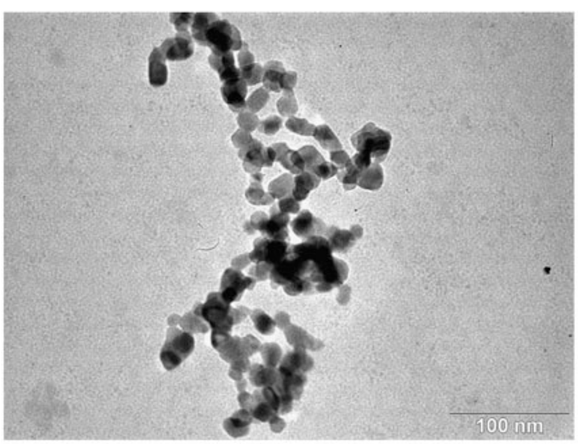

e3_17.tif

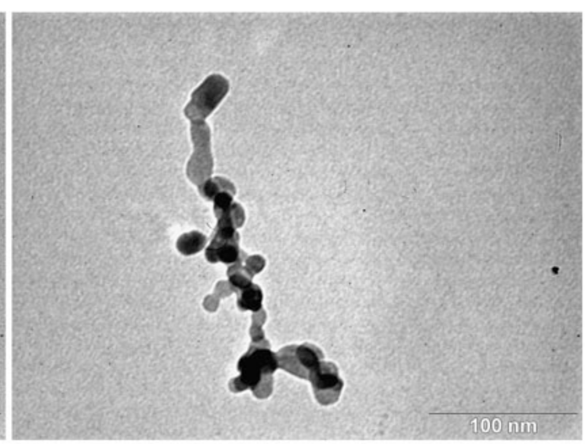

e3_18.tif

undoped SnO_2 for Yen-Hung's analysis (Prof. Sastry's student)

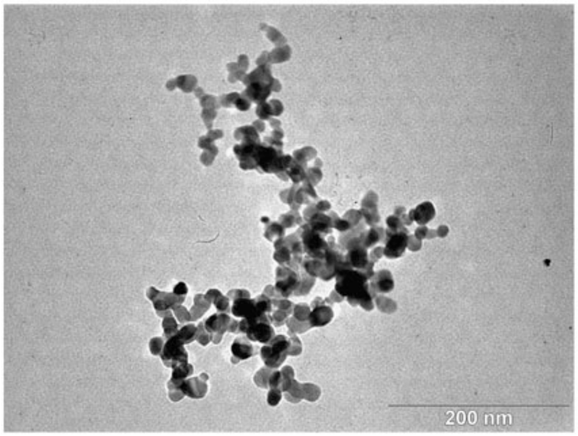

e3_19.tif

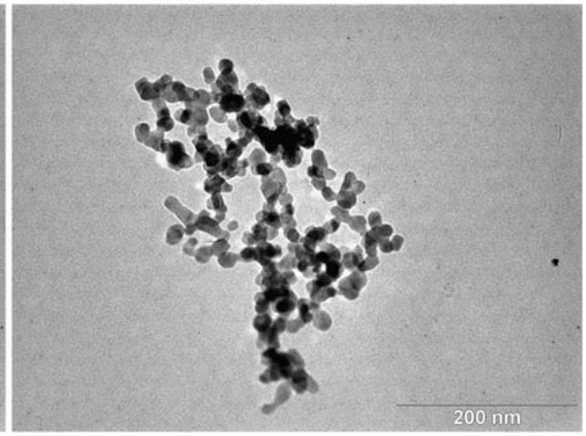

e3_20.tif

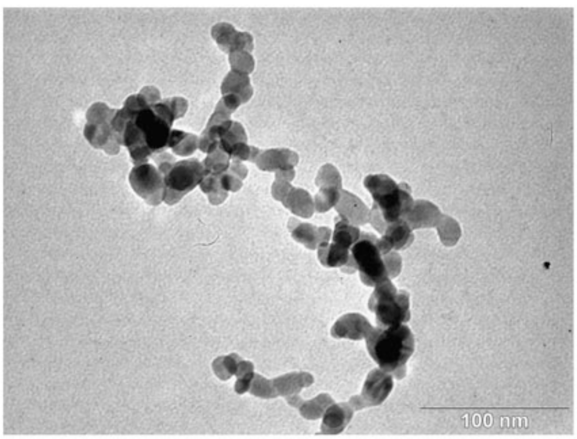

e3_21.tif

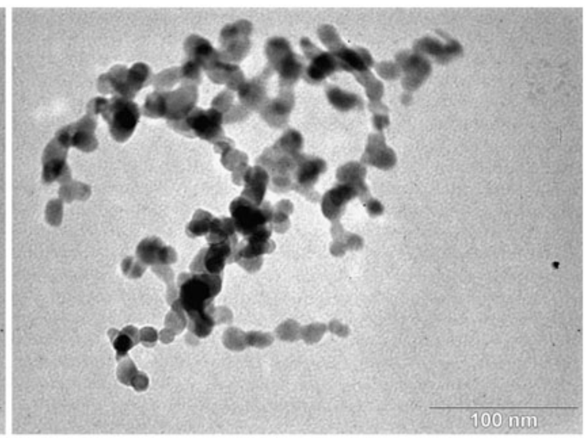

e3_22.tif

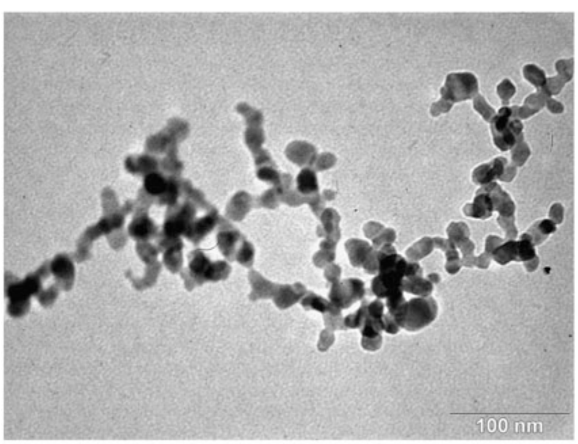

e3_23.tif

undoped SnO_2 for Yen-Hung's analysis (Prof. Sastry's student)

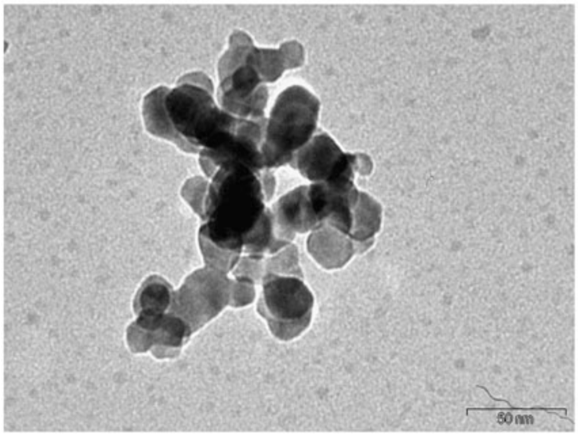

a3_a0.tif

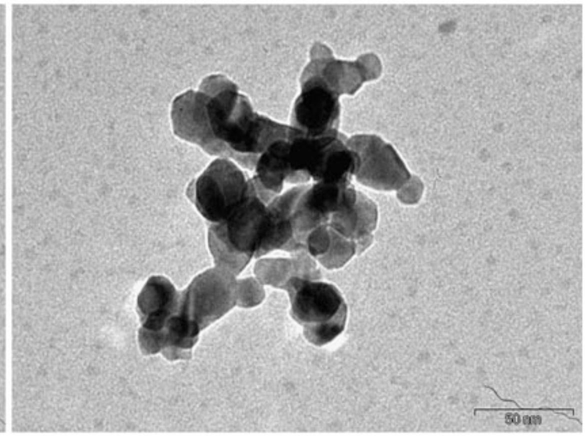

a3_an10.tif

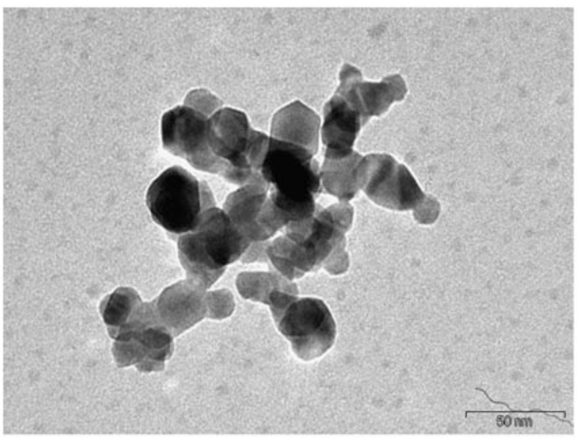

a3_an20.tif

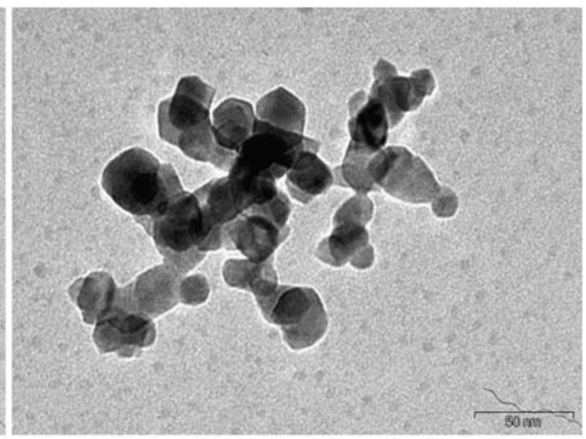

a3_an30.tif

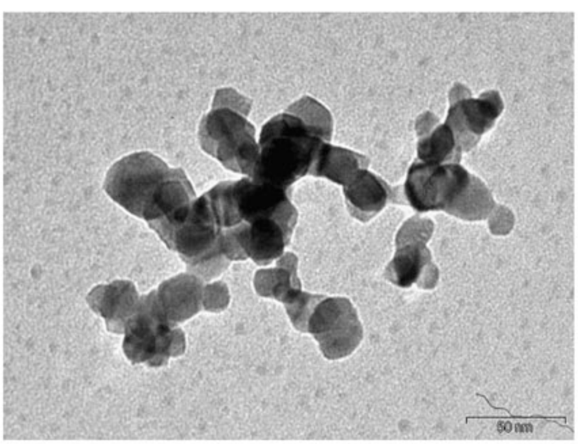

a3_an40.tif

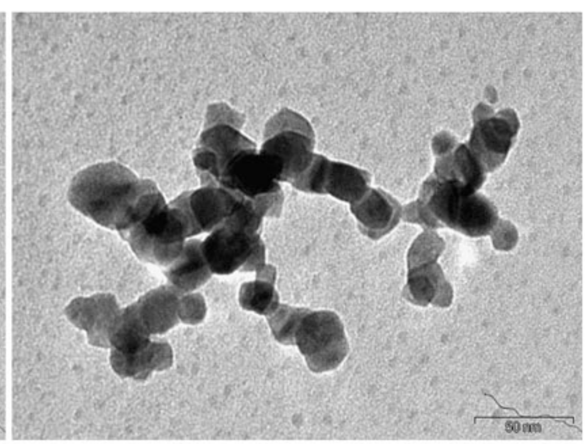

a3_an50.tif

undoped SnO_2 for Yen-Hung's analysis (Prof. Sastry's student)

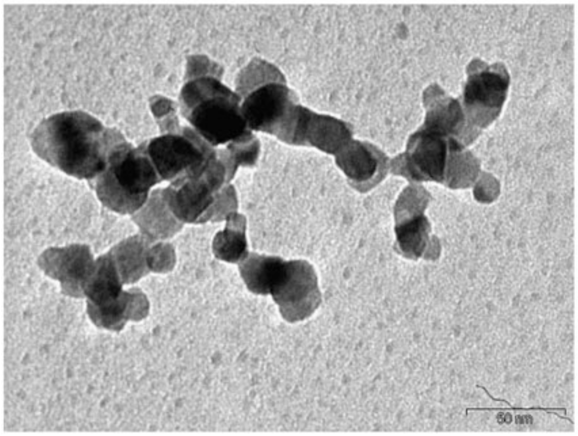

a3_an55.tif

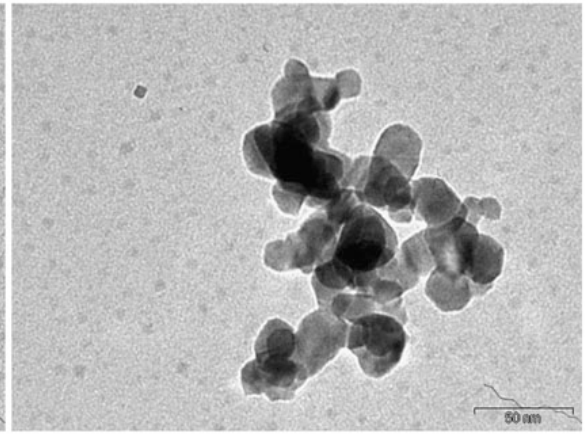

a3_ap10.tif

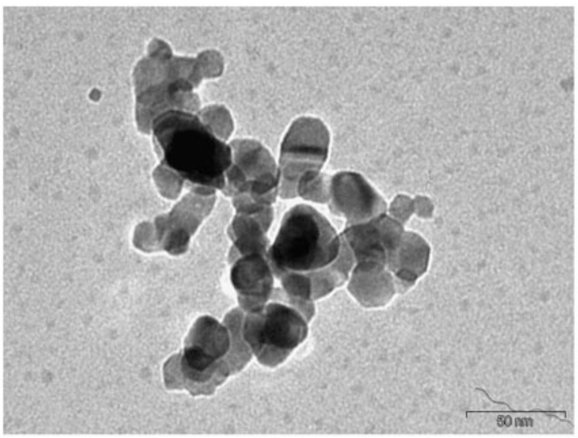

a3_ap20.tif

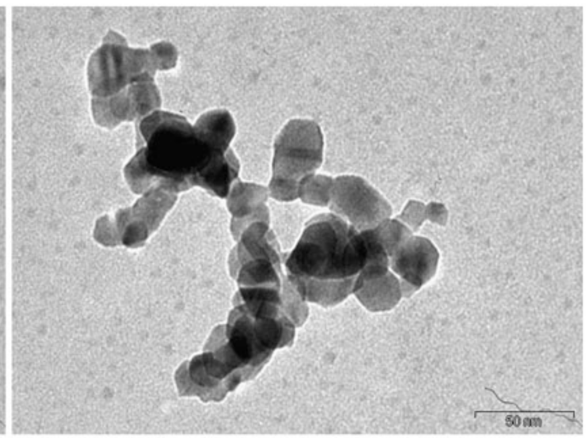

a3_ap30.tif

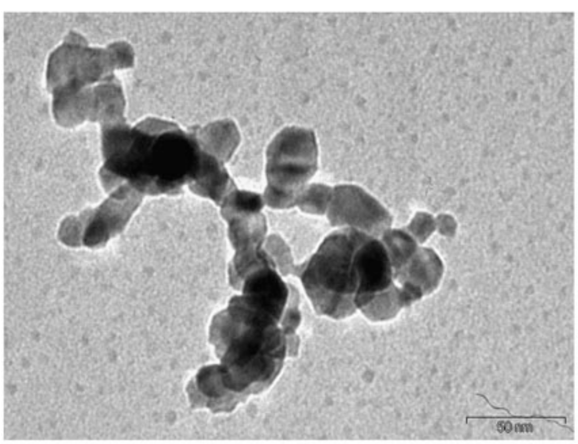

a3_ap40.tif

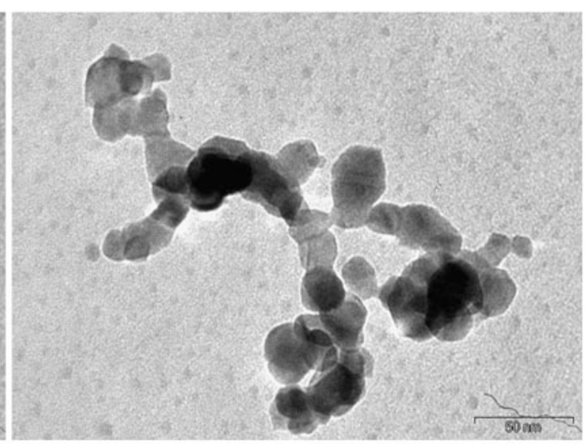

a3_ap50.tif

undoped SnO_2 for Yen-Hung's analysis (Prof. Sastry's student)

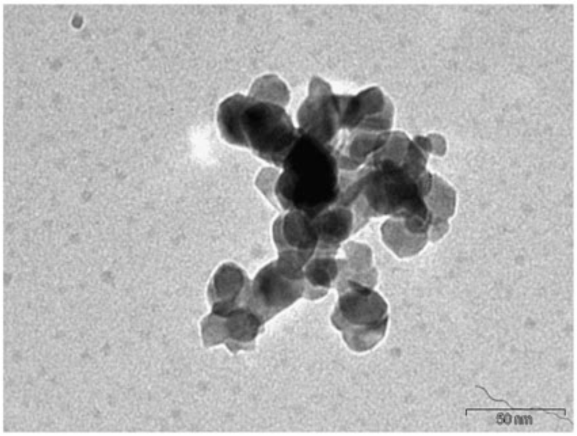

a3_bn10.tif

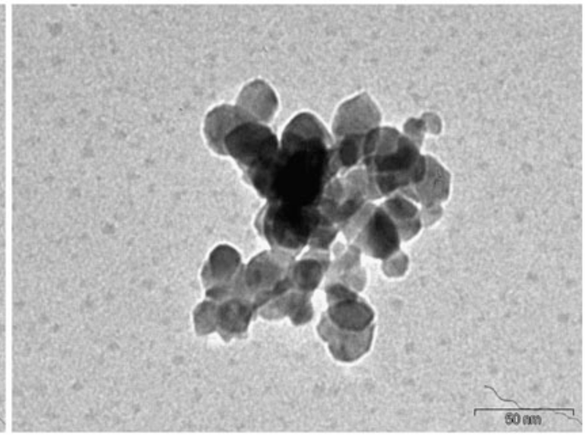

a3_bn20.tif

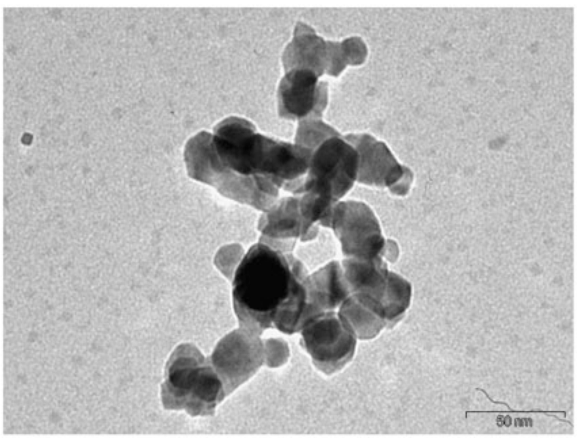

a3_bp10.tif

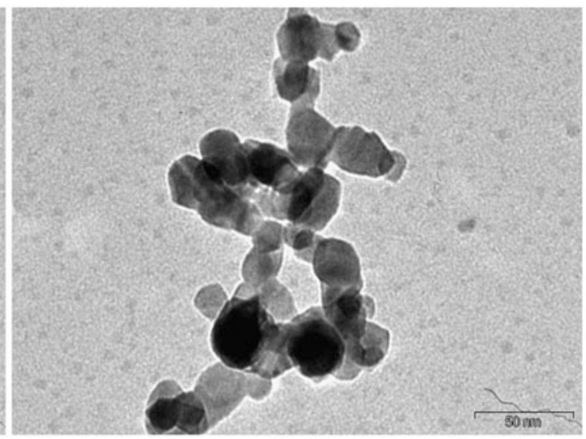

a3_bp20.tif

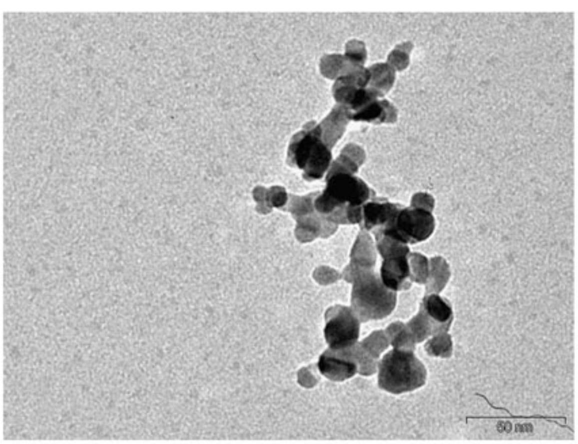

a3_an10.tif

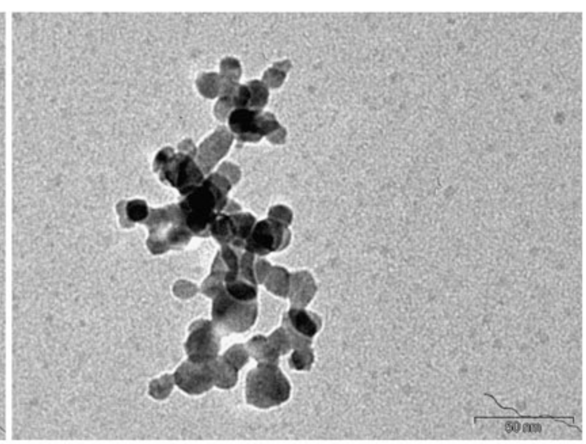

a3_an20.tif

undoped SnO_2 for Yen-Hung's rotational analysis (Prof. Sastry's student)

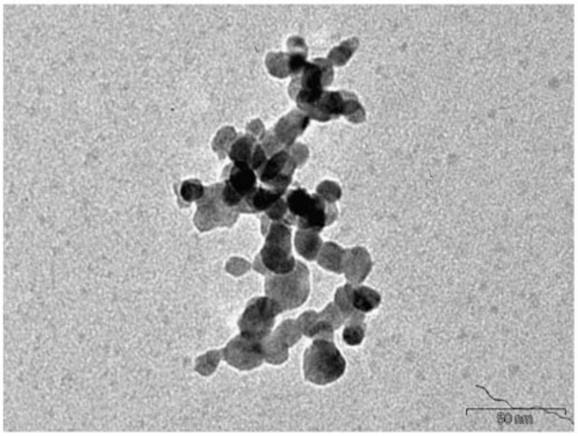

a3_an30.tif

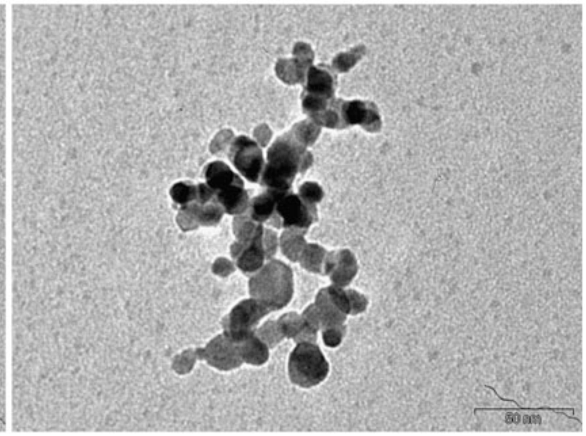

a3_an40.tif

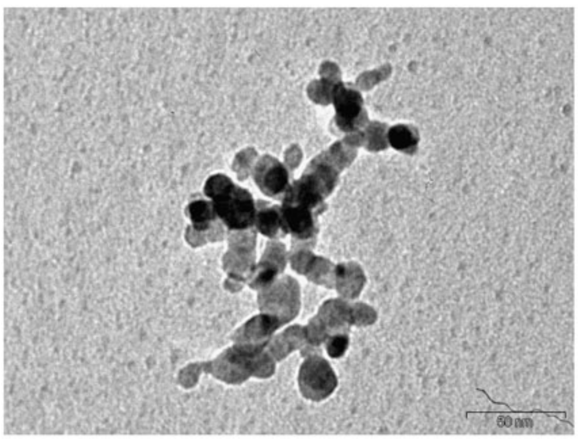

a3_an50.tif

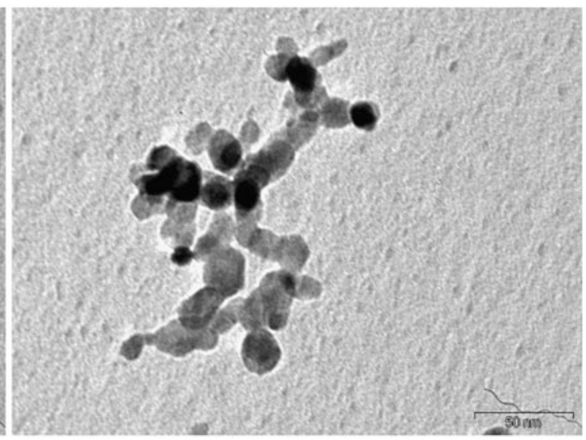

a3_an55.tif

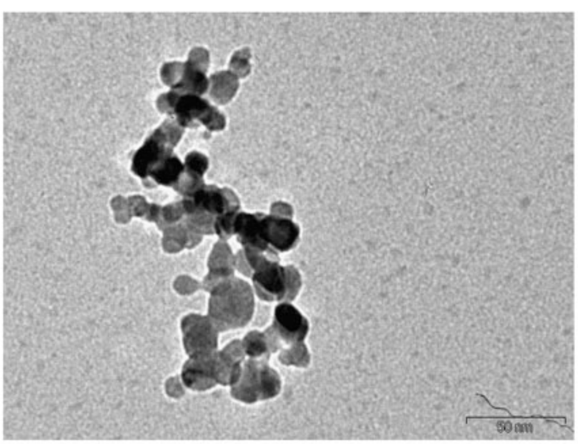

a3_ap0.tif

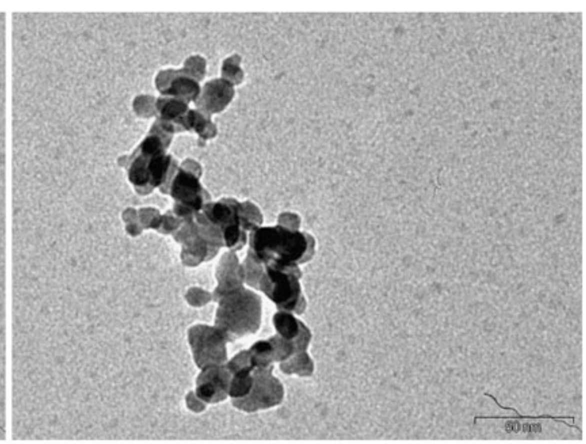

a3_ap10.tif

undoped SnO_2 for Yen-Hung's rotational analysis (Prof. Sastry's student)

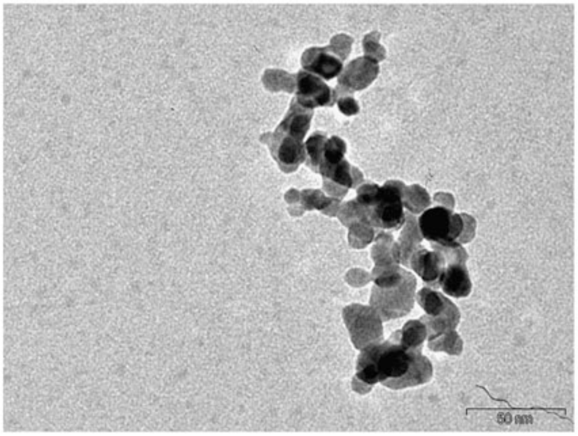

a3_ap20.tif

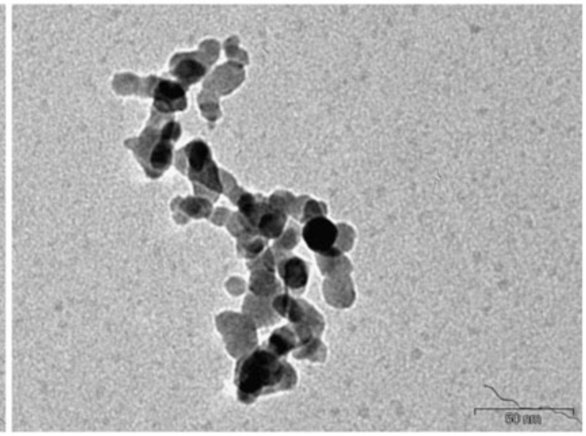

a3_ap30.tif

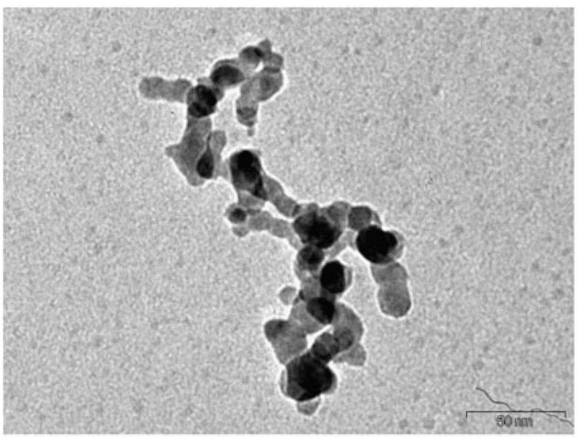

a3_ap40.tif

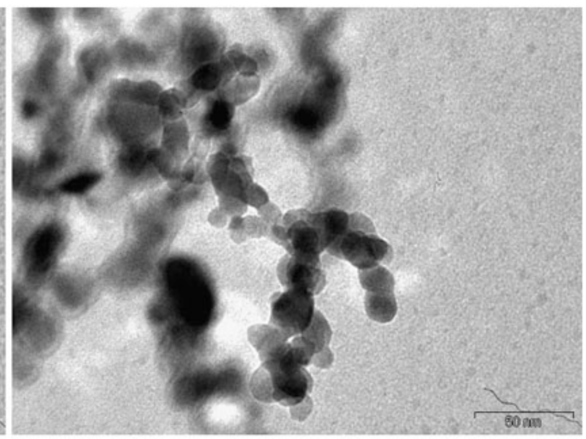

a3_ap50.tif

undoped SnO_2 for Yen-Hung's rotational analysis (Prof. Sastry's student)

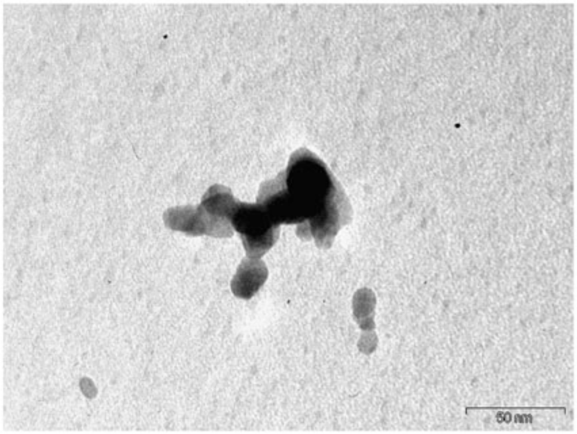

050722a3_001.tif

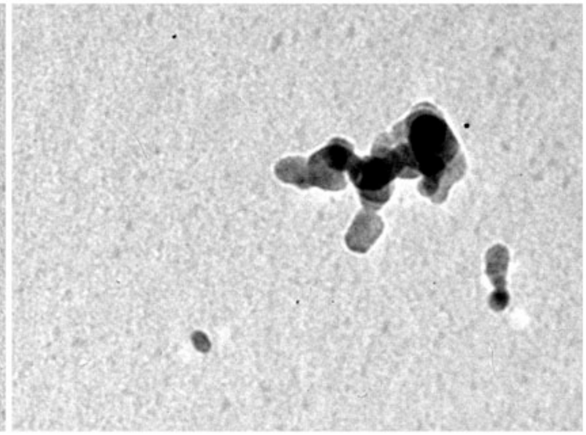

050722a3_002.tif

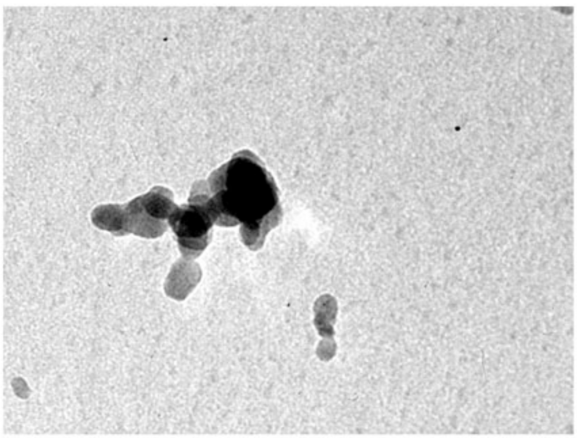

050722a3_003.tif

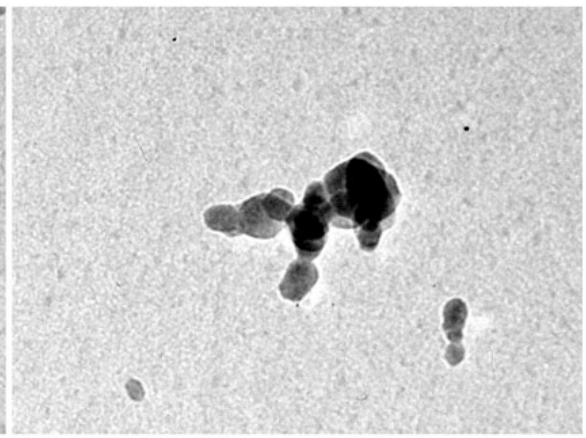

050722a3_004.tif

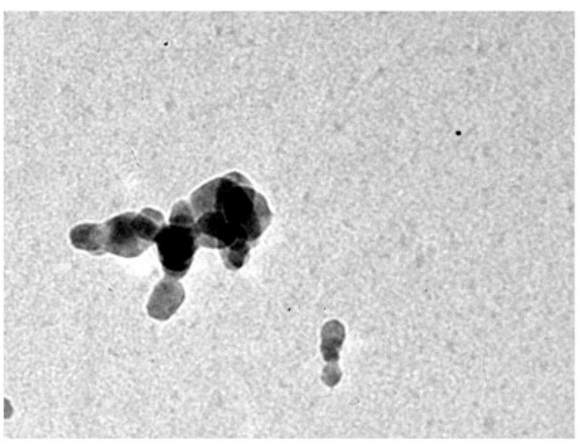

050722a3_005.tif

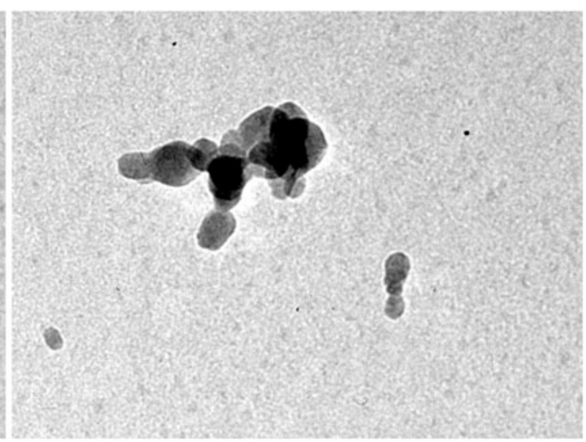

050722a3_006.tif

undoped SnO_2 for Yen-Hung's rotational analysis (Prof. Sastry's student)

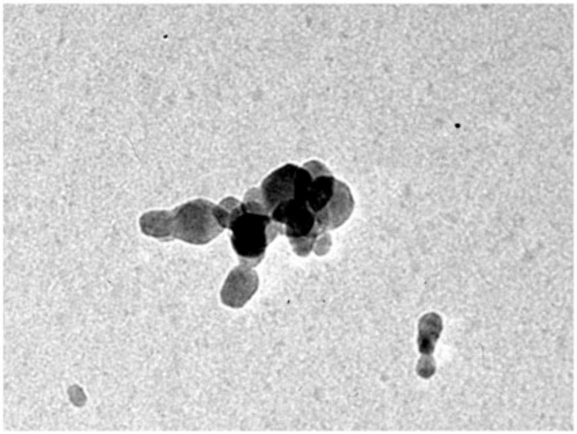

050722a3_007.tif

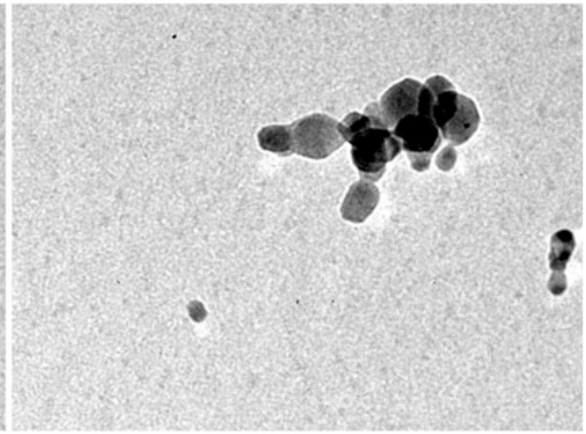

050722a3_008.tif

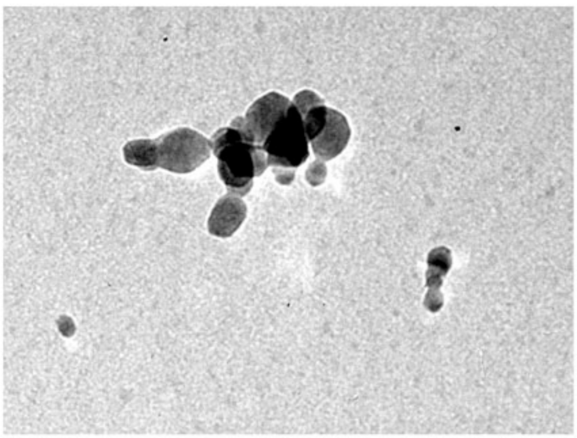

050722a3_009.tif

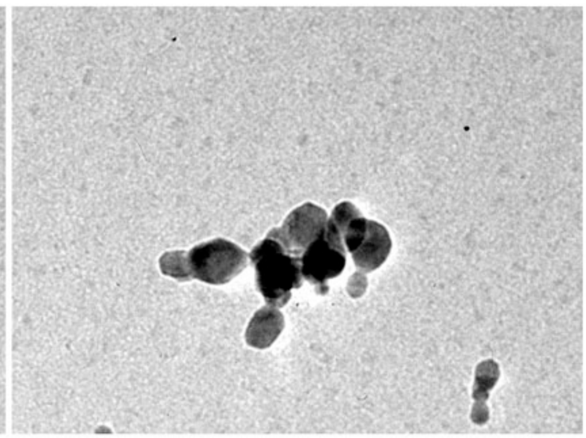

050722a3_010.tif

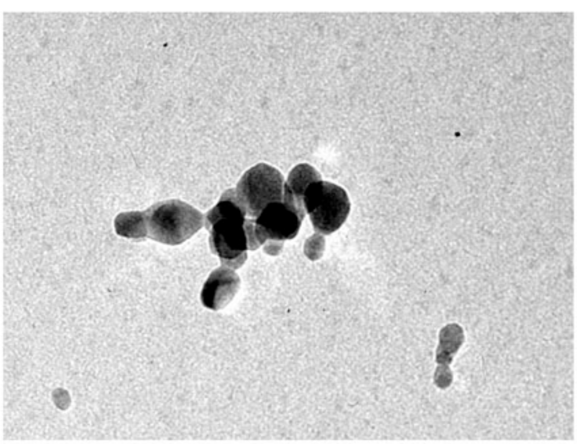

050722a3_011.tif

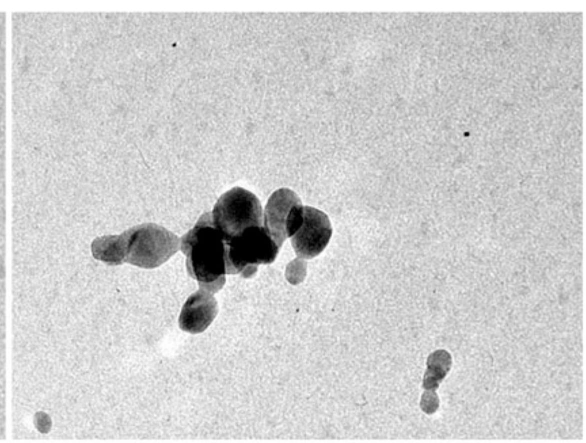

050722a3_012.tif

undoped SnO_2 for Yen-Hung's rotational analysis (Prof. Sastry's student)

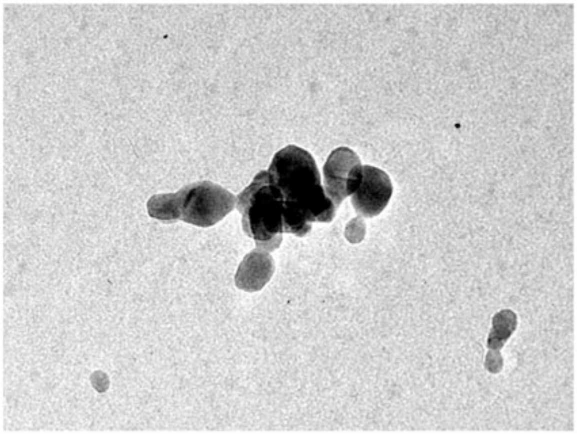

050722a3_013.tif

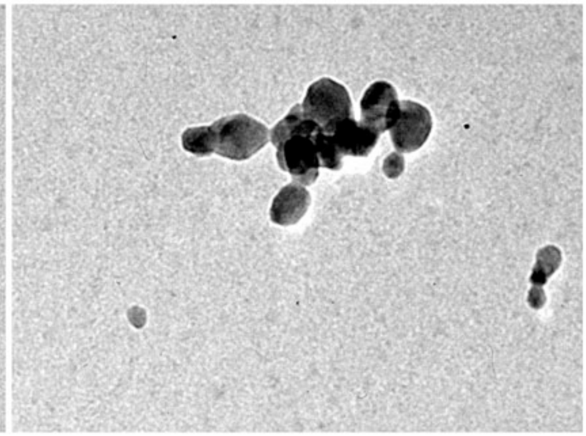

050722a3_014.tif

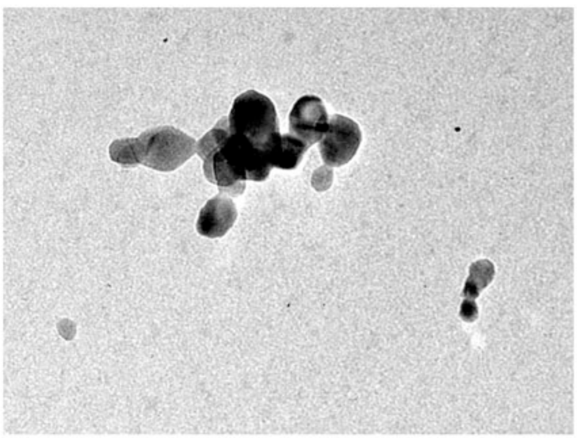

050722a3_015.tif

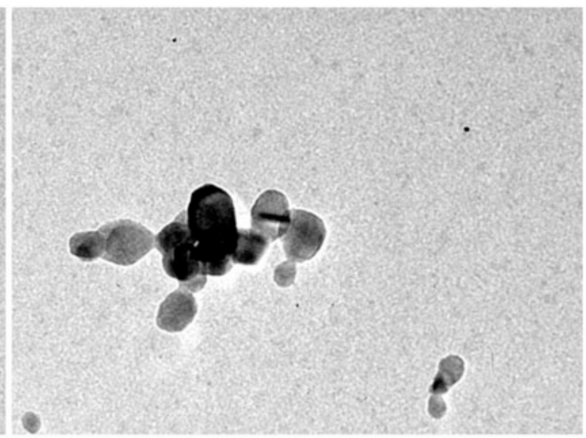

050722a3_016.tif

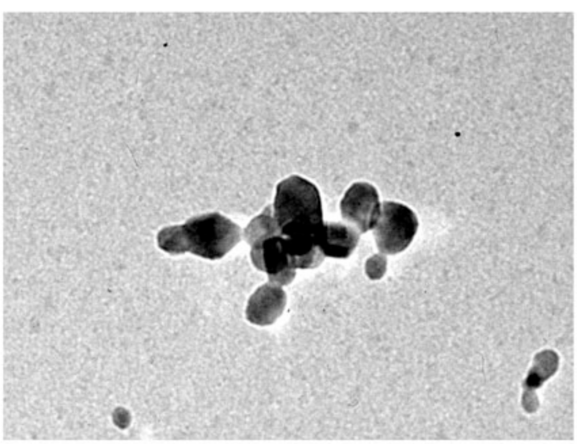

050722a3_017.tif

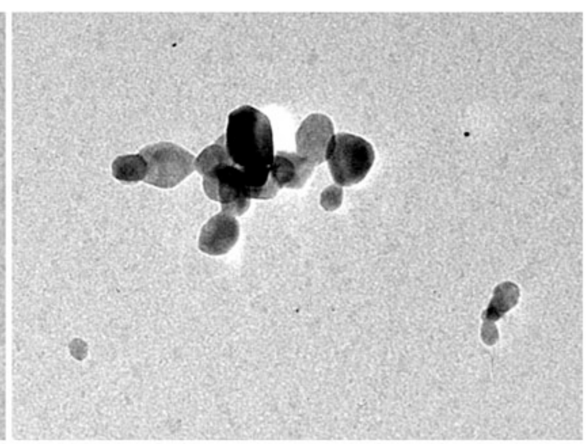

050722a3_018.tif

undoped SnO_2 for Yen-Hung's rotational analysis (Prof. Sastry's student)

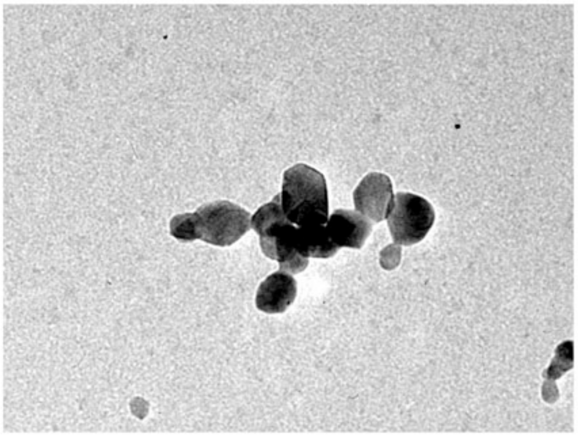

050722a3_019.tif

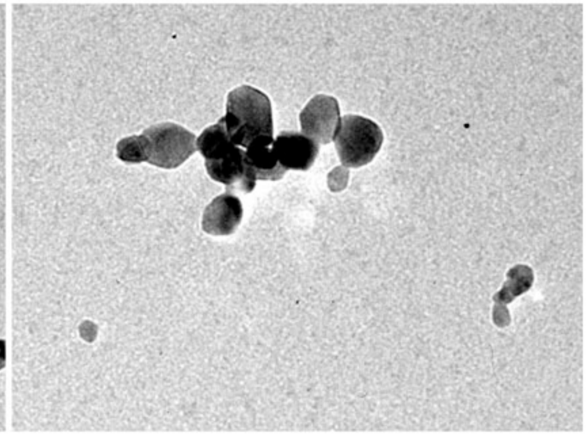

050722a3_020.tif

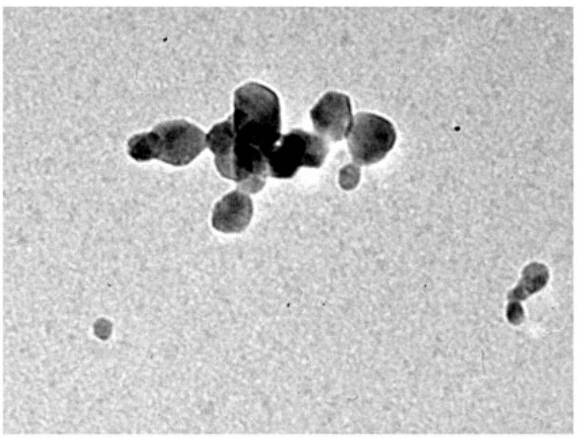

050722a3_021.tif

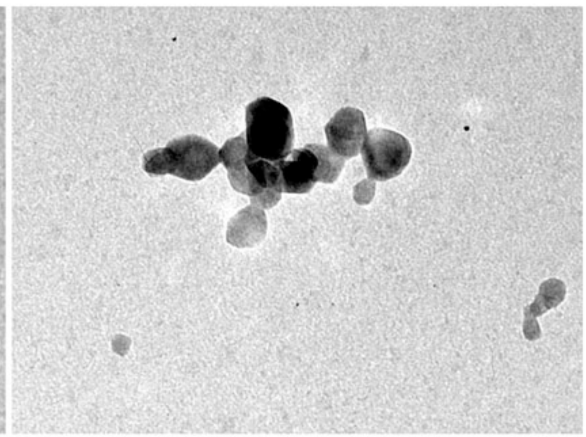

050722a3_022.tif

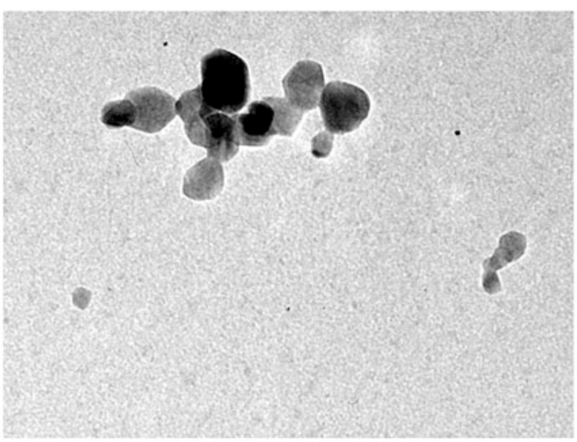

050722a3_023.tif

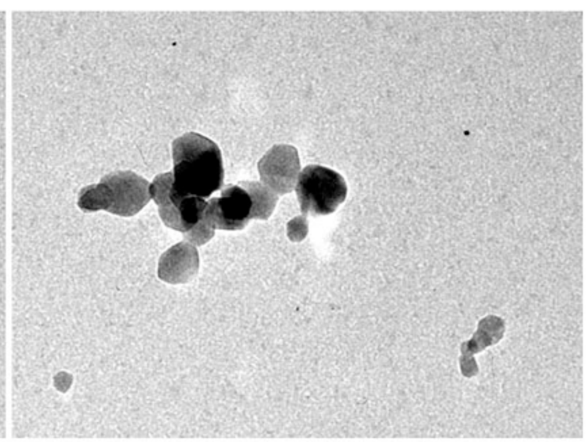

050722a3_024.tif

undoped SnO_2 for Yen-Hung's rotational analysis (Prof. Sastry's student)

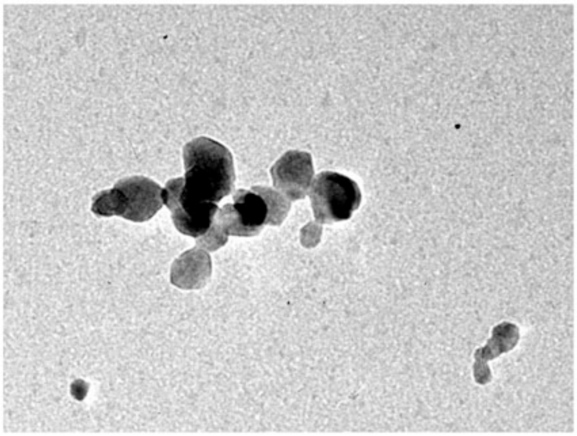

050722a3_025.tif

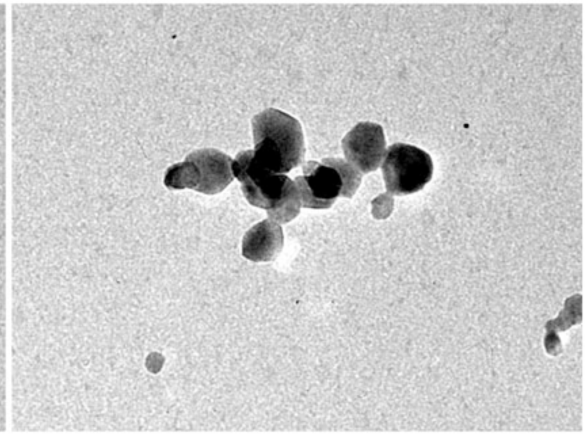

050722a3_026.tif

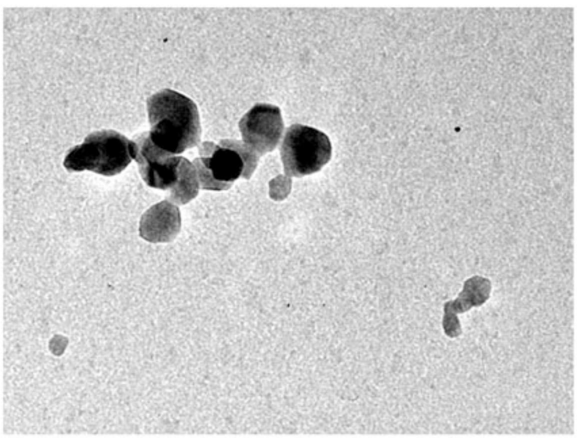

050722a3_027.tif

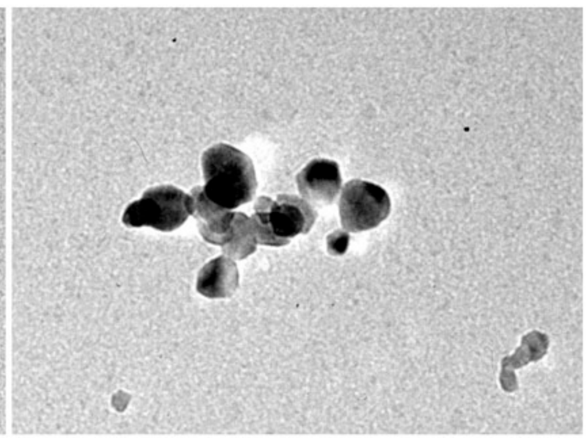

050722a3_028.tif

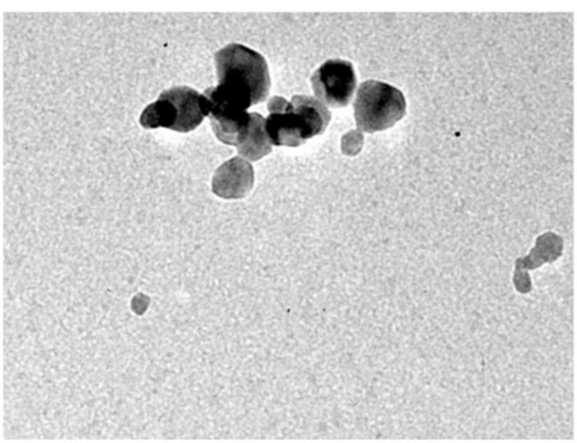

050722a3_029.tif

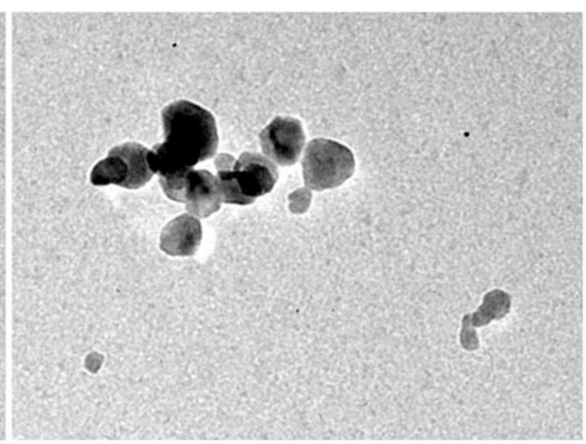

050722a3_030.tif

undoped SnO_2 for Yen-Hung's rotational analysis (Prof. Sastry's student)

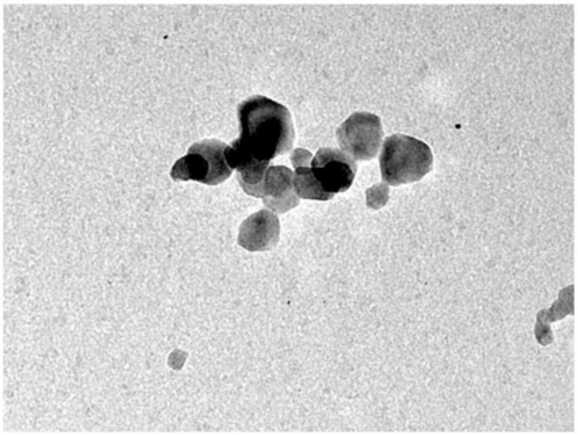

050722a3_031.tif

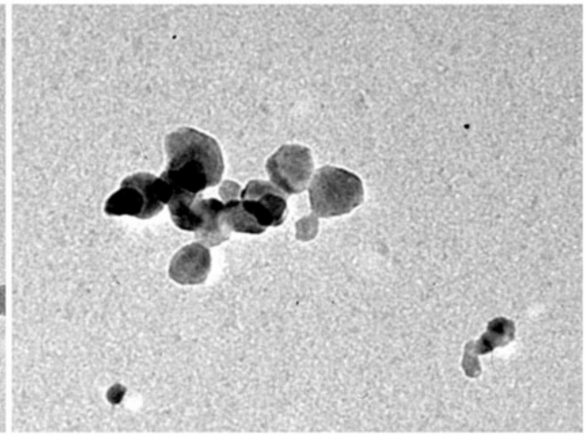

050722a3_032.tif

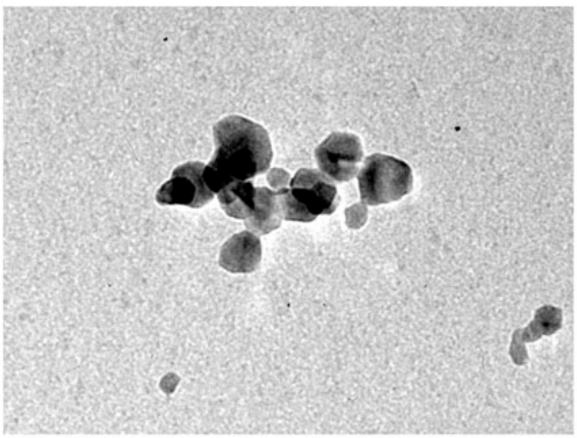

050722a3_033.tif

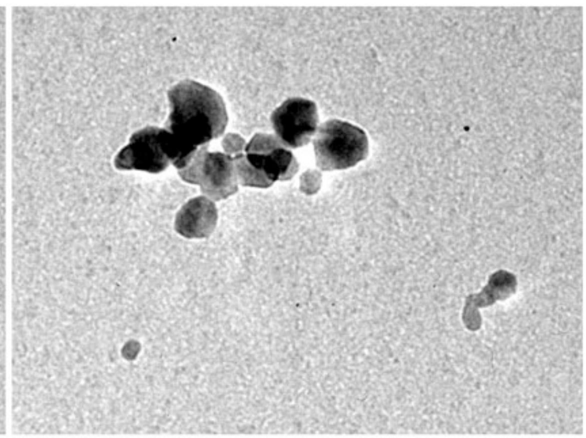

050722a3_034.tif

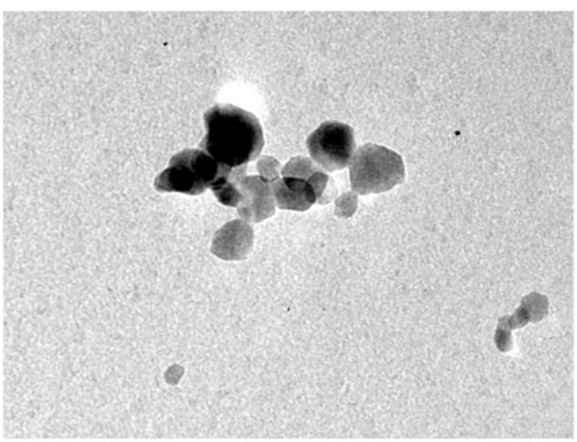

050722a3_035.tif

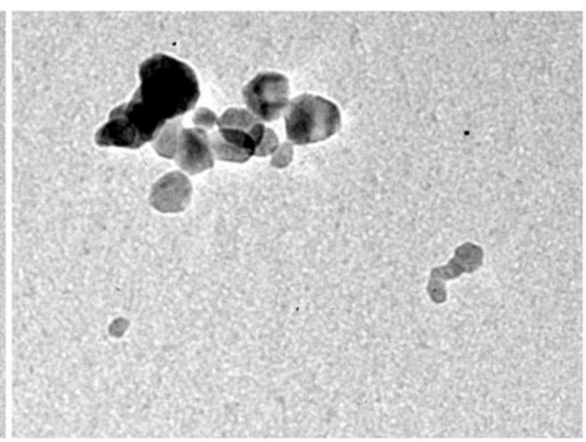

050722a3_036.tif

undoped SnO_2 for Yen-Hung's rotational analysis (Prof. Sastry's student)

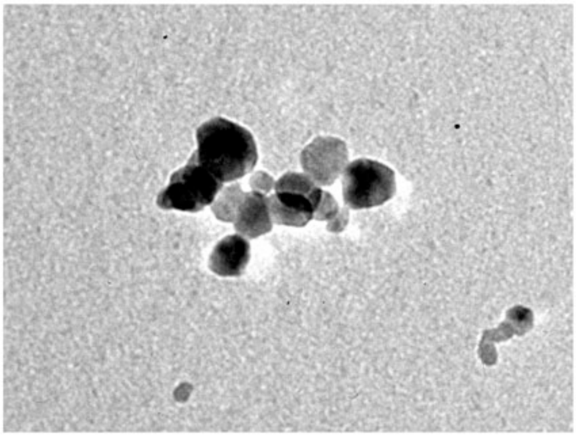

050722a3_037.tif

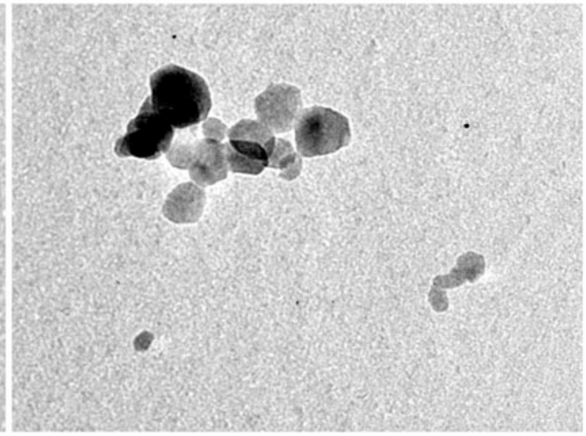

050722a3_038.tif

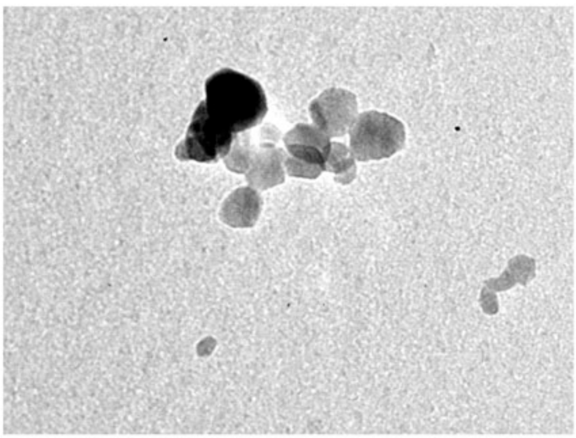

050722a3_039.tif

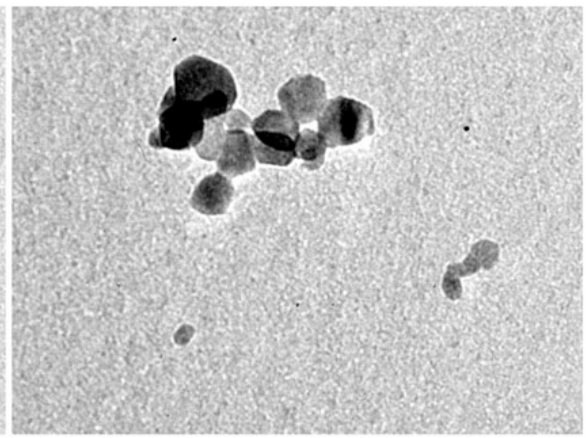

050722a3_040.tif

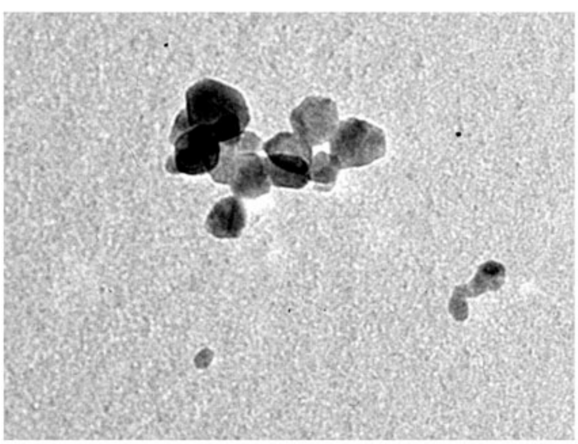

050722a3_041.tif

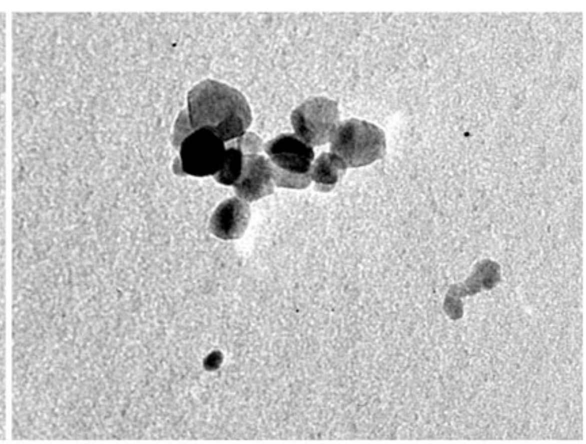

050722a3_042.tif

undoped SnO_2 for Yen-Hung's rotational analysis (Prof. Sastry's student)

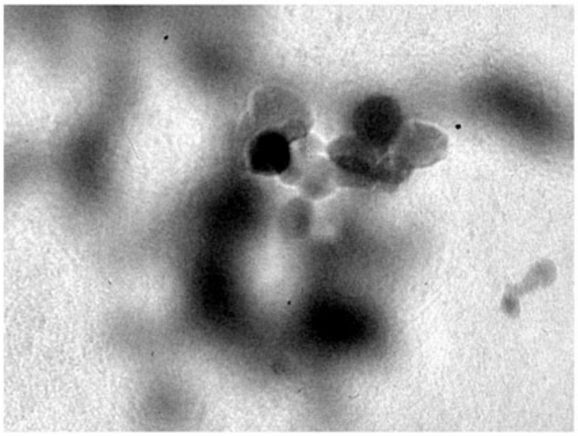

050722a3_043.tif

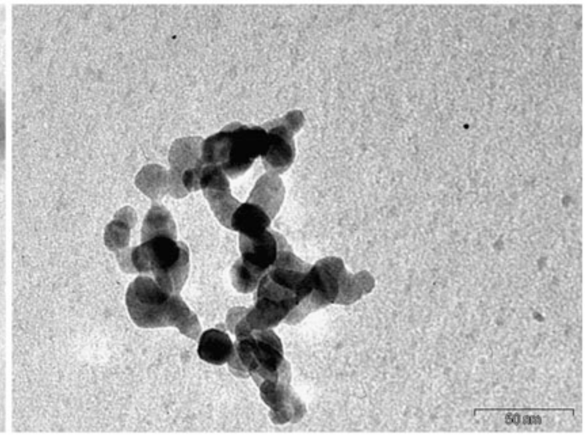

050722a3_001.tif

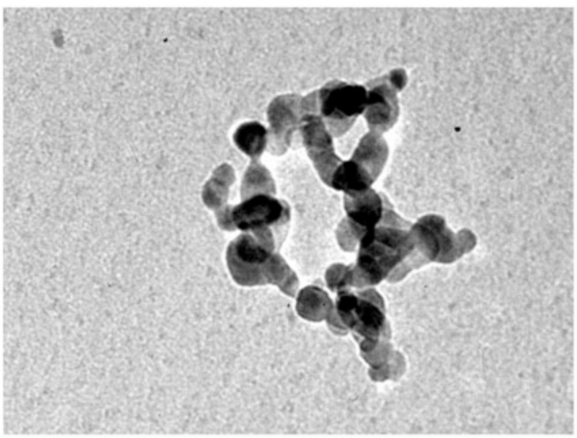

050722a3_002.tif

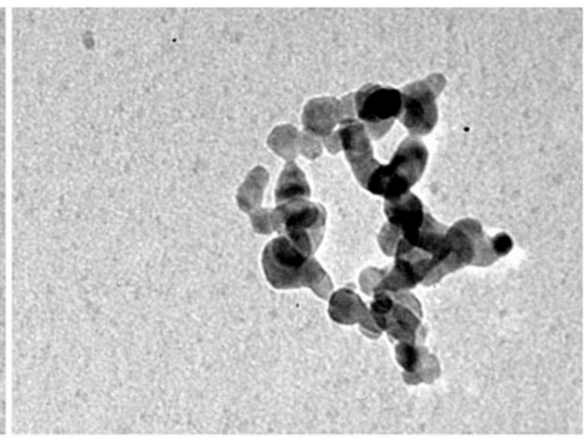

050722a3_003.tif

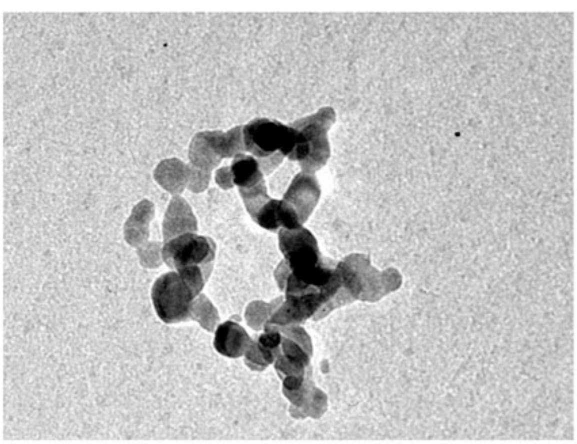

050722a3_004.tif

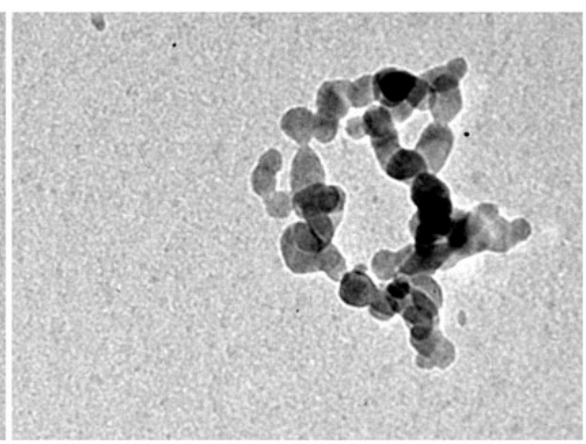

050722a3_005.tif

undoped SnO_2 for Yen-Hung's rotational analysis (Prof. Sastry's student)

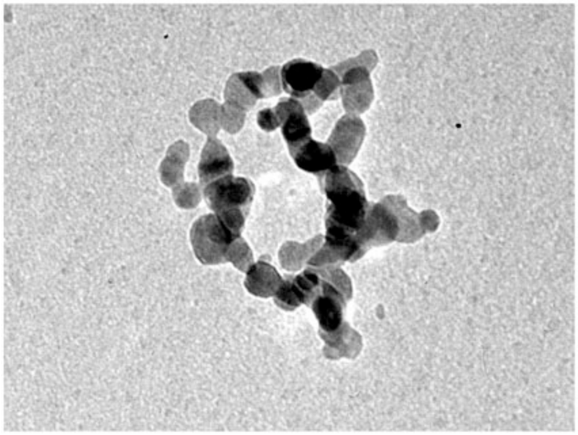

050722a3_006.tif

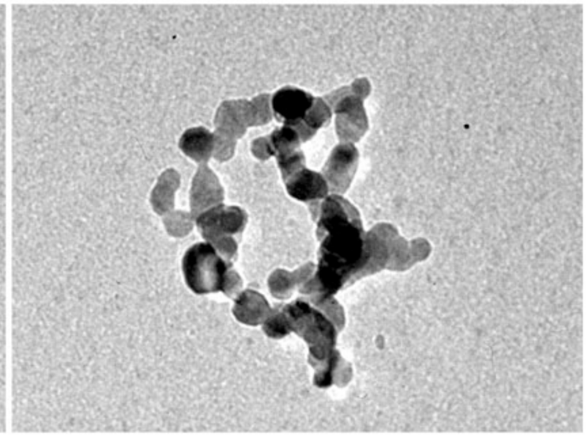

050722a3_007.tif

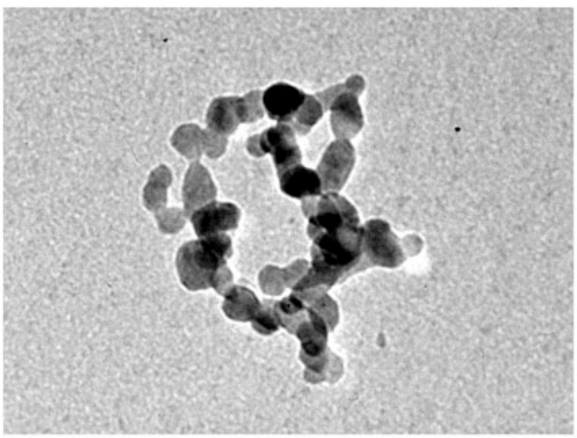

050722a3_008.tif

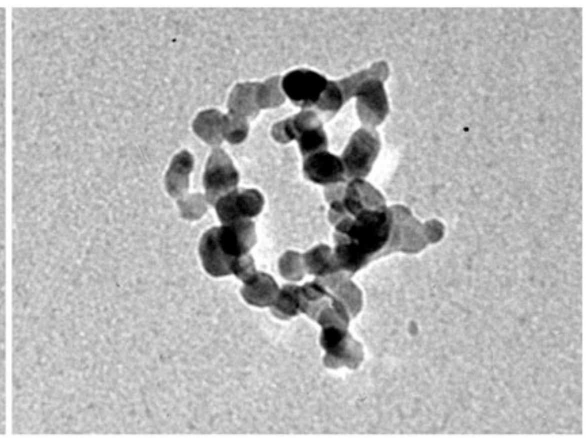

050722a3_009.tif

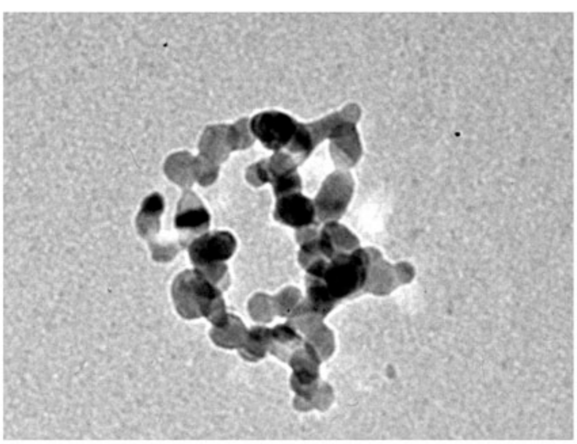

050722a3_010.tif

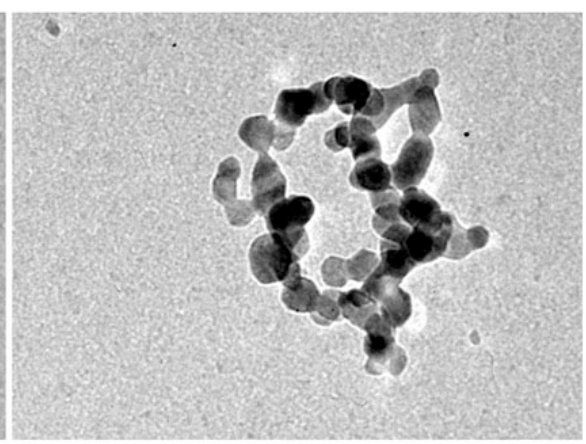

050722a3_011.tif

undoped SnO_2 for Yen-Hung's rotational analysis (Prof. Sastry's student)

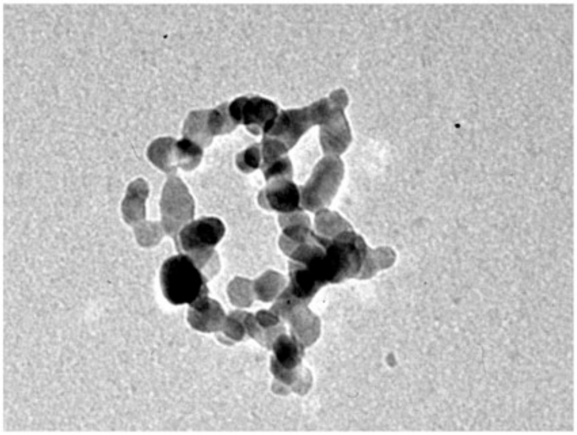

050722a3_012.tif

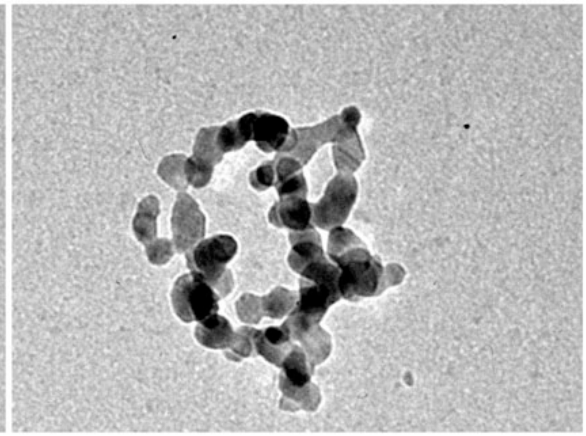

050722a3_013.tif

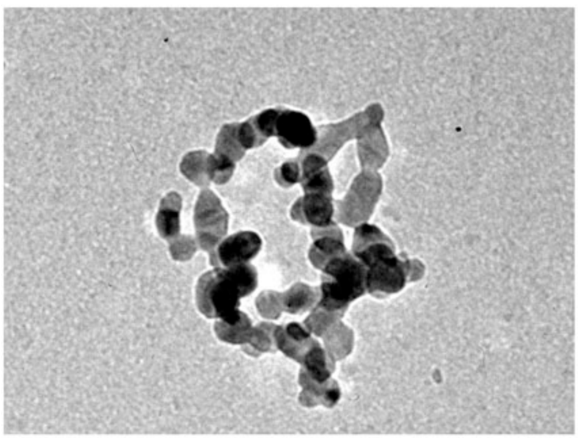

050722a3_014.tif

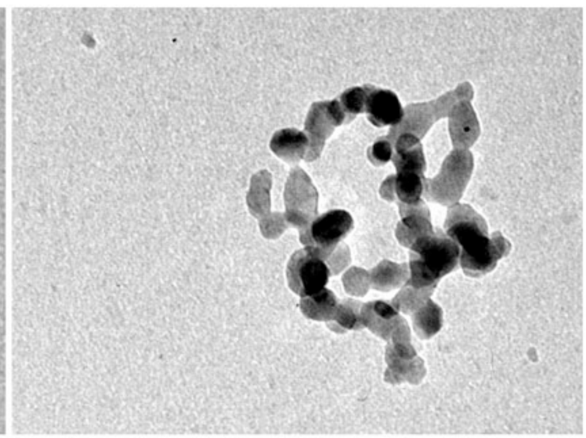

050722a3_015.tif

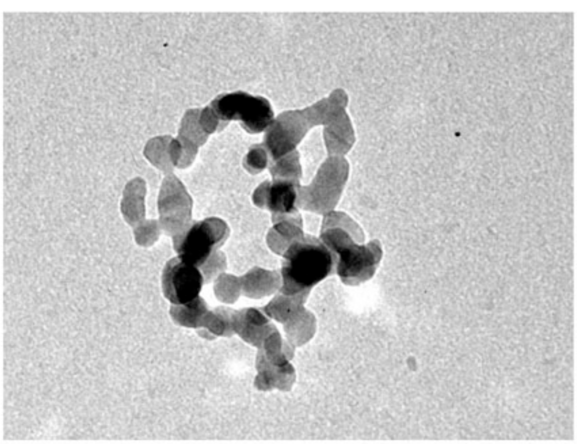

050722a3_016.tif

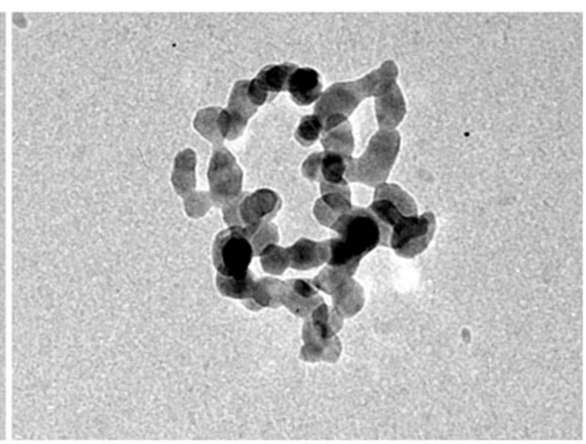

050722a3_017.tif

undoped SnO_2 for Yen-Hung's rotational analysis (Prof. Sastry's student)

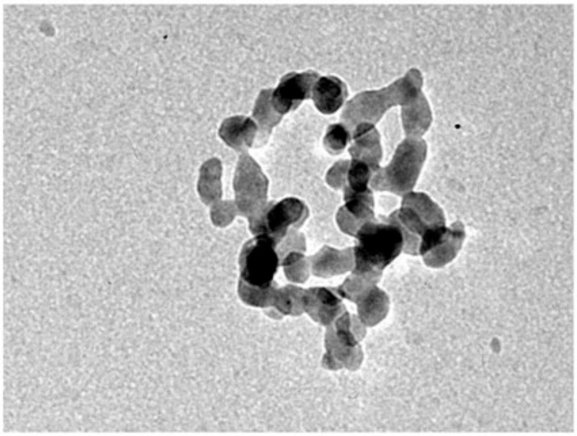

050722a3_018.tif

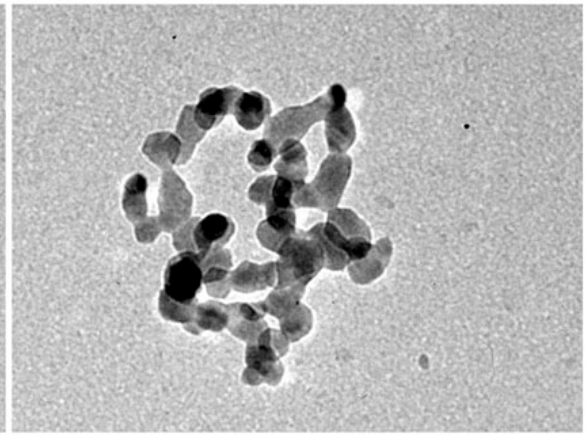

050722a3_019.tif

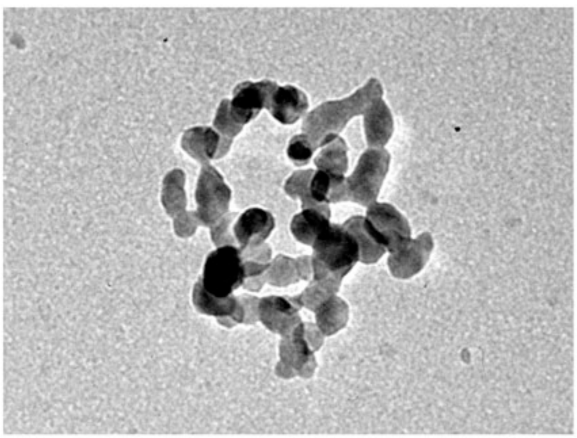

050722a3_020.tif

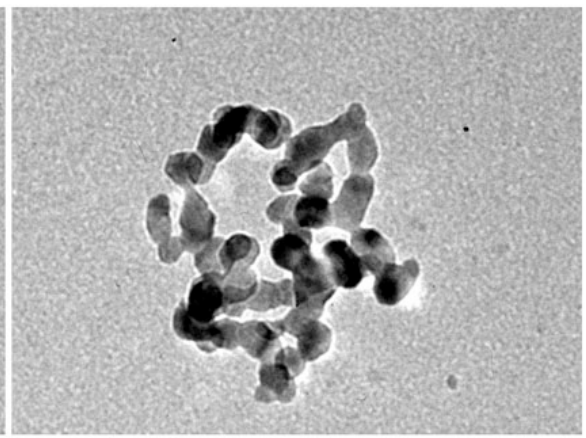

050722a3_021.tif

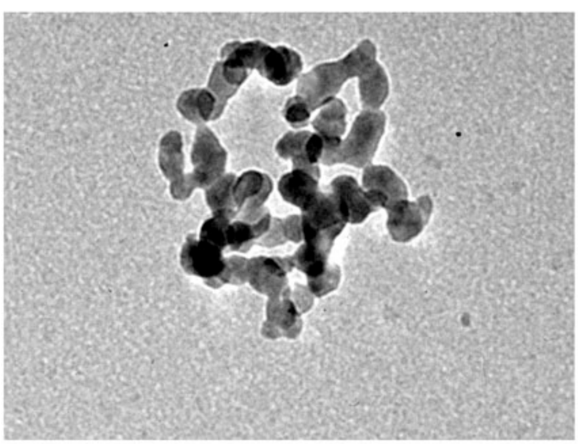

050722a3_022.tif

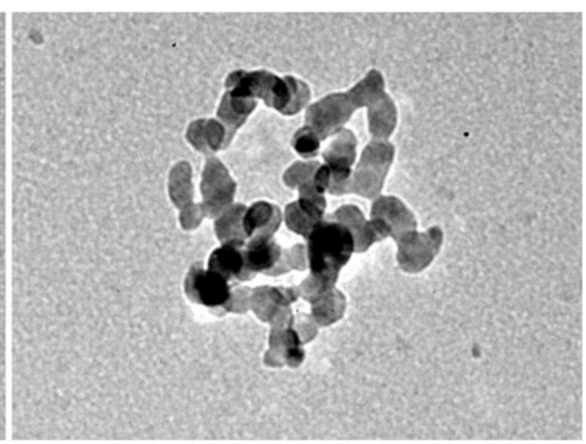

050722a3_023.tif

undoped SnO_2 for Yen-Hung's rotational analysis (Prof. Sastry's student)

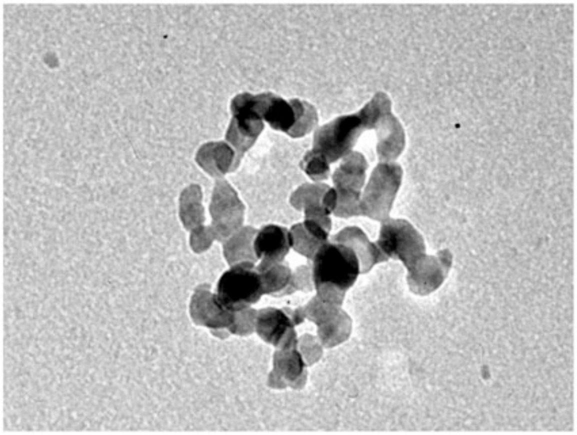

050722a3_024.tif

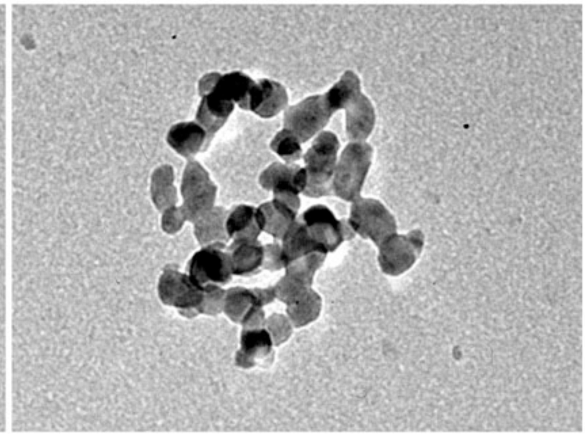

050722a3_025.tif

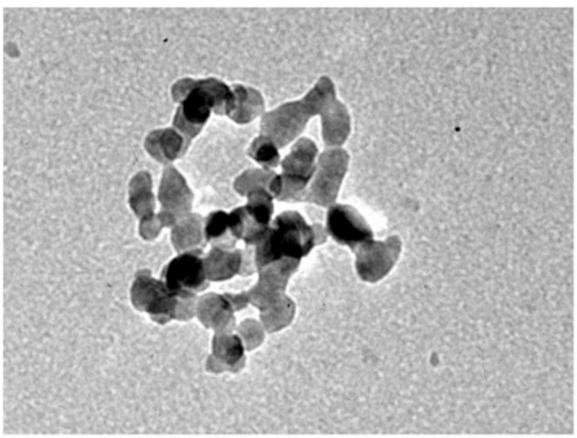

050722a3_026.tif

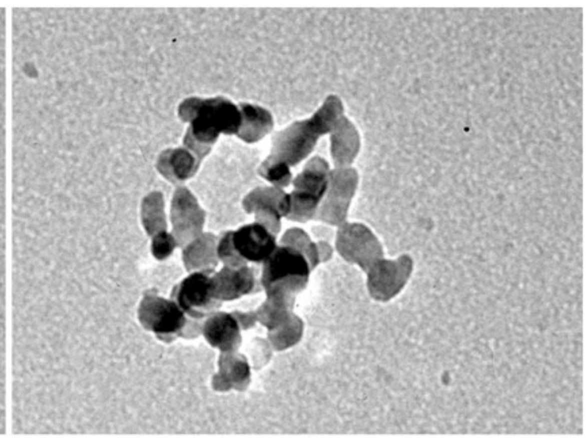

050722a3_027.tif

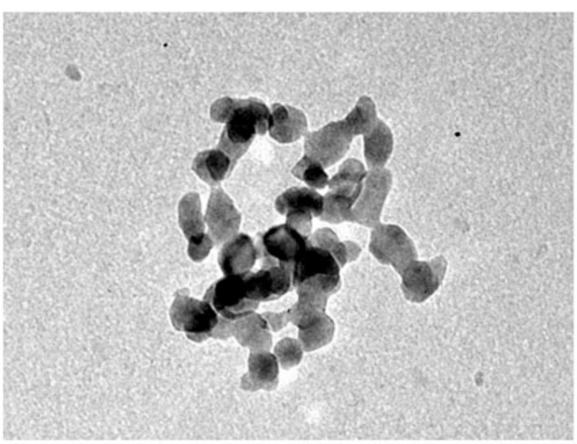

050722a3_028.tif

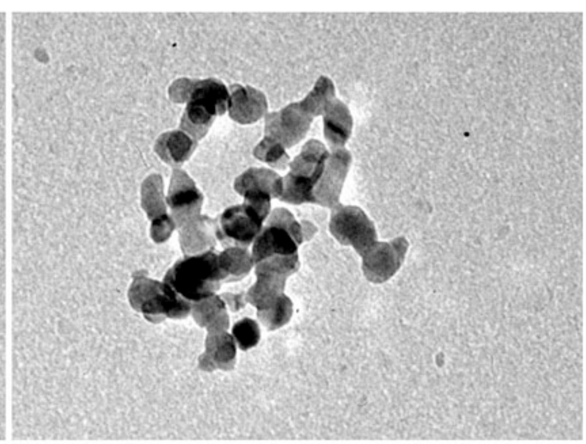

050722a3_029.tif

undoped SnO_2 for Yen-Hung's rotational analysis (Prof. Sastry's student)

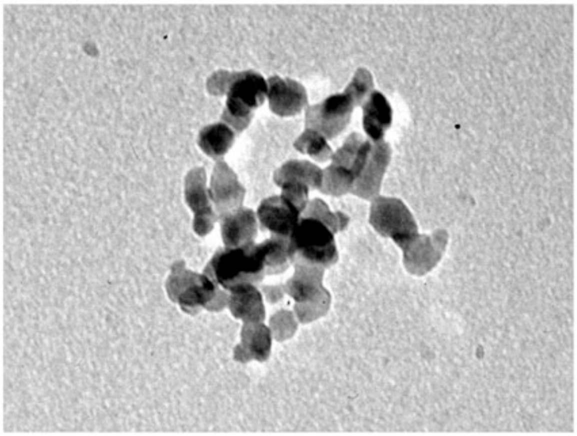

050722a3_030.tif

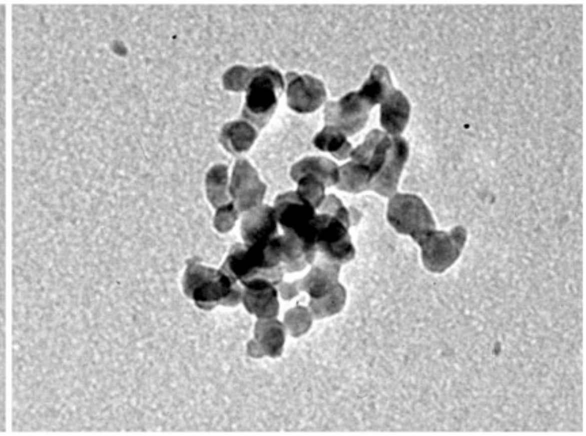

050722a3_031.tif

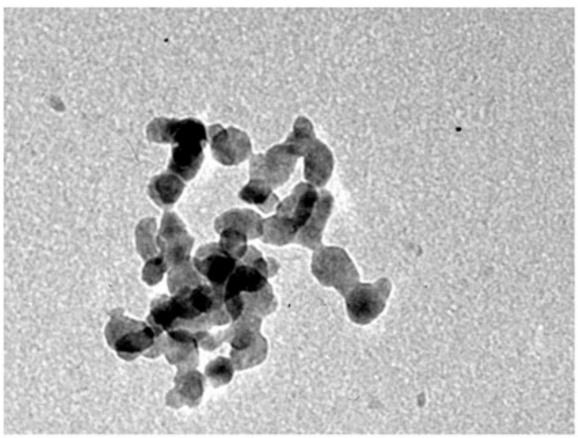

050722a3_032.tif

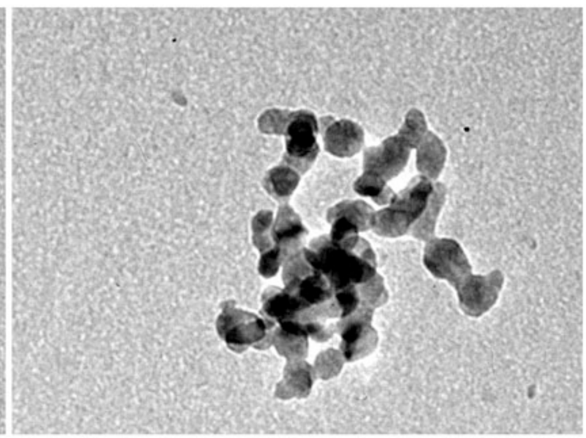

050722a3_033.tif

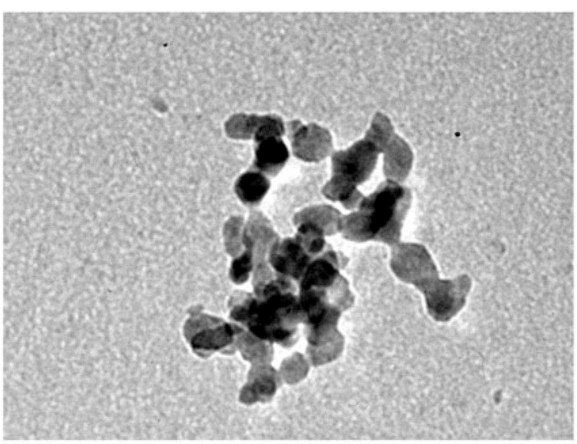

050722a3_034.tif

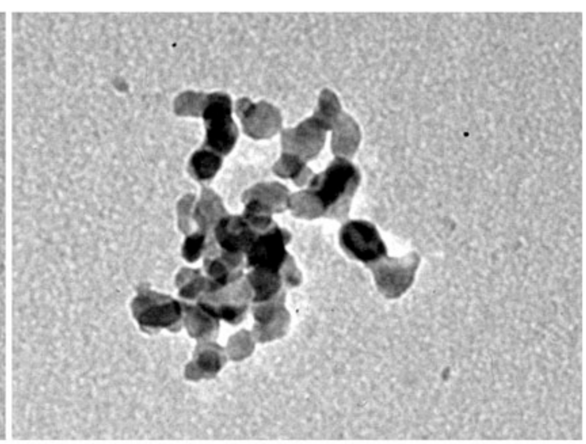

050722a3_035.tif

undoped SnO_2 for Yen-Hung's rotational analysis (Prof. Sastry's student)

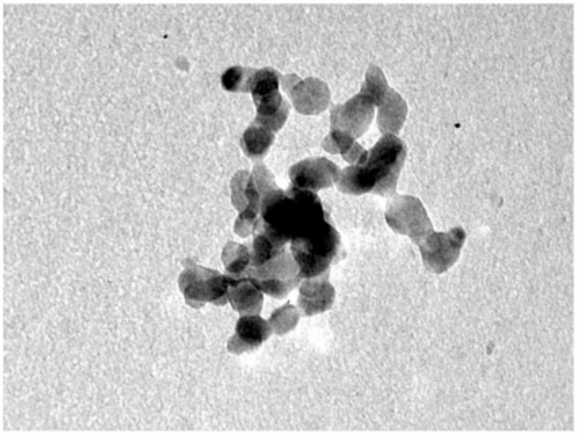

050722a3_036.tif

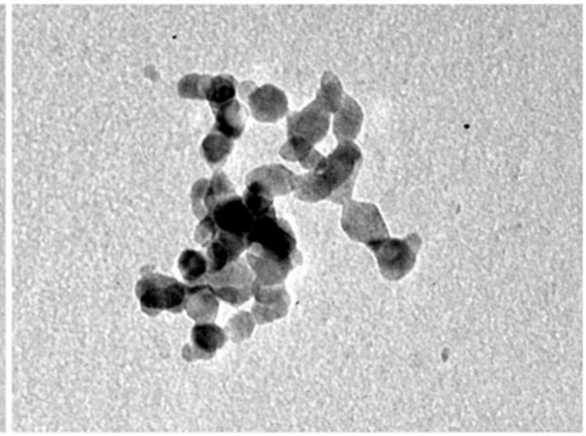

050722a3_037.tif

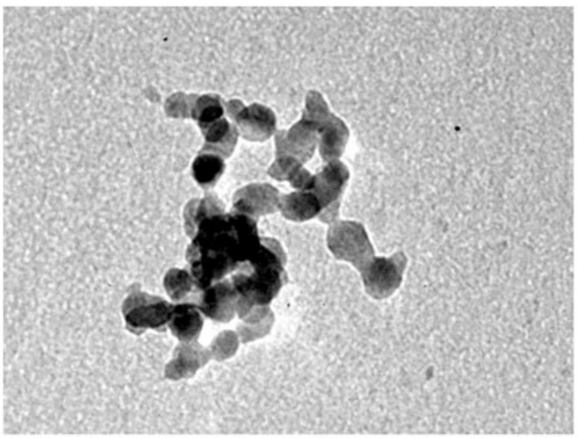

050722a3_038.tif

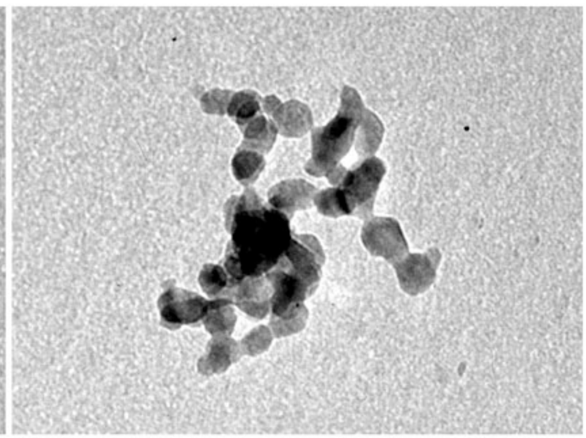

050722a3_039.tif

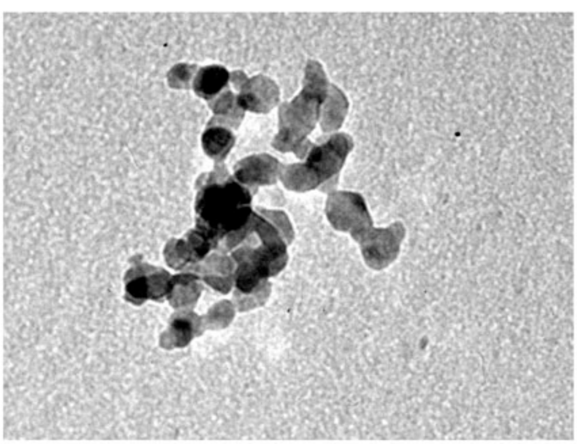

050722a3_040.tif

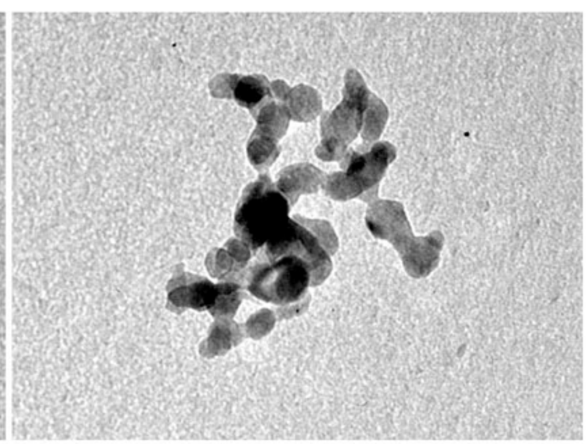

050722a3_041.tif

undoped SnO_2 for Yen-Hung's rotational analysis (Prof. Sastry's student)

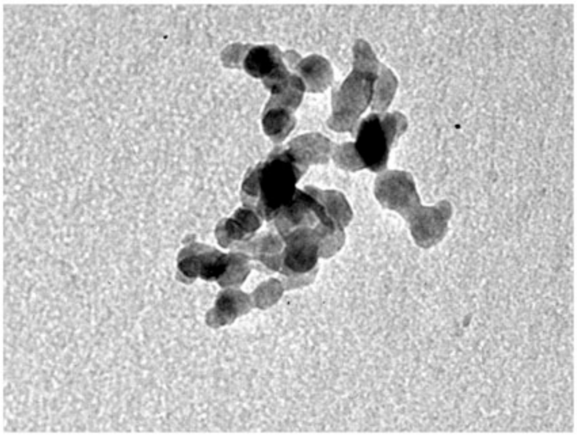

050722a3_042.tif

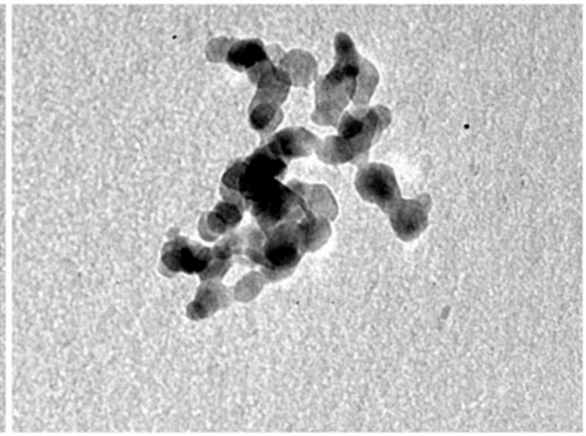

050722a3_043.tif

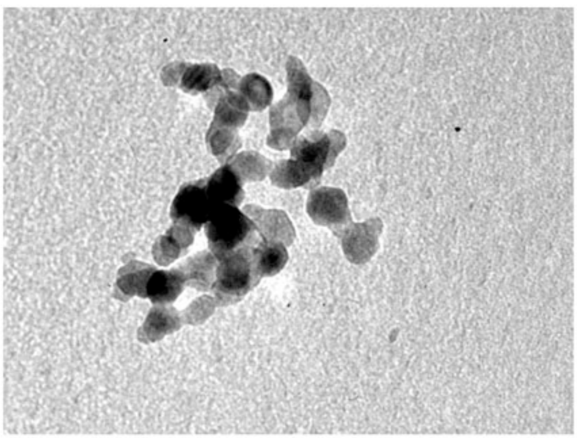

050722a3_044.tif

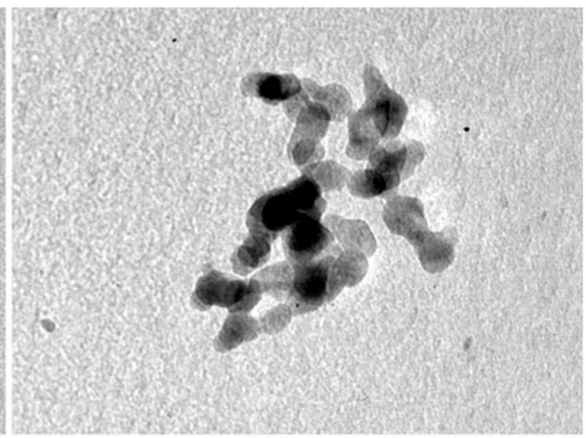

050722a3_045.tif

MACS undoped SnO_2

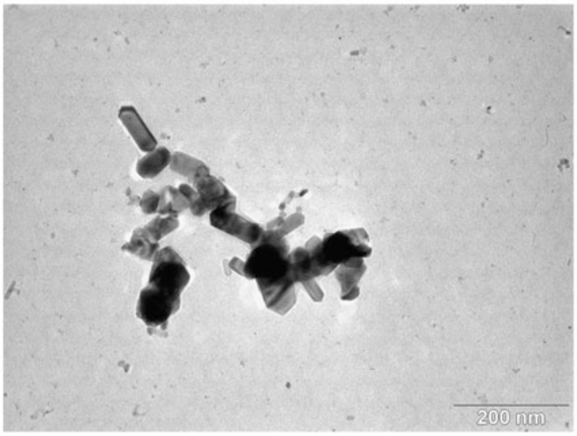

050520-c8-01.tif

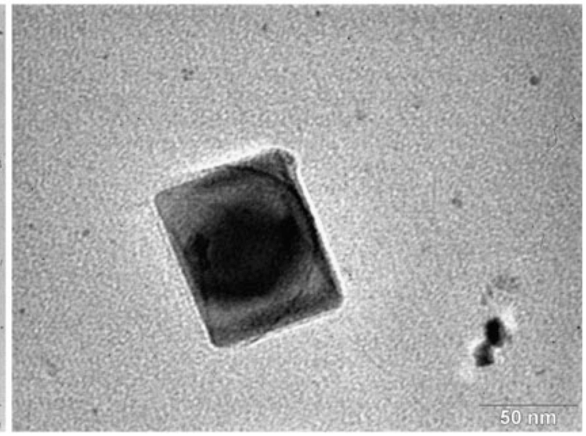

050520-c8-02.tif

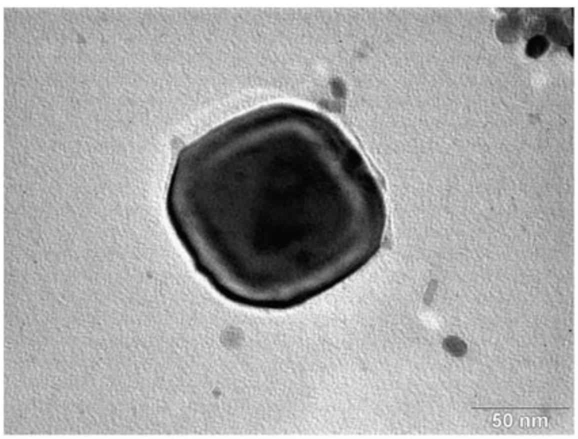

050520-c8-03.tif

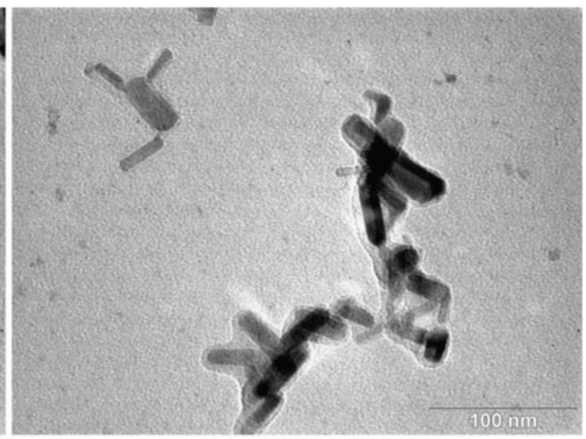

050520-c8-04.tif

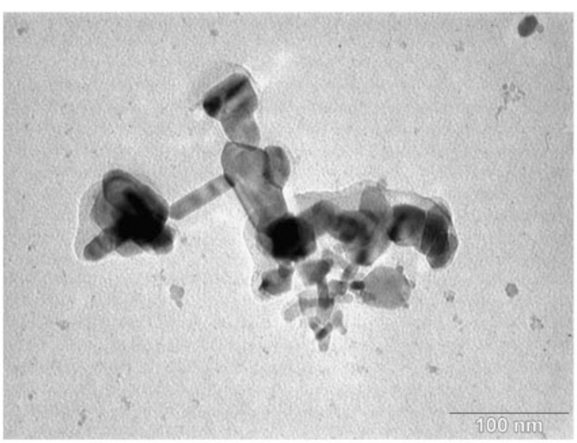

050520-c8-05.tif

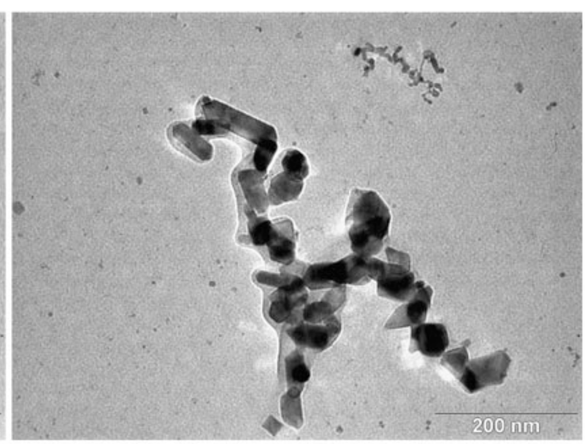

050520-c8-06.tif

MACS undoped SnO_2

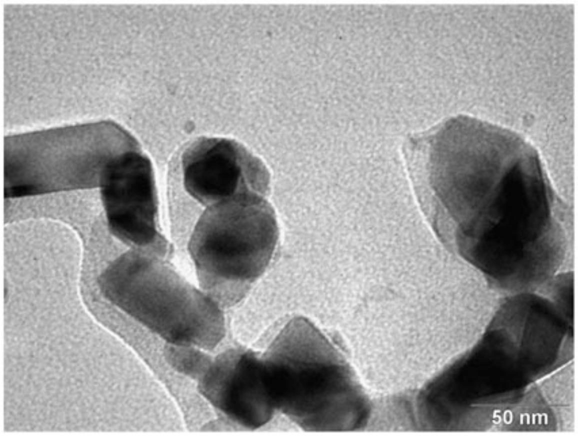

050520-c8-07.tif

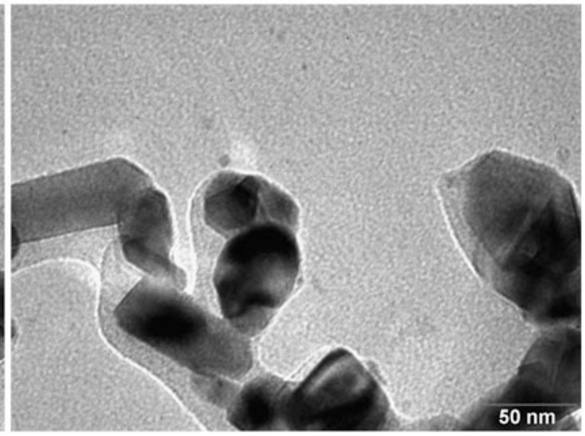

050520-c8-08.tif

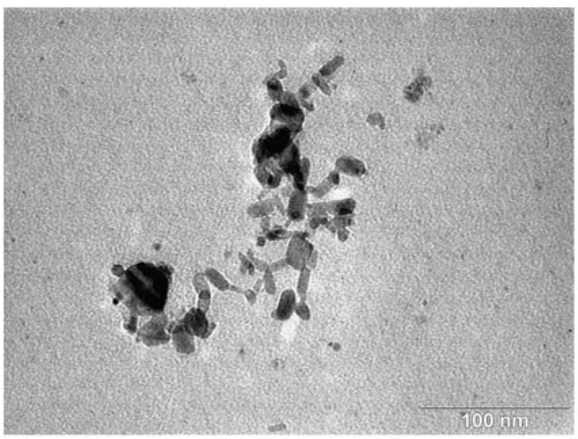

050520-c8-09.tif

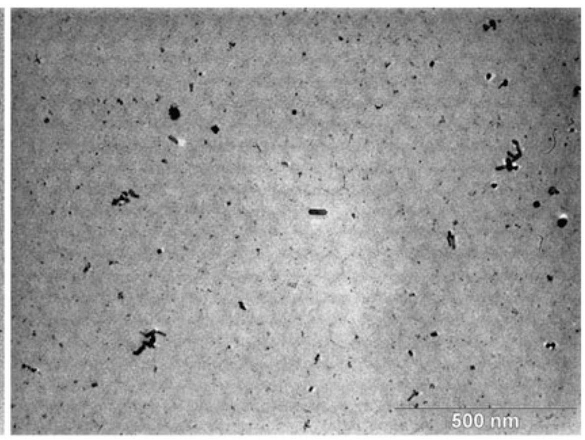

050520-c8-10.tif

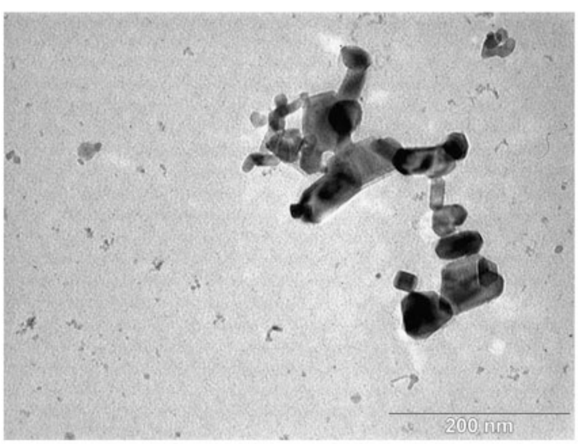

050520-c8-11.tif

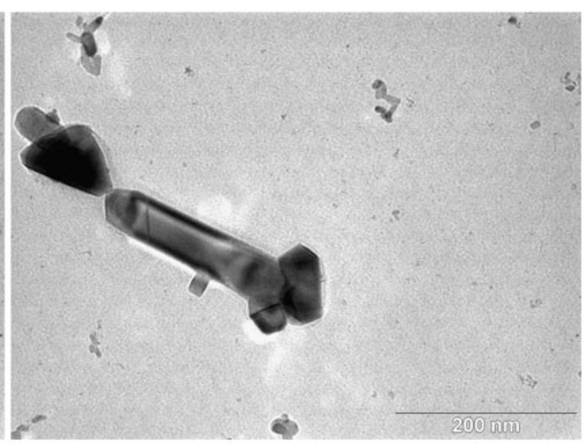

050520-c8-12.tif

MACS undoped SnO_2

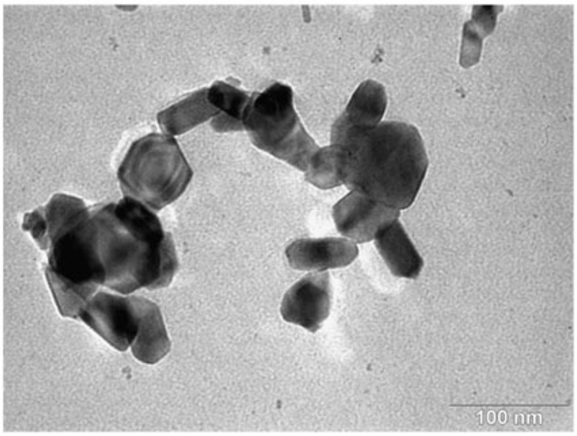

050520-c8-13.tif

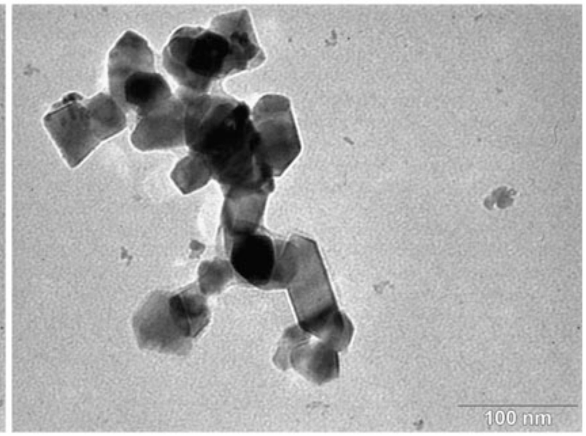

050520-c8-14.tif

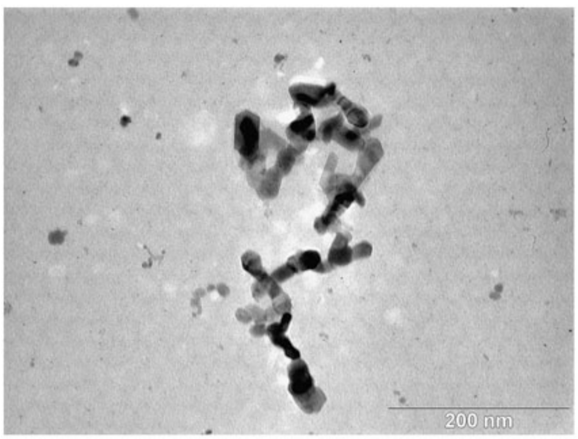

050520-c8-15.tif

MACS undoped SnO_2

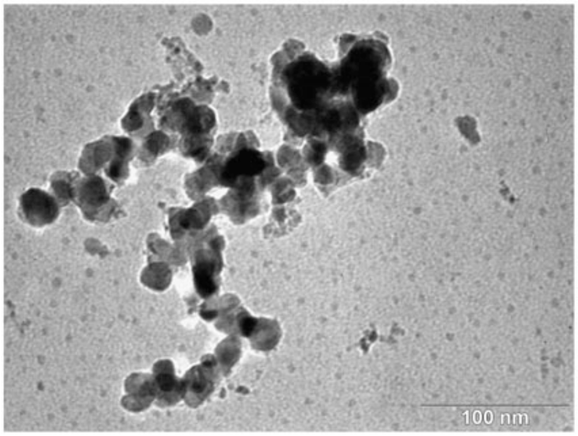

c9_1.tif

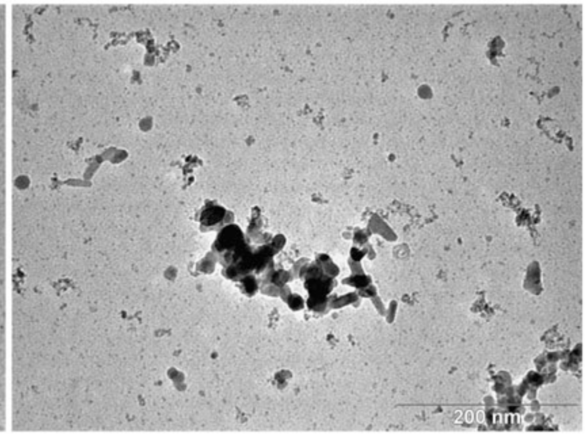

c9_10.tif

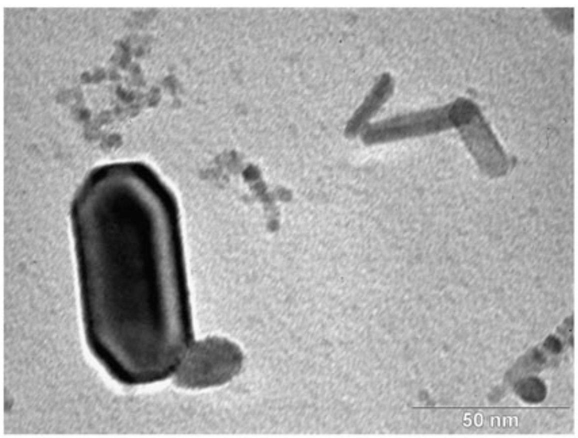

c9_11.tif

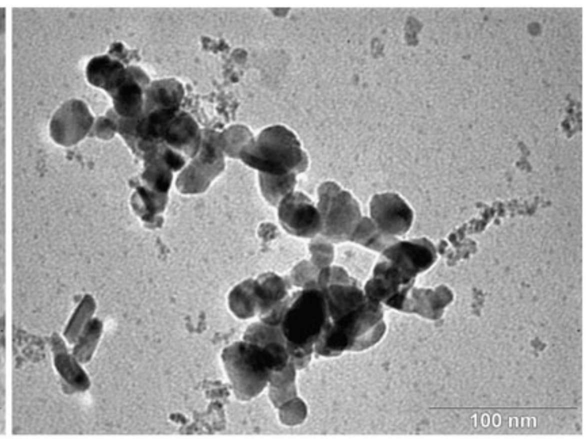

c9_12.tif

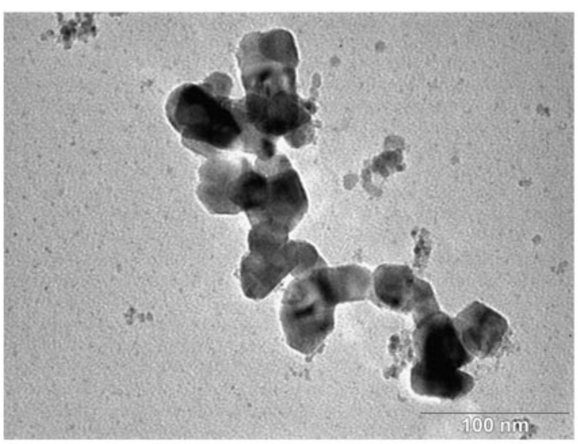

c9_13.tif

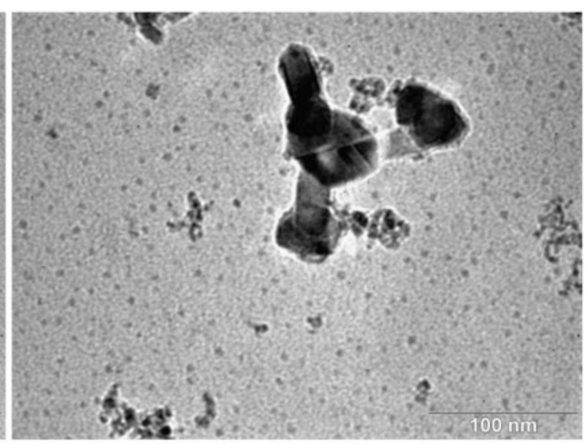

c9_2.tif

MACS undoped SnO_2

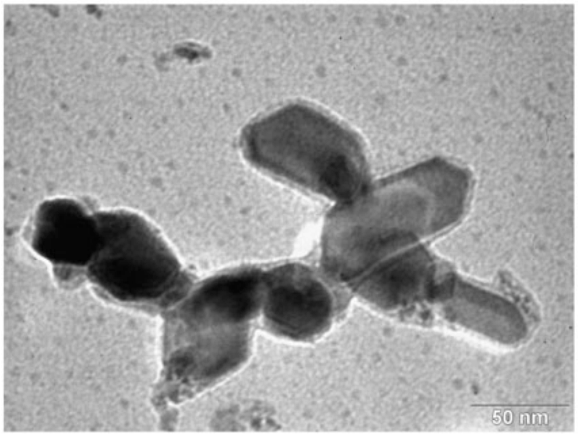

c9_3.tif

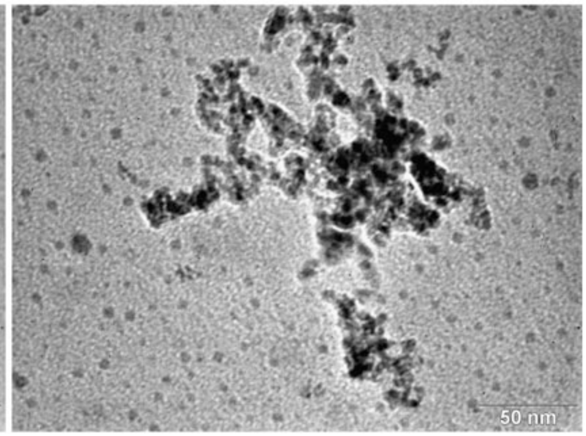

c9_4.tif

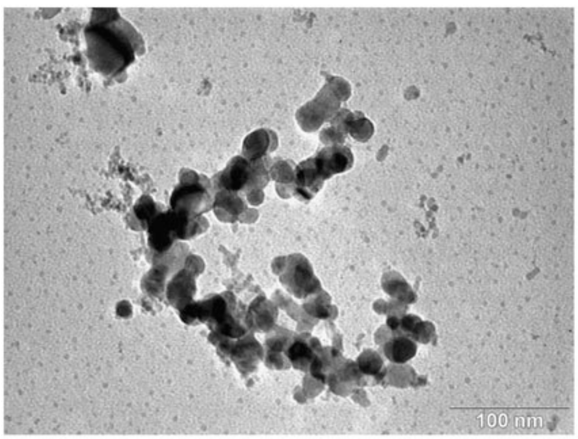

c9_5.tif

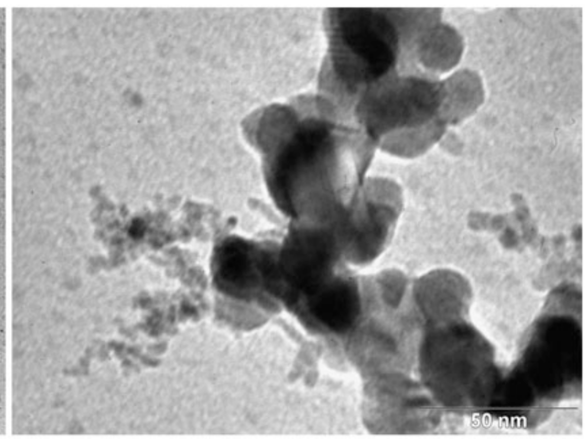

c9_5_1.tif

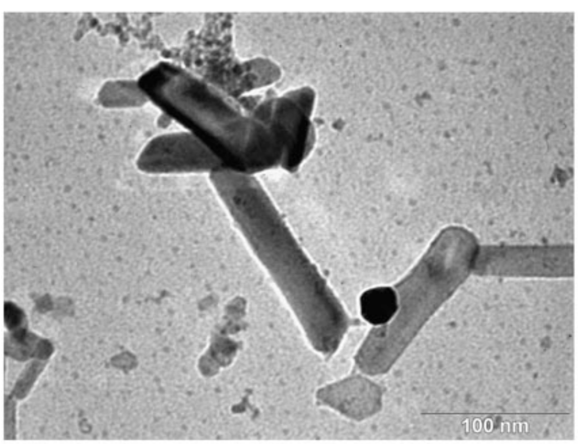

c9_6.tif

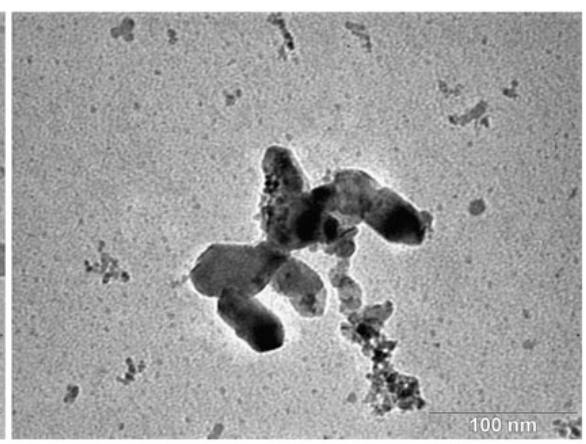

c9_7.tif

MACS undoped SnO_2

c9_8.tif

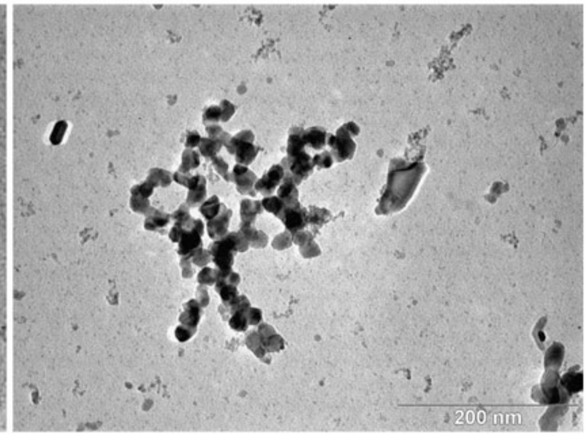

c9_9.tif

MACS undoped SnO_2

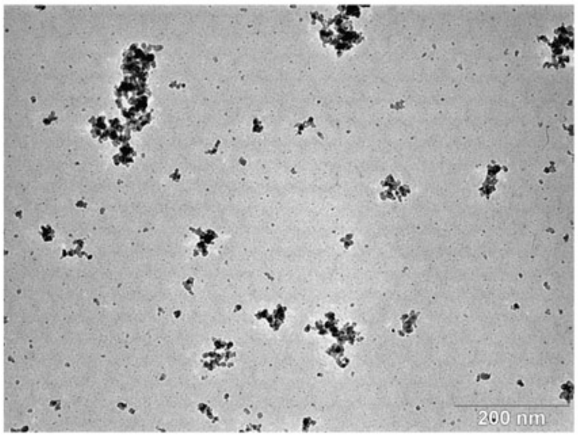

c10_01.tif

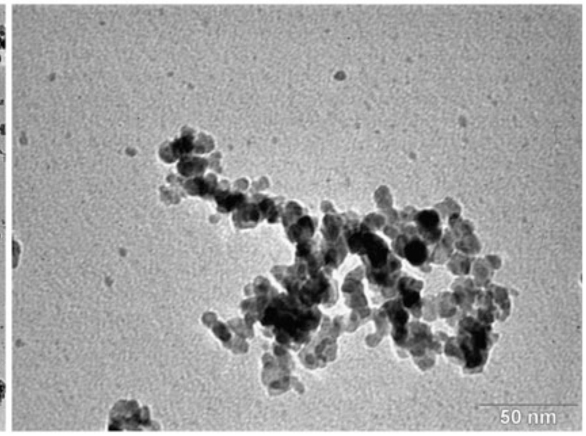

c10_02.tif

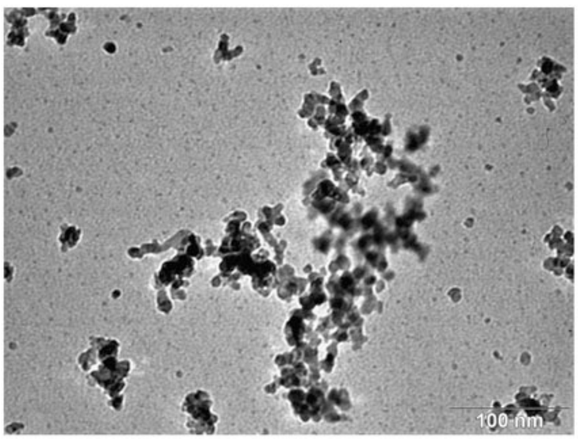

c10_03.tif

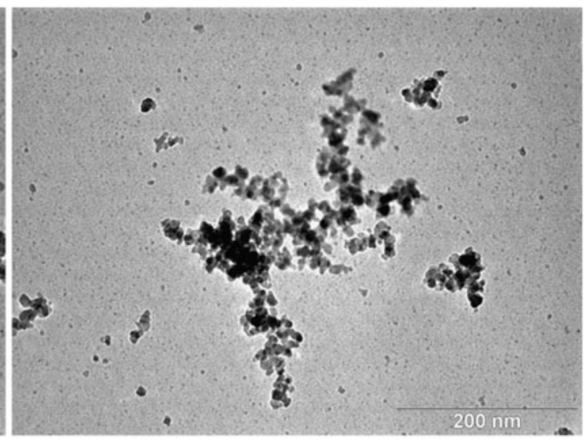

c10_04.tif

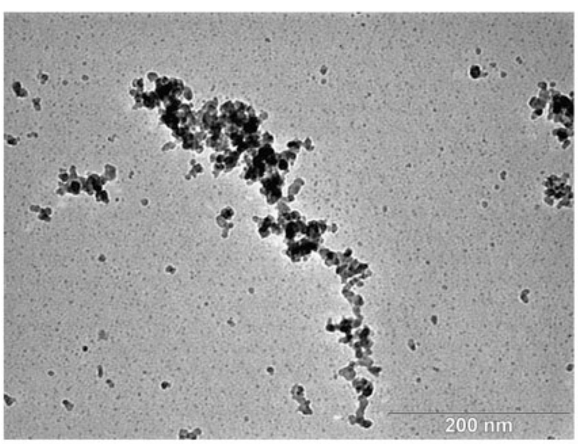

c10_05.tif

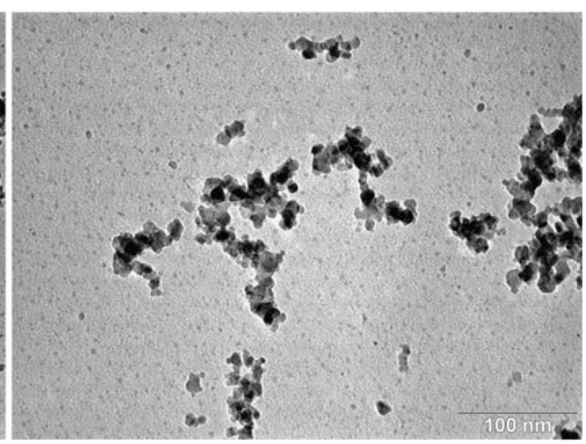

c10_06.tif

MACS undoped SnO_2

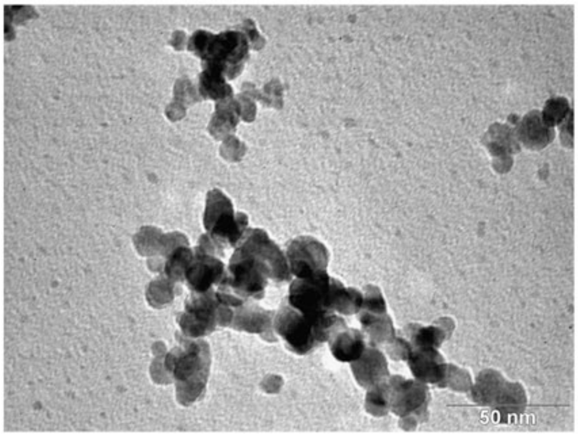

c10_07.tif

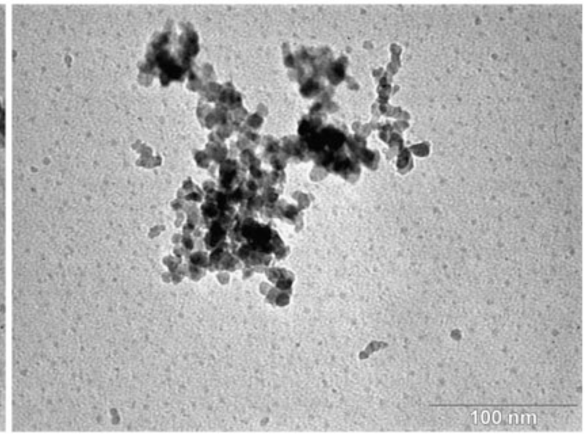

c10_08.tif

MACS undoped SnO_2 height study - sampled at 1 cm

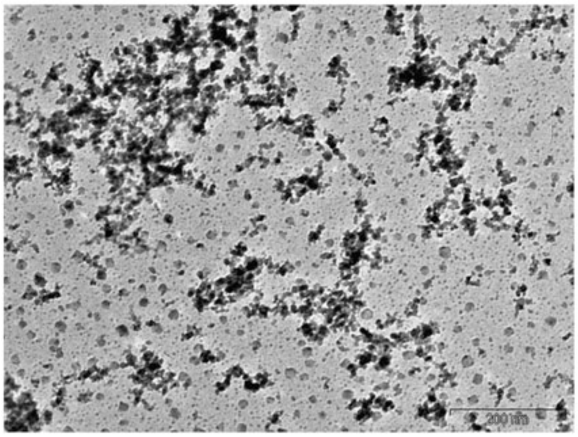

050722_a6_01.tif

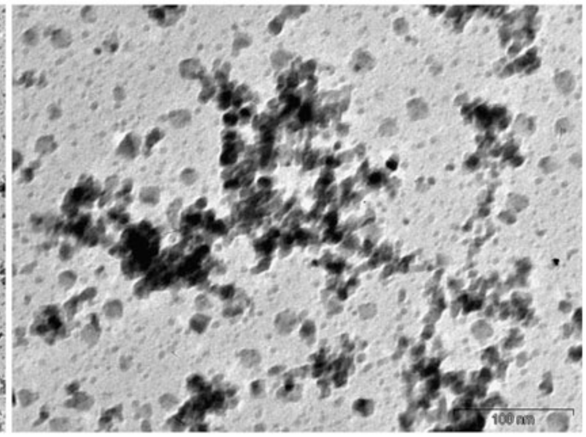

050722_a6_02.tif

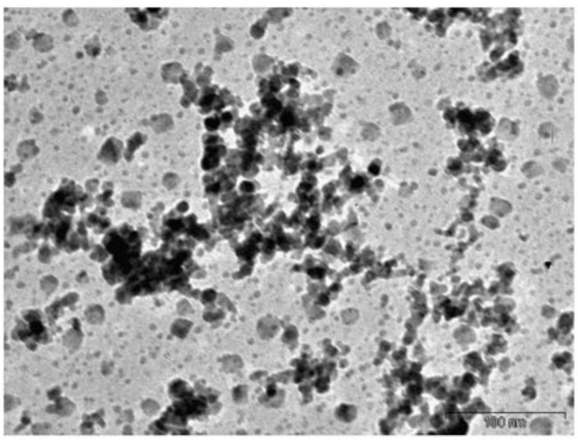

050722_a6_03.tif

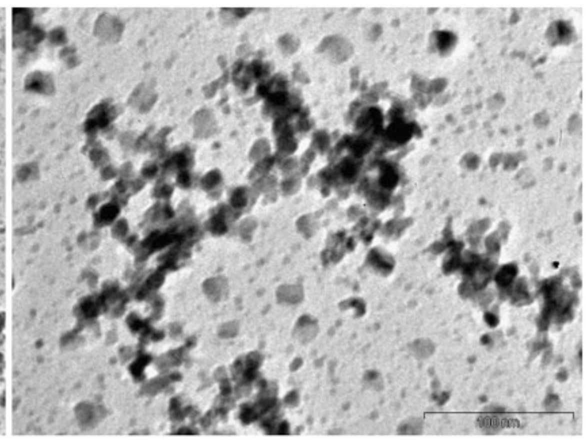

050722_a6_04.tif

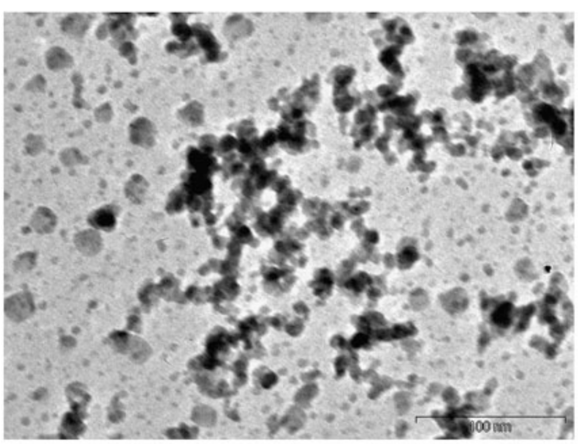

050722_a6_05.tif

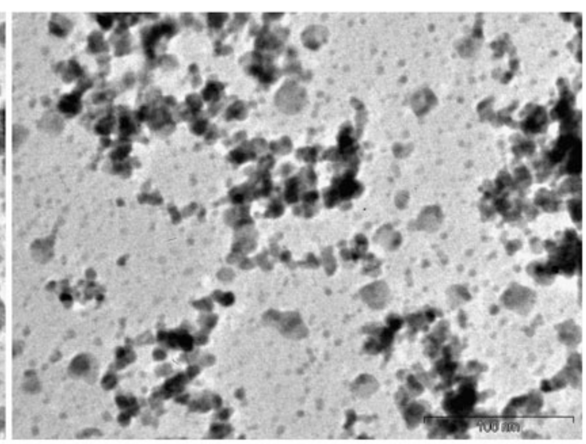

050722_a6_06.tif

MACS undoped SnO_2 height study - sampled at 1 cm

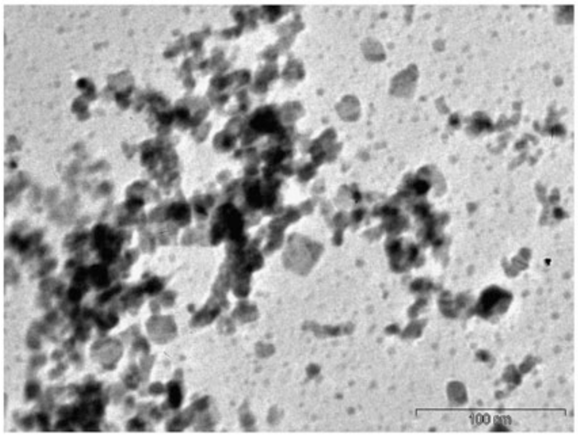

050722_a6_07.tif

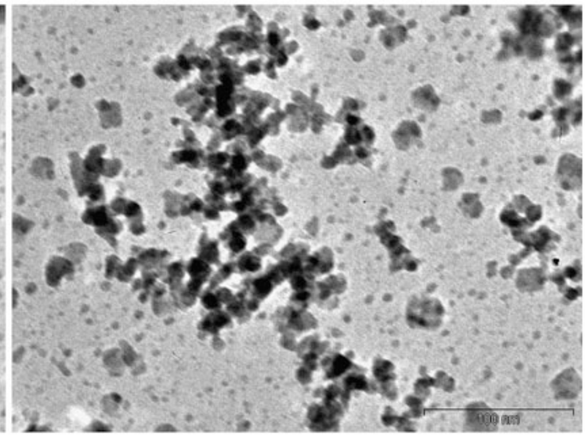

050722_a6_08.tif

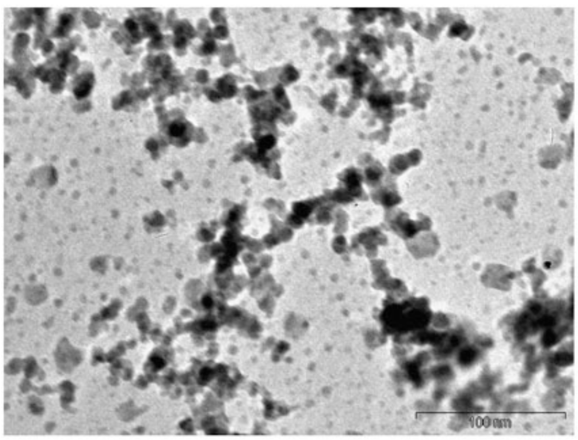

050722_a6_09.tif

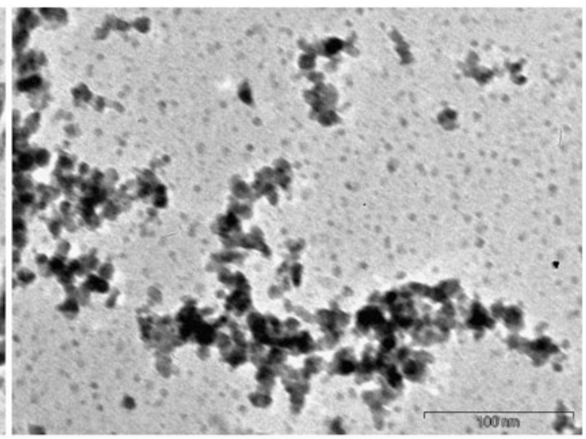

050722_a6_10.tif

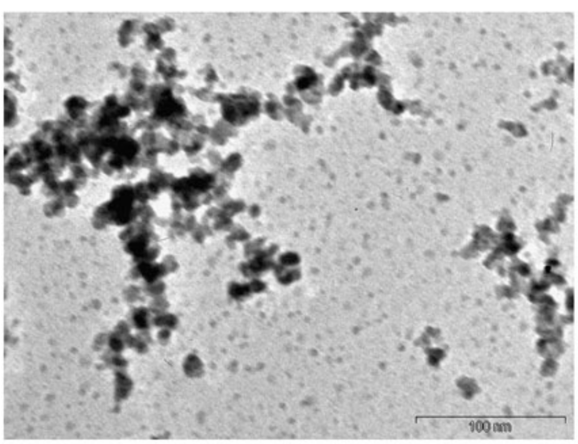

050722_a6_11.tif

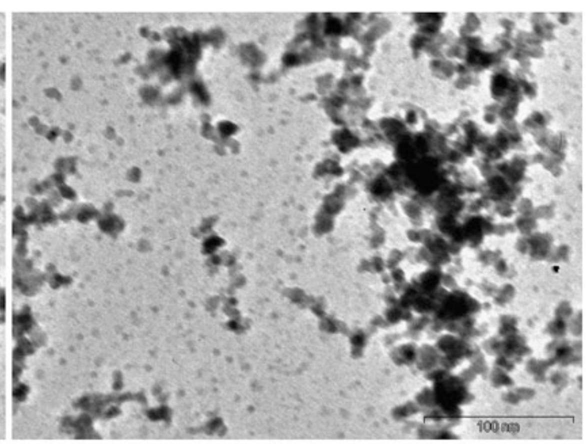

050722_a6_12.tif

MACS undoped SnO_2 height study - sampled at 2 cm

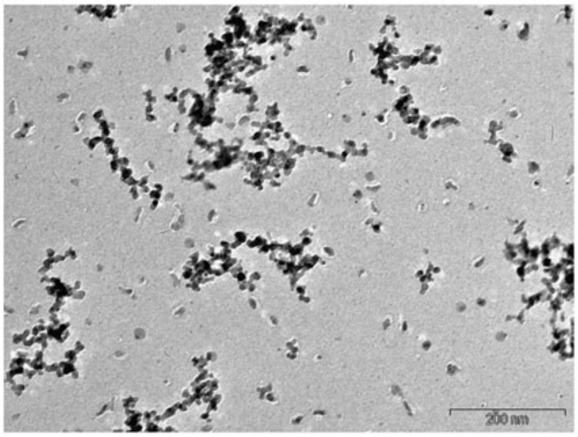

050722_a7_01.tif

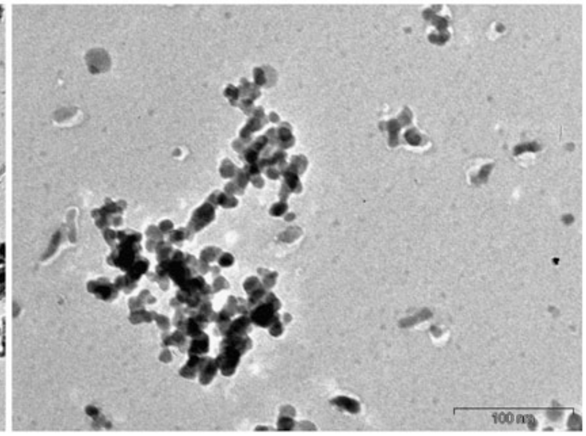

050722_a7_02.tif

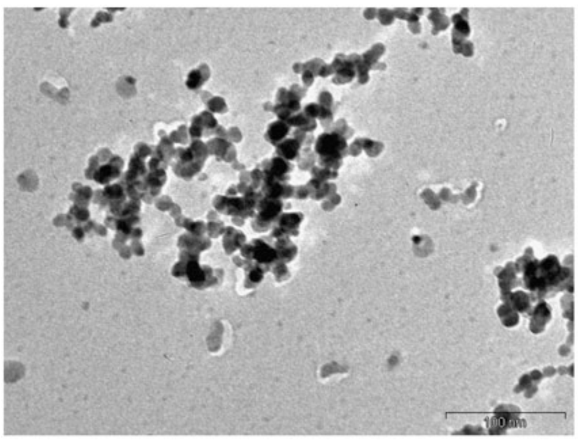

050722_a7_03.tif

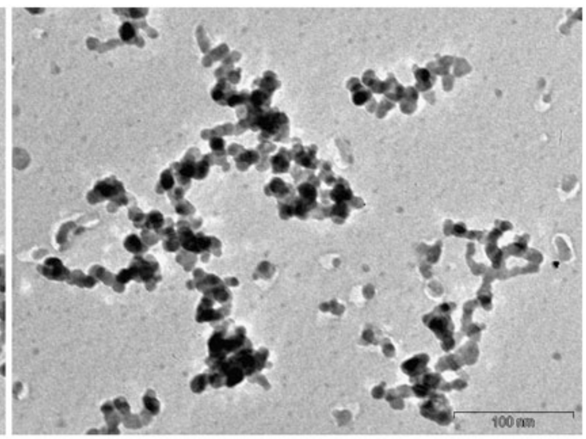

050722_a7_04.tif

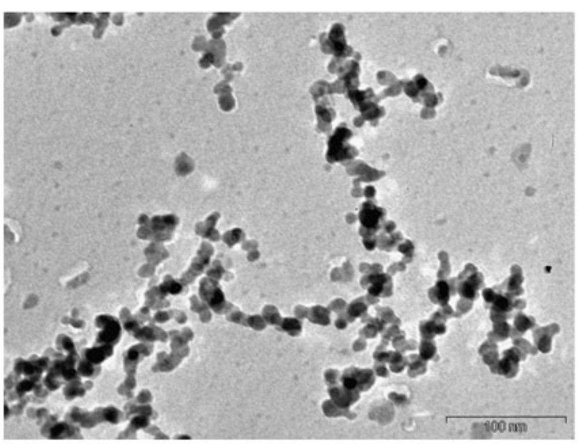

050722_a7_05.tif

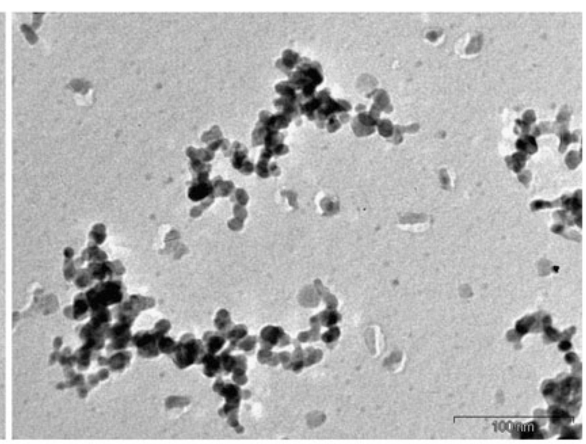

050722_a7_06.tif

MACS undoped SnO_2 height study - sampled at 2 cm

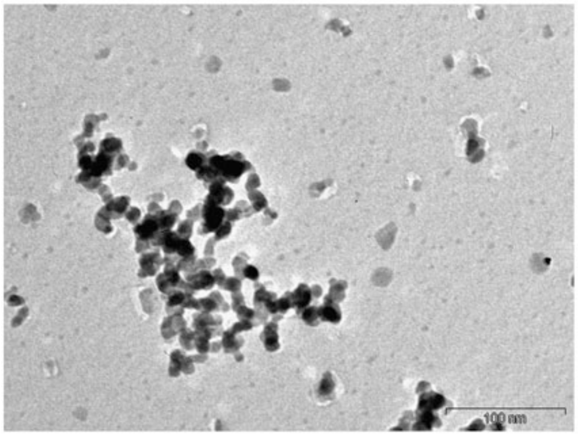

050722_a7_07.tif

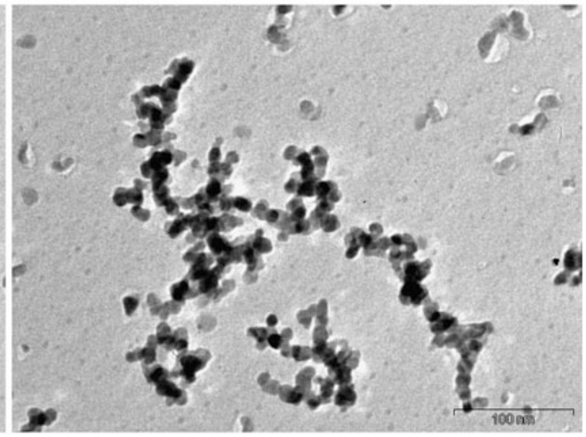

050722_a7_08.tif

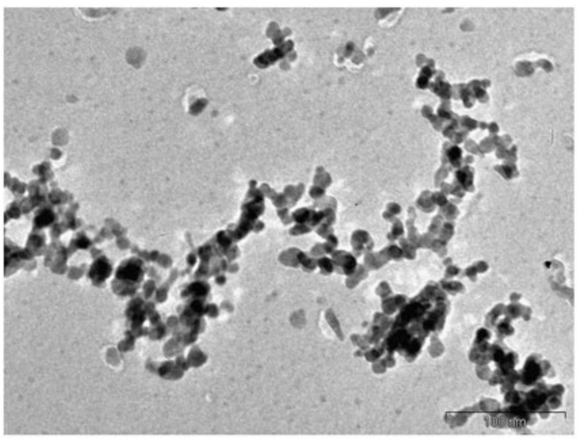

050722_a7_09.tif

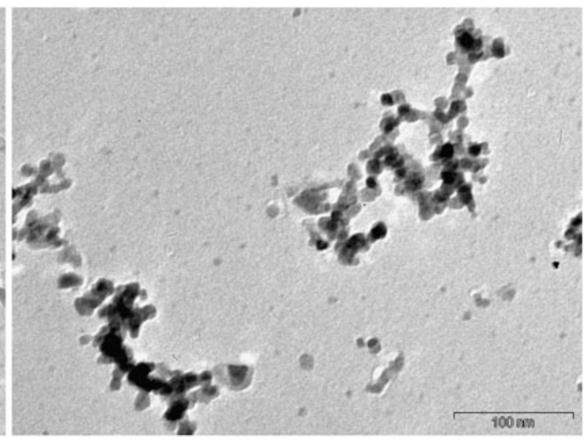

050722_a7_10.tif

MACS undoped SnO_2 height study - sampled at 5 cm

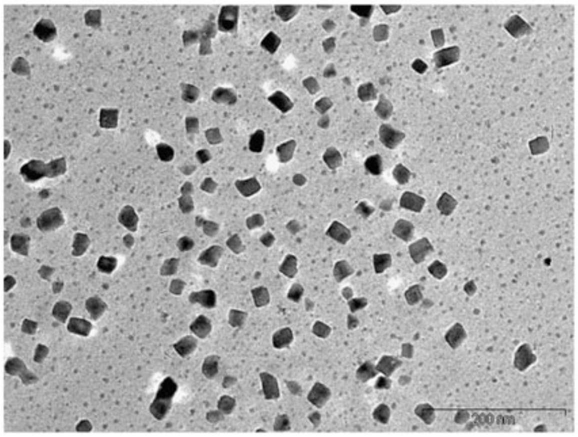

050722_a8_01.tif

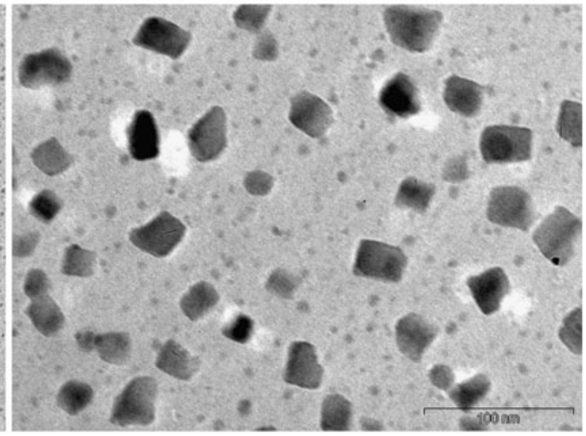

050722_a8_02.tif

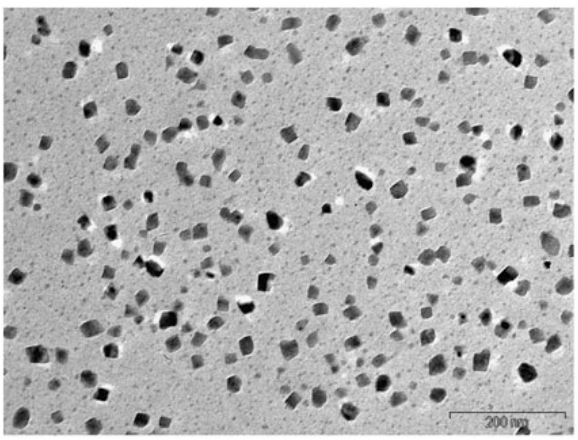

050722_a8_03.tif

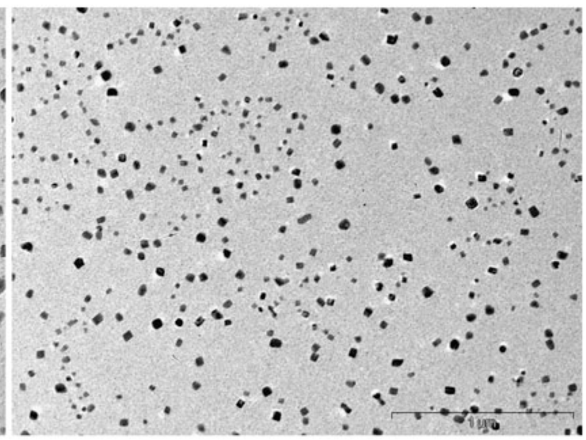

050722_a8_04.tif

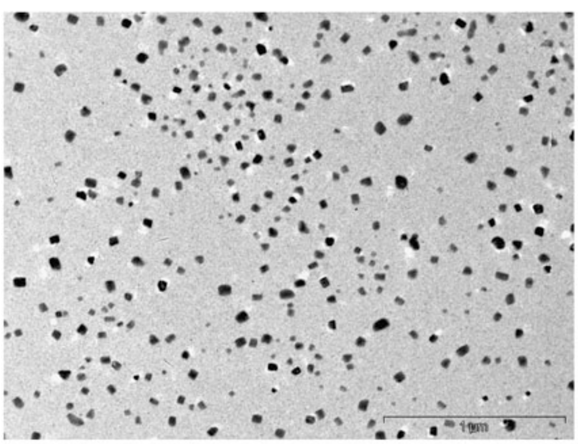

050722_a8_05.tif

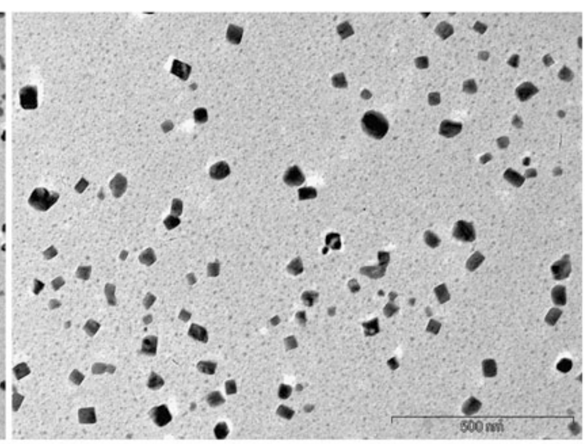

050722_a8_06.tif

MACS undoped SnO_2 height study - sampled at 5 cm

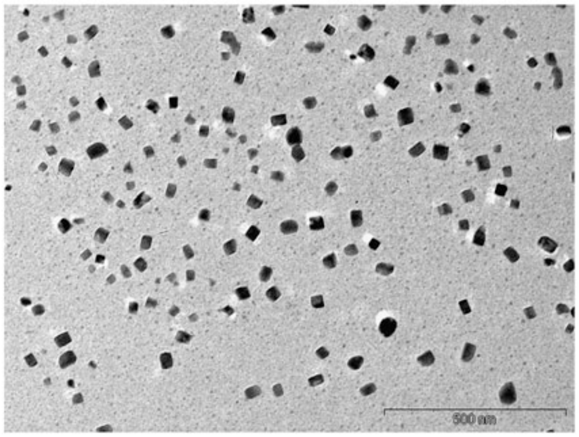

050722_a8_07.tif

MACS undoped SnO_2 height study - sampled at 5 cm

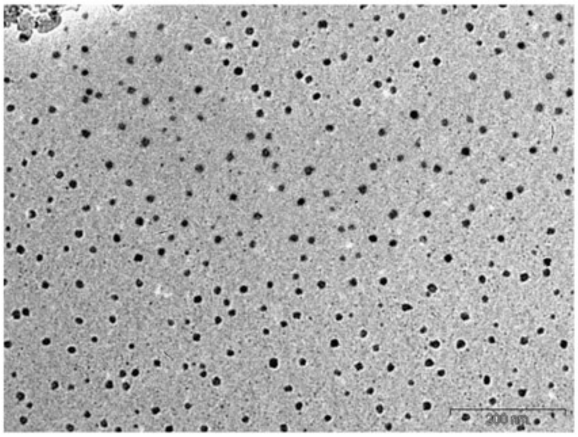
050722_b5_01.tif

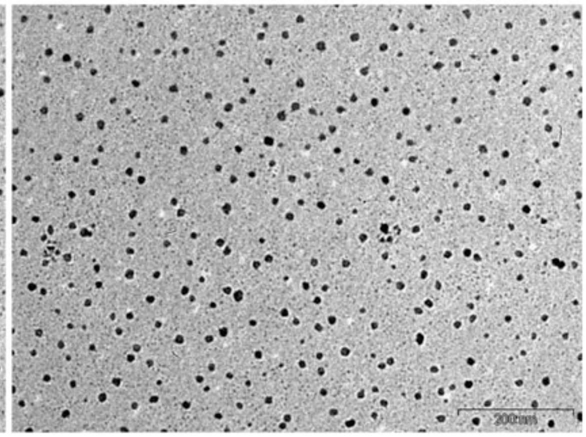
050722_b5_02.tif

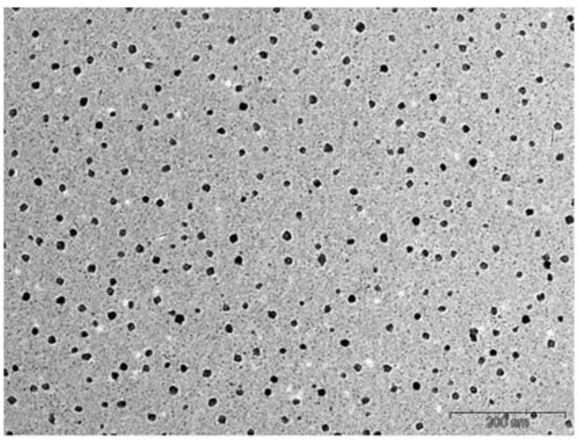
050722_b5_03.tif

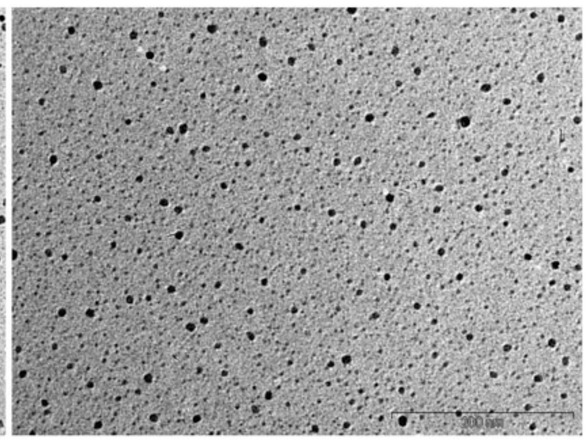
050722_b5_04.tif

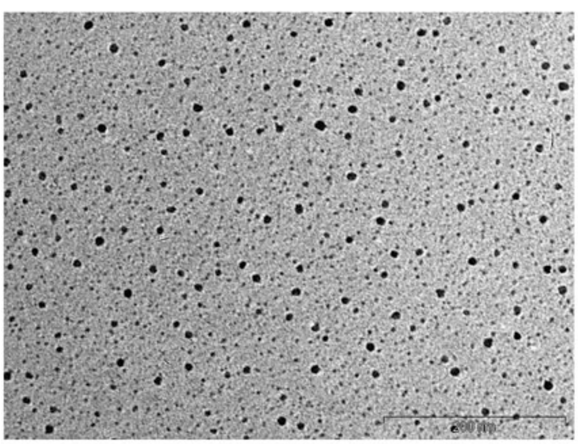
050722_b5_05.tif

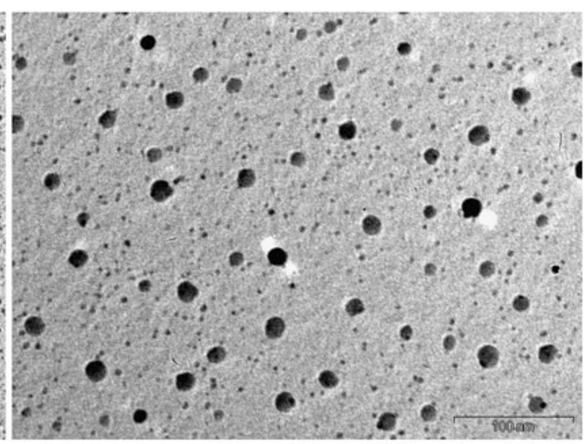
050722_b5_06.tif

MACS undoped SnO_2 height study - sampled at 9 cm

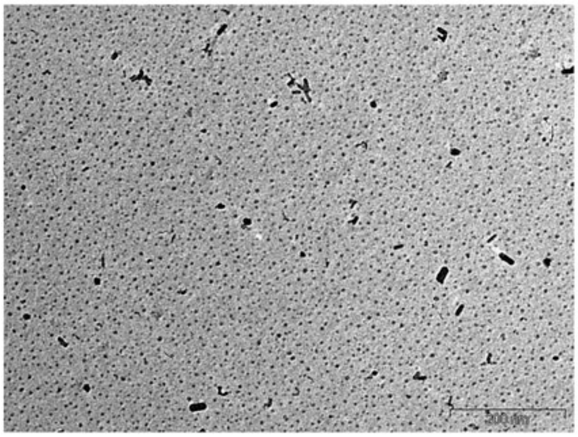

050722_a9_01.tif

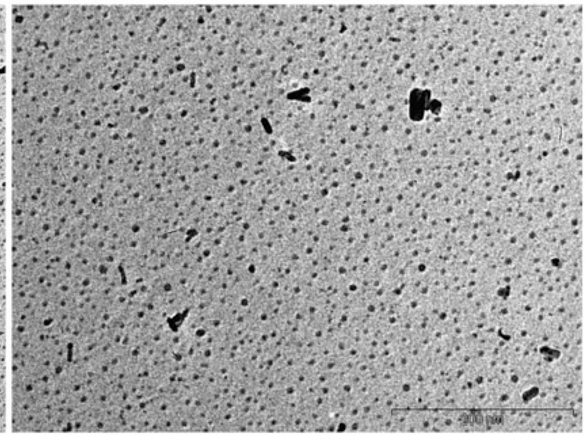

050722_a9_02.tif

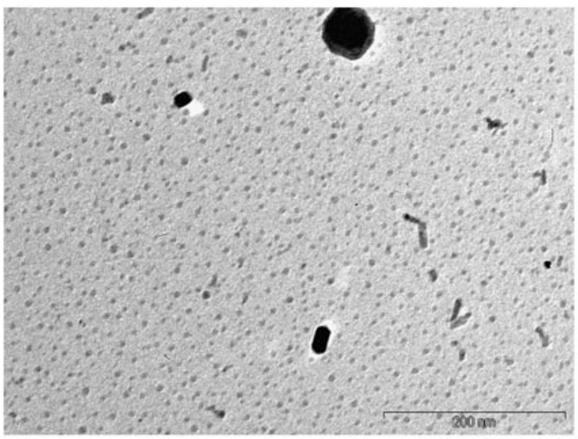

050722_a9_03.tif

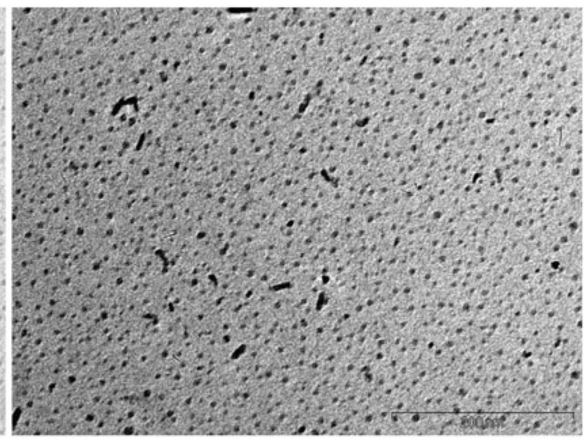

050722_a9_04.tif

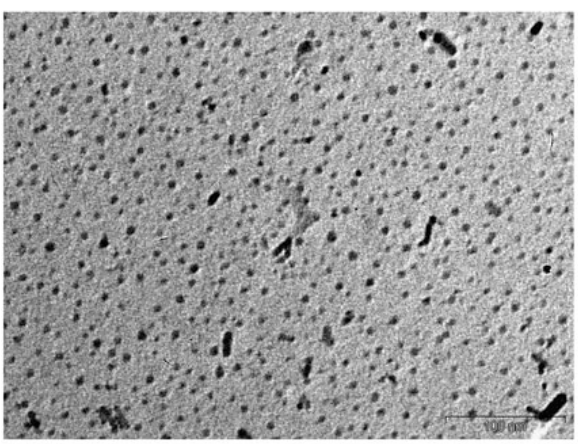

050722_a9_05.tif

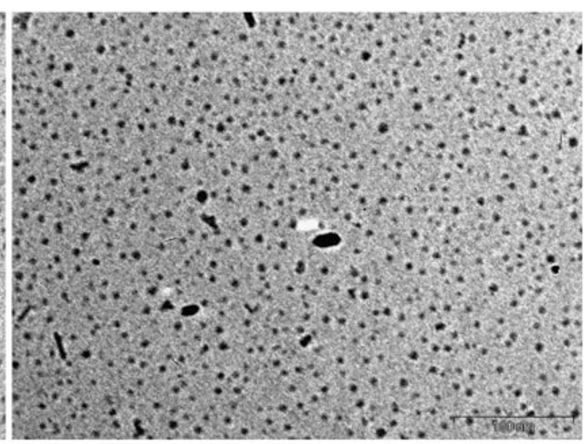

050722_a9_06.tif

MACS undoped SnO_2 height study - sampled at 9 cm

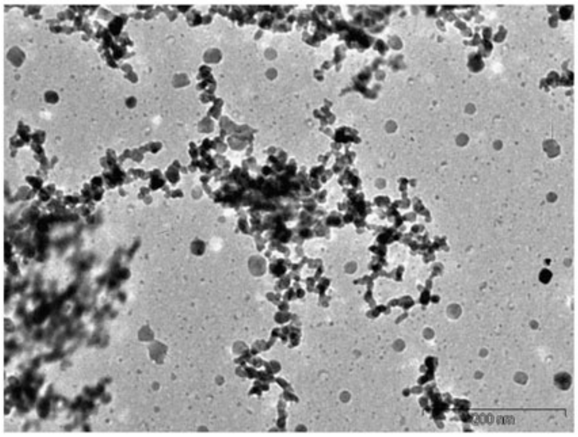

050722_b6_01.tif

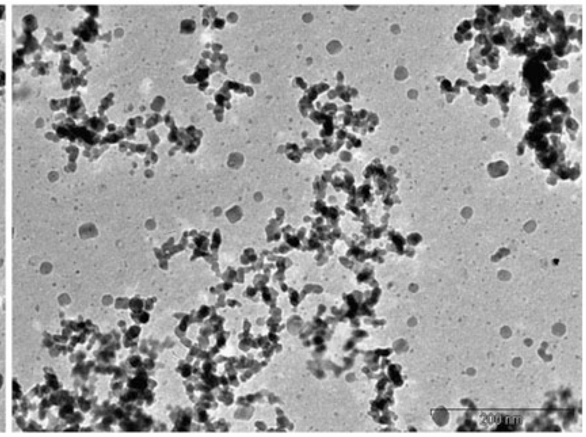

050722_b6_02.tif

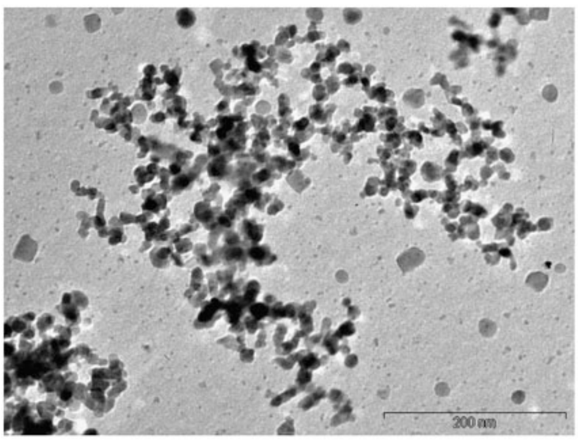

050722_b6_03.tif

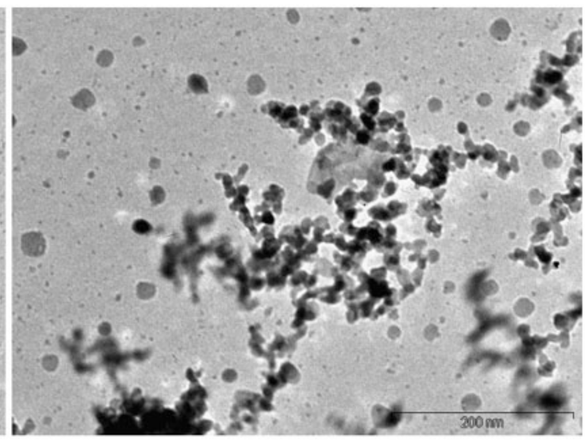

050722_b6_04.tif

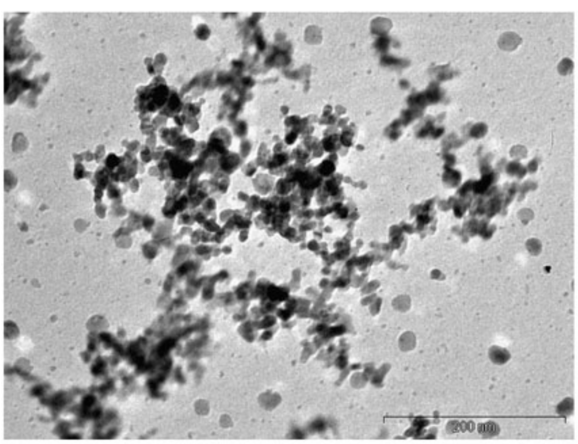

050722_b6_05.tif

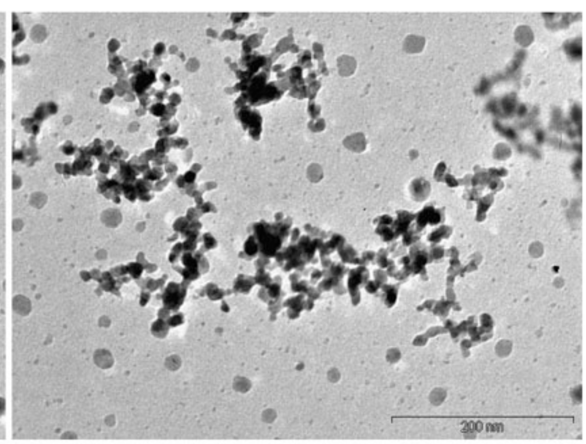

050722_b6_06.tif

MACS undoped SnO_2 height study - sampled at 9 cm

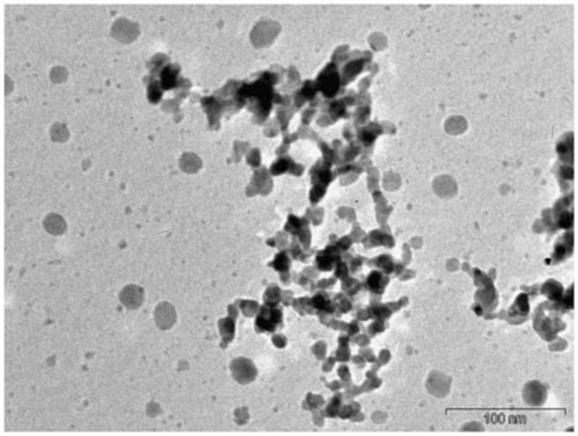

050722_b6_07.tif

MACS undoped SnO_2 height study - sampled at 13 cm

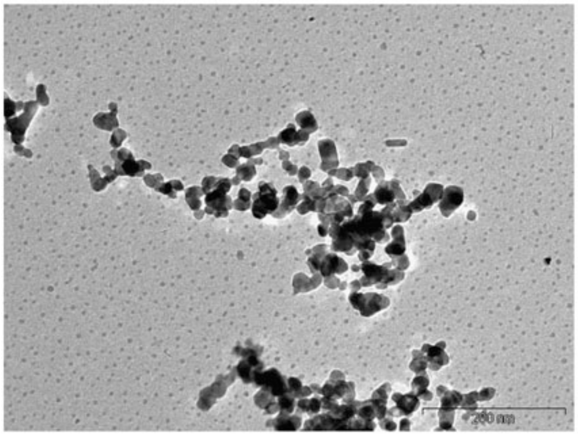

050722_a10_01.tif

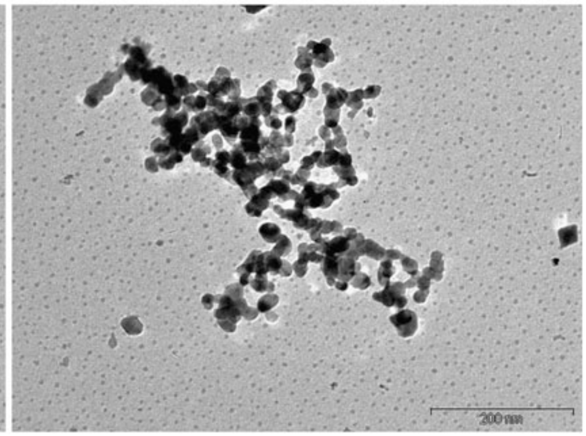

050722_a10_02.tif

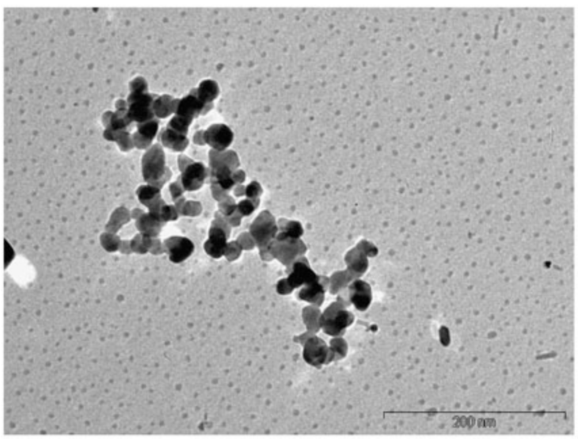

050722_a10_03.tif

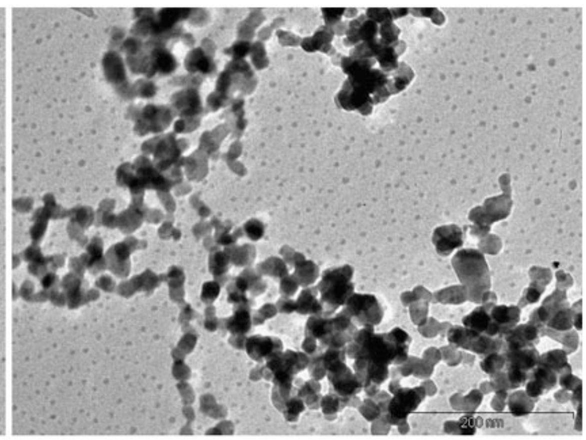

050722_a10_04.tif

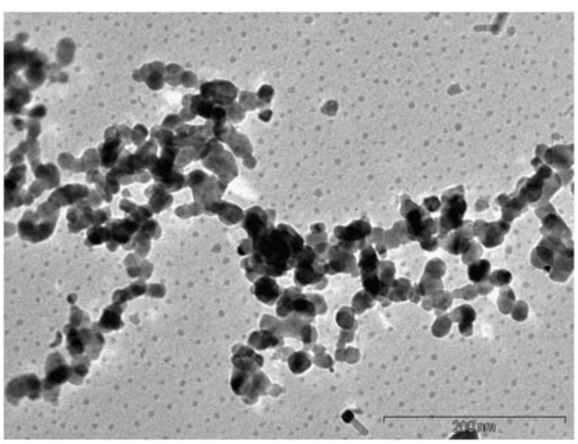

050722_a10_05.tif

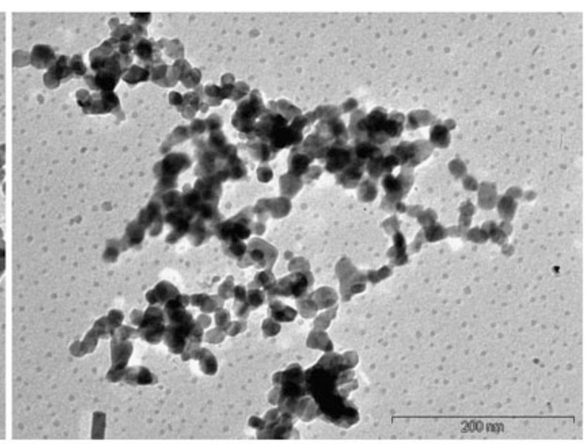

050722_a10_06.tif

MACS undoped SnO_2 height study - sampled at 13 cm

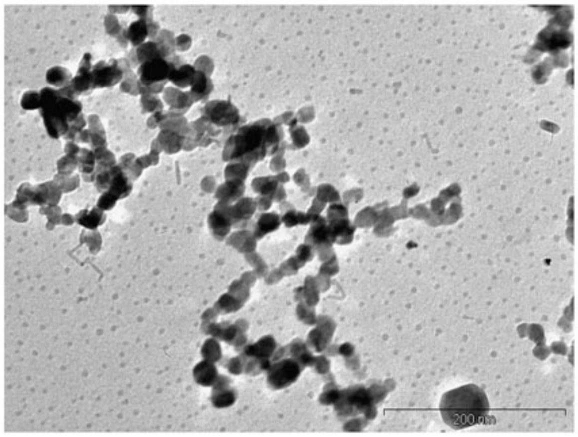

050722_a10_07.tif

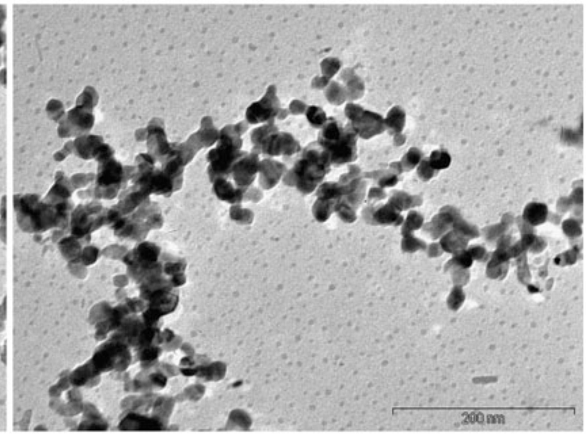

050722_a10_08.tif

MACS undoped SnO_2 height study - sampled at 9 cm

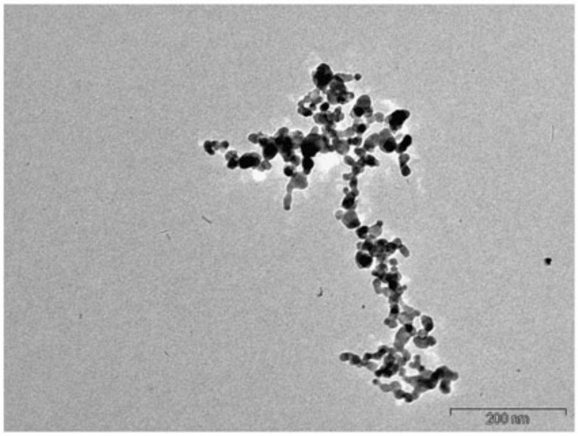

050722_b3_01.tif

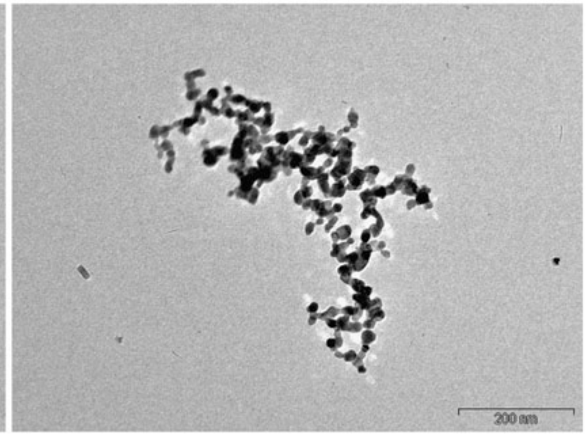

050722_b3_02.tif

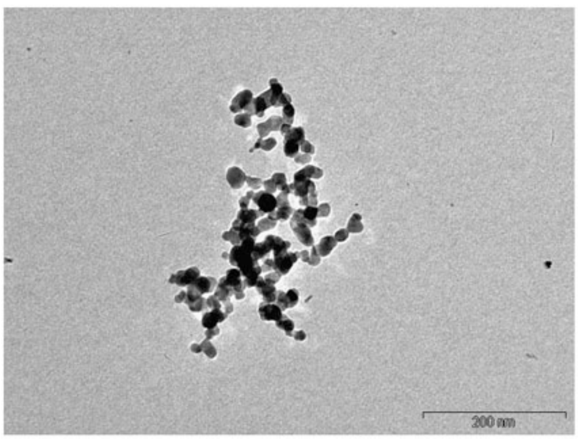

050722_b3_03.tif

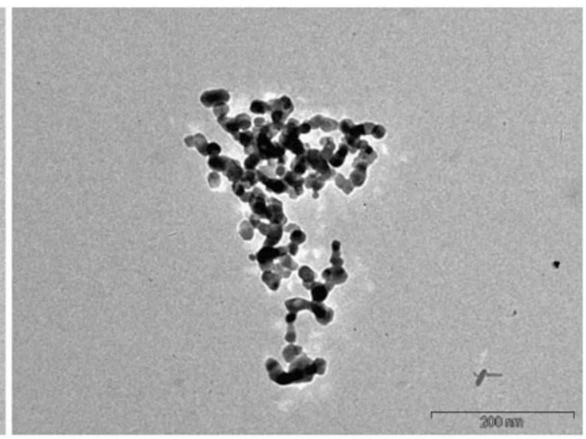

050722_b3_04.tif

MACS undoped SnO_2 height study - sampled at 9 cm

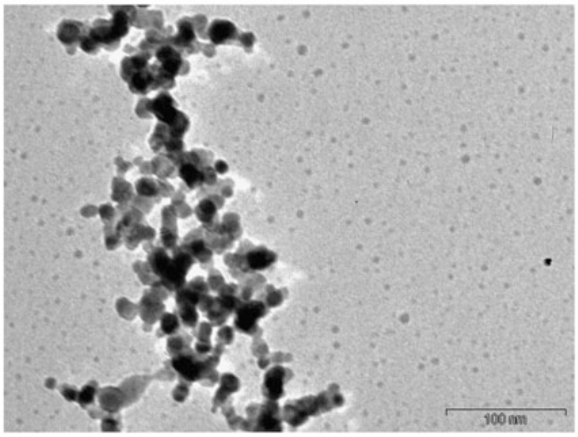

050722_b7_07.tif

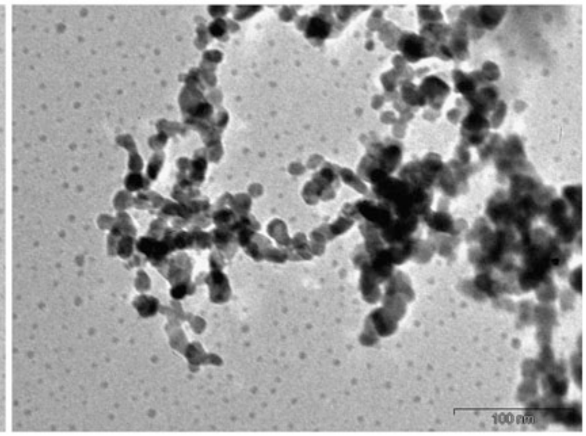

050722_b7_08.tif

MACS undoped SnO_2 height study - sampled at 9 cm

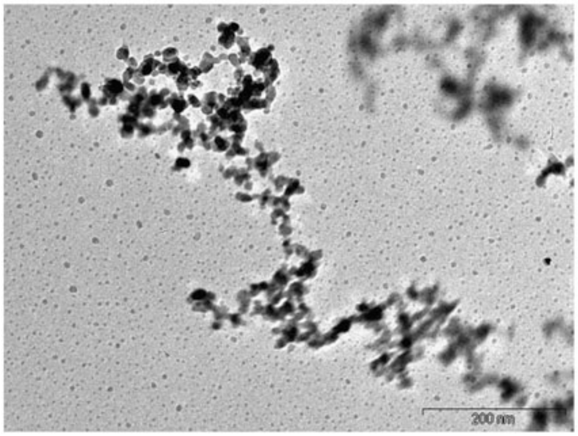

050722_b7_01.tif

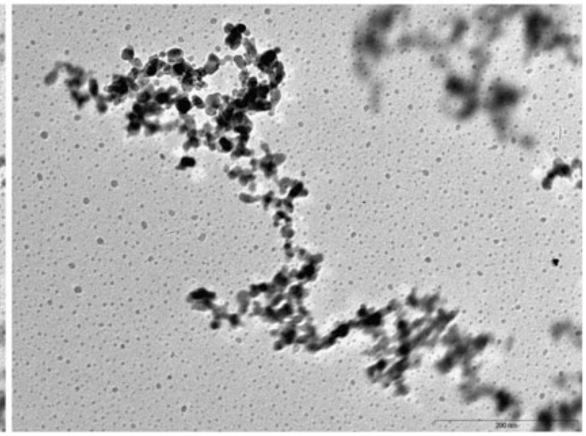

050722_b7_02.tif

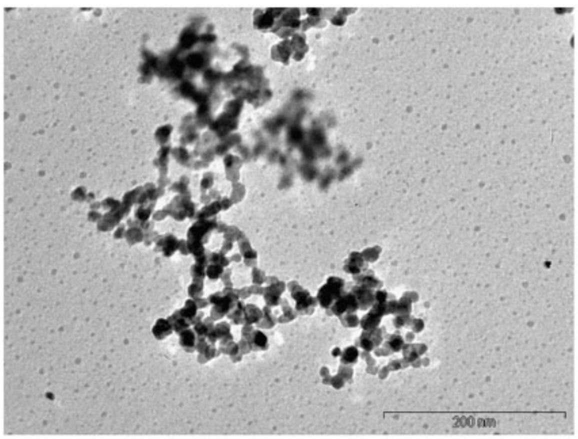

050722_b7_03.tif

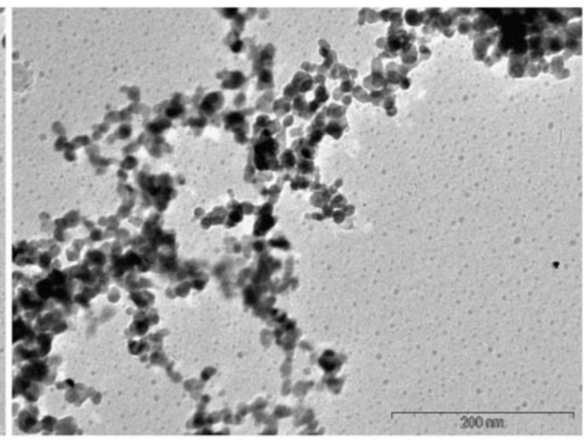

050722_b7_04.tif

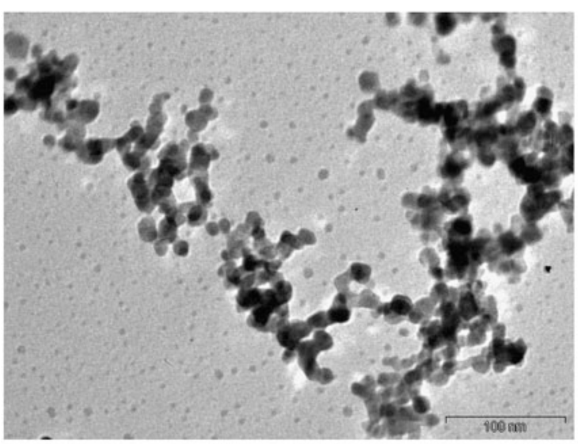

050722_b7_05.tif

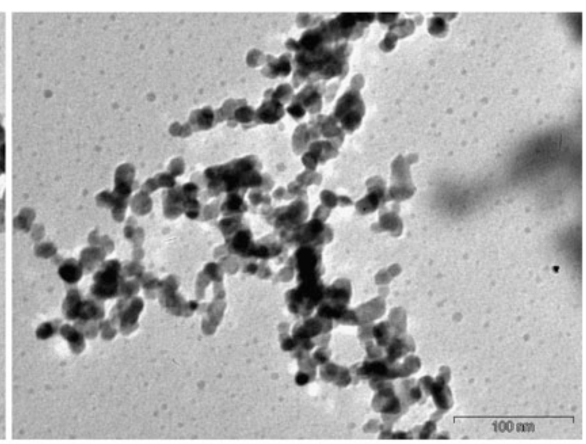

050722_b7_06.tif

MACS undoped SnO_2 height study - sampled at 9 cm

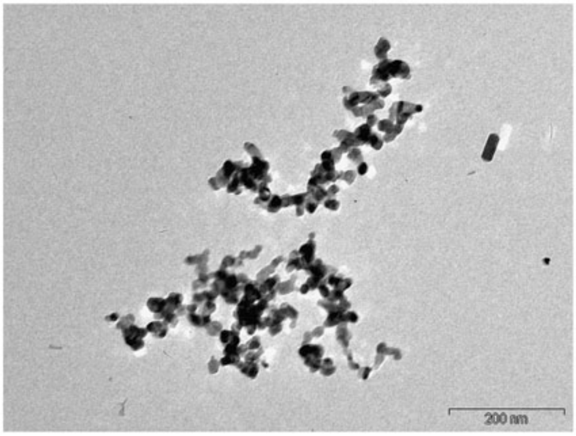

050722_b4_01.tif

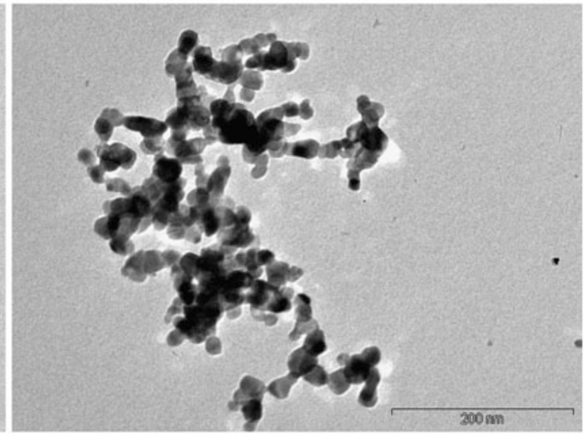

050722_b4_02.tif

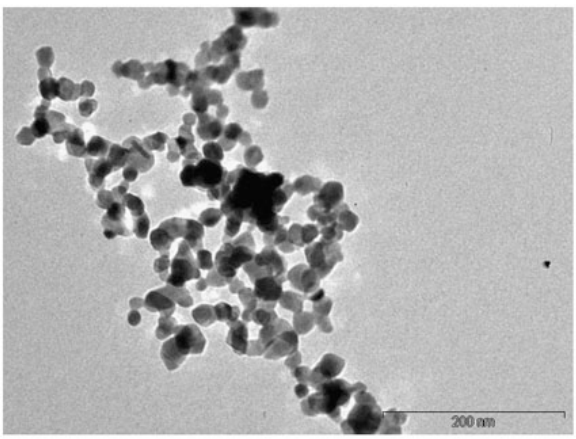

050722_b4_03.tif

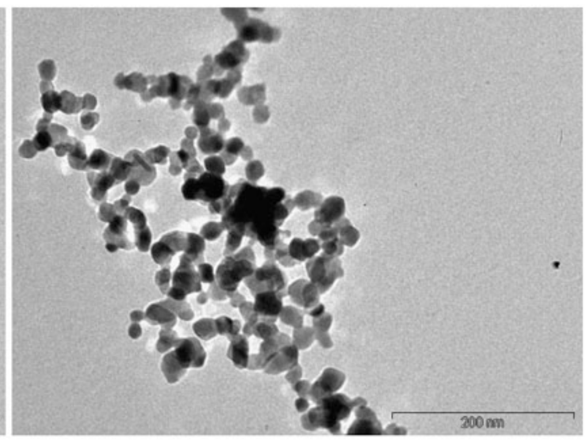

050722_b4_04.tif

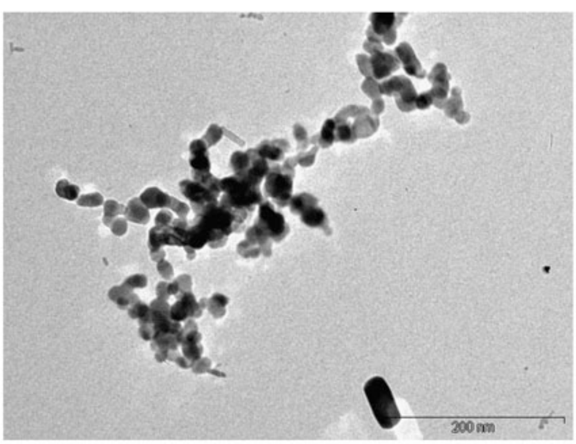

050722_b4_05.tif

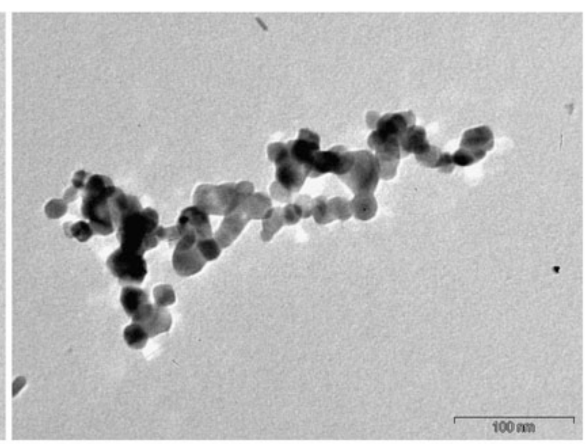

050722_b4_06.tif

MACS undoped SnO_2 height study - sampled at 9 cm

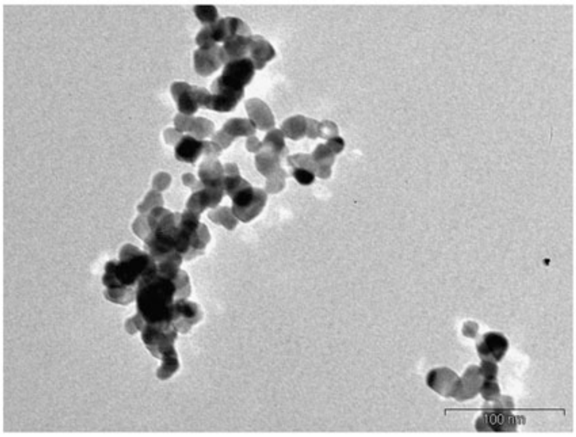

050722_b4_07.tif

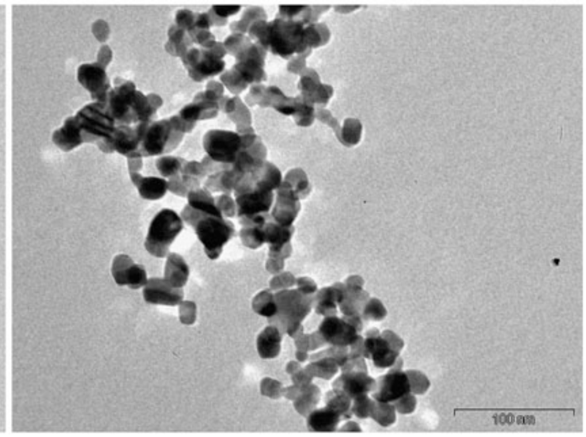

050722_b4_08.tif

MACS undoped SnO_2 - high resolution TEM

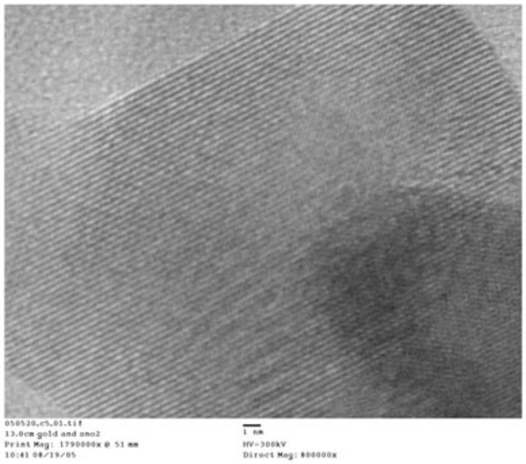

050520_c5_01.tif

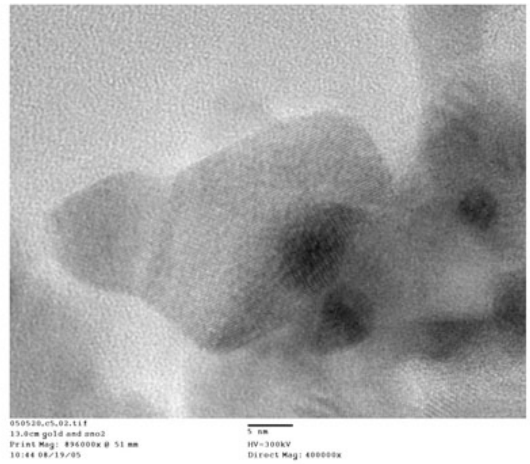

050520_c5_02.tif

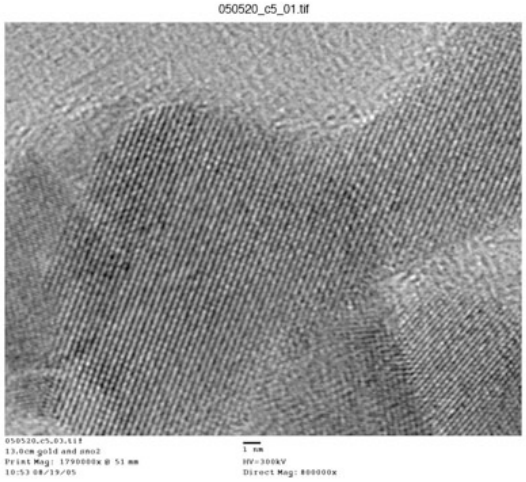

050520_c5_03.tif

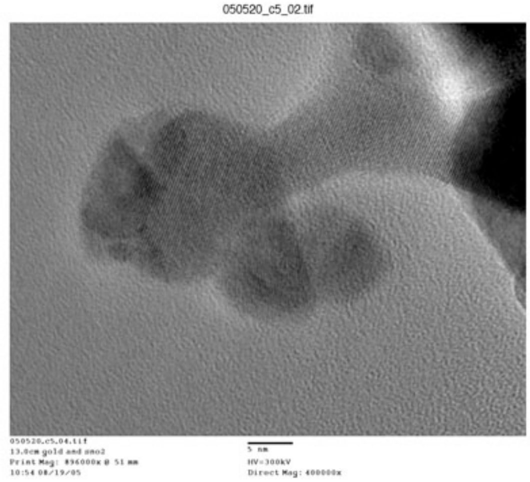

050520_c5_04.tif

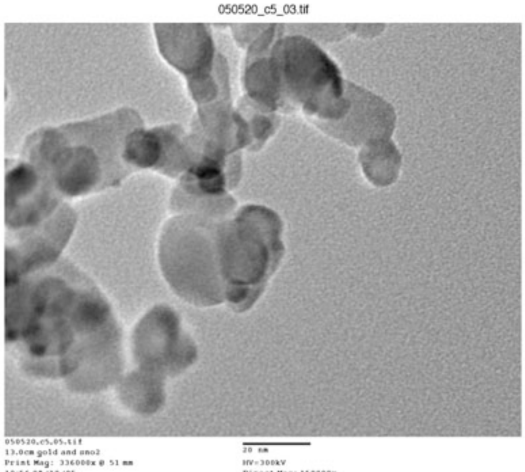

050520_c5_05.tif

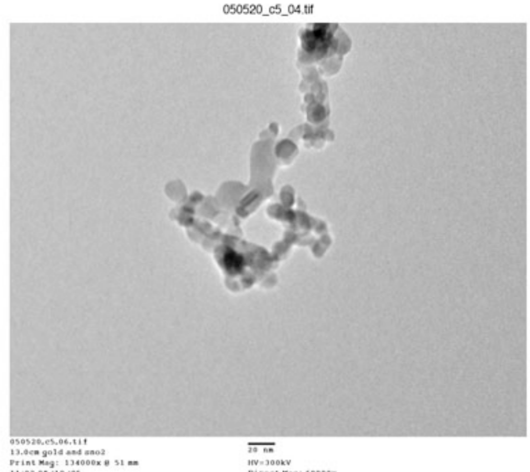

050520_c5_06.tif

MACS undoped SnO_2 - high resolution TEM

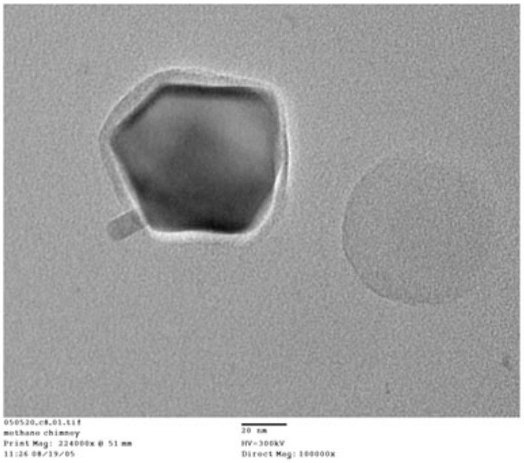

050520_c8_01.tif

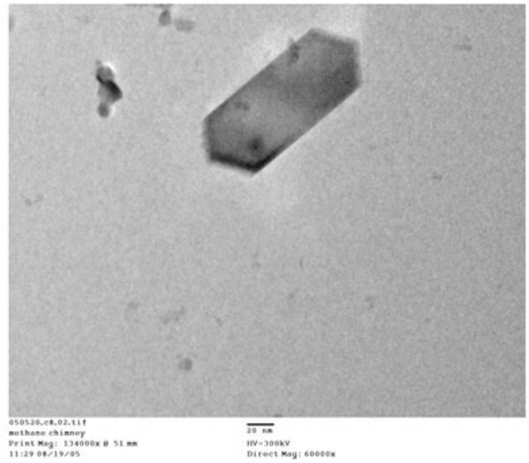

050520_c8_02.tif

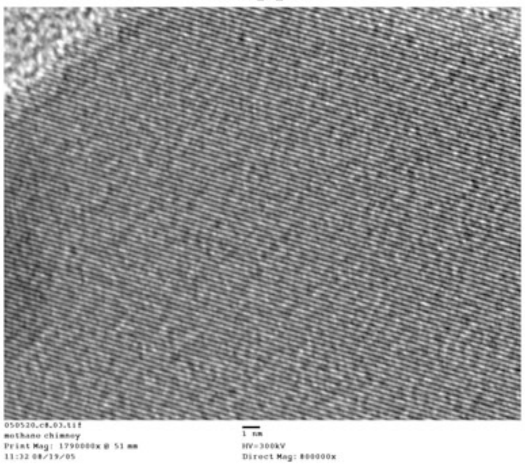

050520_c8_03.tif

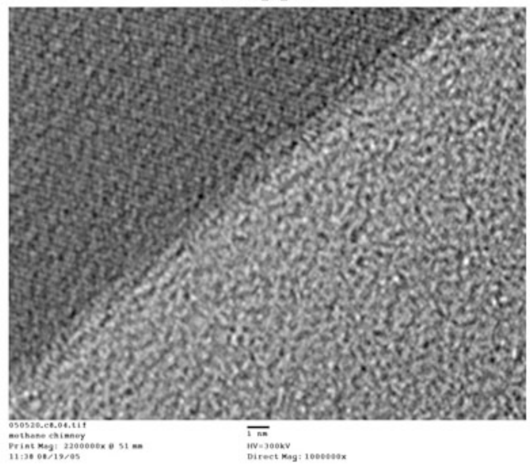

050520_c8_04.tif

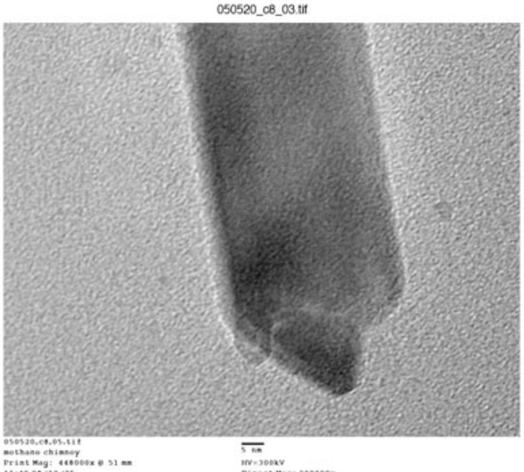

050520_c8_05.tif

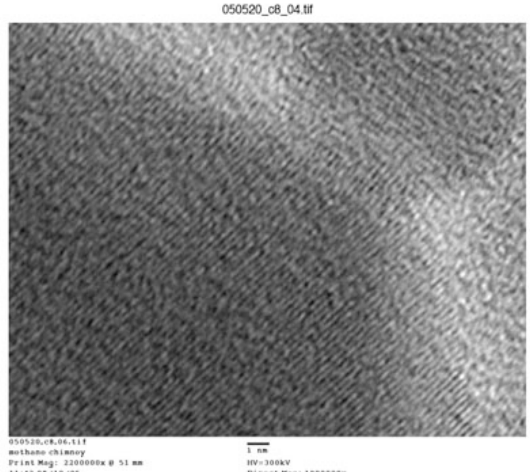

050520_c8_06.tif

MACS undoped SnO_2 - high resolution TEM

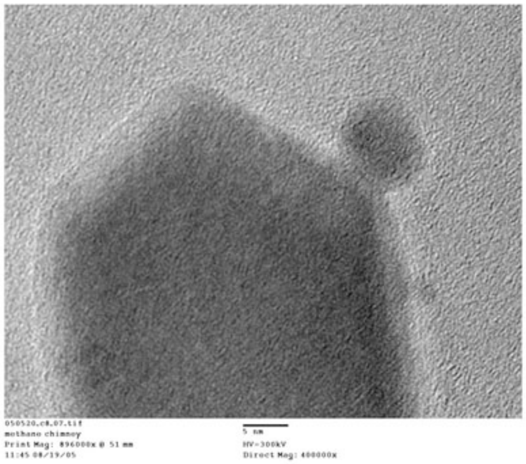

050520_c8_07.tif

MACS undoped SnO_2 - high resolution TEM

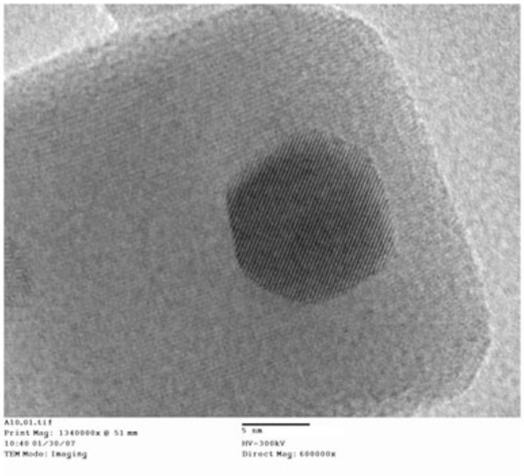

A10_01.tif

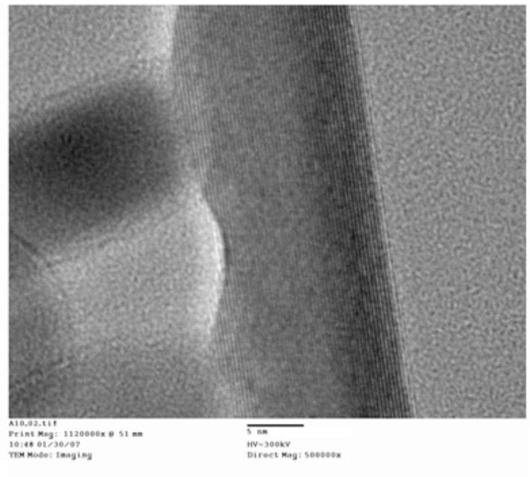

A10_02.tif

A10_03.tif

SAED-01.tif

MACS gold-doped SnO_2

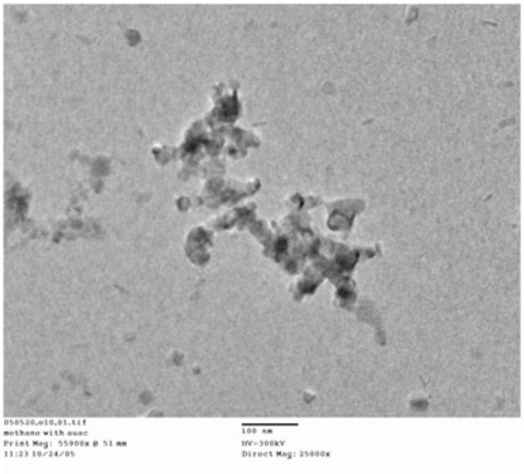

050520_e10_01.tif

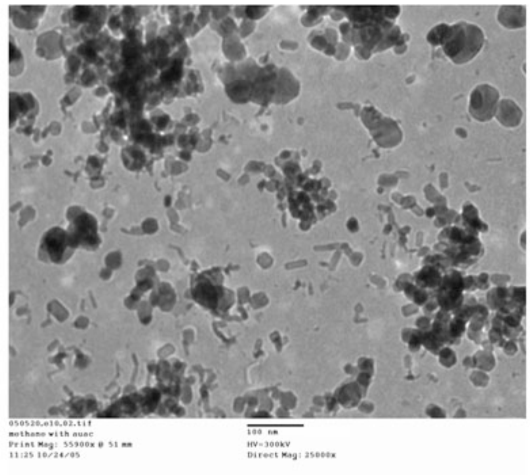

050520_e10_02.tif

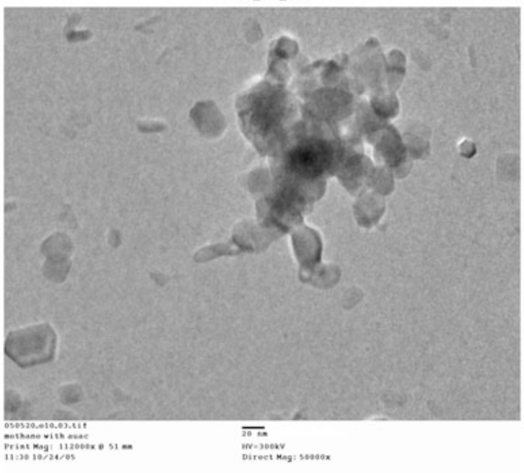

050520_e10_03.tif

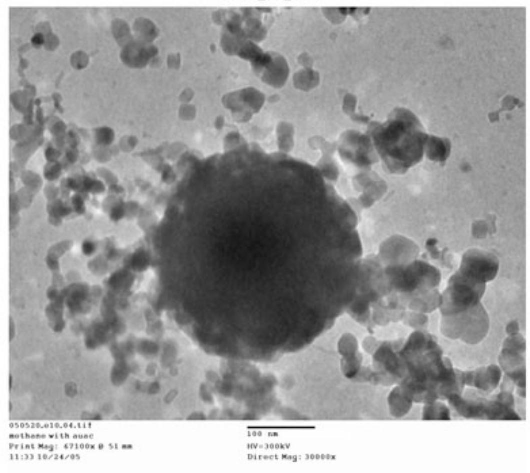

050520_e10_04.tif

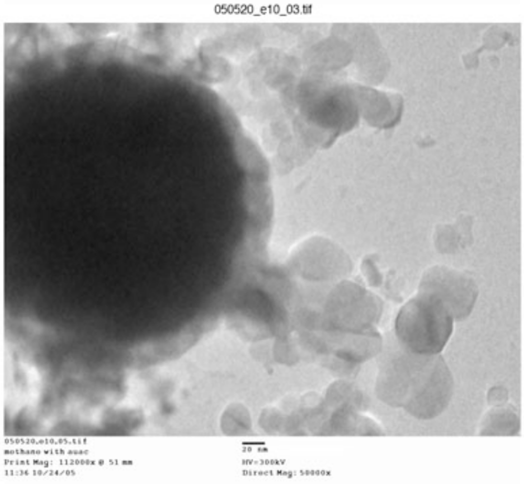

050520_e10_05.tif

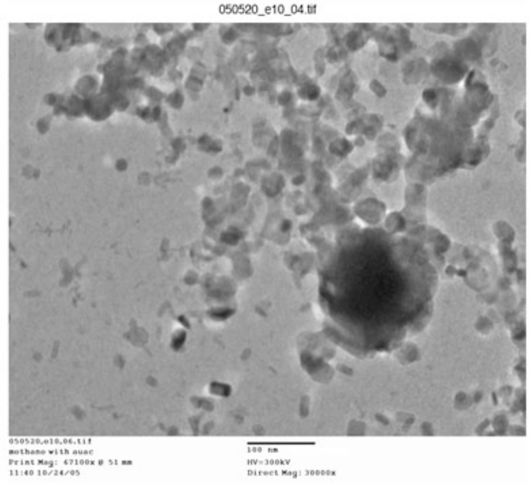

050520_e10_06.tif

MACS gold-doped SnO_2

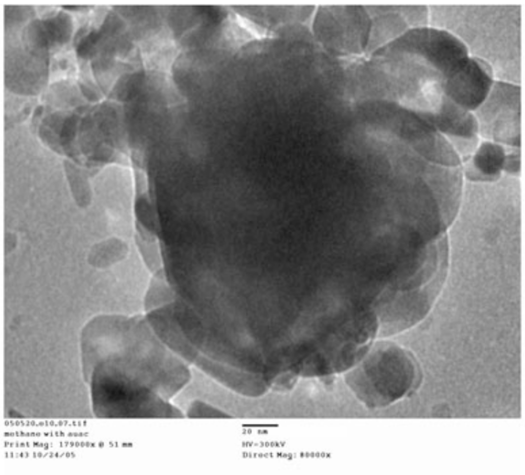

050520_e10_07.tif

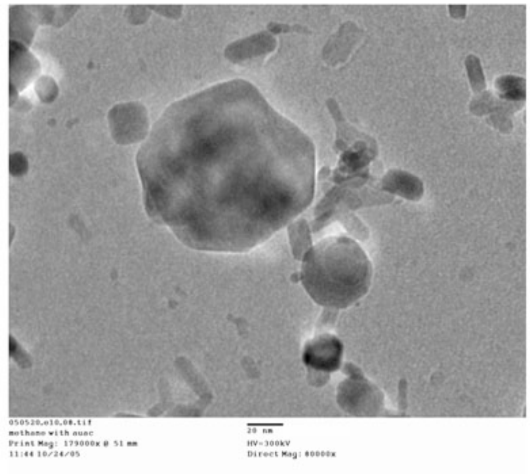

050520_e10_08.tif

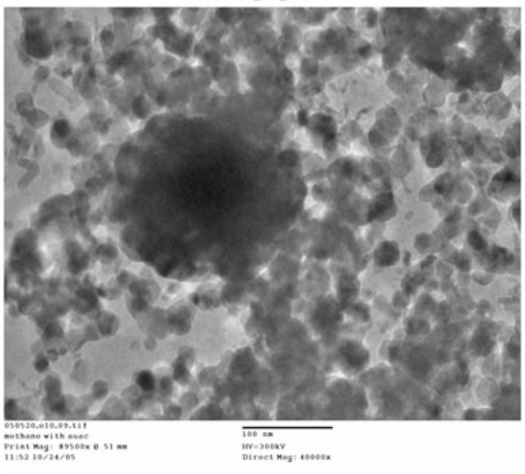

050520_e10_09.tif

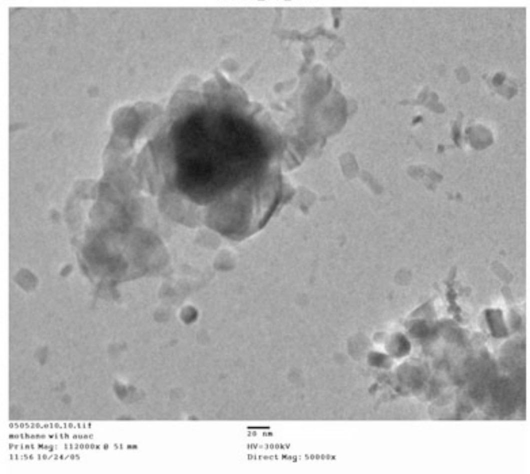

050520_e10_10.tif

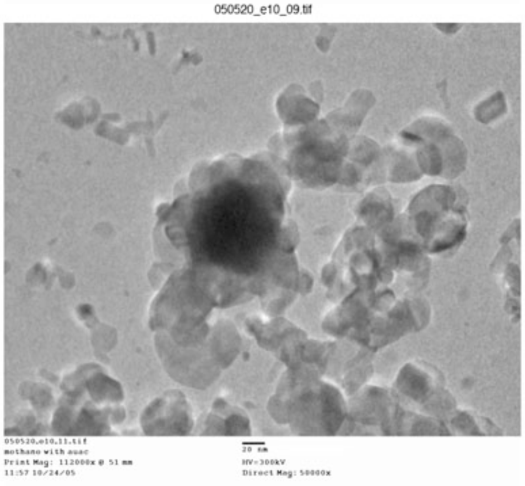

050520_e10_11.tif

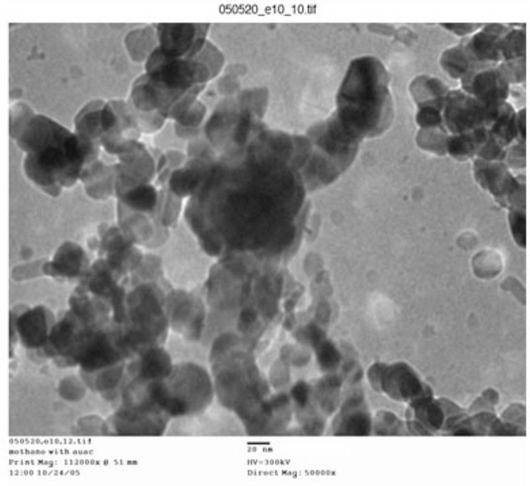

050520_e10_12.tif

MACS aluminum-doped SnO_2

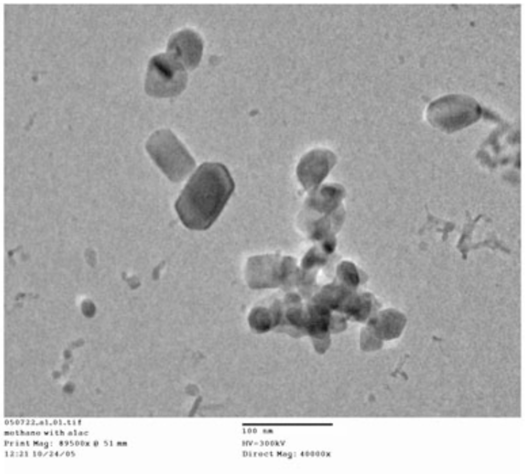

050722_a2_01.tif

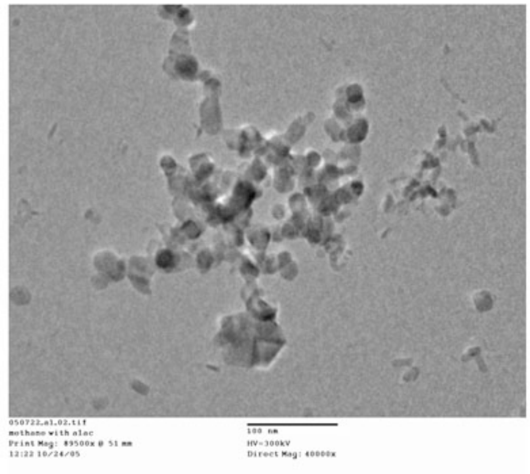

050722_a2_02.tif

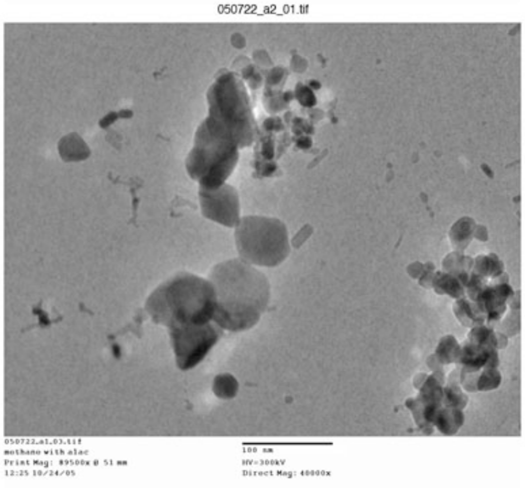

050722_a2_03.tif

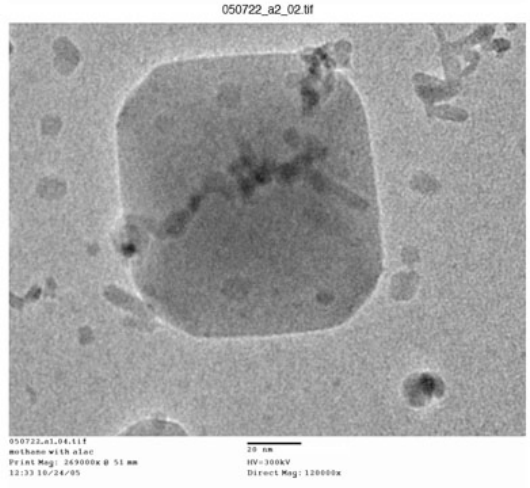

050722_a2_04.tif

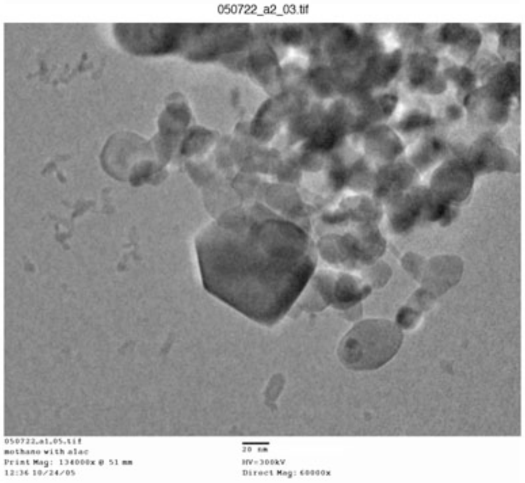

050722_a2_05.tif

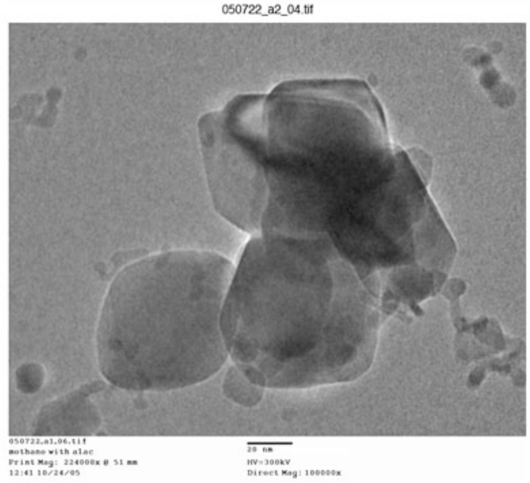

050722_a2_06.tif

MACS aluminum-doped SnO_2

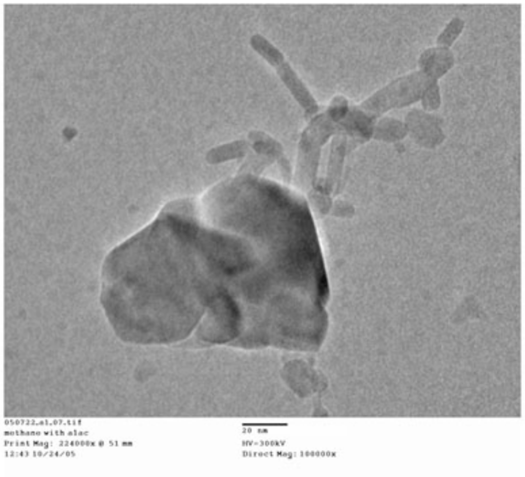

050722_a2_07.tif

MACS platinum-doped SnO_2

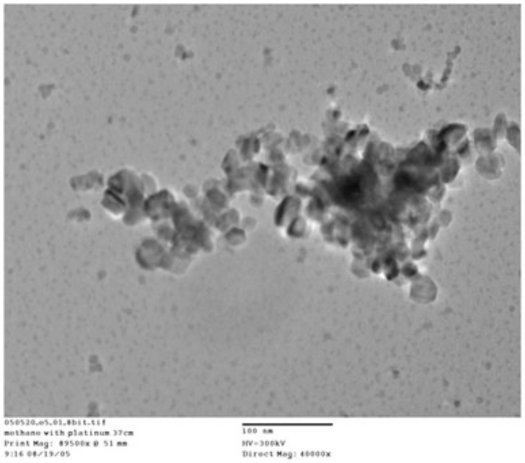

050520_e5_01.tif

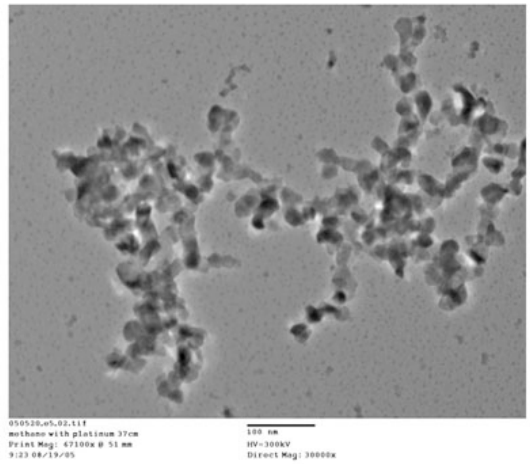

050520_e5_02.tif

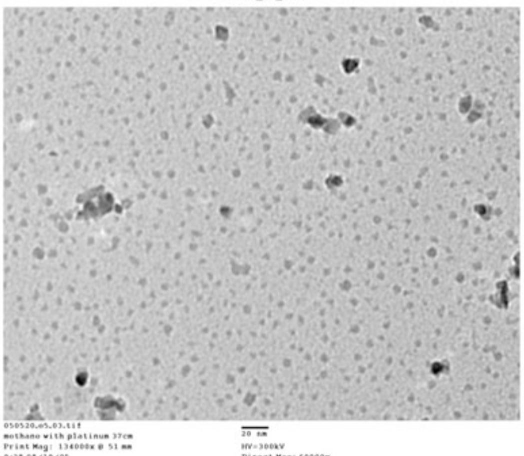

050520_e5_03.tif

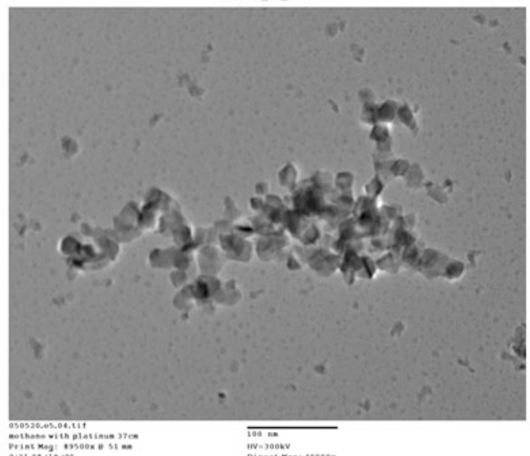

050520_e5_04.tif

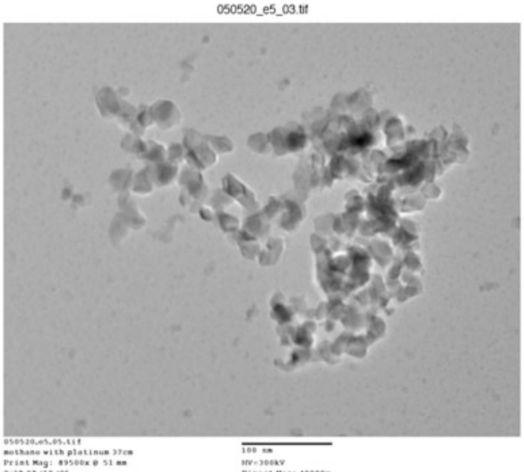

050520_e5_05.tif

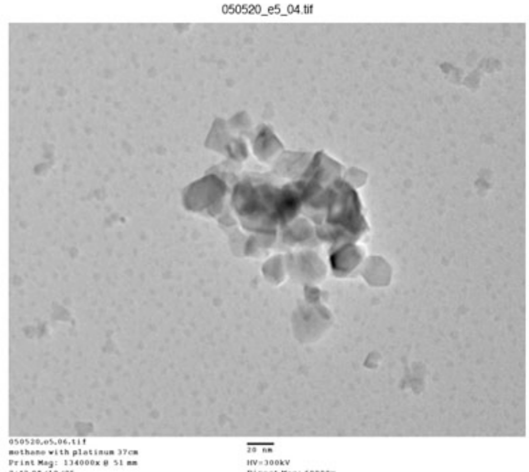

050520_e5_06.tif

MACS aluminum-doped SnO_2

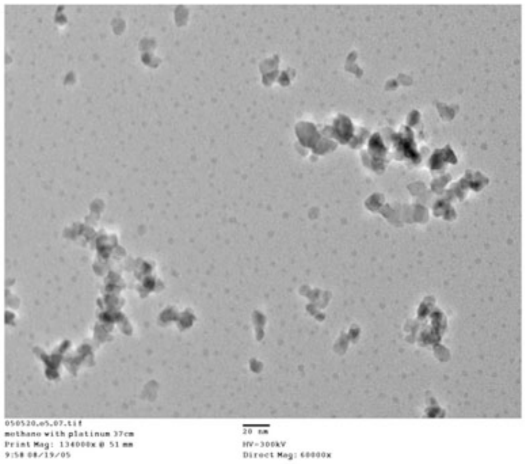

050520_e5_07.tif

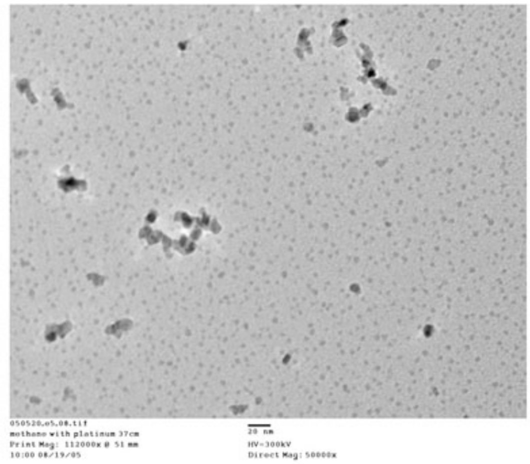

050520_e5_08.tif

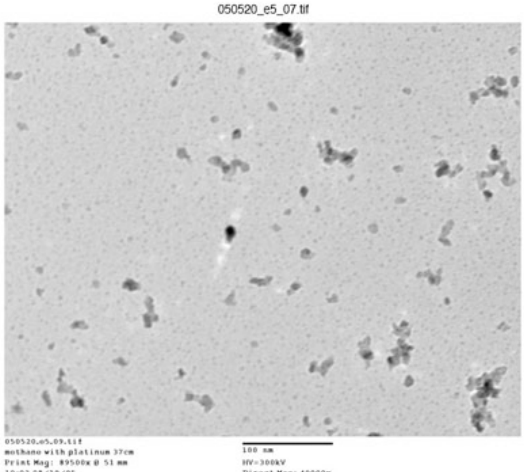

050520_e5_09.tif

Gold acetate decomposition study on hot-plate

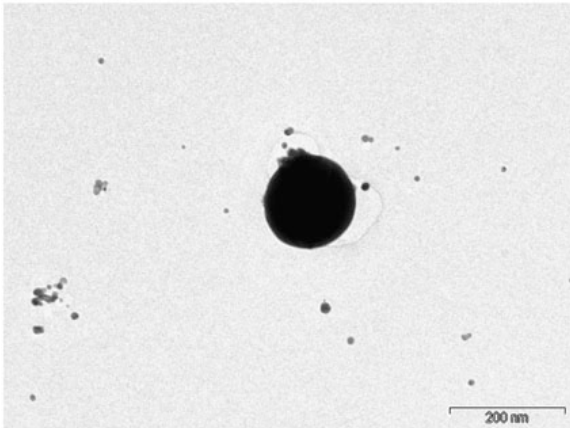

060929_b2_01.tif

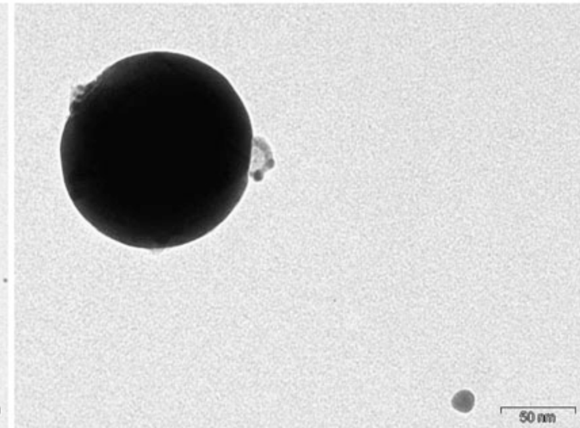

060929_b2_02.tif

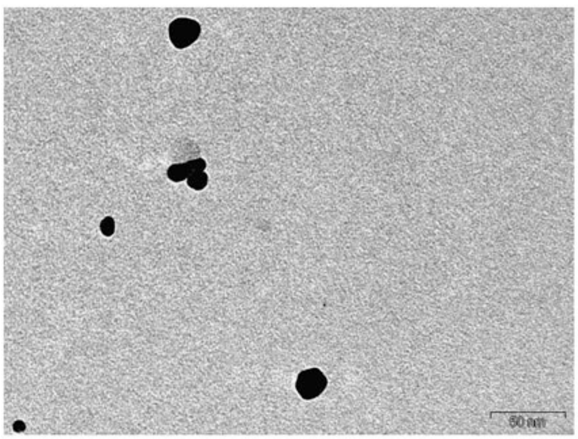

060929_b2_03.tif

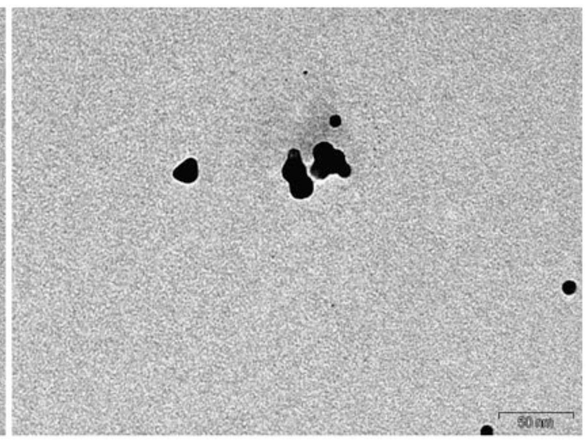

060929_b2_04.tif

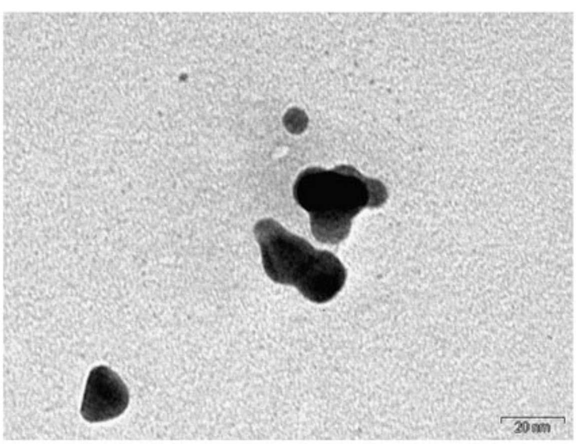

060929_b2_05.tif

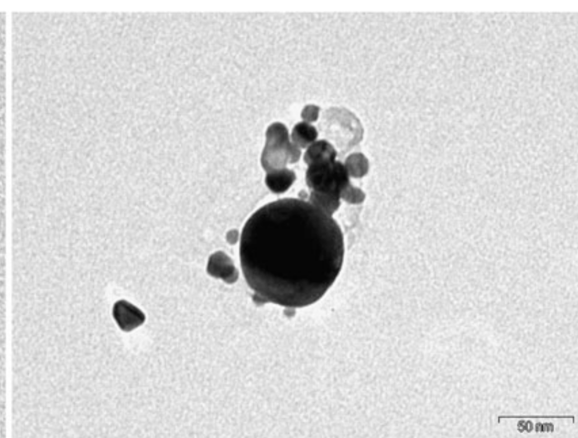

060929_b2_06.tif

Gold acetate decomposition study on hot-plate

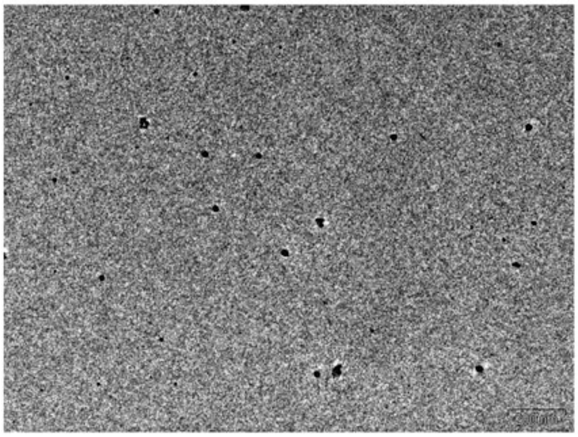

060929_b2_07.tif

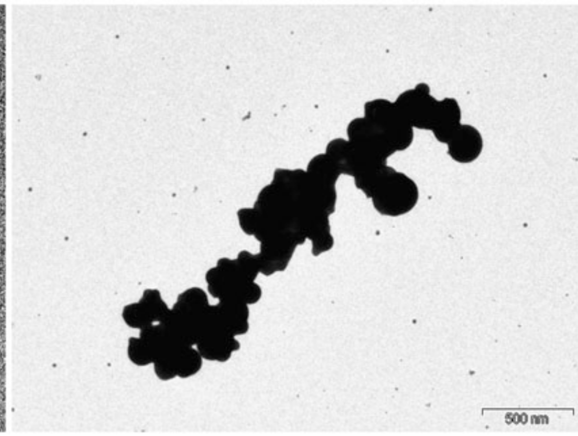

060929_b2_08.tif

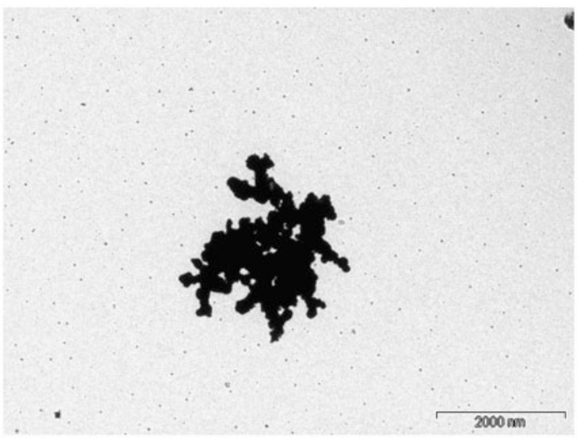

060929_b2_09.tif

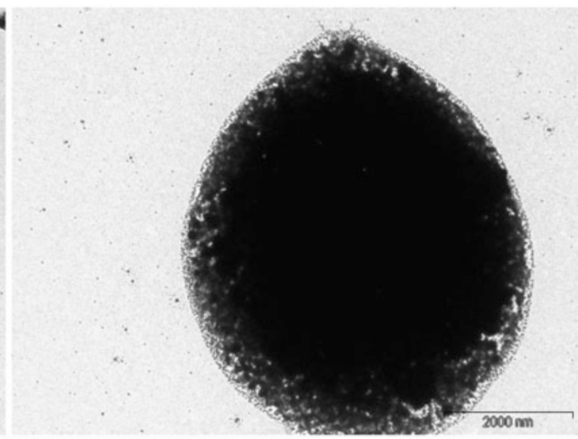

060929_b2_10.tif

060929_b2_11.tif

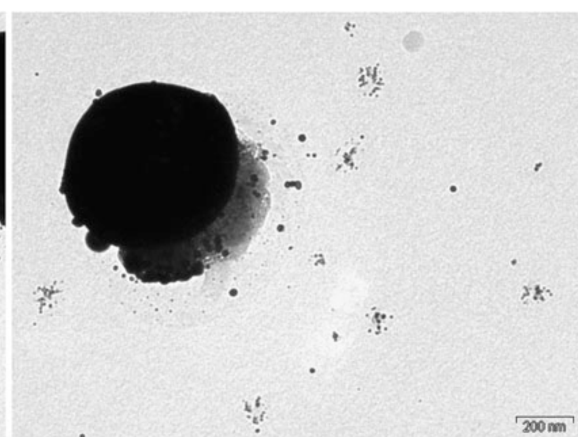

060929_b2_12.tif

Gold acetate decomposition study on hot-plate

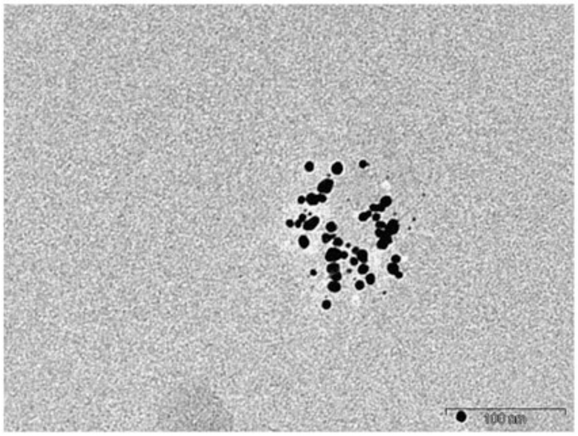

060929_b2_13.tif

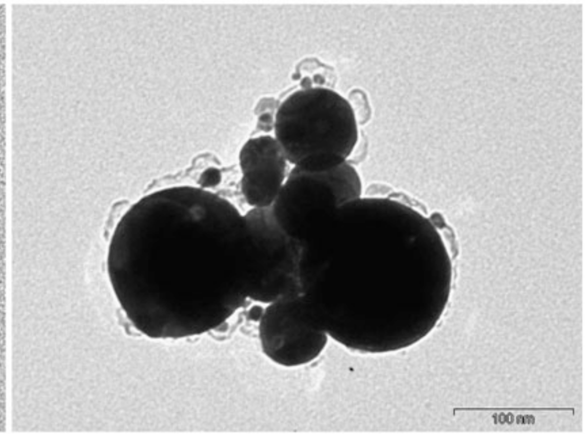

060929_b1_01.tif

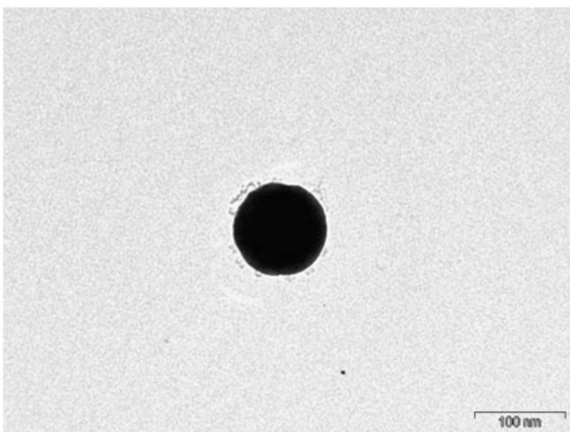

060929_b1_02.tif

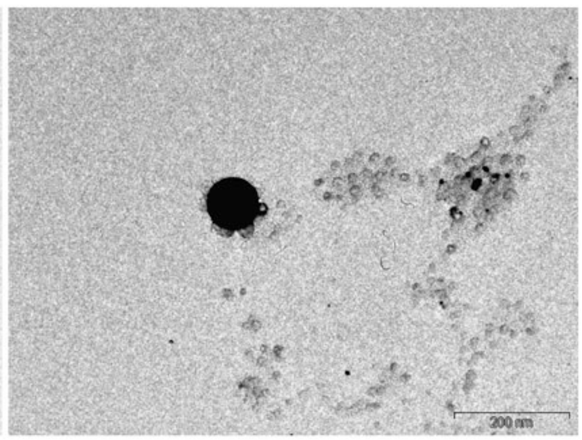

060929_b1_03.tif

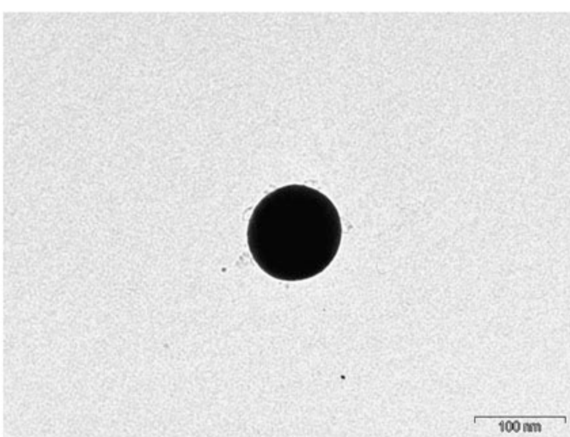

060929_b1_04.tif

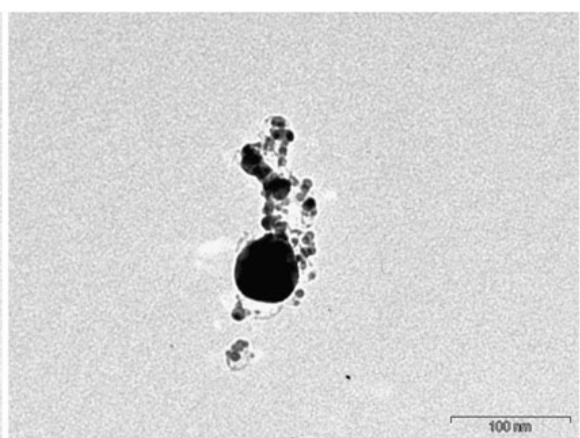

060929_b1_05.tif

Gold acetate decomposition study on hot-plate

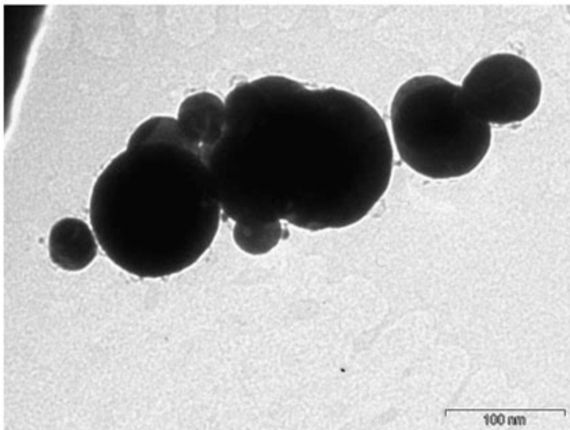

060929_b1_06.tif

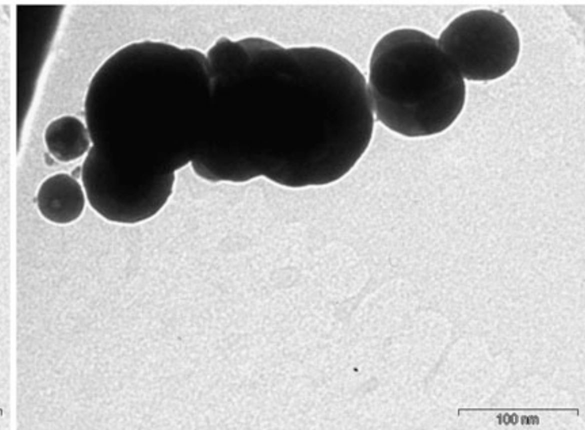

060929_b1_07.tif

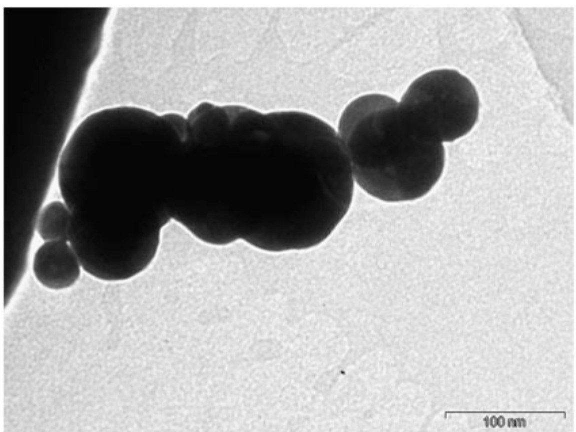

060929_b1_08.tif

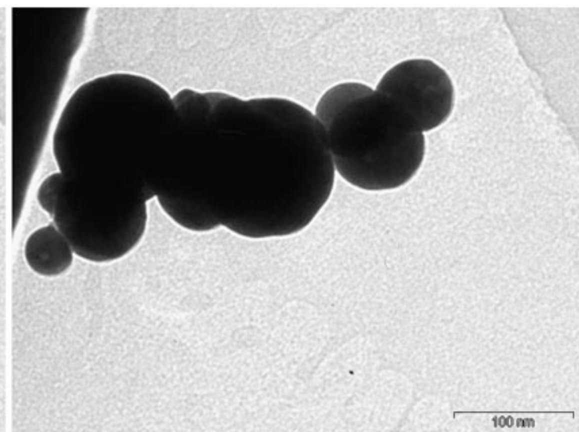

060929_b1_09.tif

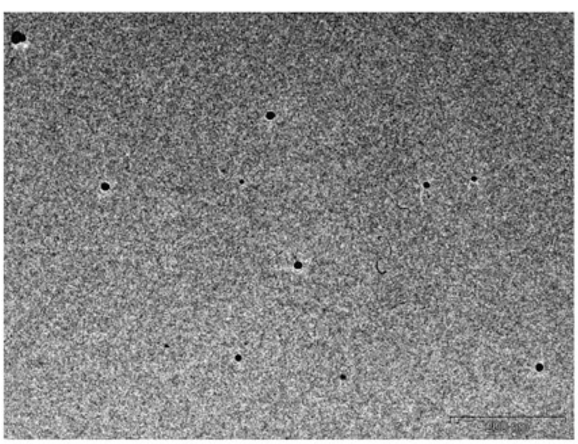

060929_b2_01.tif

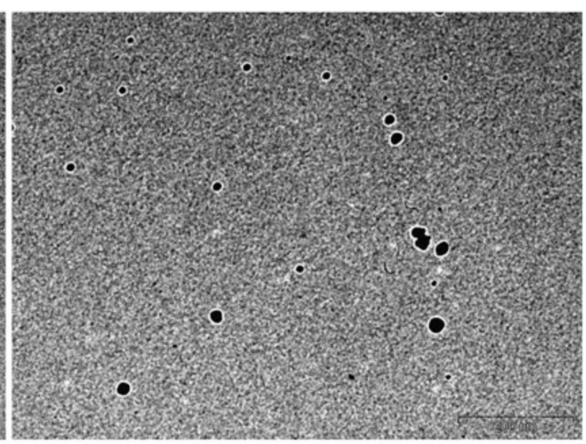

060929_b2_02.tif

Gold acetate decomposition study on hot-plate

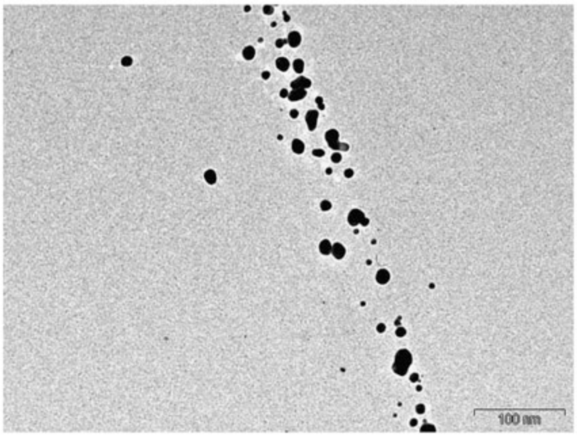

060929_b2_03.tif

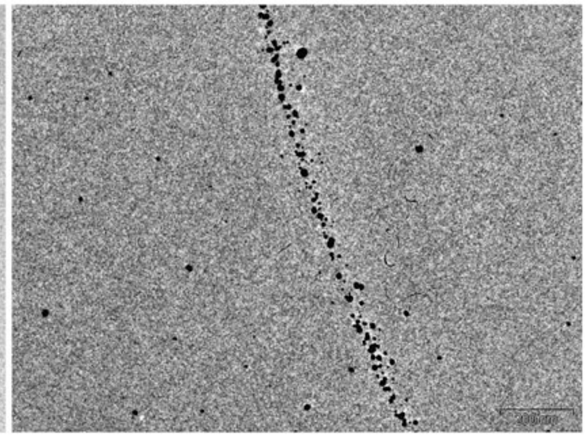

060929_b2_04.tif

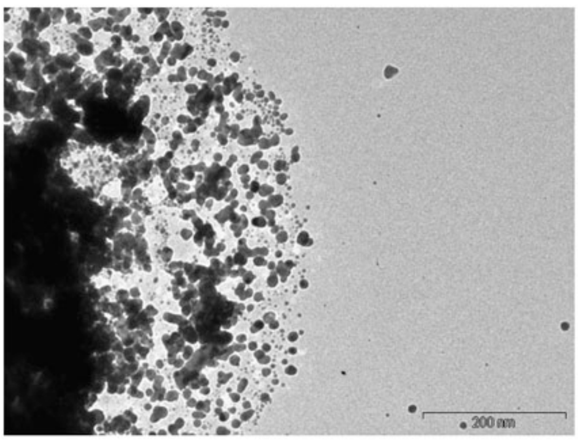

060929_b2_05.tif

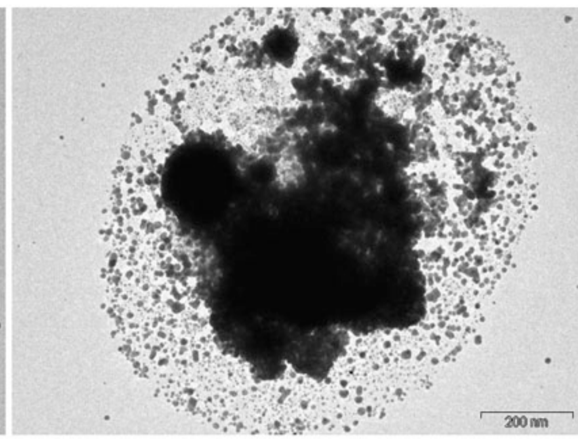

060929_b2_06.tif

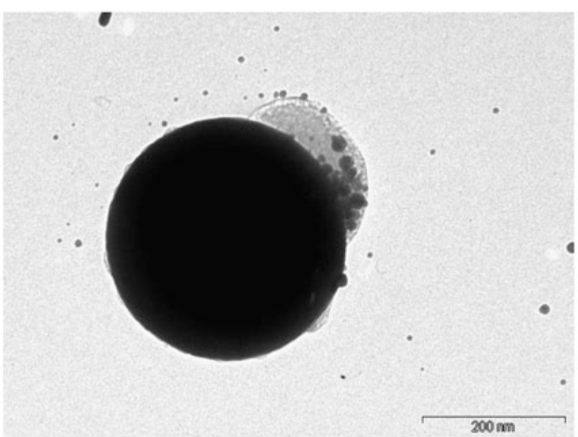

060929_b2_07.tif

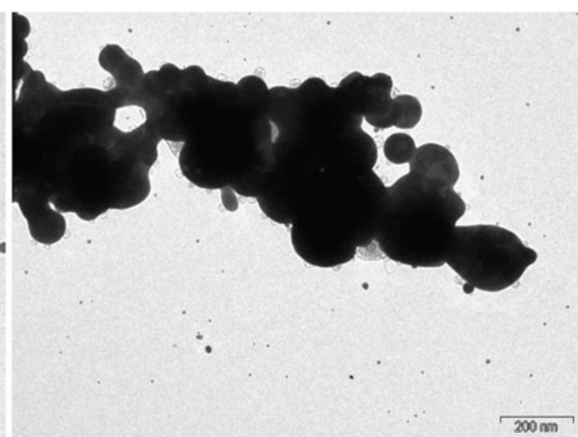

060929_b2_08.tif

Gold acetate decomposition study on hot-plate

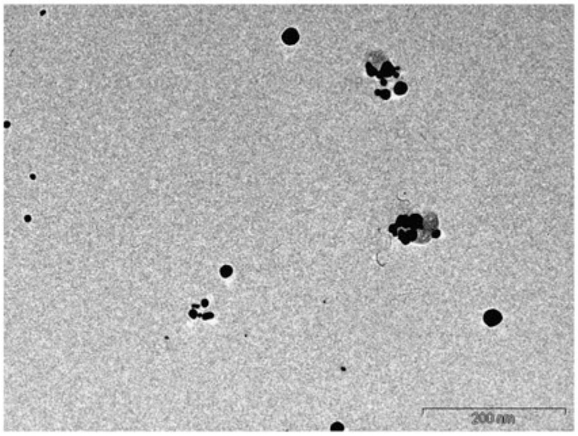

060929_b2_09.tif

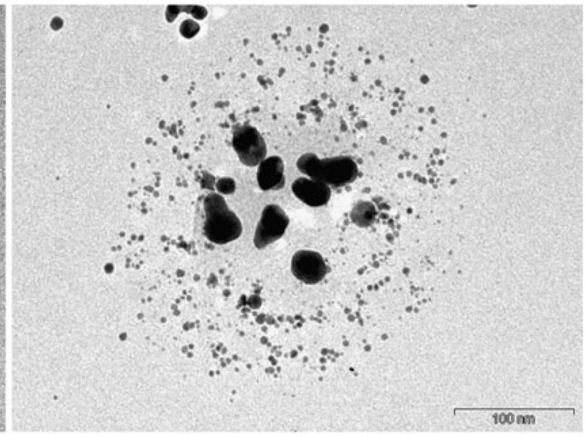

060929_b2_10.tif

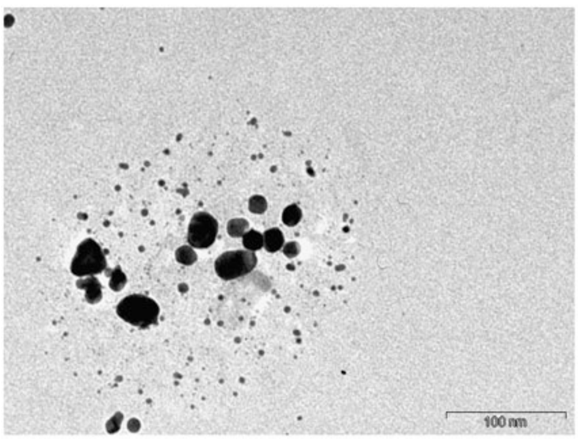

060929_b2_11.tif

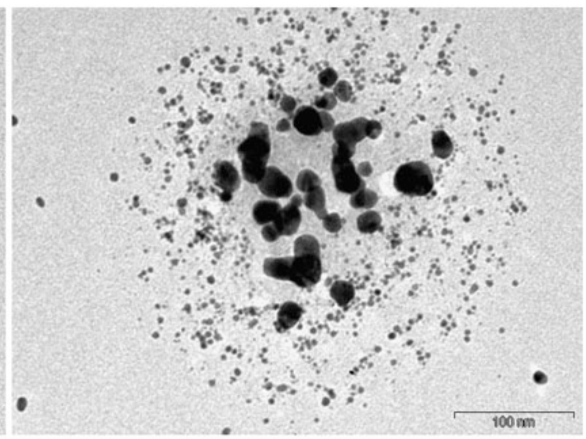

060929_b2_12.tif

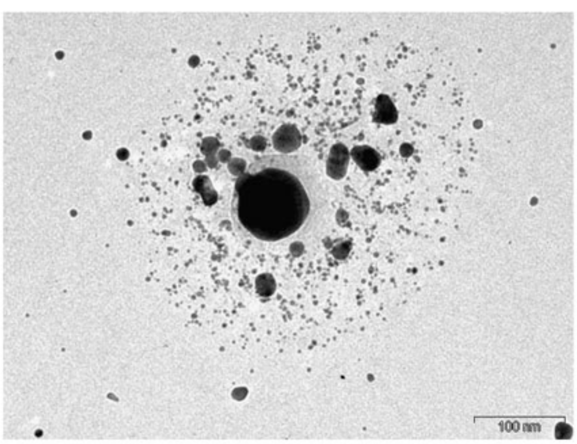

060929_b2_13.tif

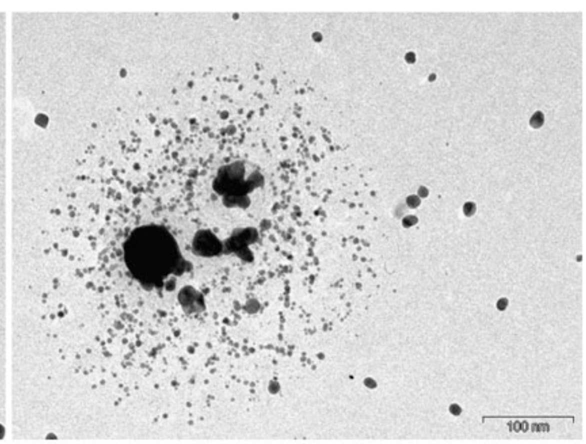

060929_b2_14.tif

Gold acetate decomposition study on hot-plate

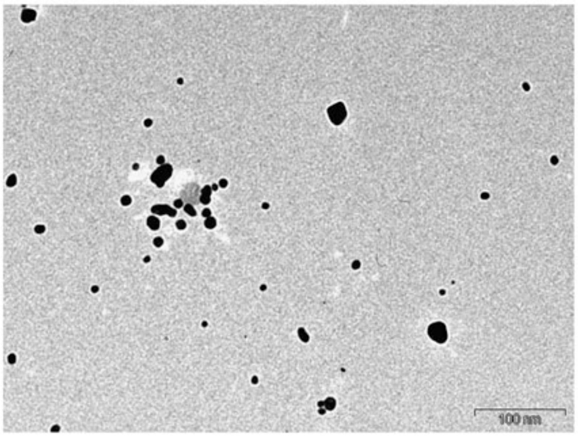

060929_b2_15.tif

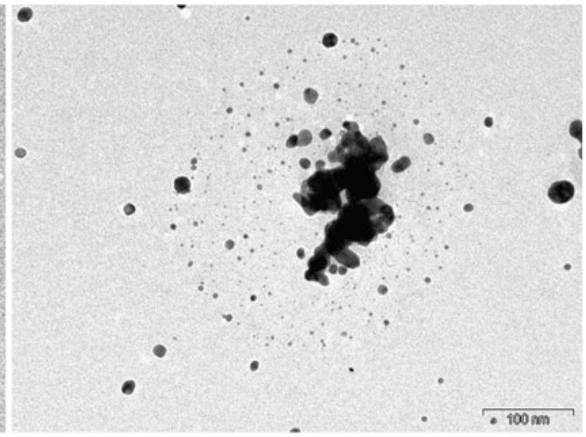

060929_b2_16.tif

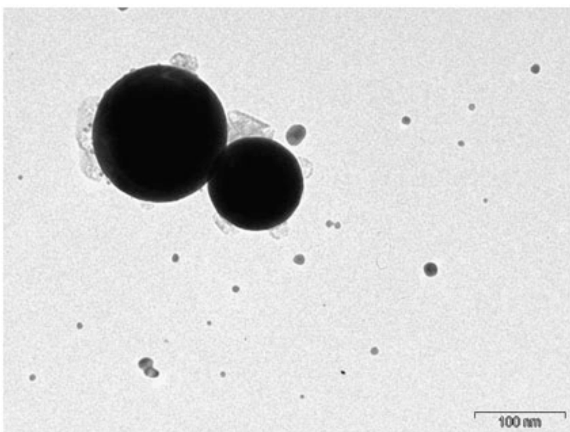

060929_b2_17.tif

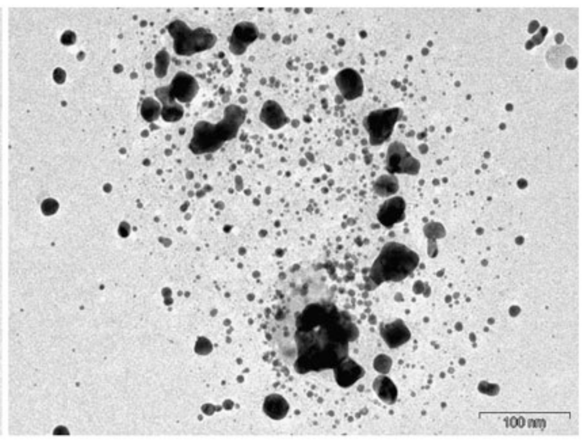

060929_b2_18.tif

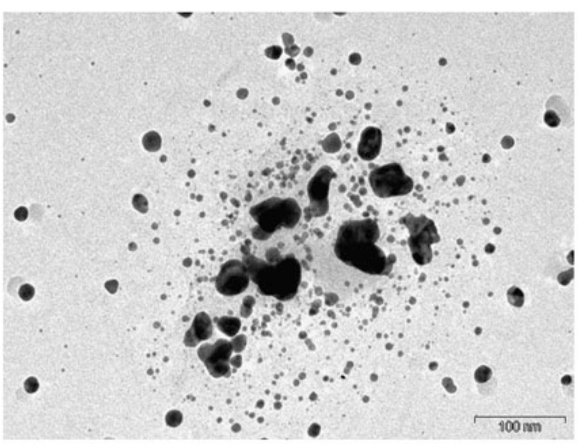

060929_b2_19.tif

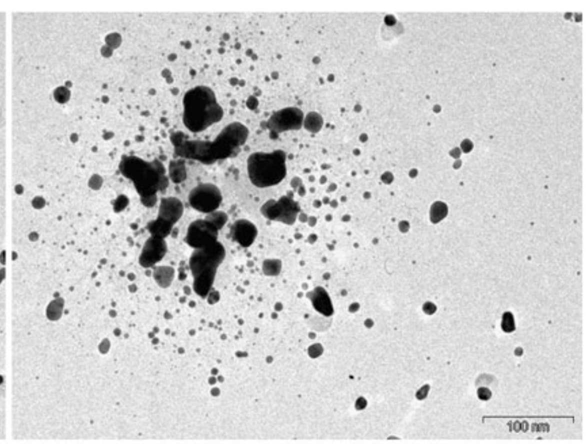

060929_b2_20.tif

Gold acetate decomposition study on hot-plate

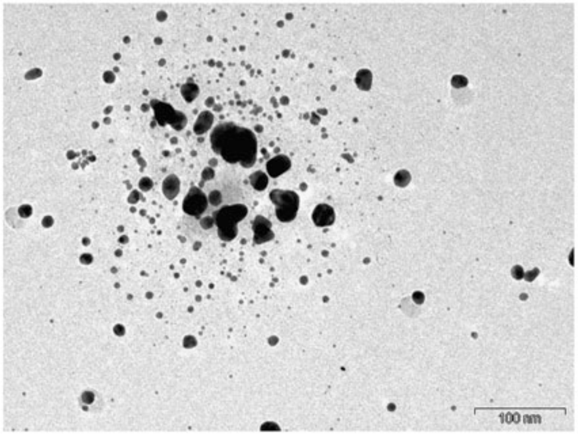

060929_b2_21.tif

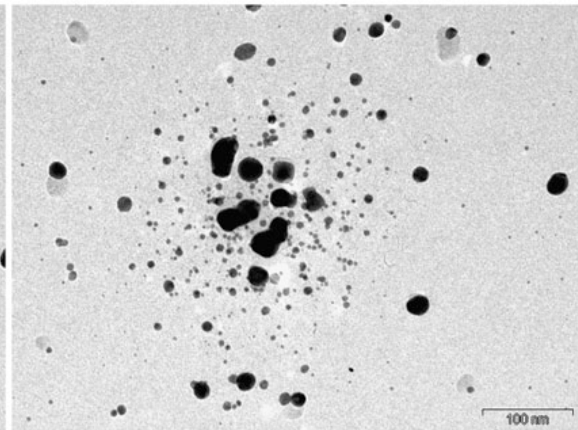

060929_b2_22.tif

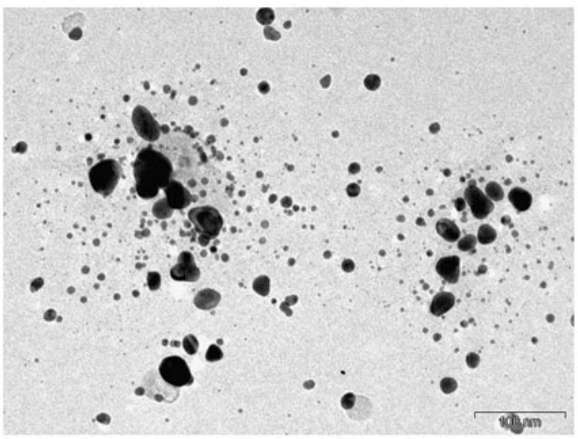

060929_b2_23.tif

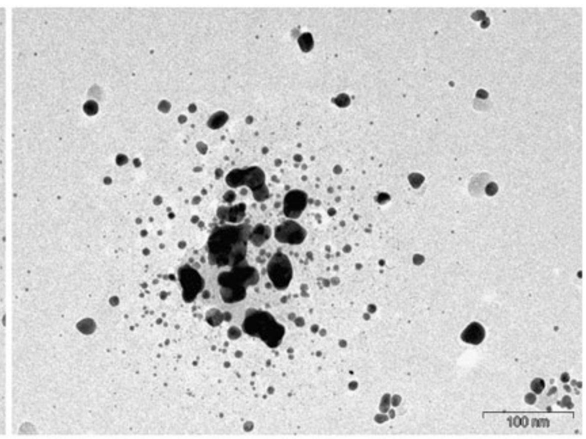

060929_b2_24.tif

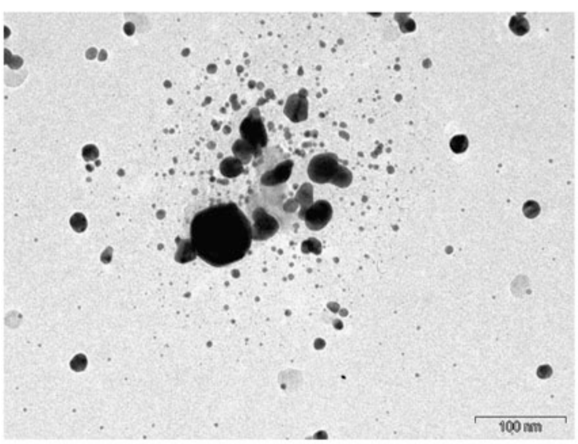

060929_b2_25.tif

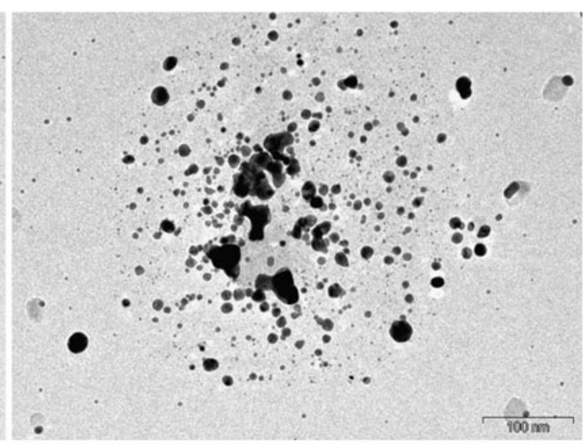

060929_b2_26.tif

Gold acetate decomposition study on hot-plate

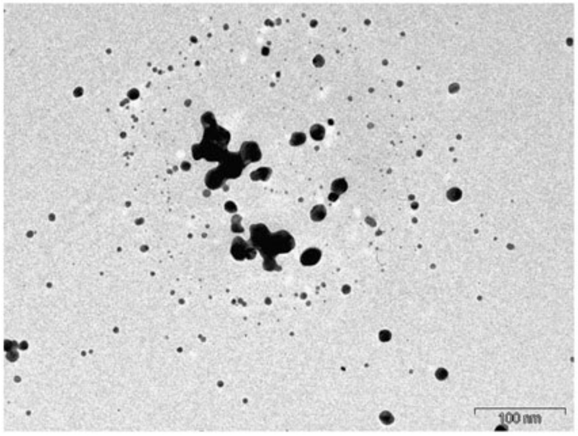

060929_b2_27.tif

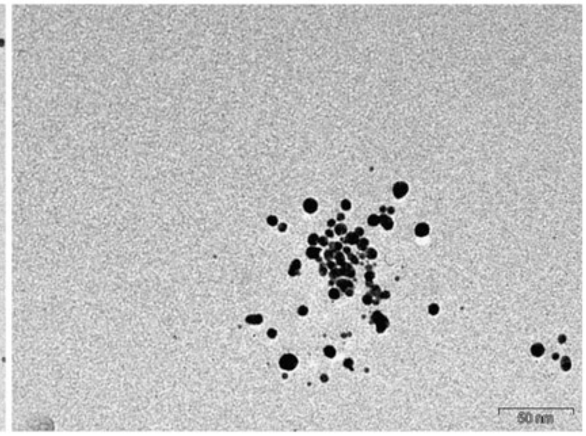

060929_b2_28.tif

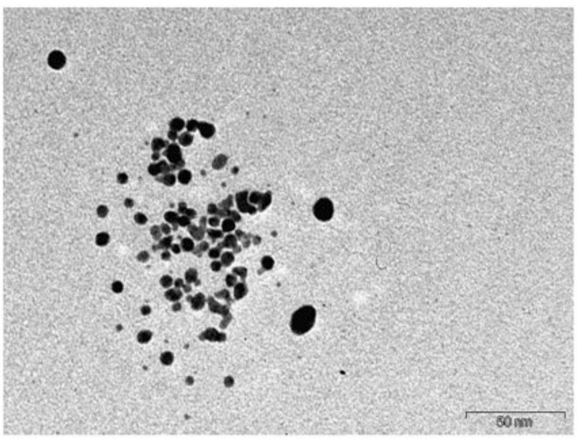

060929_b2_29.tif

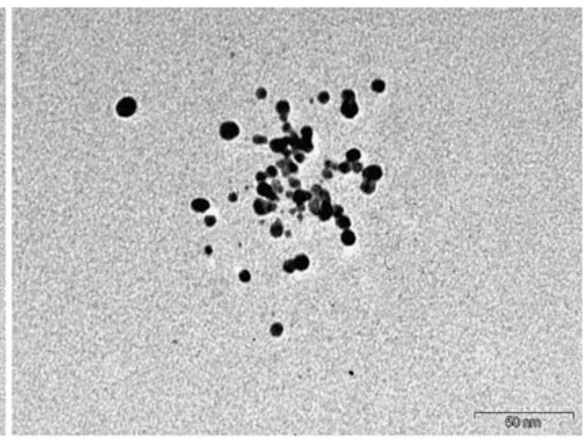

060929_b2_30.tif

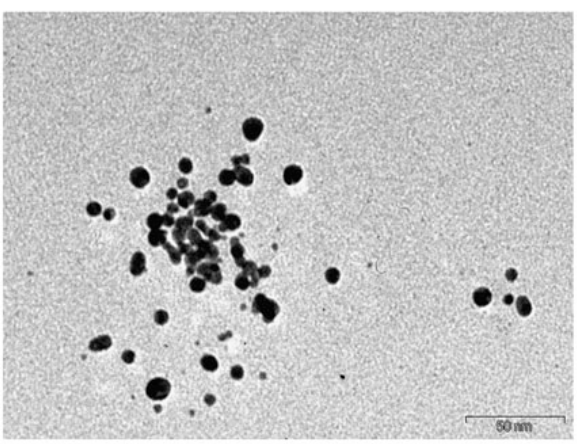

060929_b2_31.tif

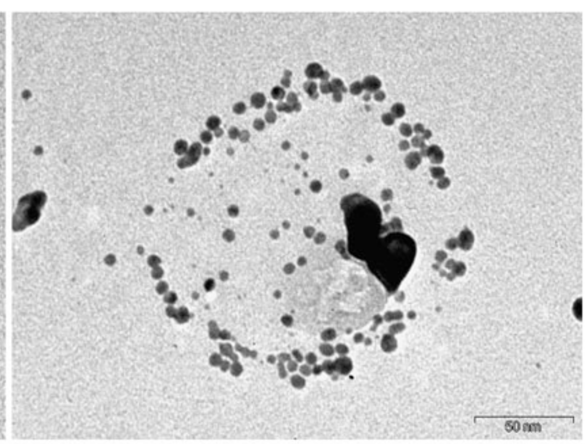

060929_b2_32.tif

Gold acetate decomposition study on hot-plate

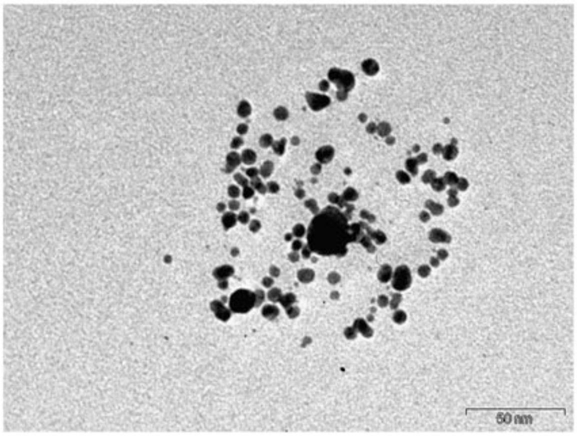

060929_b2_33.tif

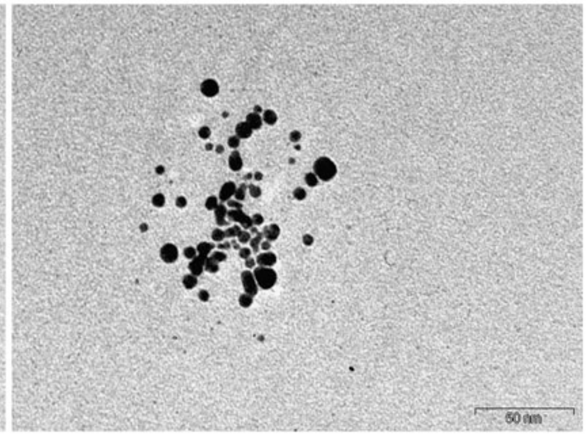

060929_b2_34.tif

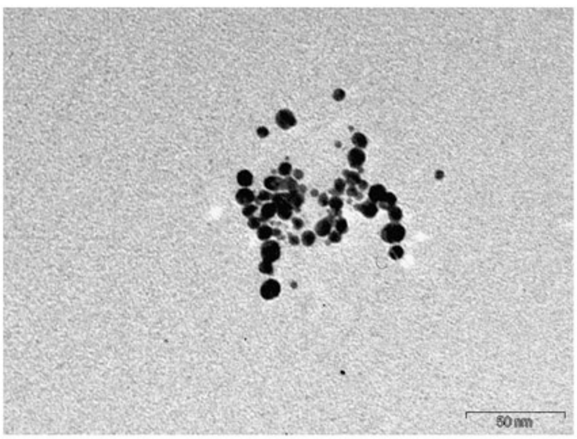

060929_b2_35.tif

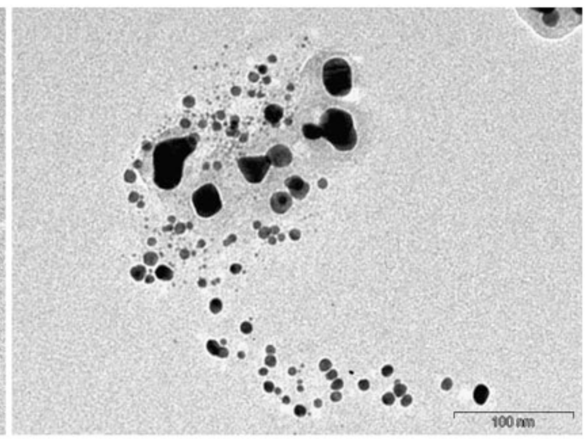

060929_b2_36.tif

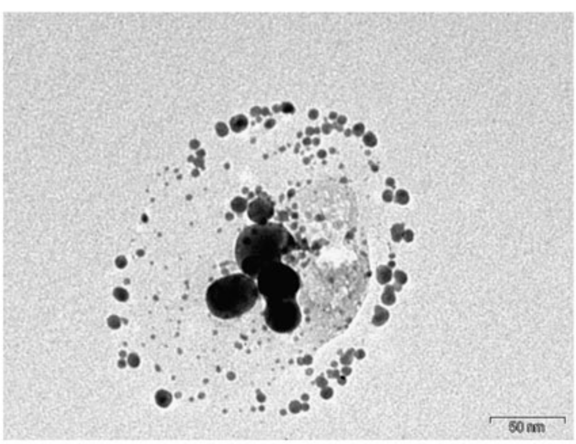

060929_b2_37.tif

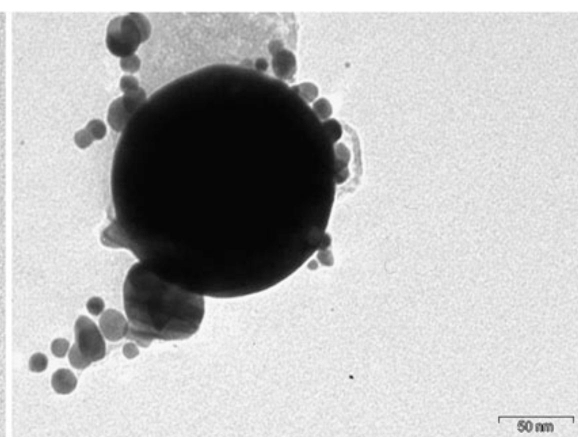

060929_b2_38.tif

Gold acetate decomposition study on hot-plate

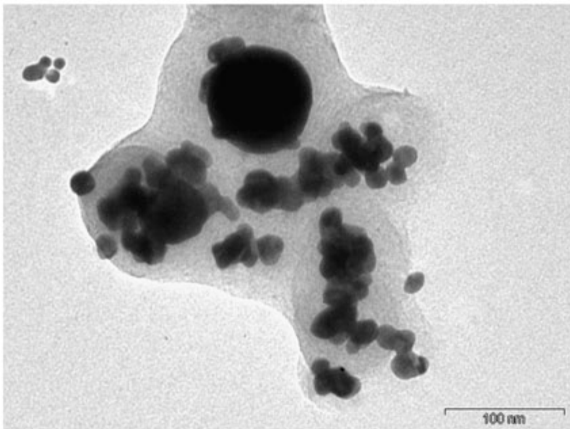

060929_b2_39.tif

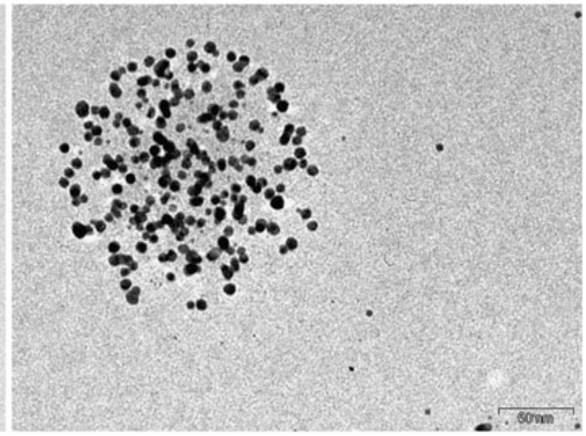

060929_b2_40.tif

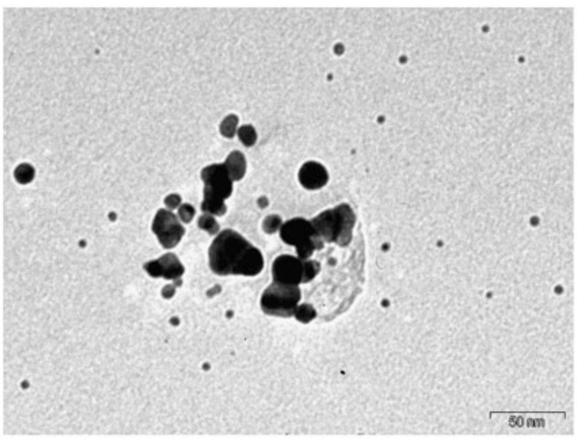

060929_b2_41.tif

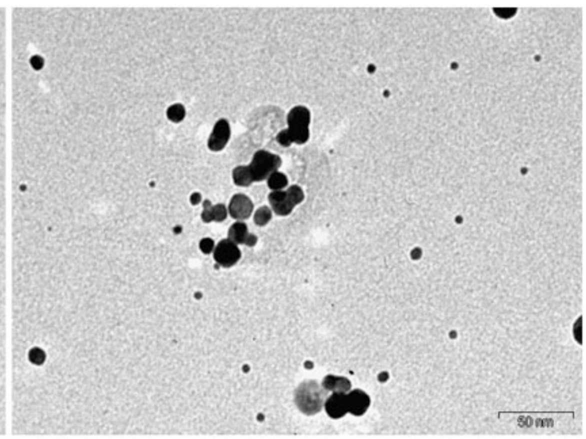

060929_b2_42.tif

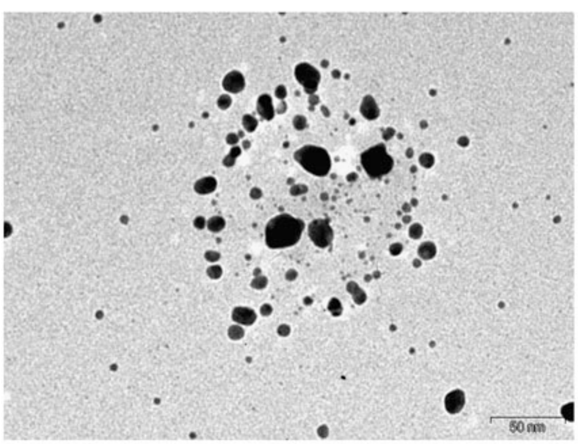

060929_b2_43.tif

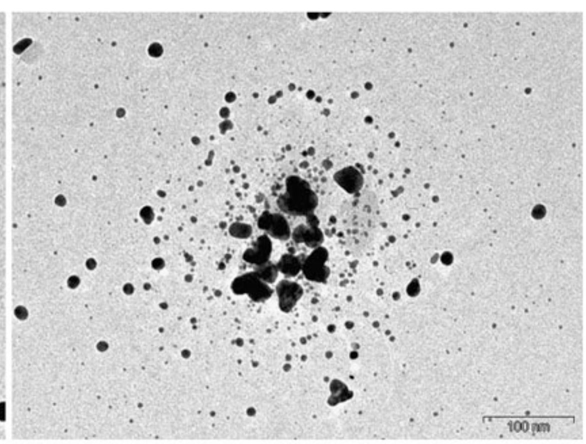

060929_b2_44.tif

Gold acetate decomposition study on hot-plate

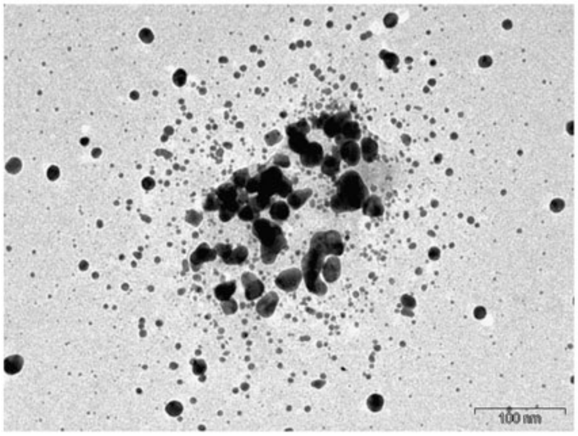

060929_b2_45.tif

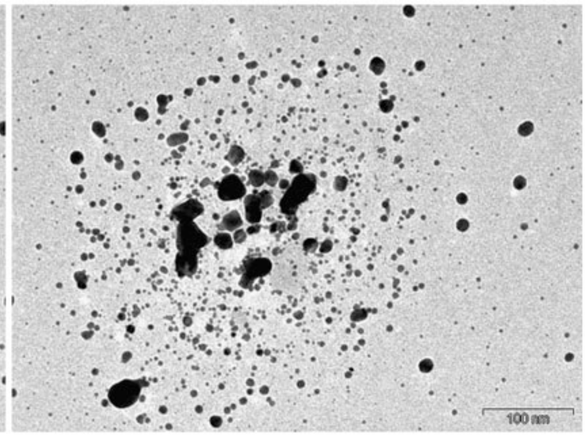

060929_b2_46.tif

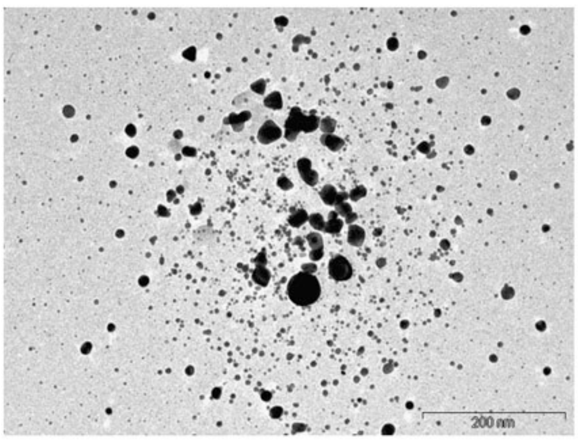

060929_b2_47.tif

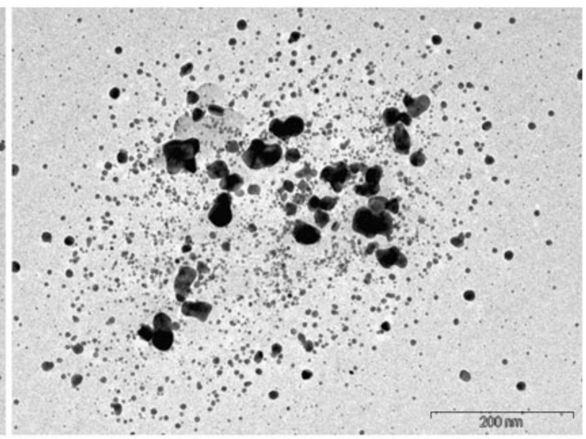

060929_b2_48.tif

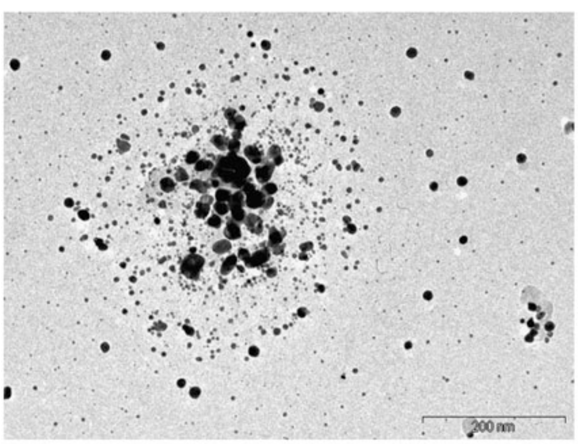

060929_b2_49.tif

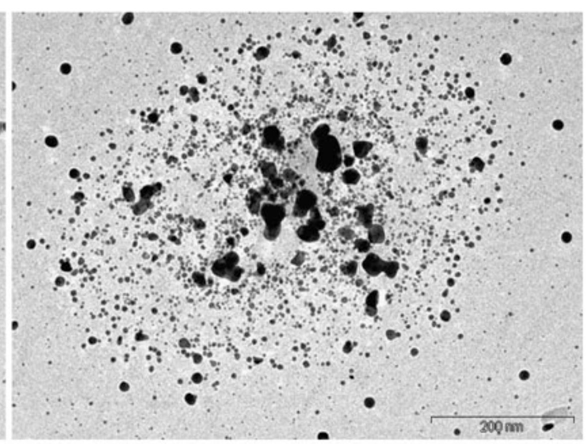

060929_b2_50.tif

Gold acetate decomposition study - sampled 1 mm away

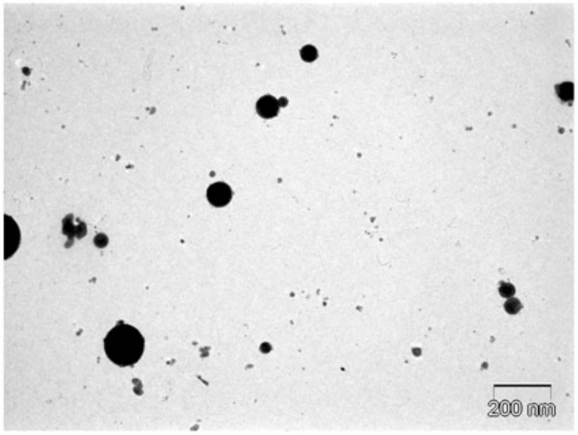

060929_a8_01.tif

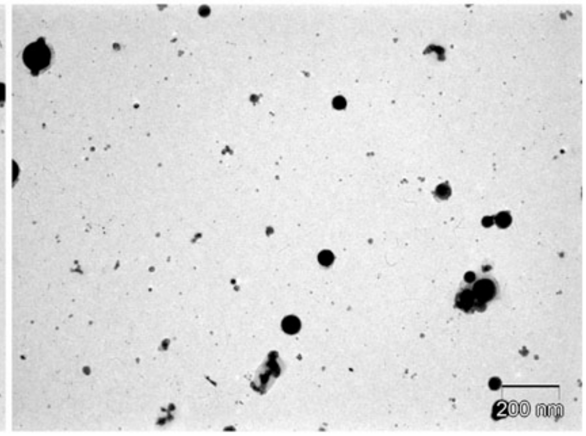

060929_a8_02.tif

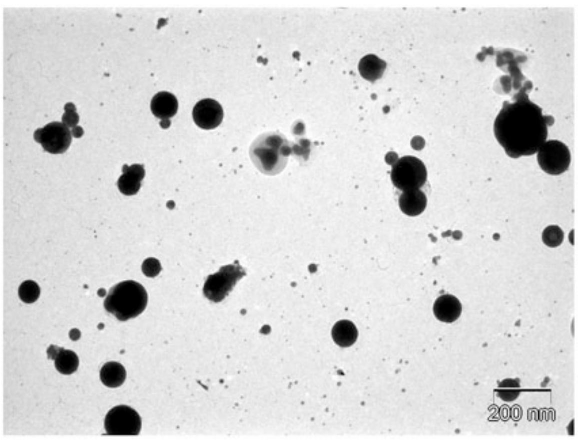

060929_a8_03.tif

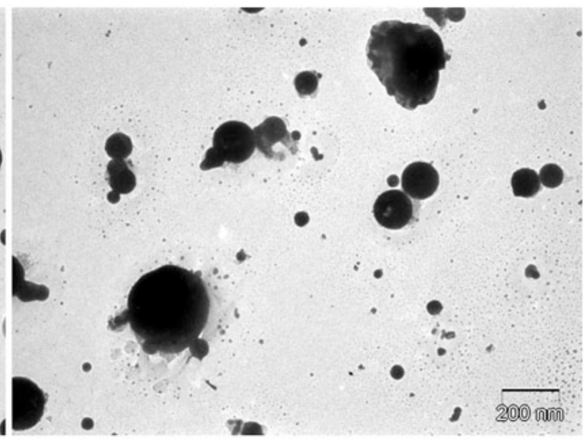

060929_a8_04.tif

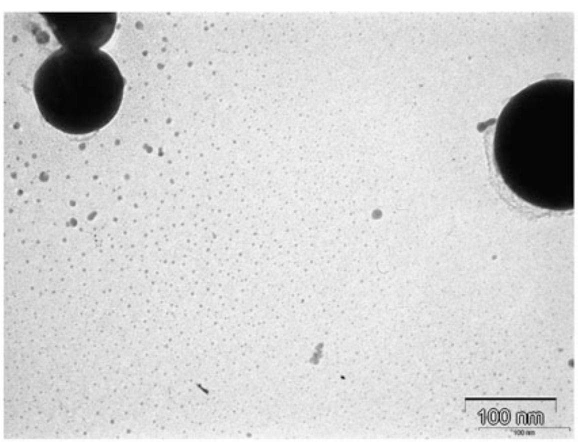

060929_a8_05.tif

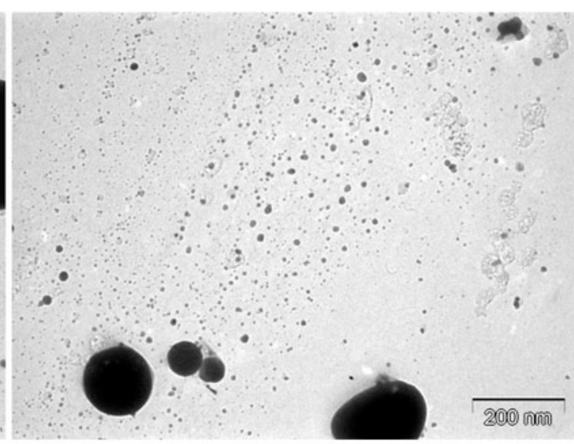

060929_a8_06.tif

Gold acetate decomposition study - sampled 1 mm away

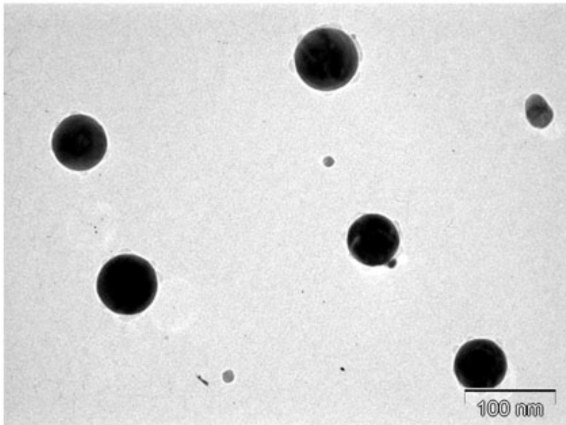

060929_a8_07.tif

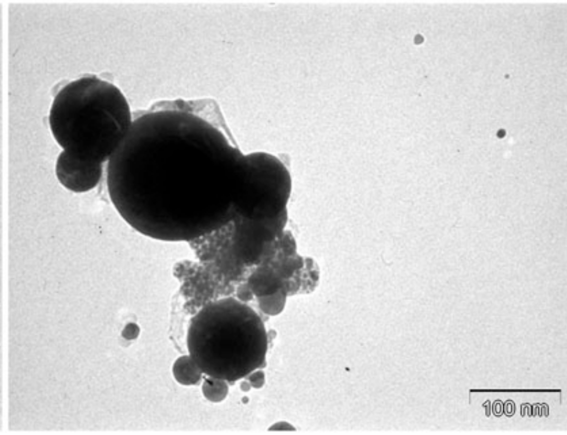

060929_a8_08.tif

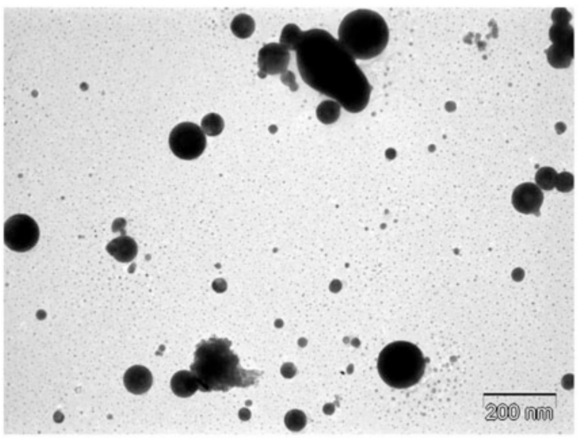

060929_a8_09.tif

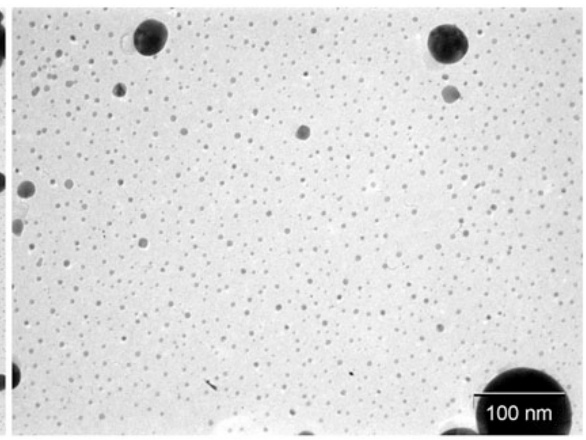

060929_a8_10.tif

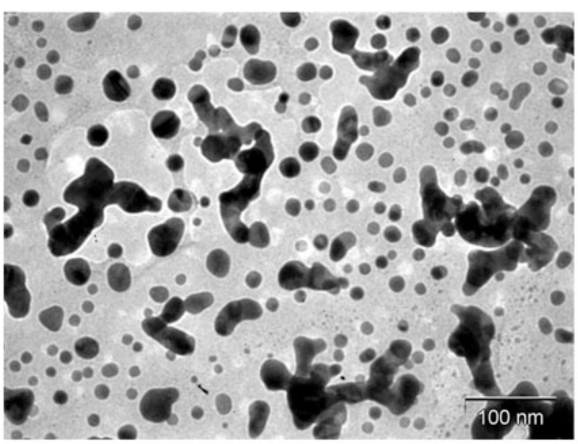

060929_a8_11.tif

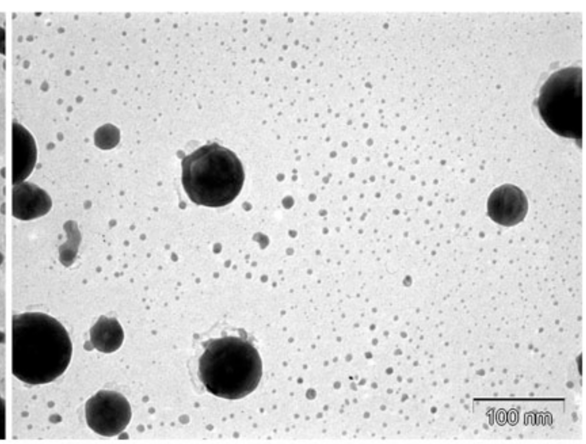

060929_a8_12.tif

Gold acetate decomposition study - sampled 1 mm away

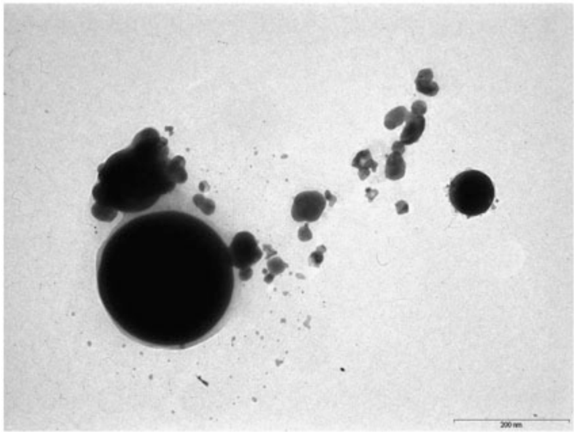

060929_a9_01.tif

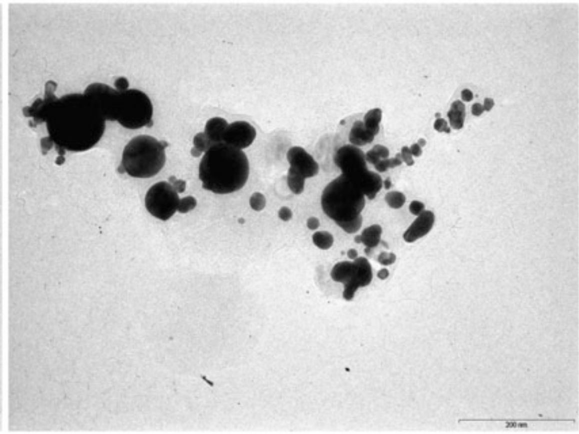

060929_a9_02.tif

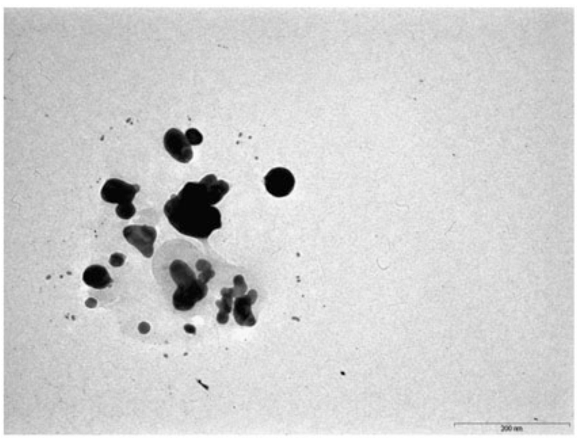

060929_a9_03.tif

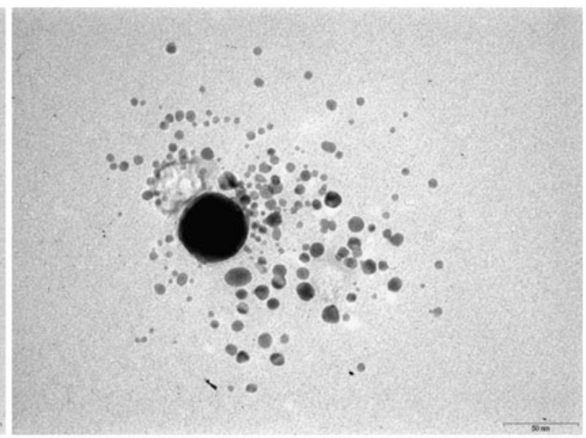

060929_a9_04.tif

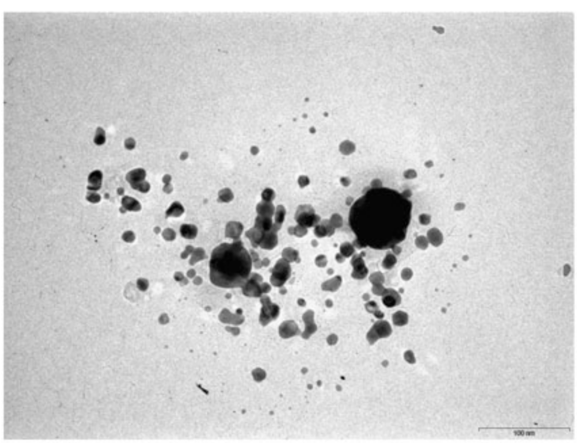

060929_a9_05.tif

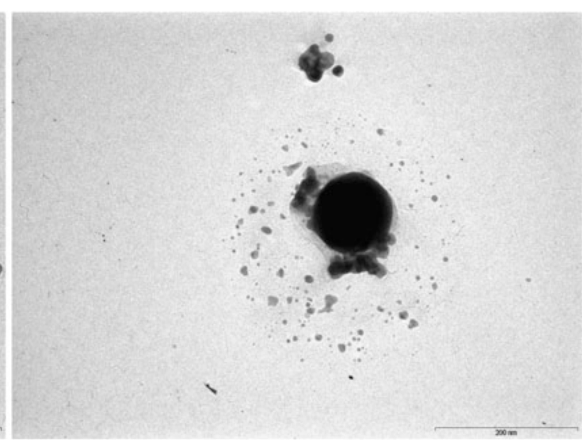

060929_a9_06.tif

Gold acetate decomposition study - sampled 1 mm away

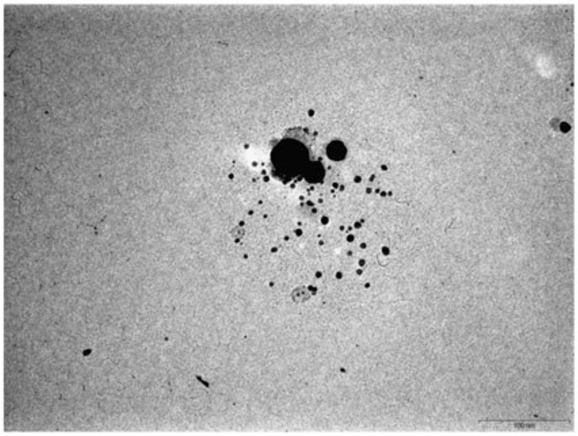

060929_a9_07.tif

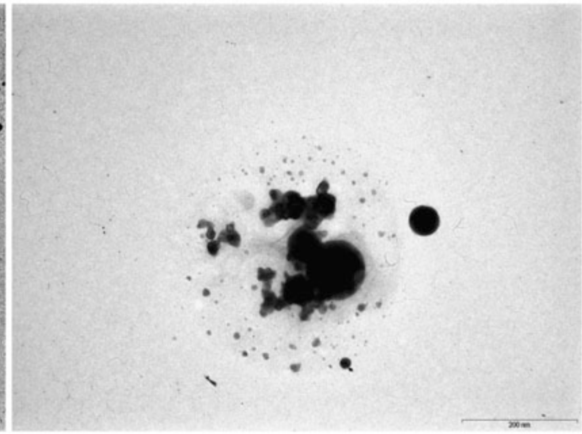

060929_a9_08.tif

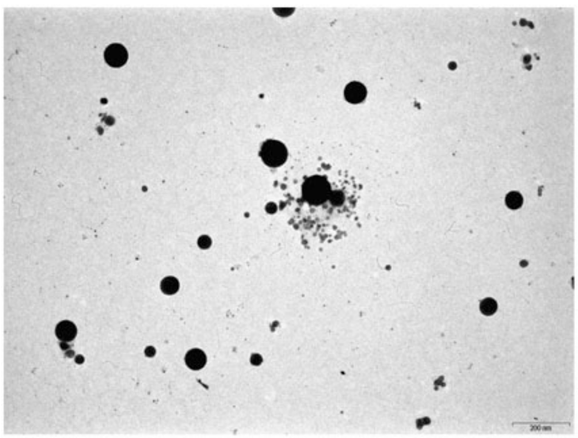

060929_a9_09.tif

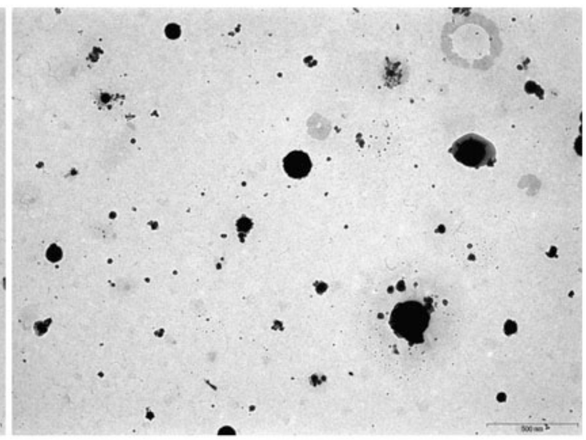

060929_a9_10.tif

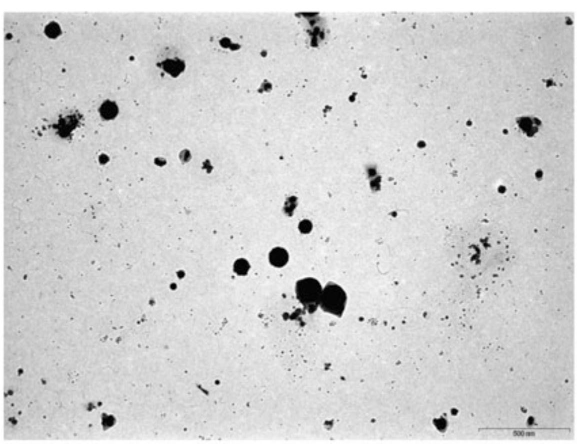

060929_a9_11.tif

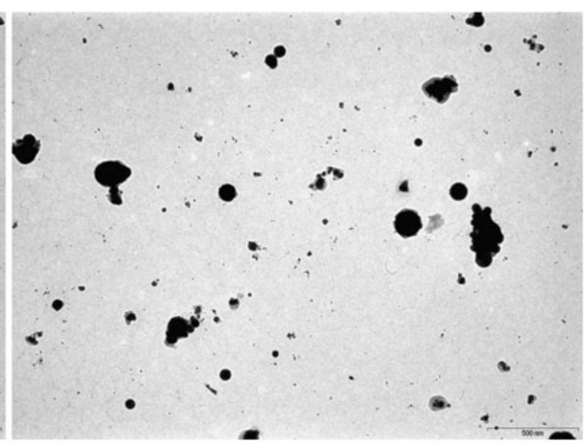

060929_a9_12.tif

Gold acetate decomposition study - sampled 2 mm away

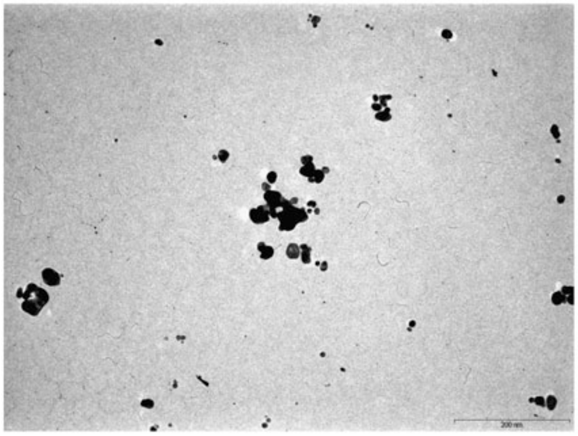

060929_d10_01.tif

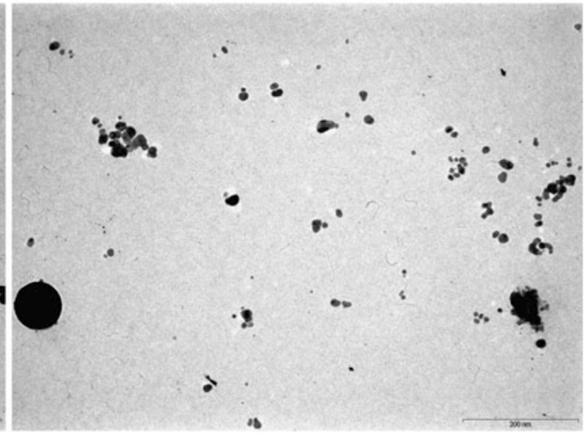

060929_d10_02.tif

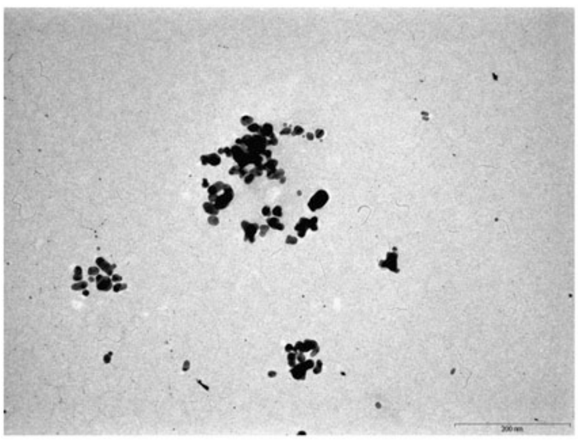

060929_d10_03.tif

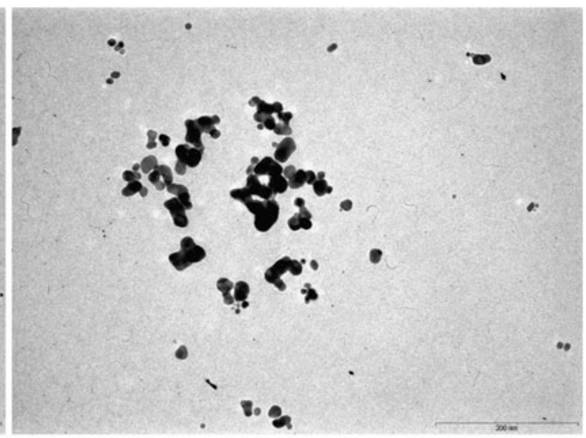

060929_d10_04.tif

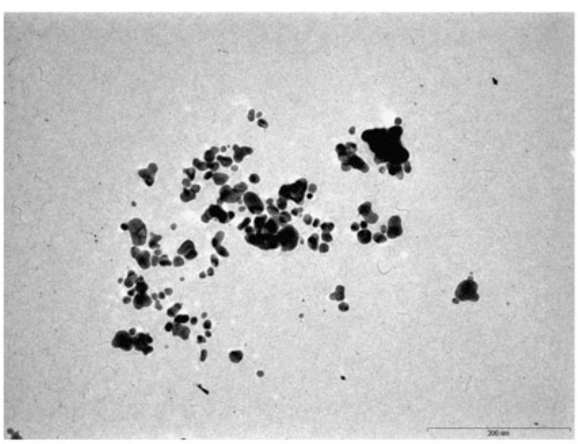

060929_d10_05.tif

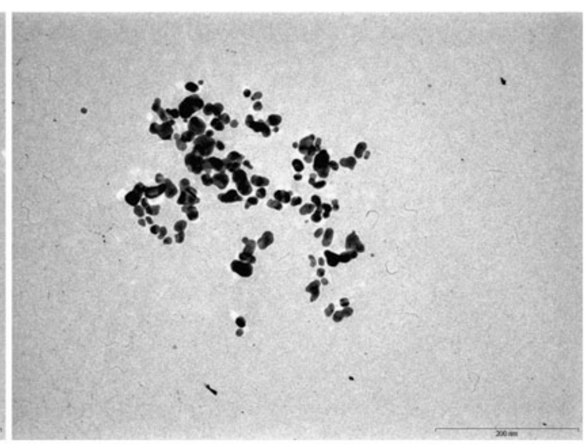

060929_d10_06.tif

Gold acetate decomposition study - sampled 2 mm away

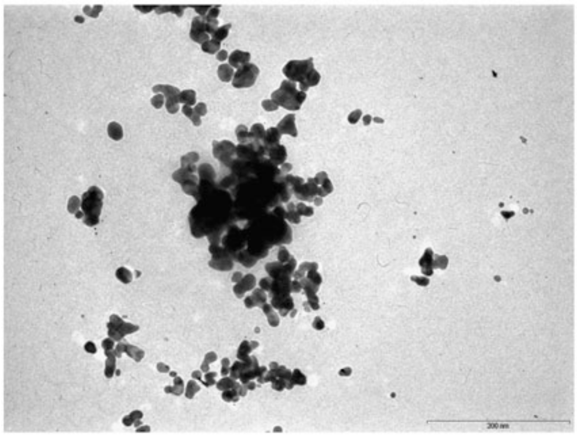

060929_d10_07.tif

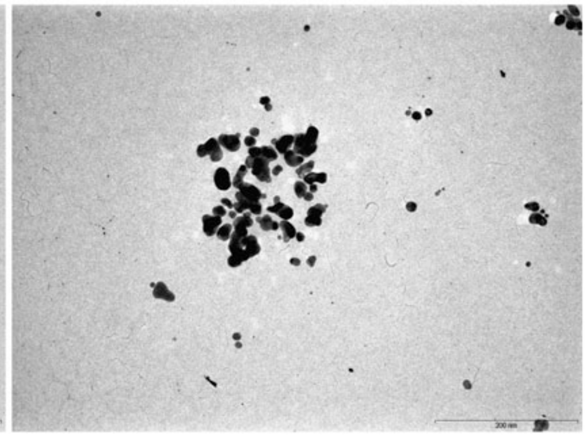

060929_d10_08.tif

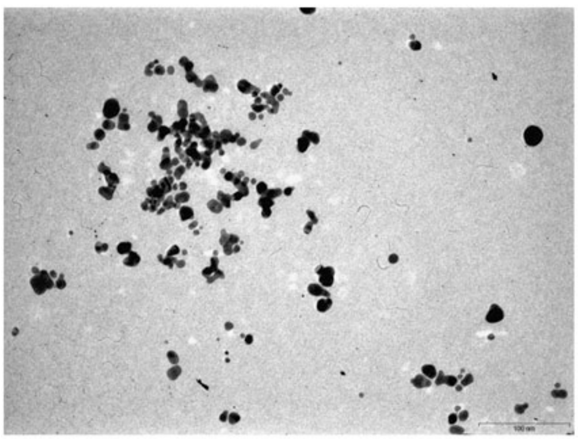

060929_d10_09.tif

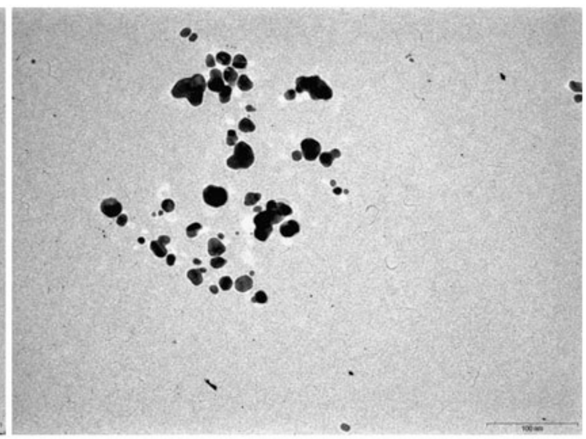

060929_d10_10.tif

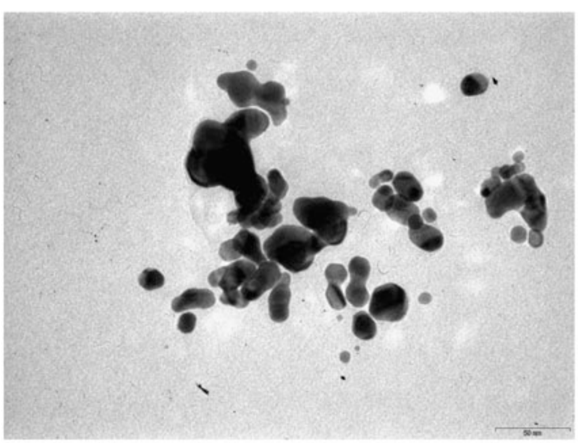

060929_d10_12.tif

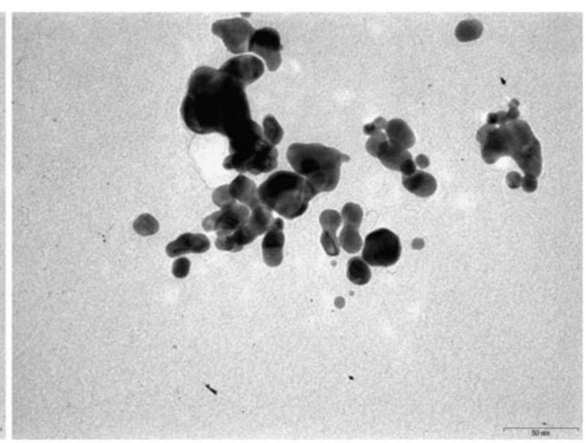

060929_d10_13.tif

Gold acetate decomposition study - sampled 2 mm away

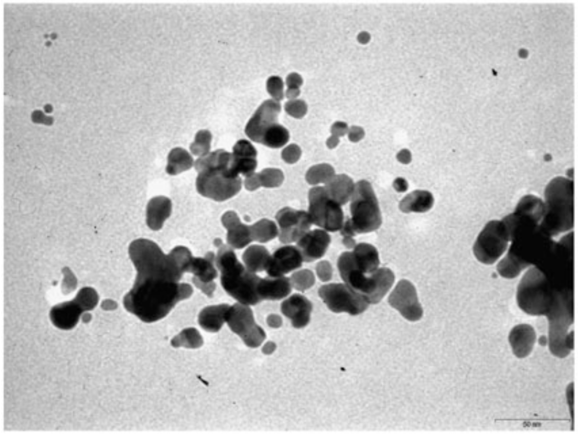

060929_d10_14.tif

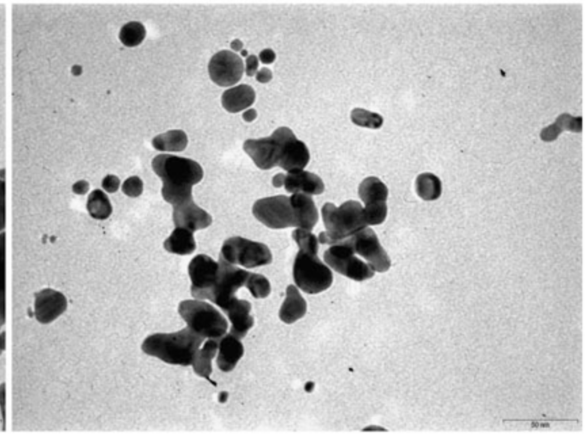

060929_d10_15.tif

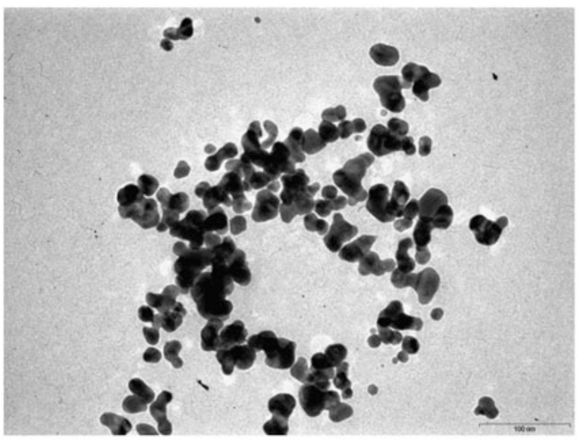

060929_d10_16.tif

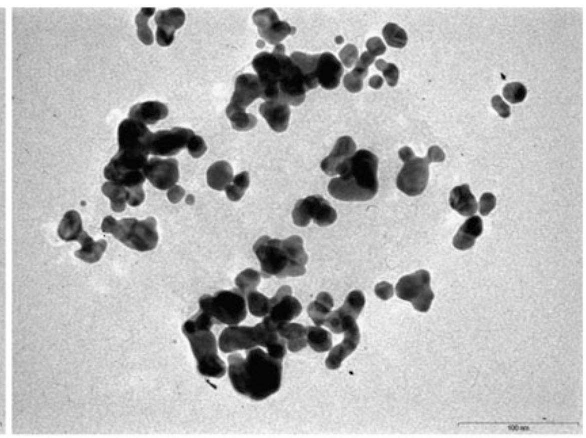

060929_d10_17.tif

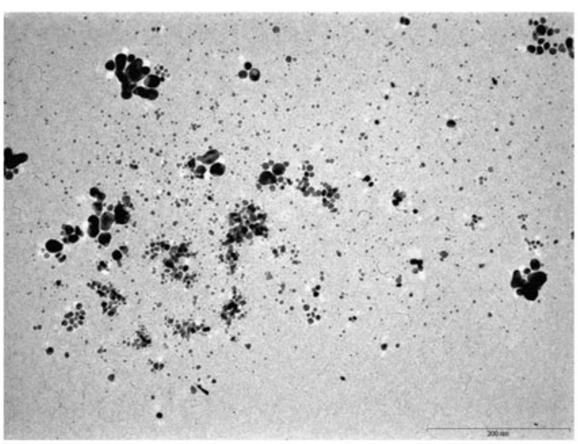

060929_d9_1.tif

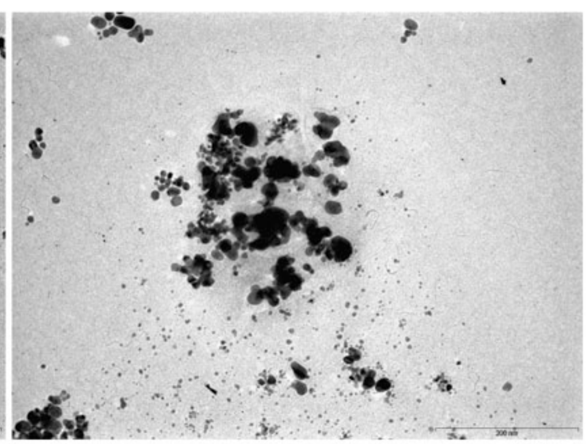

060929_d9_2.tif

Gold acetate decomposition study - sampled 2 mm away

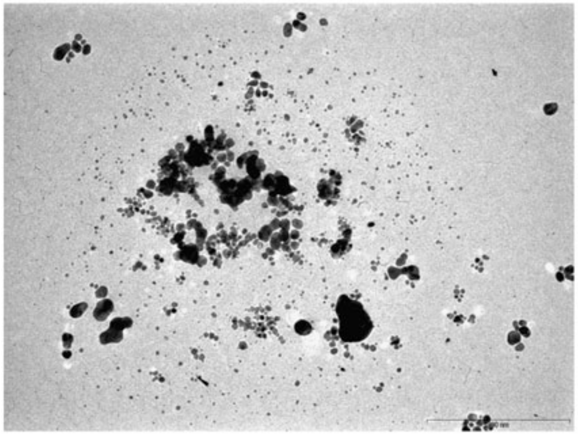

060929_d9_3.tif

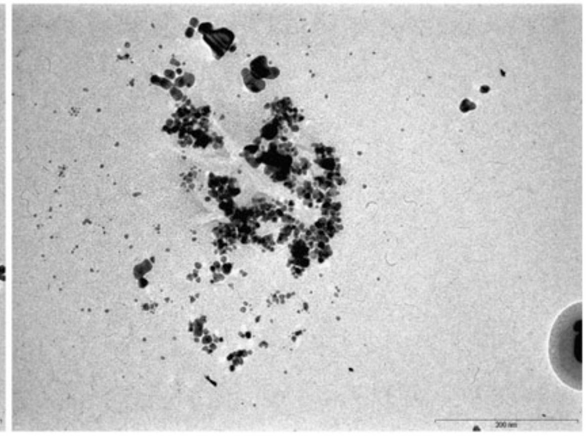

060929_d9_4.tif

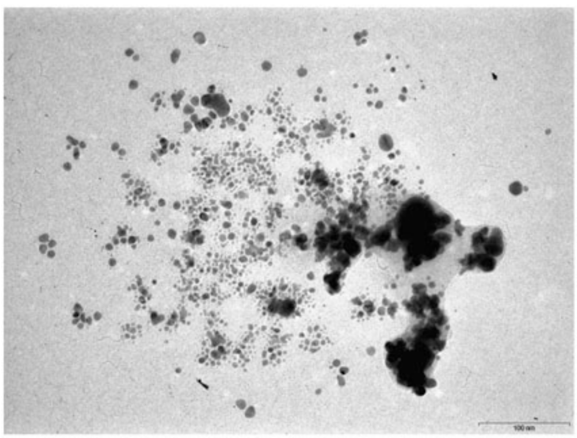

060929_d9_5.tif

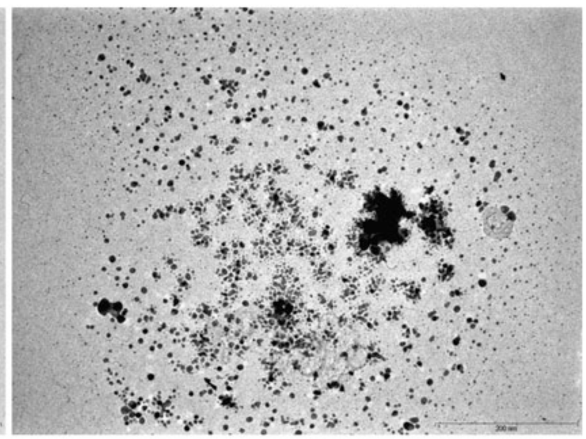

060929_d9_6.tif

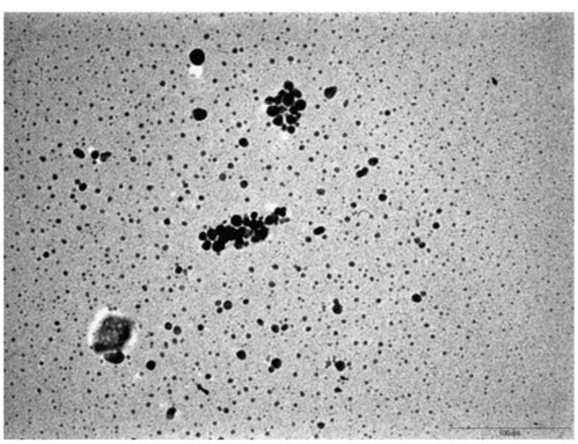

060929_d9_7.tif

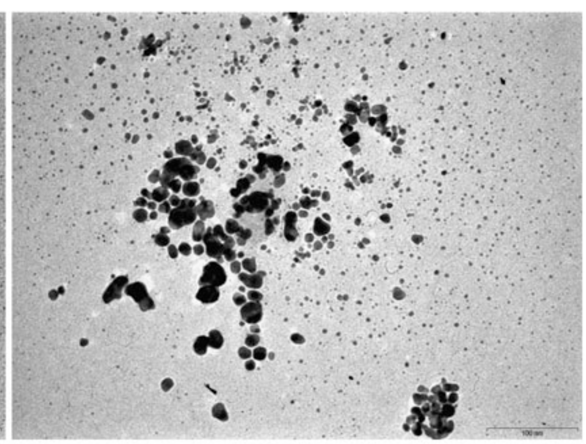

060929_d9_8.tif

Gold acetate decomposition study - sampled 4 mm away

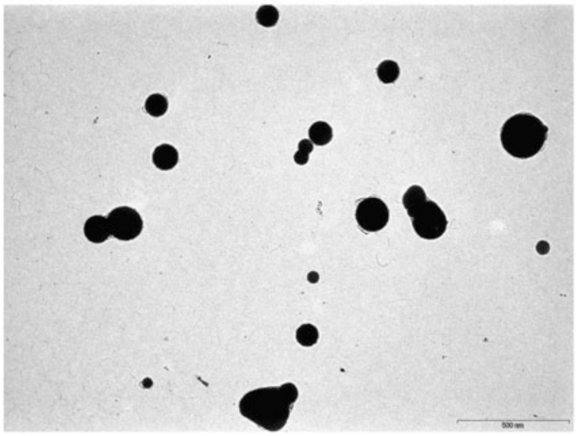

060929_b10_01.tif

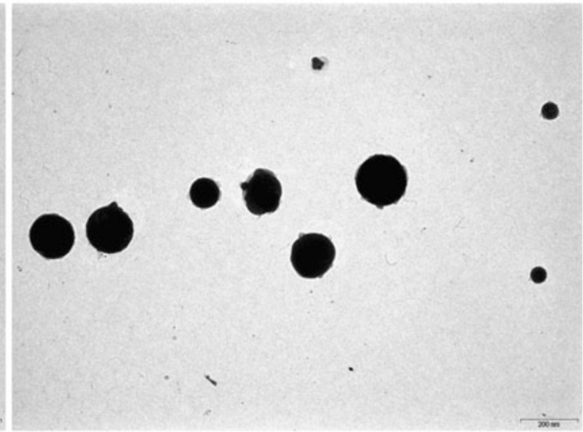

060929_b10_02.tif

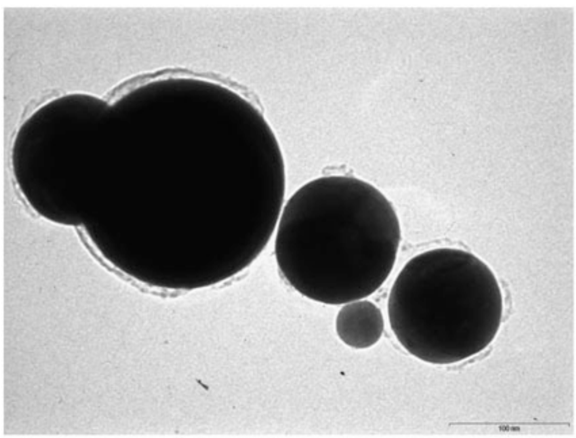

060929_b10_03.tif

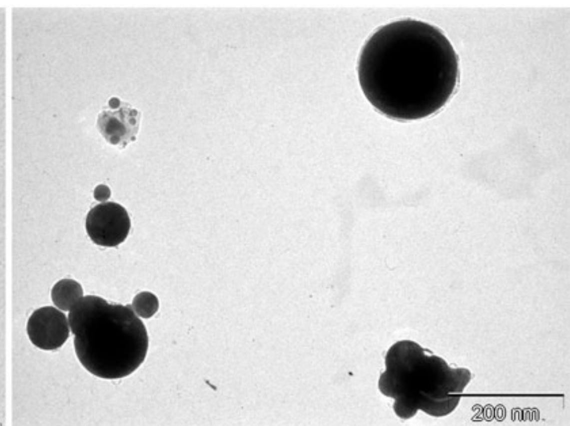

060929_b7_01.tif

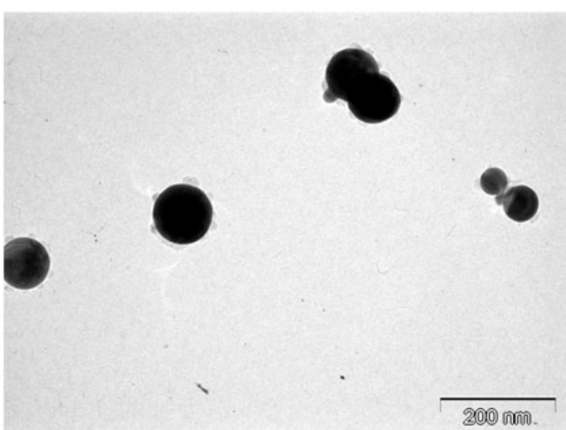

060929_b7_02.tif

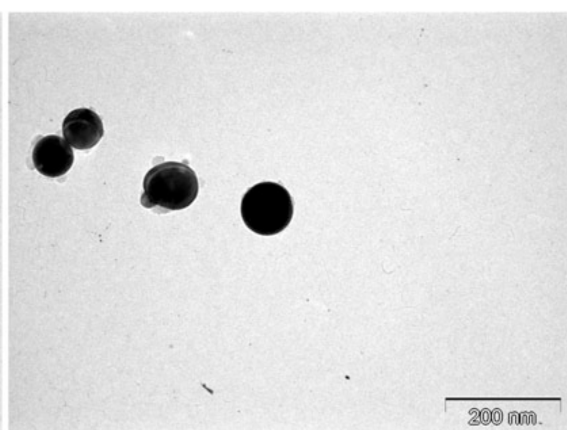

060929_b7_03.tif

Gold acetate decomposition study - sampled 4 mm away

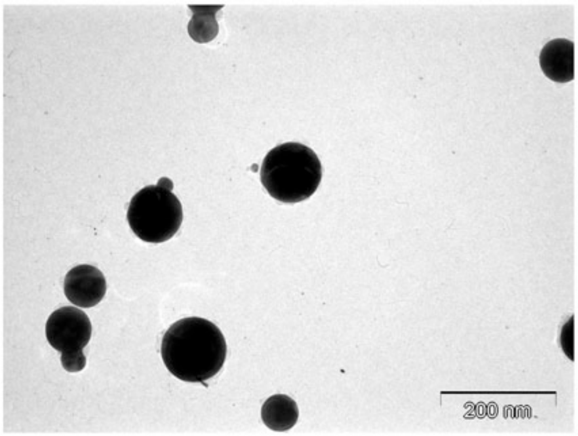

060929_b7_04.tif

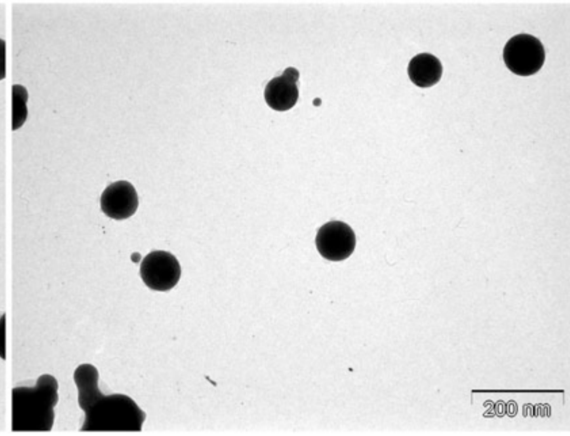

060929_b7_05.tif

Gold acetate decomposition study

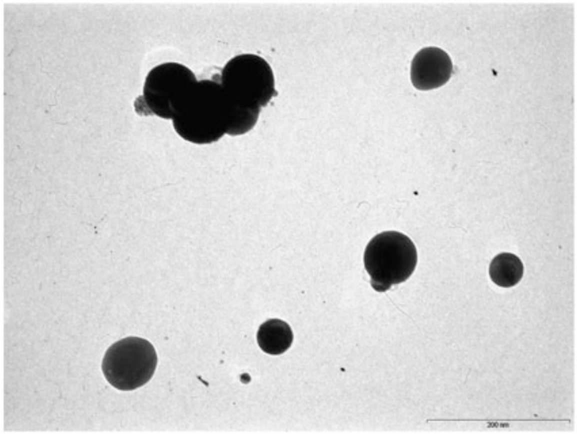

060929_c4_01.tif

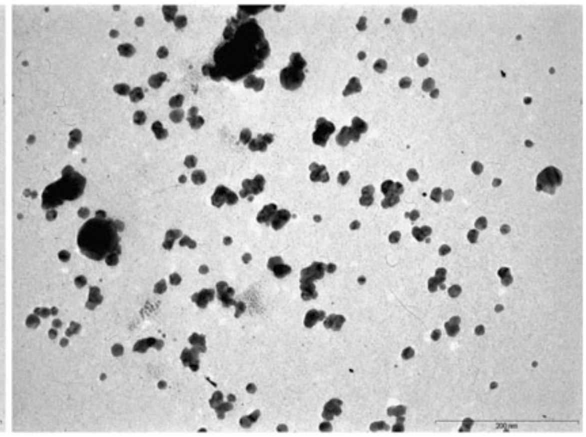

060929_c4_02.tif

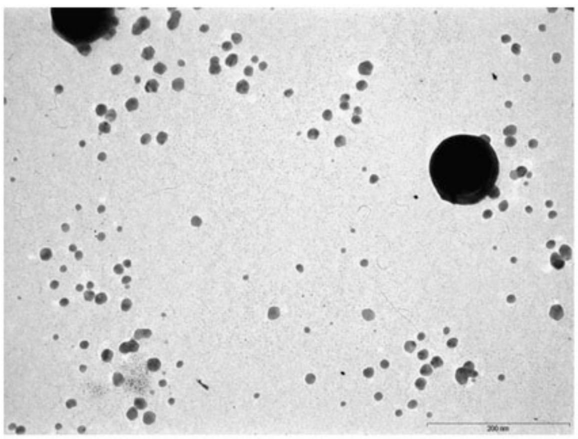

060929_c4_03.tif

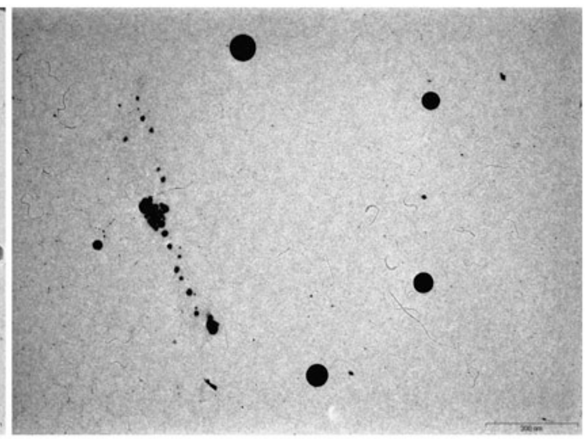

060929_c4_04.tif

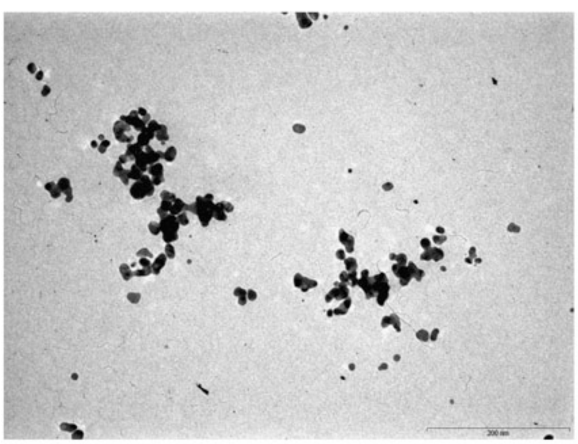

060929_d10_01.tif

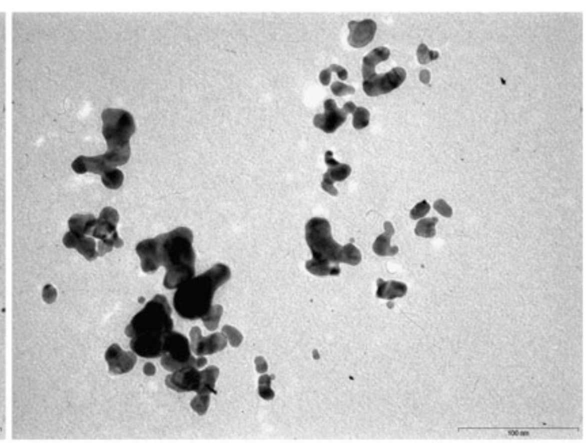

060929_d10_02.tif

Gold acetate decomposition study

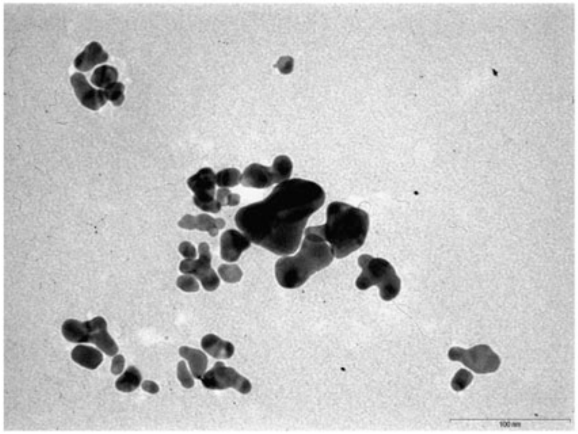

060929_d10_03.tif

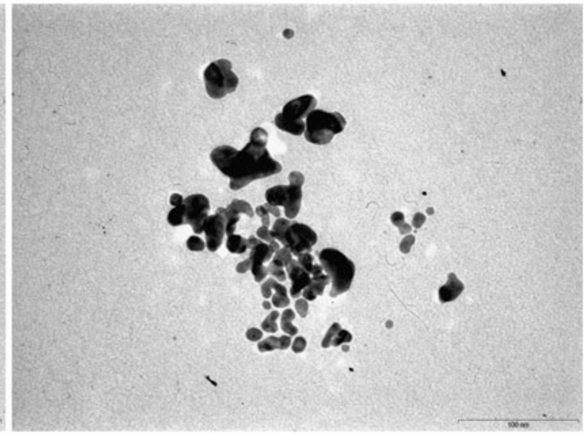

060929_d10_04.tif

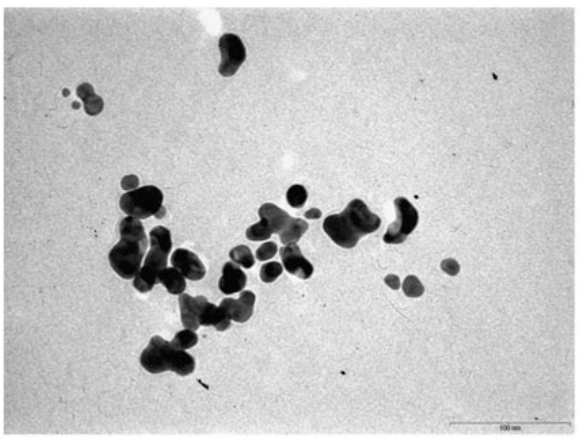

060929_d10_05.tif

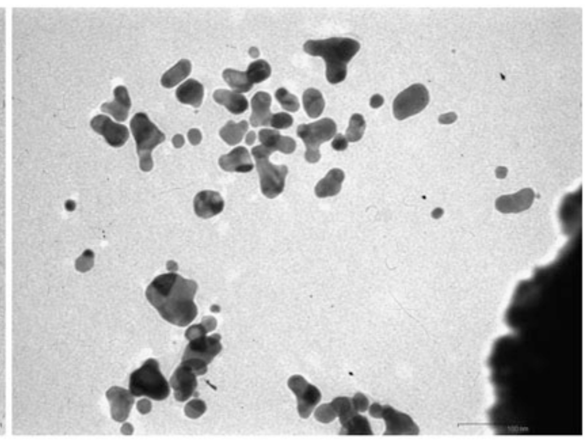

060929_d10_06.tif

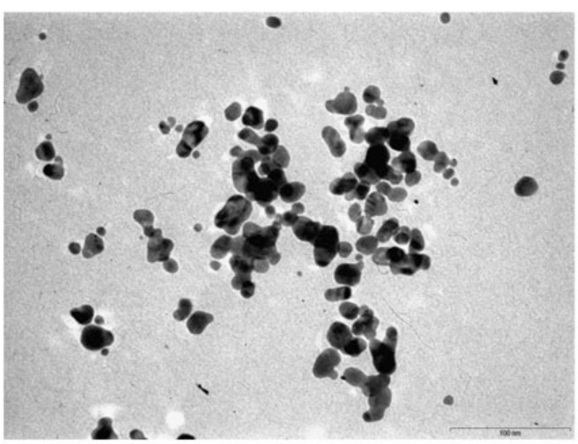

060929_d10_07.tif

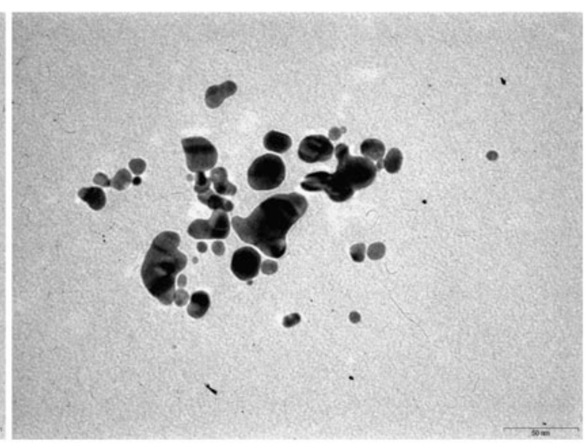

060929_d10_08.tif

Gold acetate decomposition study

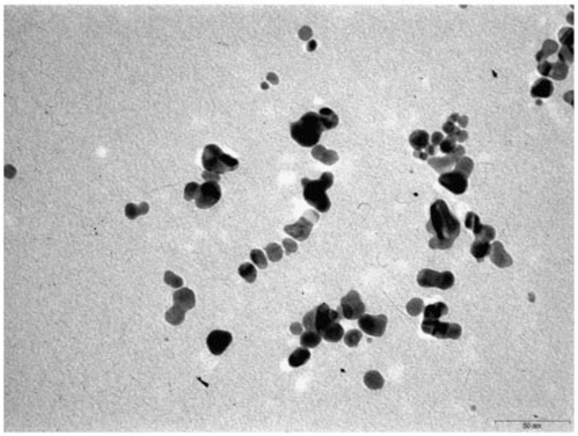

060929_d10_09.tif

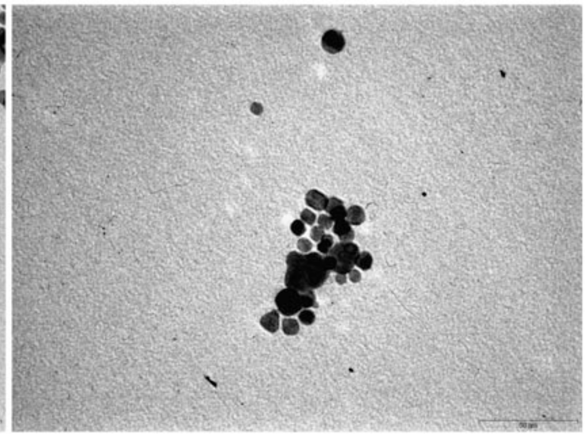

060929_d10_10.tif

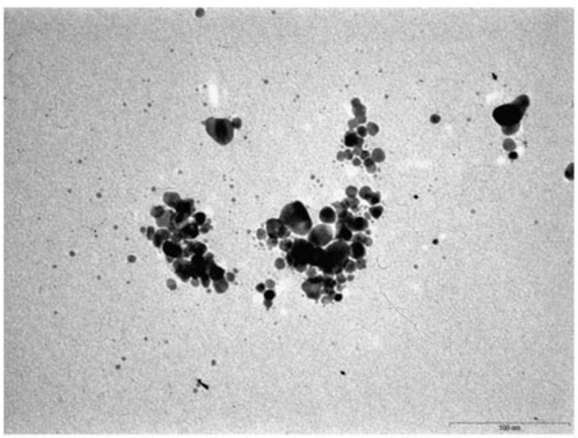

060929_d10_11.tif

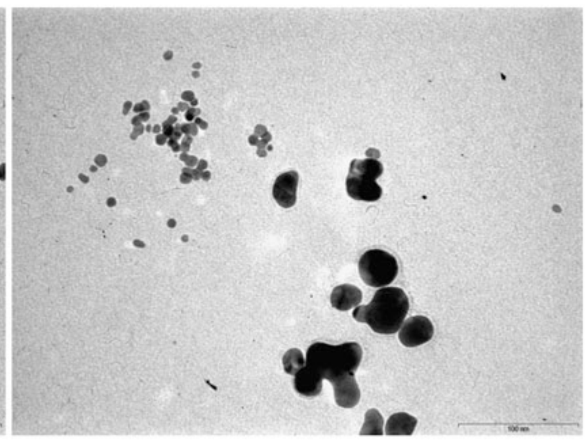

060929_d10_12.tif

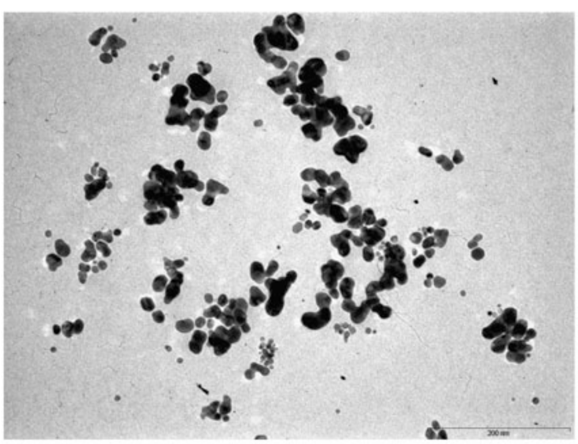

060929_d10_13.tif

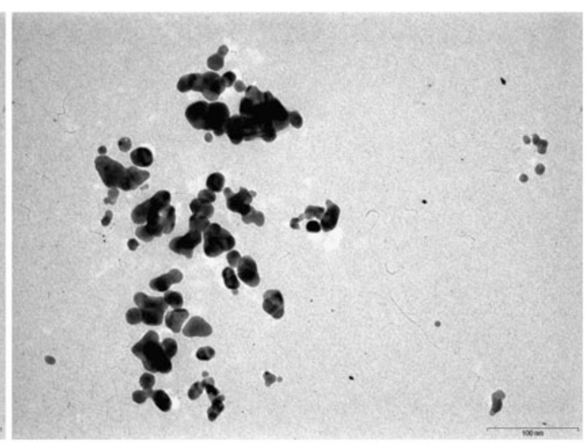

060929_d10_14.tif

Gold acetate decomposition study

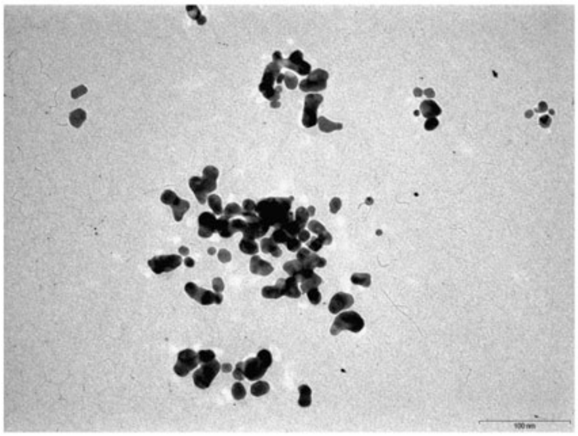

060929_d10_21.tif

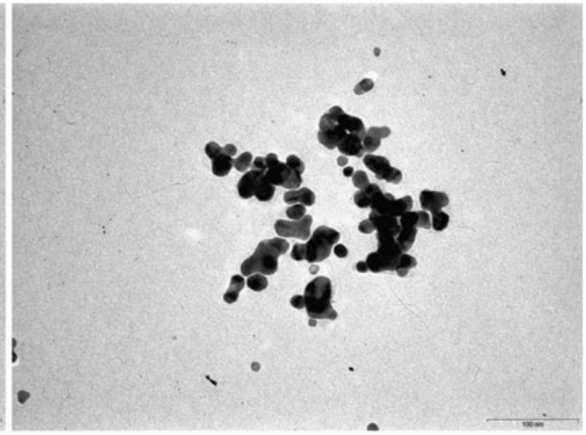

060929_d10_22.tif

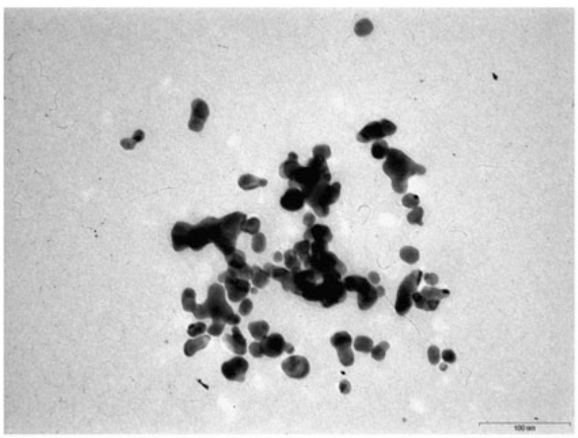

060929_d10_23.tif

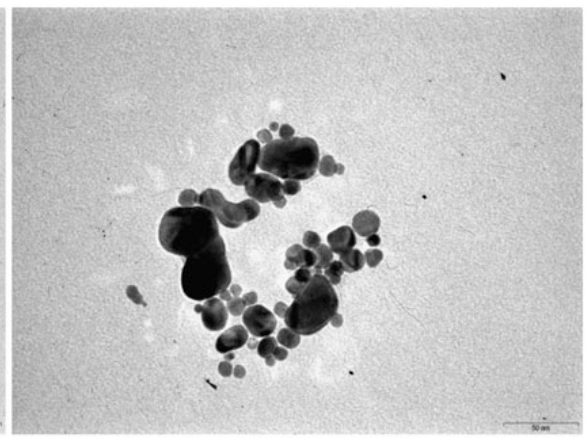

060929_d10_24.tif

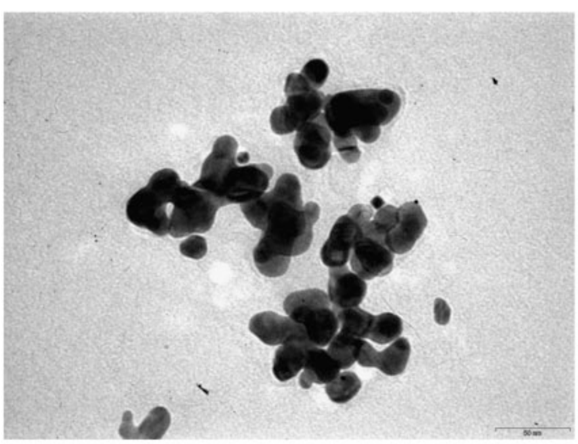

060929_d10_25.tif

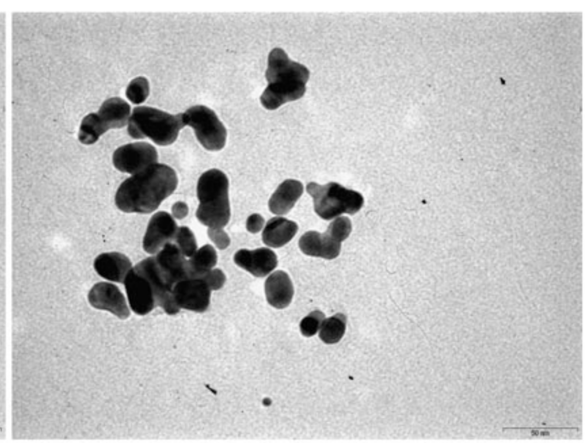

060929_d10_26.tif

Gold acetate decomposition study

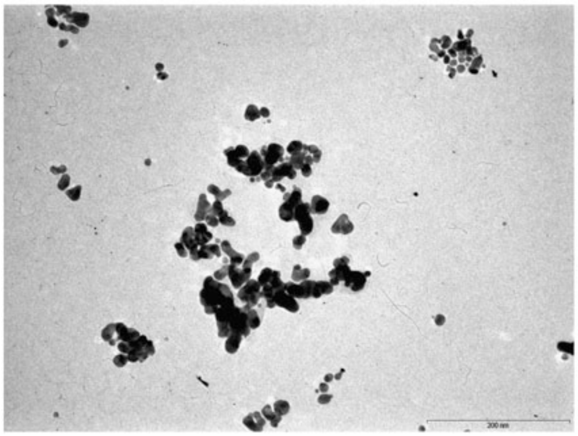

060929_d10_27.tif

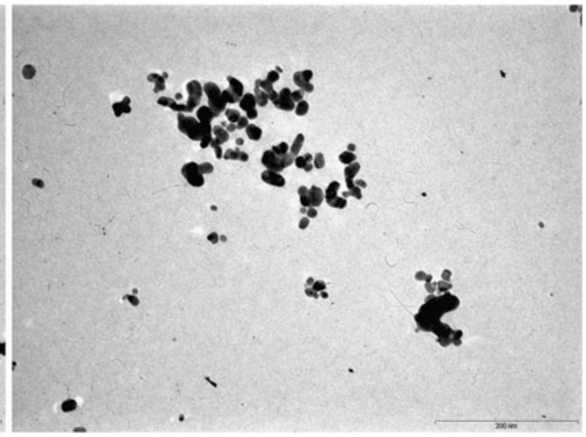

060929_d10_28.tif

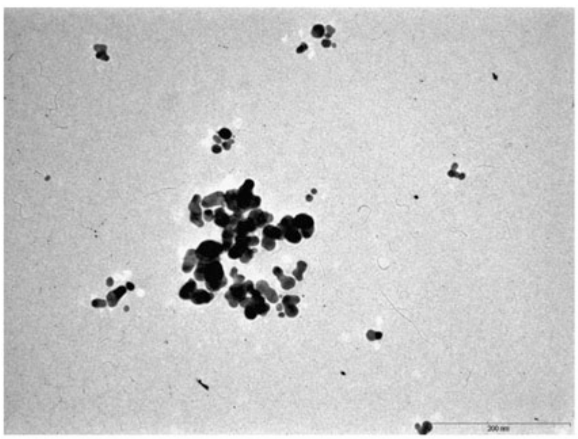

060929_d10_29.tif

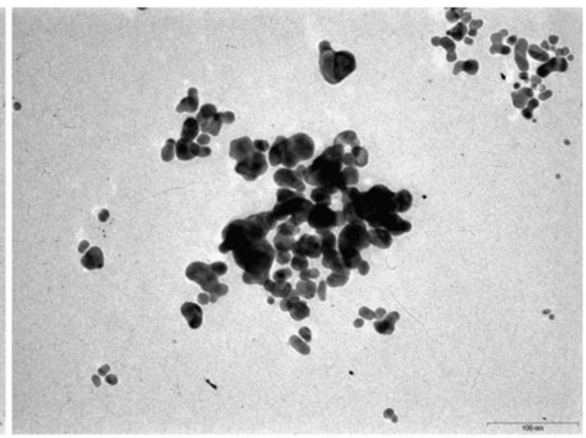

060929_d10_30.tif

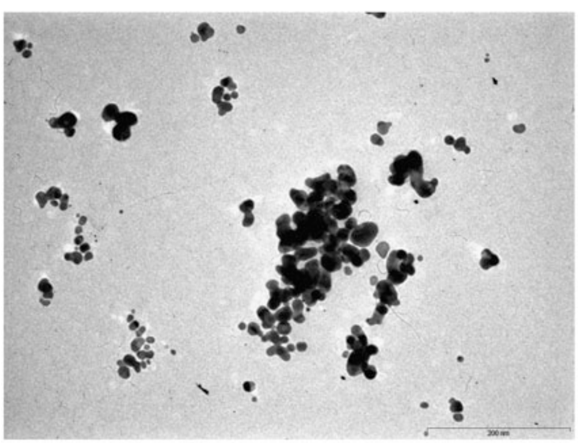

060929_d10_31.tif

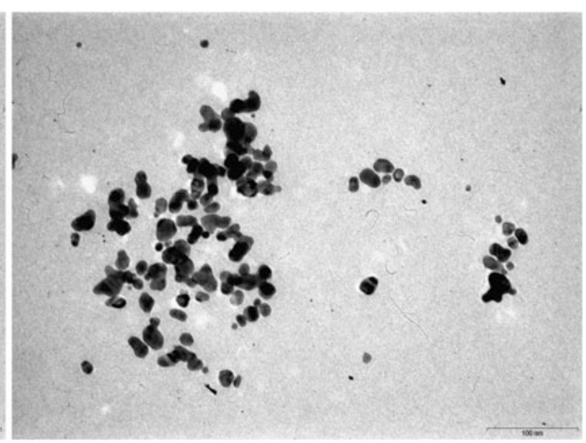

060929_d10_32.tif

Gold acetate decomposition study

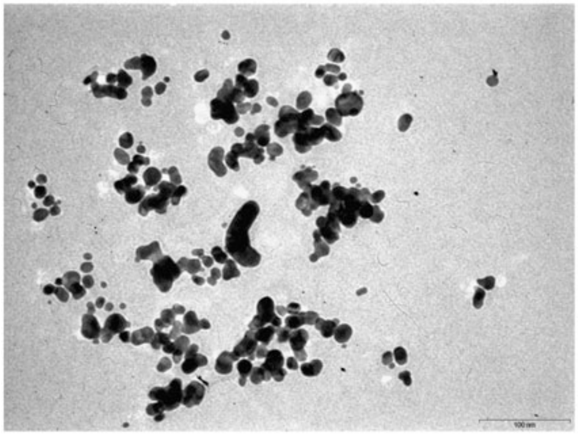

060929_d10_33.tif

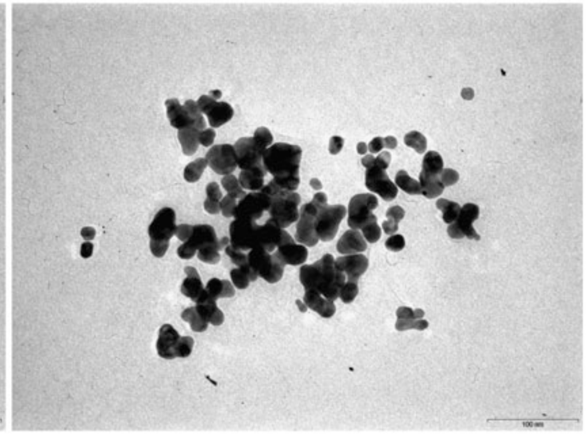

060929_d10_34.tif

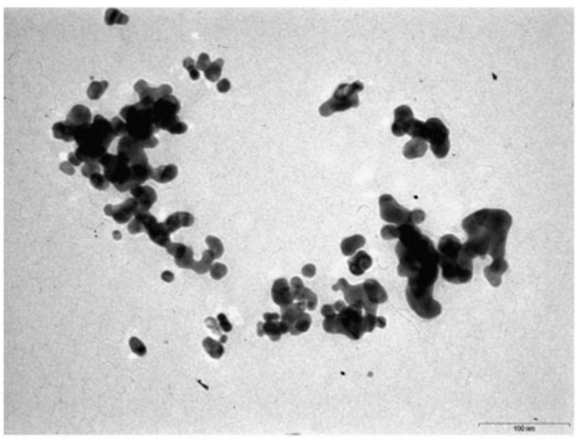

060929_d10_35.tif

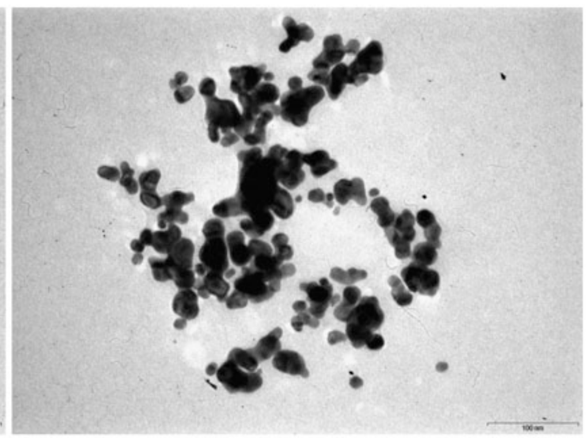

060929_d10_36.tif

Gold acetate decomposition study

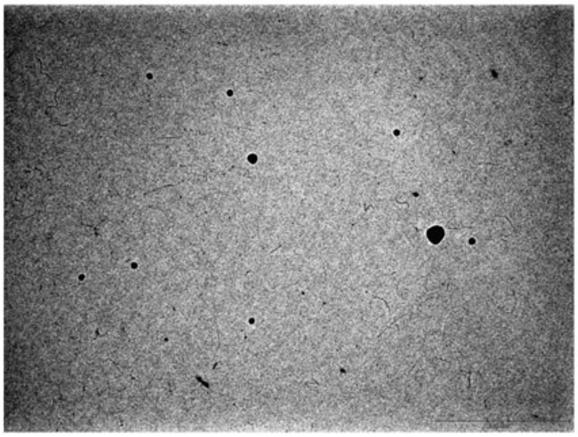

060929_b2_01.tif

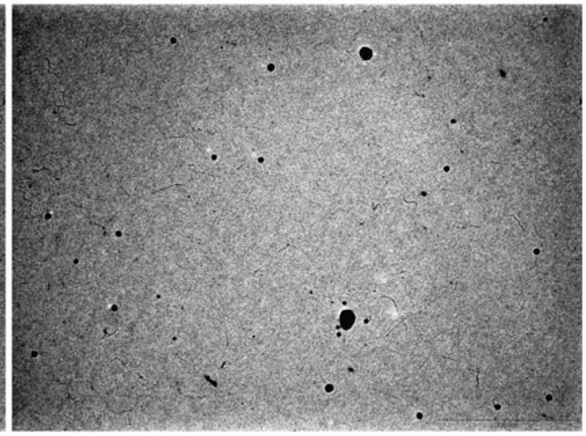

060929_b2_02.tif

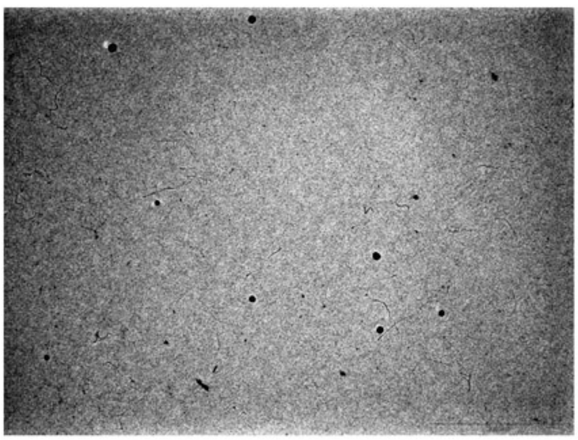

060929_b2_03.tif

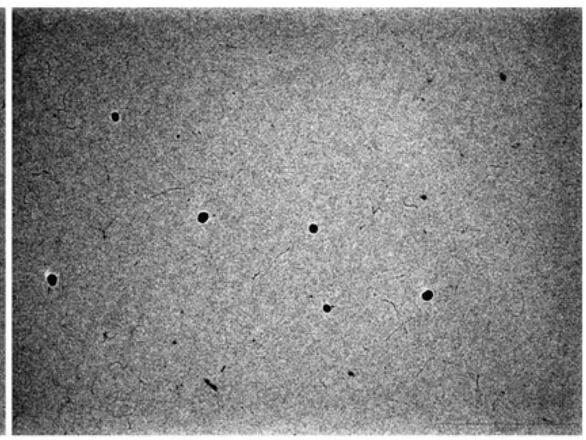

060929_b2_04.tif

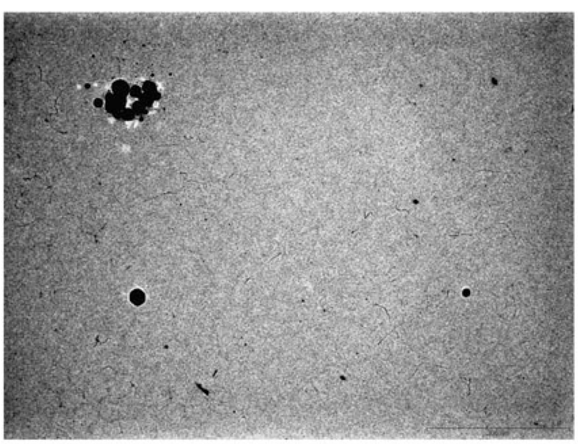

060929_b2_05.tif

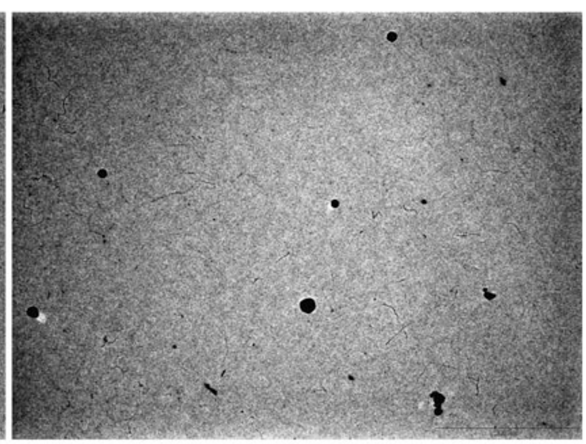

060929_b2_06.tif

Gold acetate decomposition study

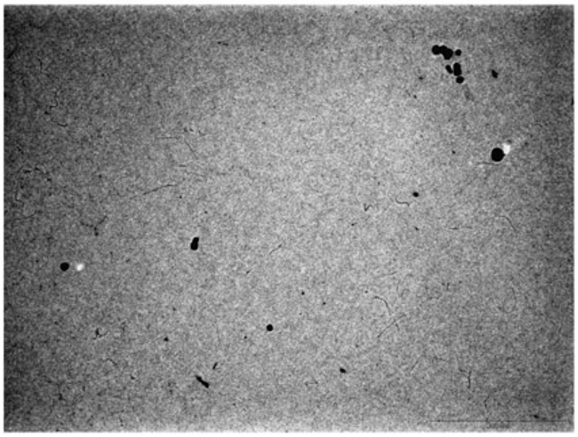

060929_b2_07.tif

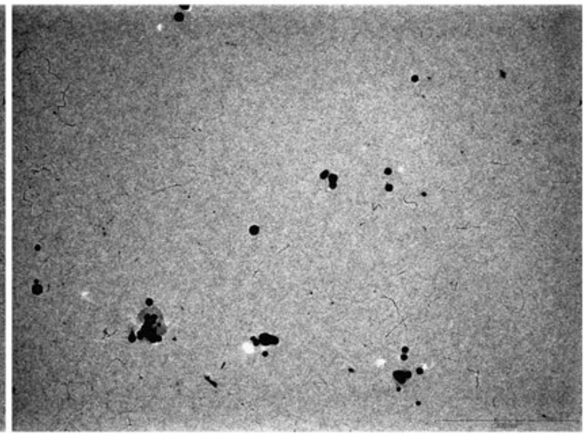

060929_b2_08.tif

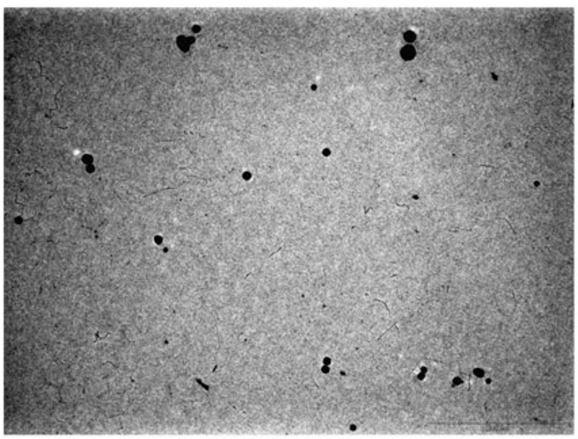

060929_b2_09.tif

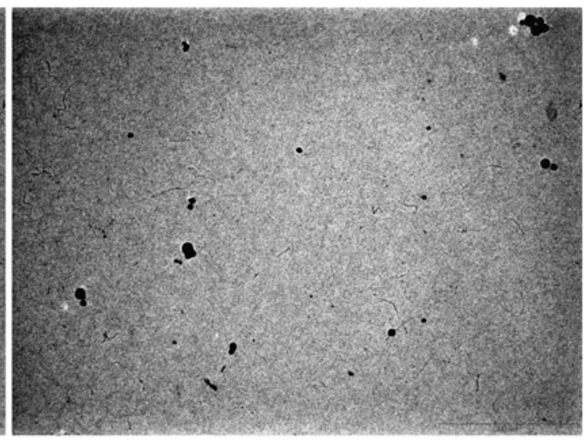

060929_b2_10.tif

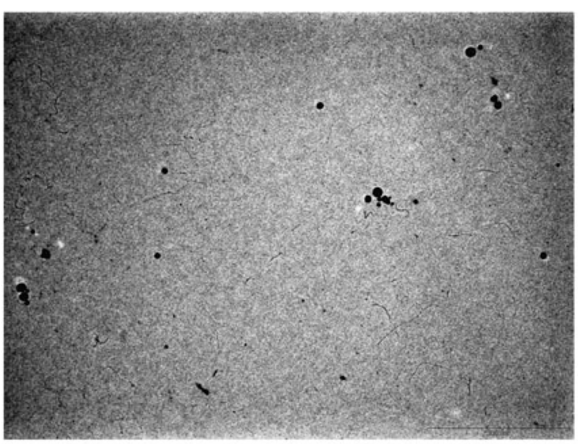

060929_b2_11.tif

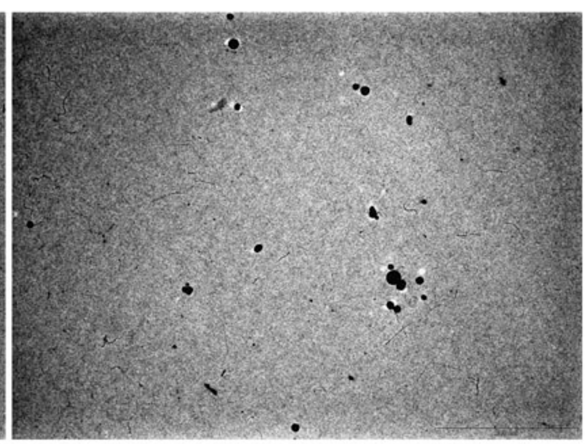

060929_b2_12.tif

Gold acetate decomposition study

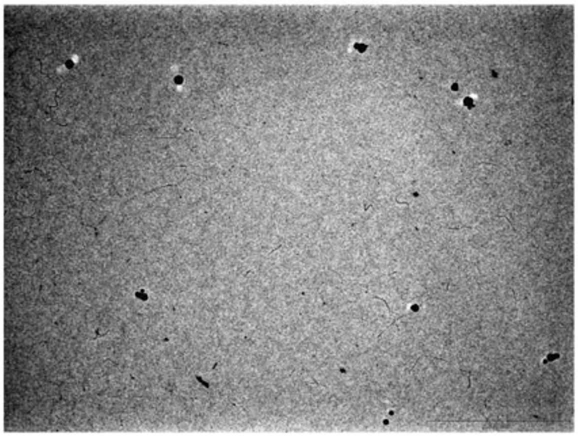

060929_b2_13.tif

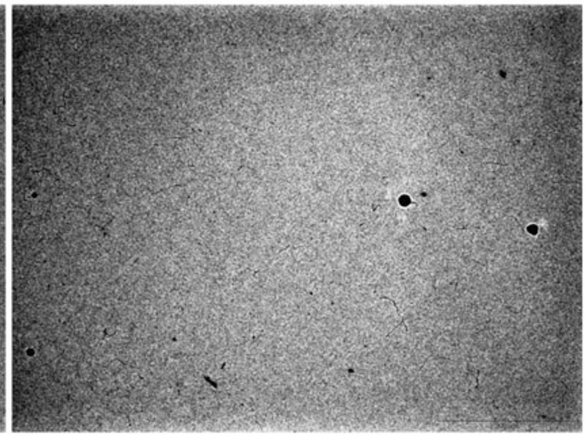

060929_b2_14.tif

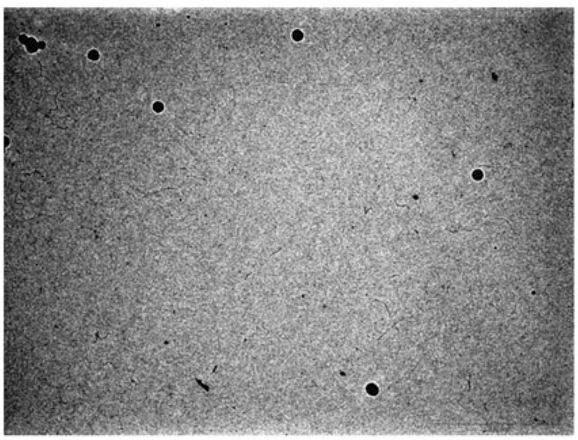

060929_b2_15.tif

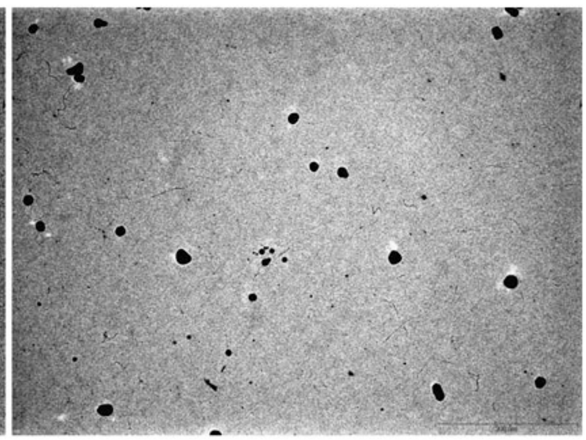

060929_b2_16.tif

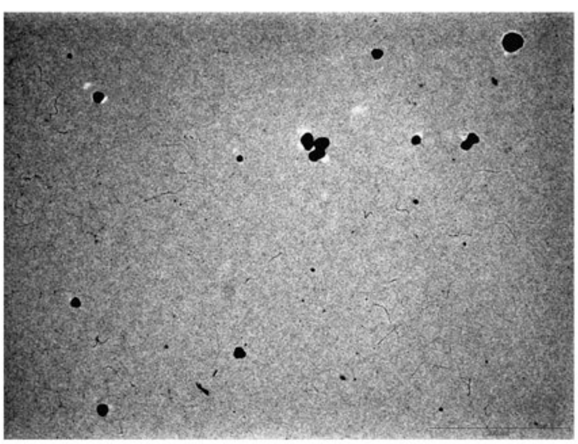

060929_b2_17.tif

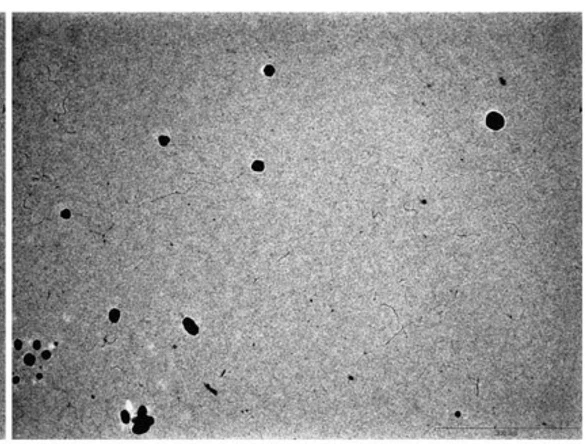

060929_b2_18.tif

Gold acetate decomposition study

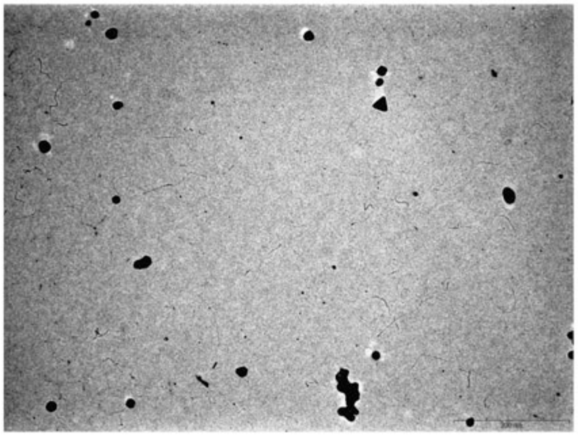

060929_b2_19.tif

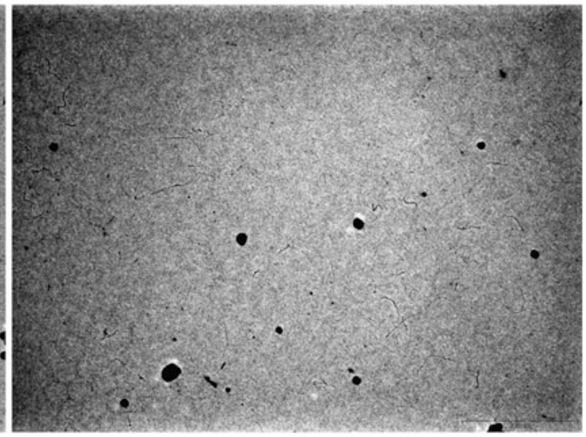

060929_b2_20.tif

SnO_2 dispersion-drop film on TEM grid

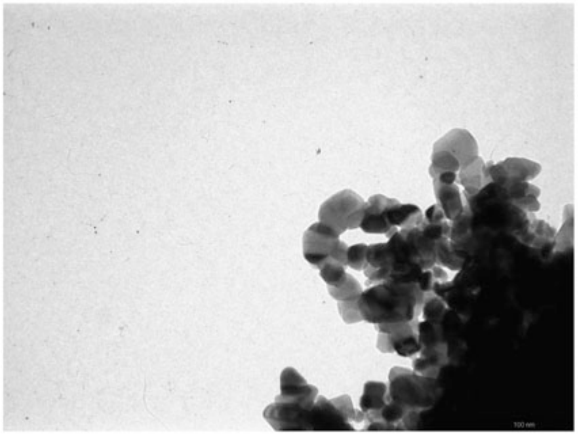

060929_e1_01.tif

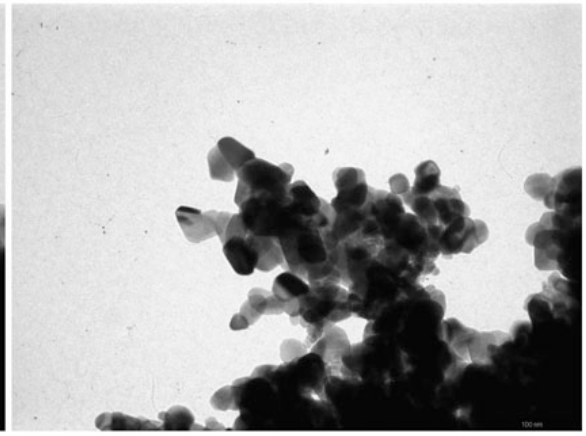

060929_e1_02.tif

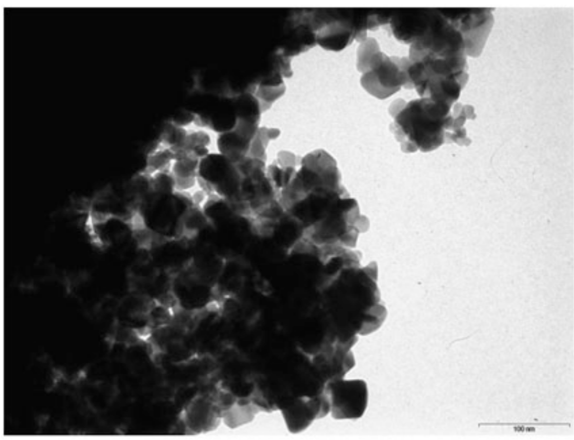

060929_e1_03.tif

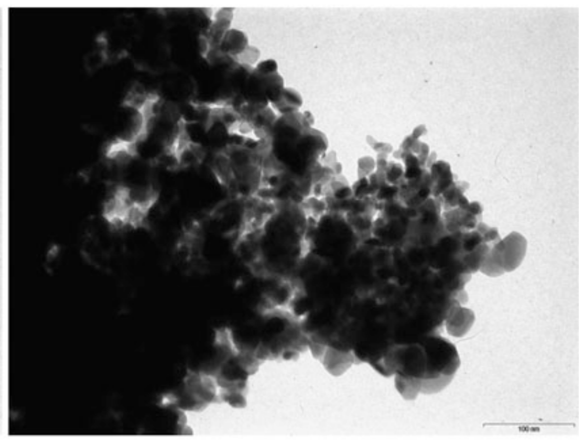

060929_e1_04.tif

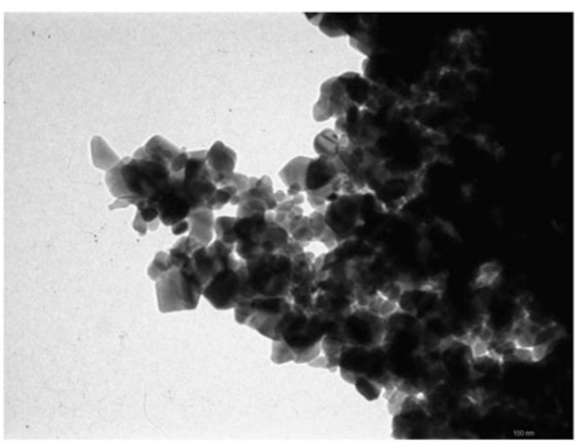

060929_e1_05.tif

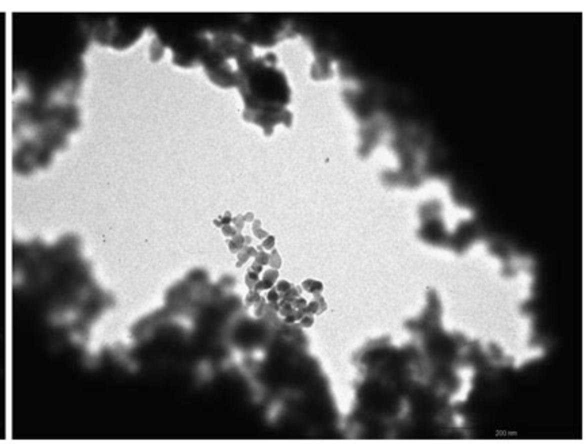

060929_e1_06.tif

SnO_2 dispersion-drop film on TEM grid

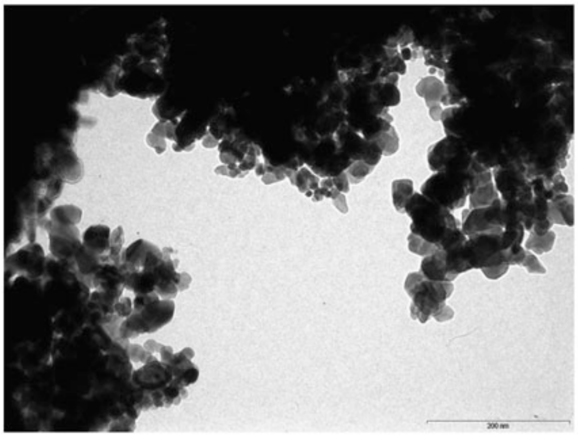

060929_e1_07.tif

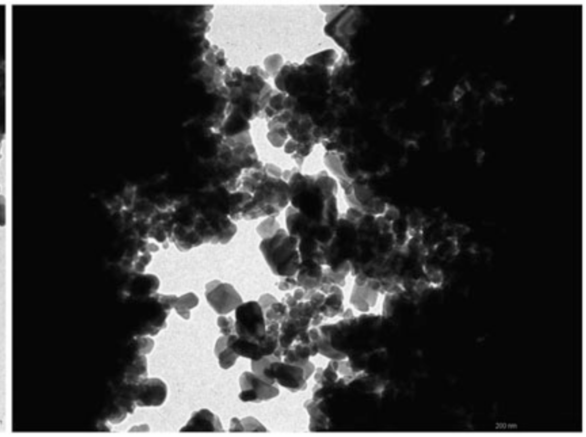

060929_e1_08.tif

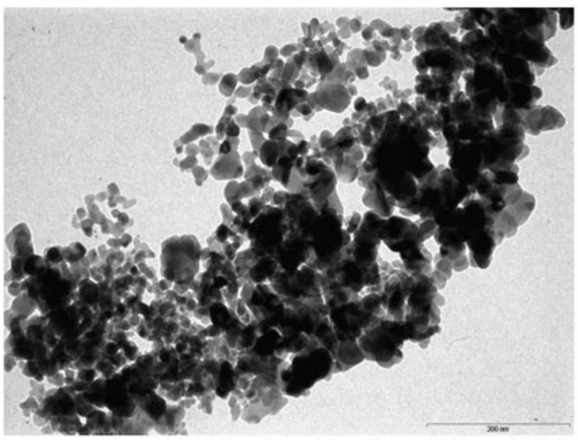

060929_e1_09.tif

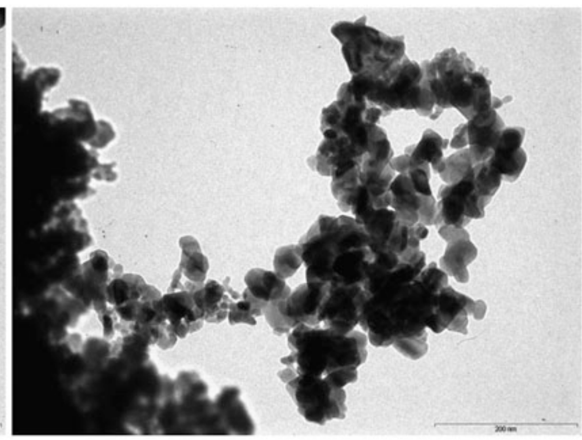

060929_e1_10.tif

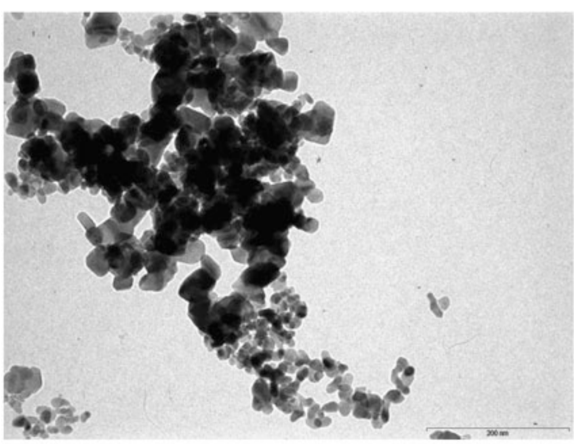

060929_e1_11.tif

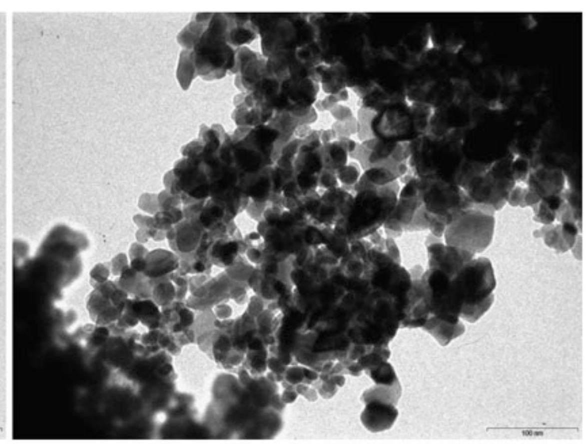

060929_e1_12.tif

SnO_2 dispersion-drop film on TEM grid

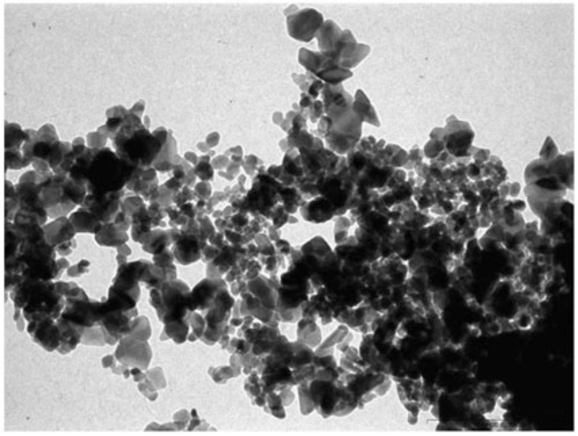

060929_e1_13.tif

Gold-doped SnO_2 dispersion-drop film on TEM grid

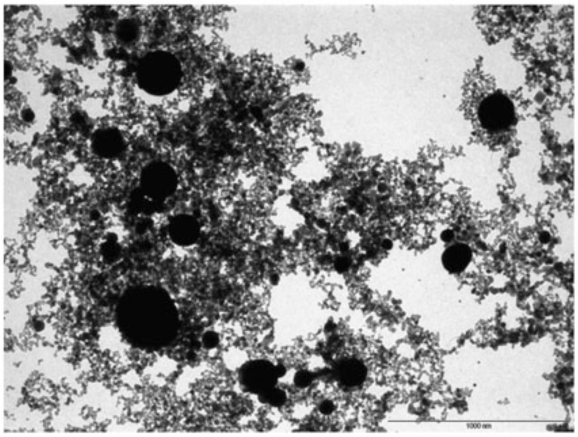

060929_e2_01.tif

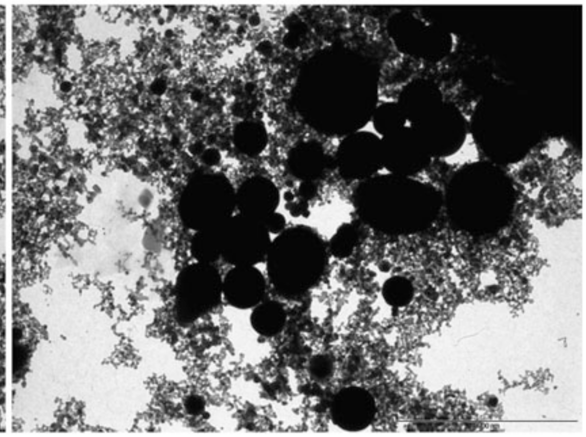

060929_e2_02.tif

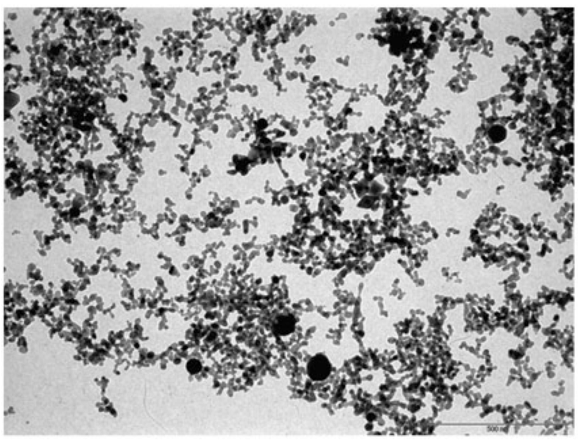

060929_e2_03.tif

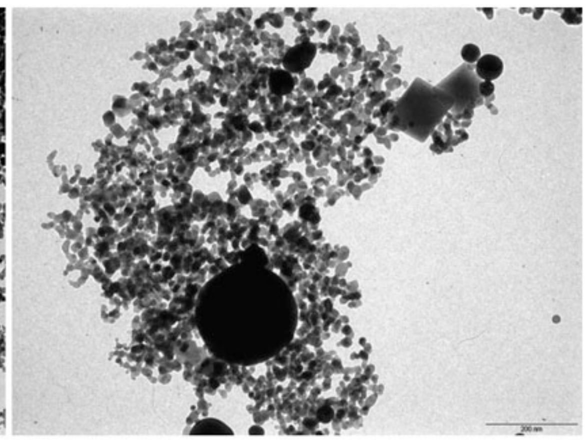

060929_e2_04.tif

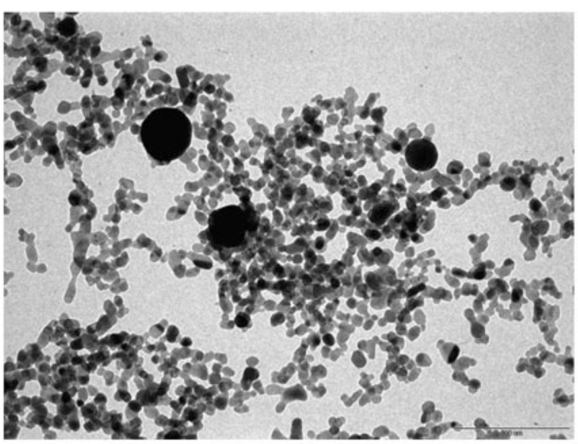

060929_e2_05.tif

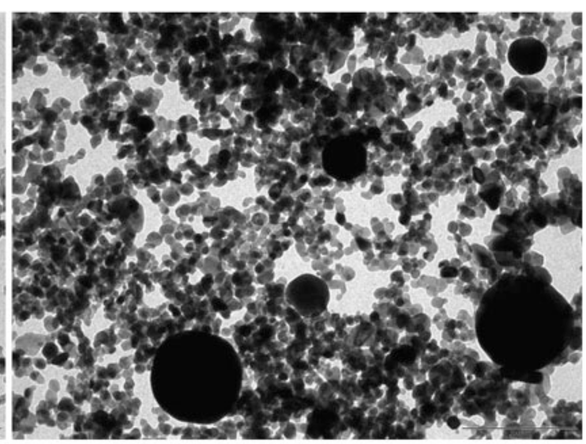

060929_e2_06.tif

Gold-doped SnO_2 dispersion-drop film on TEM grid

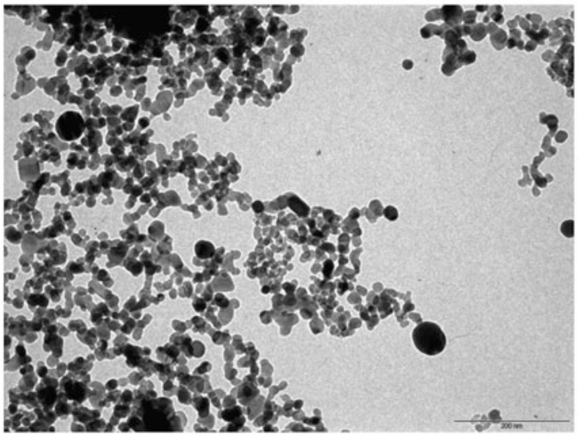

060929_e2_07.tif

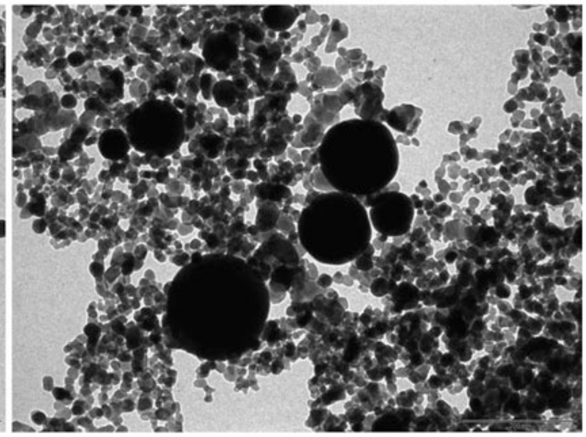

060929_e2_08.tif

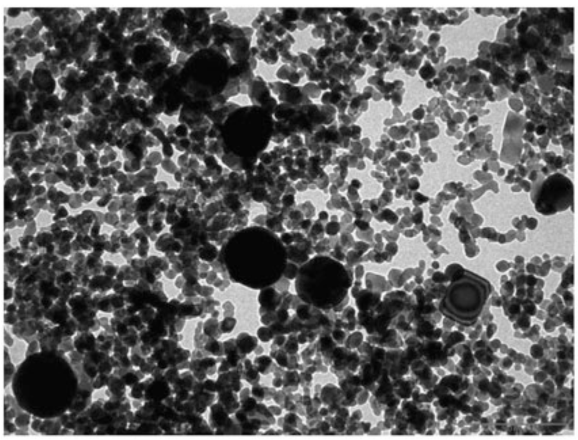

060929_e2_09.tif

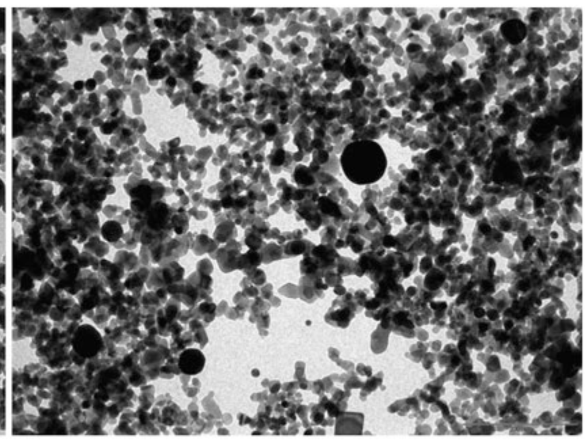

060929_e2_10.tif

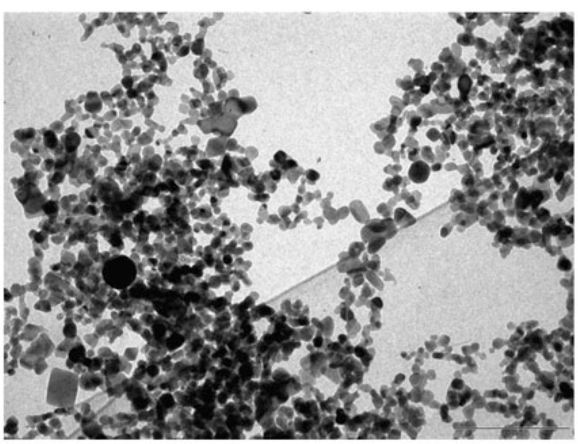

060929_e2_11.tif

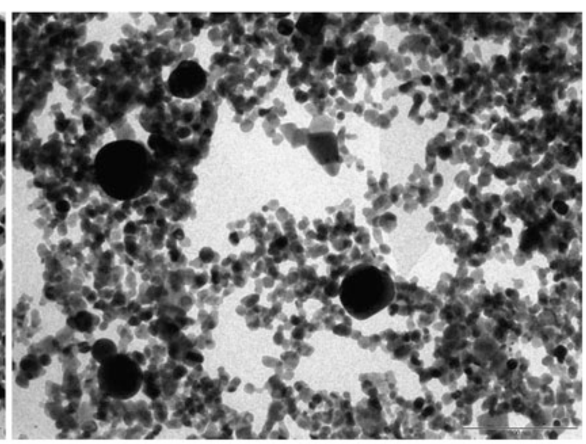

060929_e2_12.tif

Gold-doped SnO_2 dispersion-drop film on TEM grid

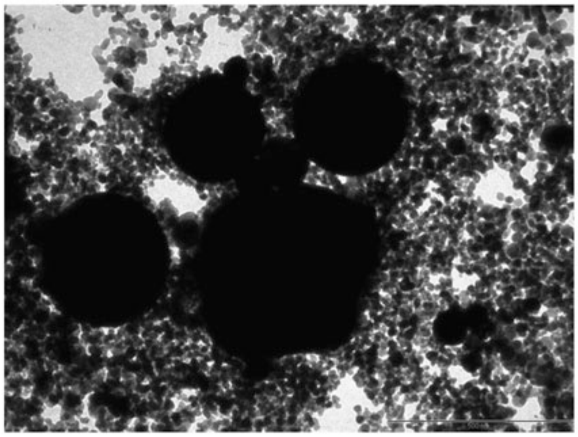

060929_e2_13.tif

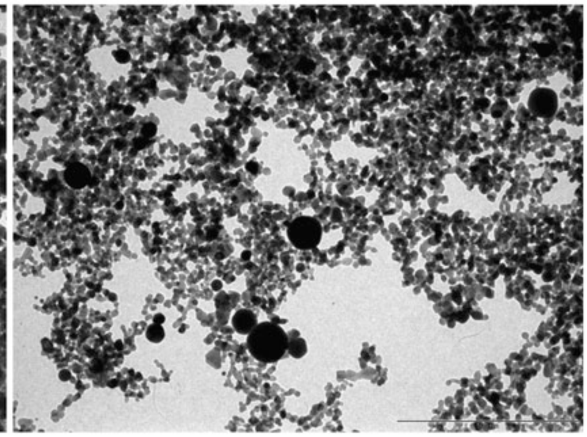

060929_e2_14.tif

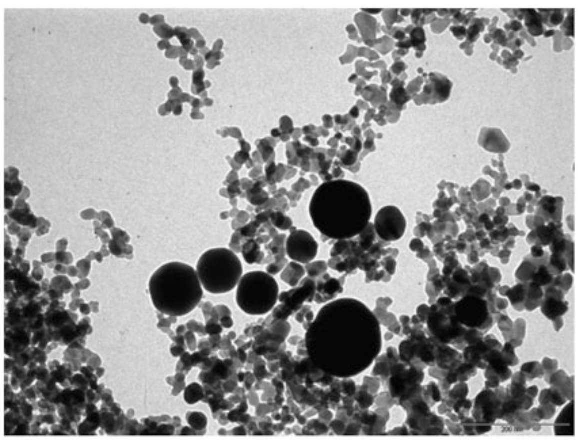

060929_e2_15.tif

Palladium-doped SnO_2 dispersion-drop film on TEM grid

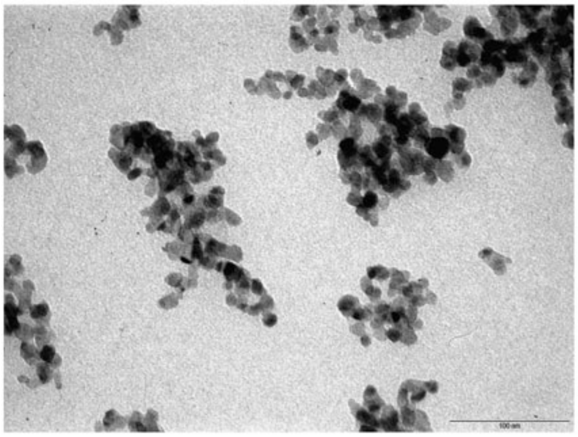

060929_e4_01.tif

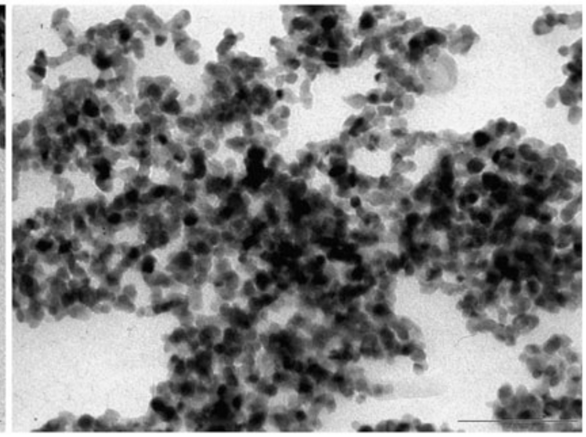

060929_e4_02.tif

C.6 SEM images

C.6.1 Precursor particles

Metallic gold powder, Sigma Aldrich

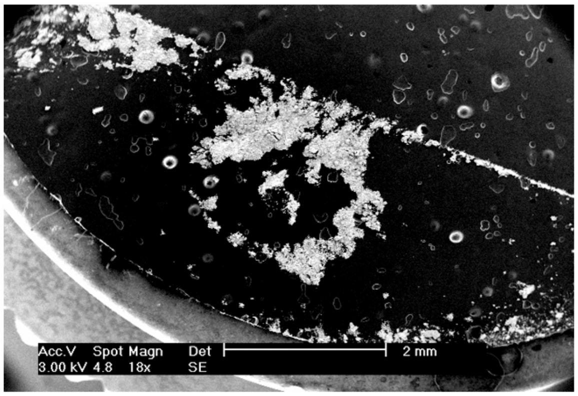

AU_POST1.TIF

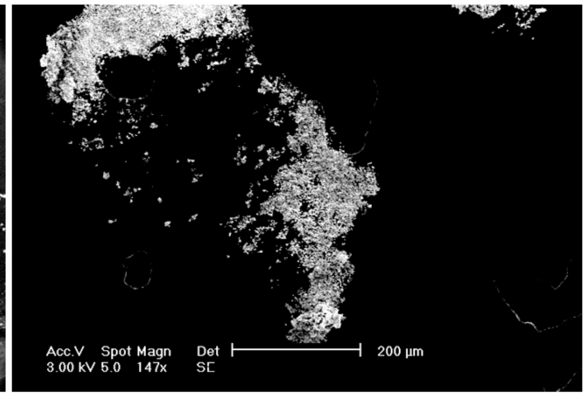

AU_POST2.TIF

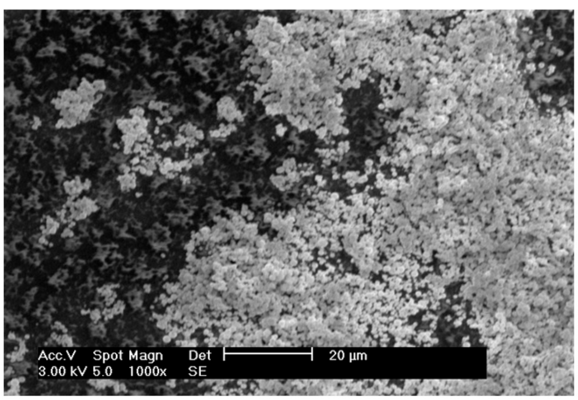

AU_POST3.TIF

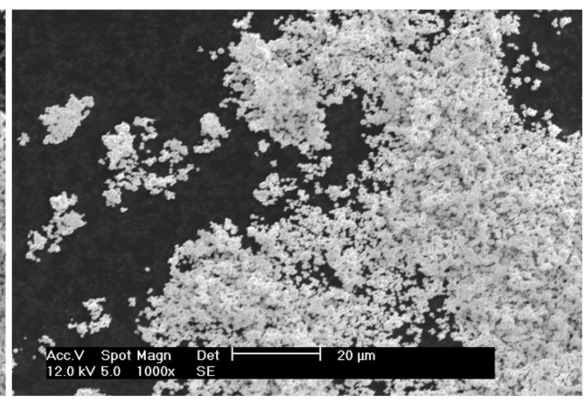

AU_POST4.TIF

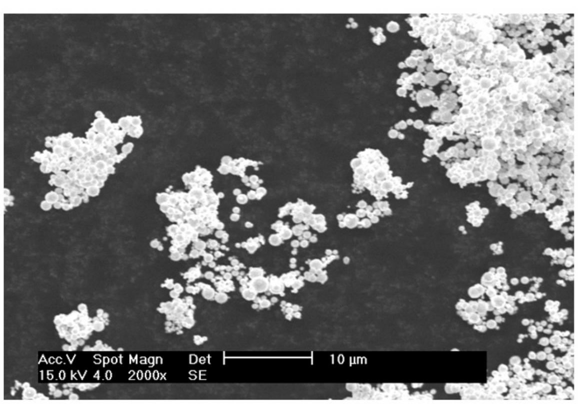

AU_POST5.TIF

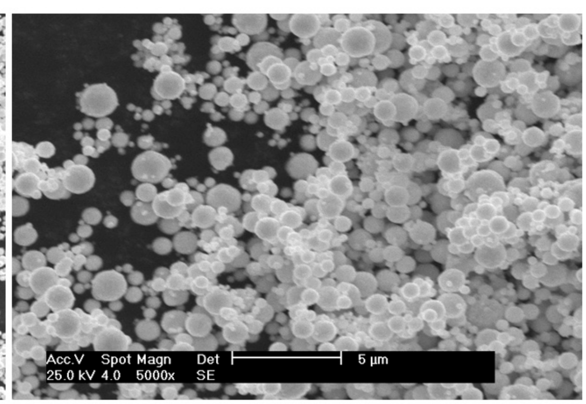

AU_POST6.TIF

Metallic gold powder, Sigma Aldrich

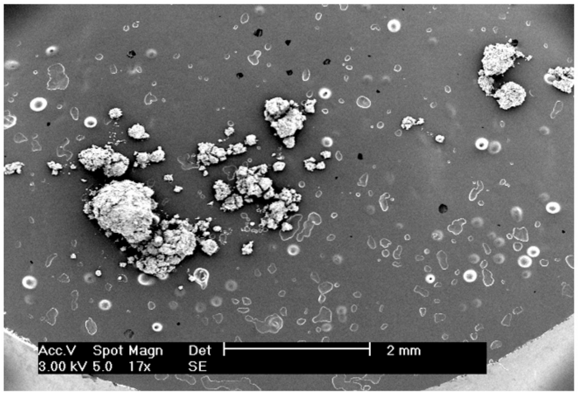

AU_PRE1.TIF

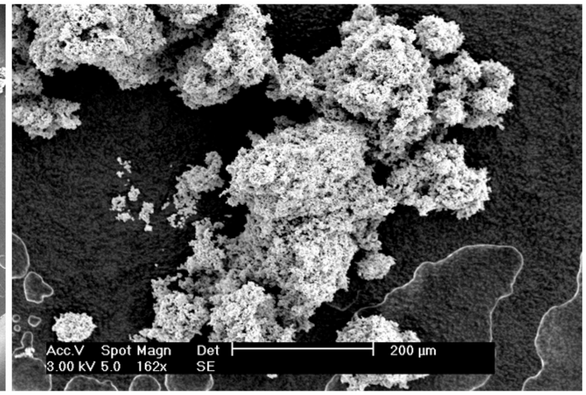

AU_PRE2.TIF

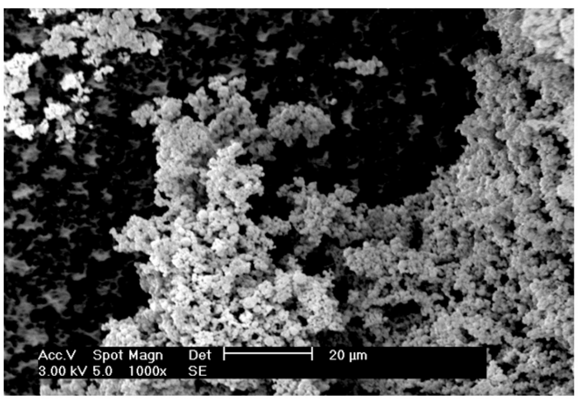

AU_PRE3.TIF

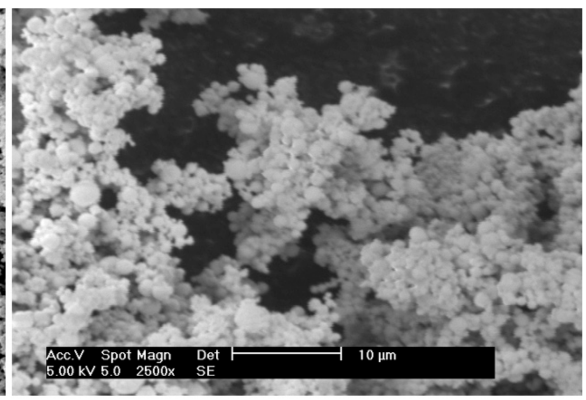

AU_PRE4.TIF

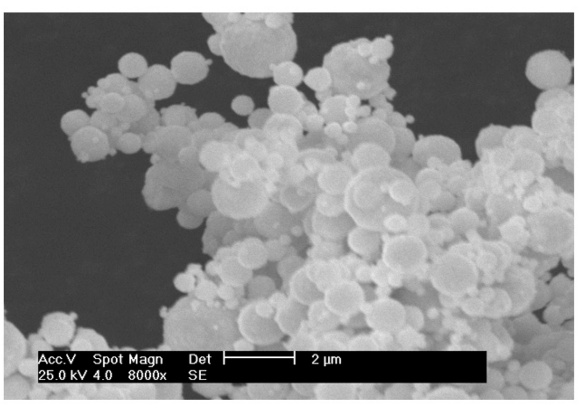

AU_PRE5.TIF

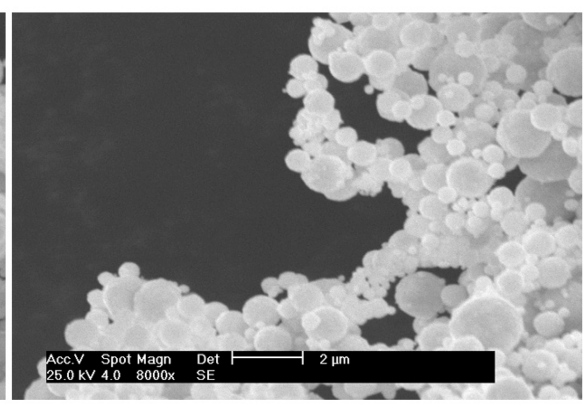

AU_PRE6.TIF

Metallic palladium powder, Sigma Aldrich

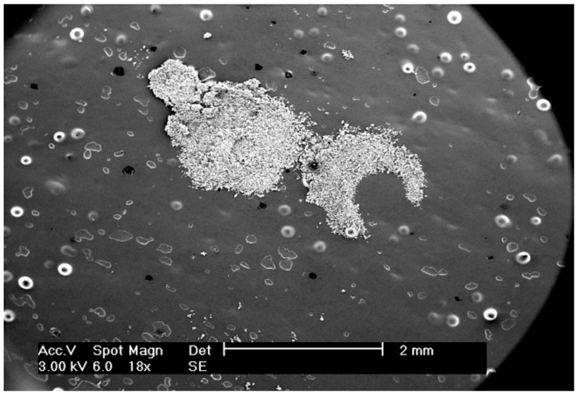

PD_POST1.TIF

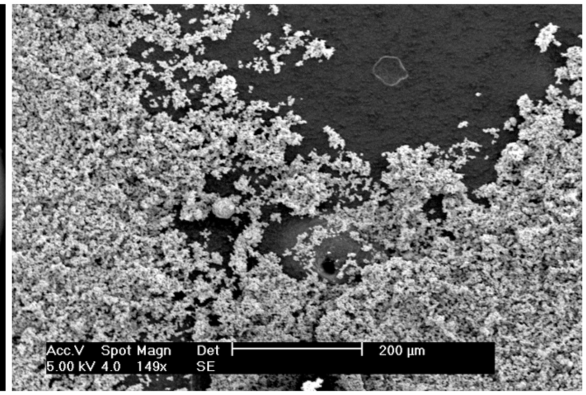

PD_POST2.TIF

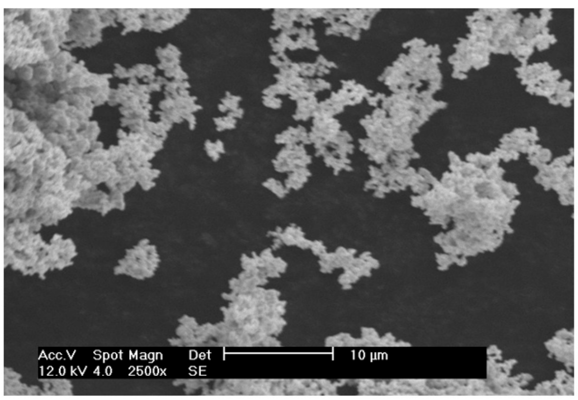

PD_POST3.TIF

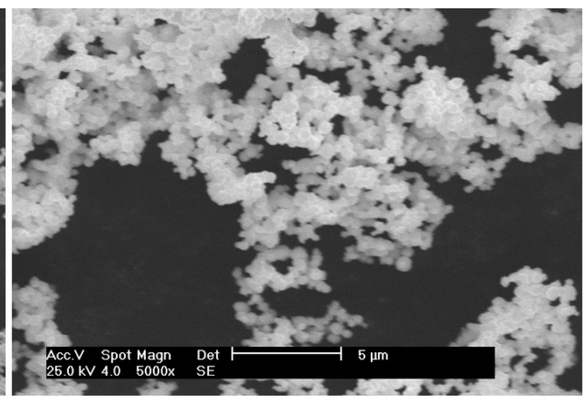

PD_POST4.TIF

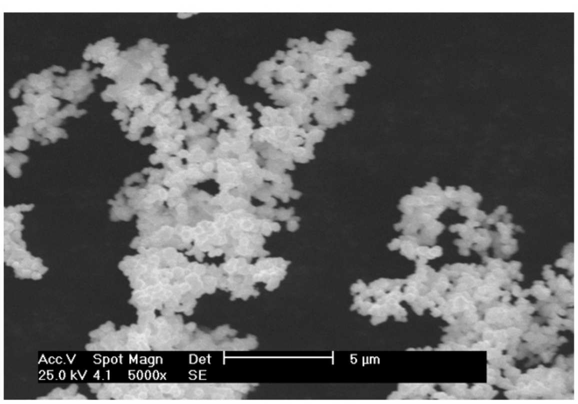

PD_POST5.TIF

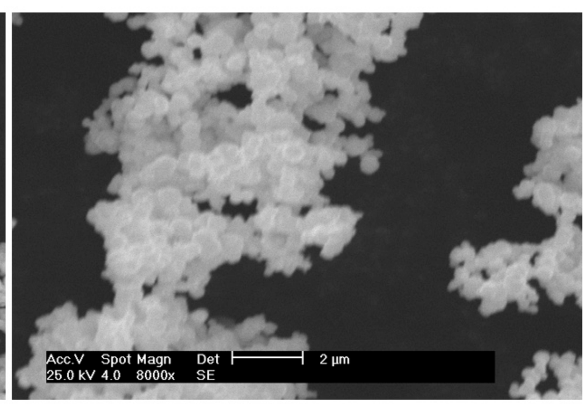

PD_POST6.TIF

As-received gold acetate powders, unsputtered

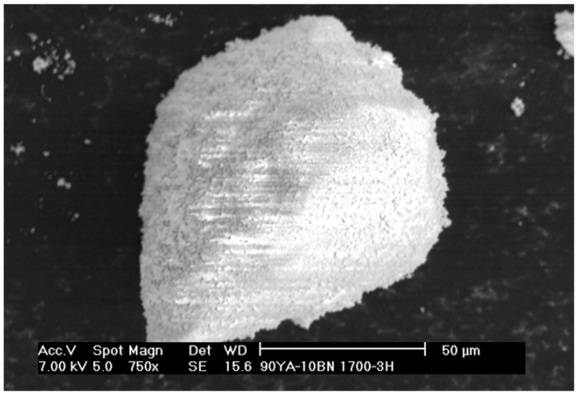

AUAC01.TIF

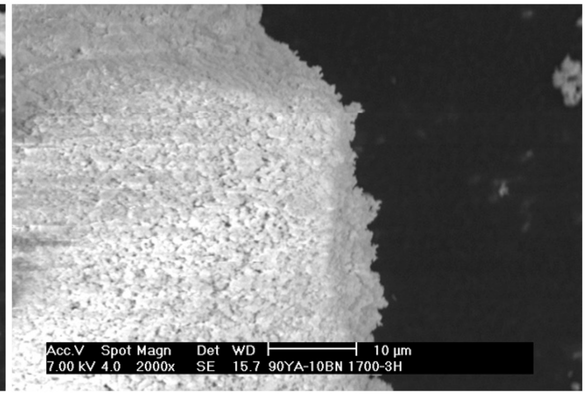

AUAC02.TIF

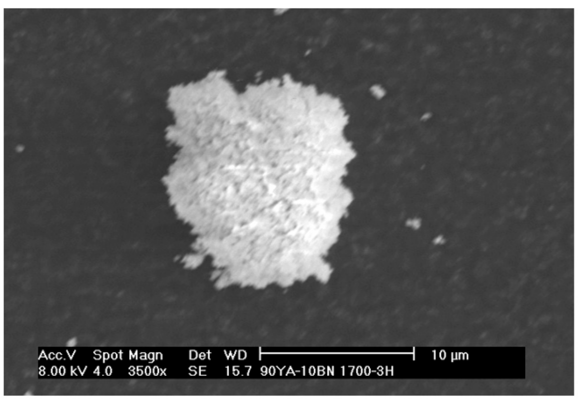

AUAC03.TIF

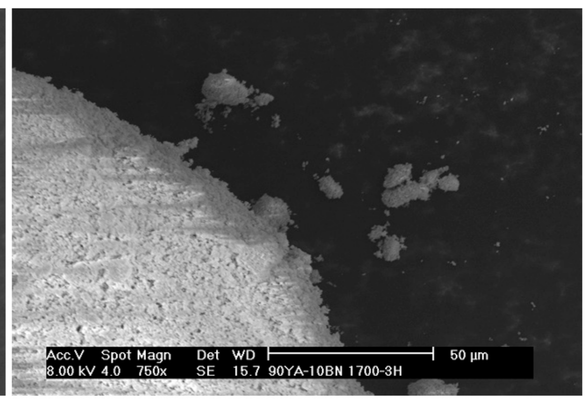

AUAC04.TIF

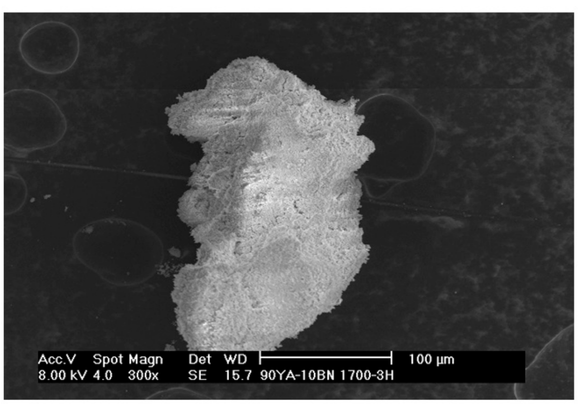

AUAC05.TIF

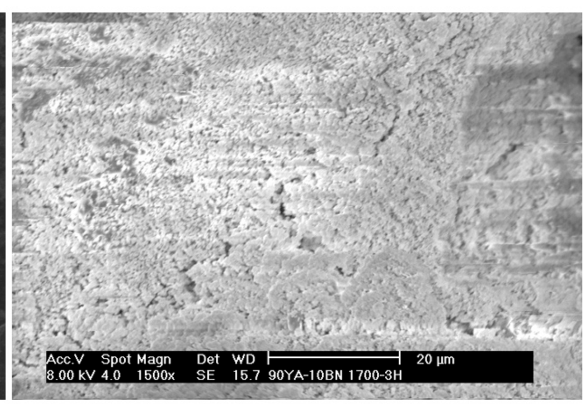

AUAC06.TIF

Gold acetate powders, sputtered

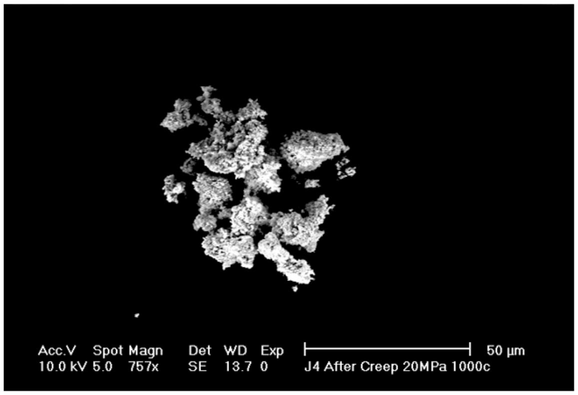

AUACB01.TIF

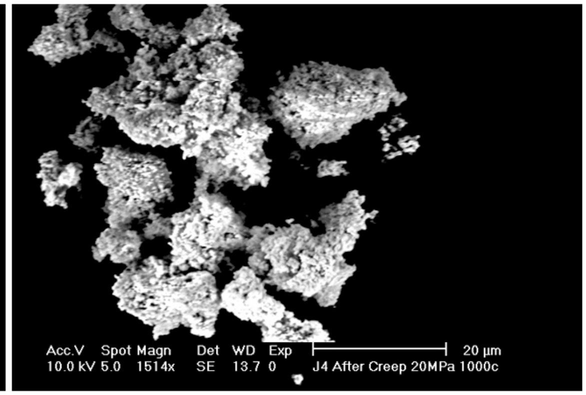

AUACB02.TIF

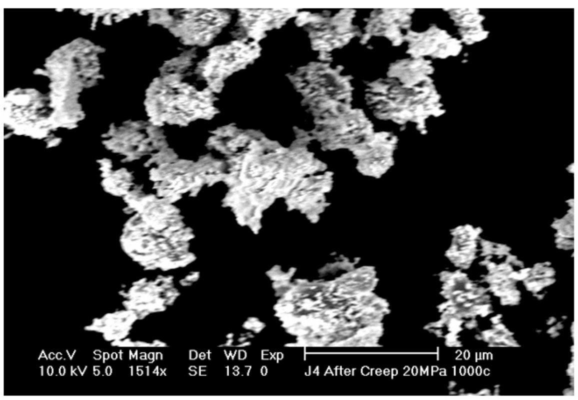

AUACB03.TIF

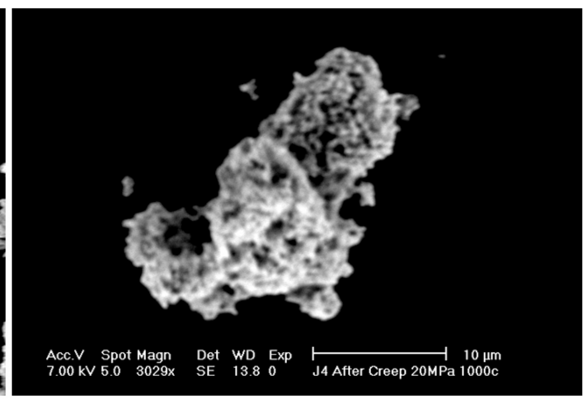

AUACB04.TIF

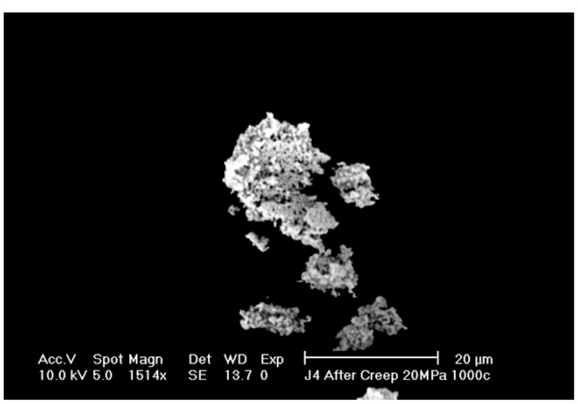

AUACB05.TIF

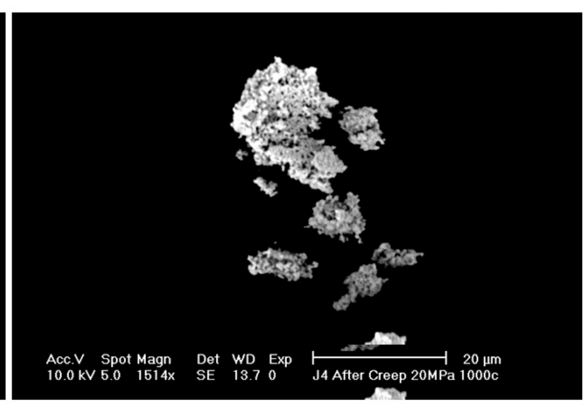

AUACB06.TIF

Gold acetate powders, sputtered

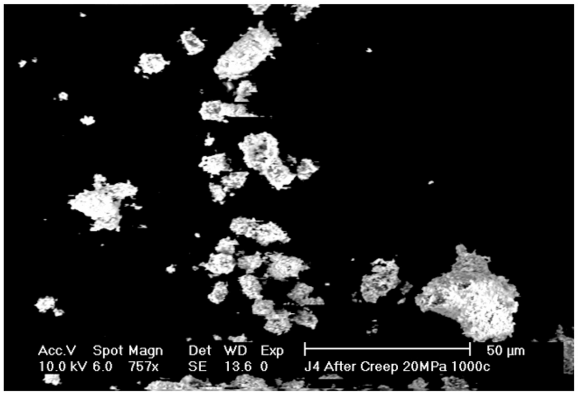

AUACB07.TIF

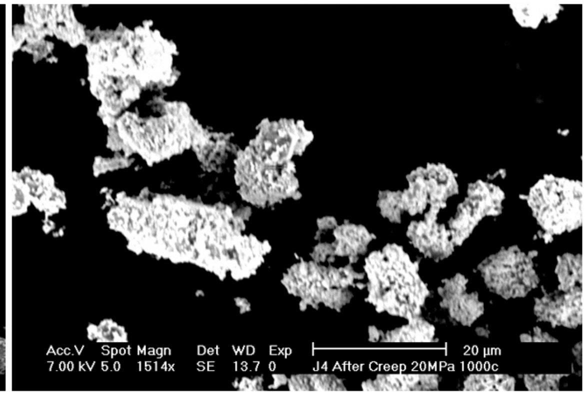

AUACB08.TIF

As-received aluminum acetate powders, unsputtered

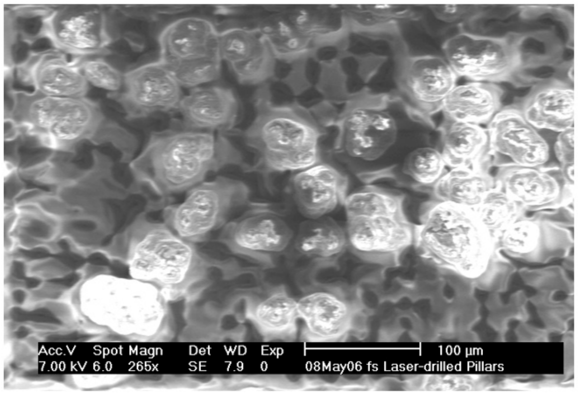

ALAC01.TIF

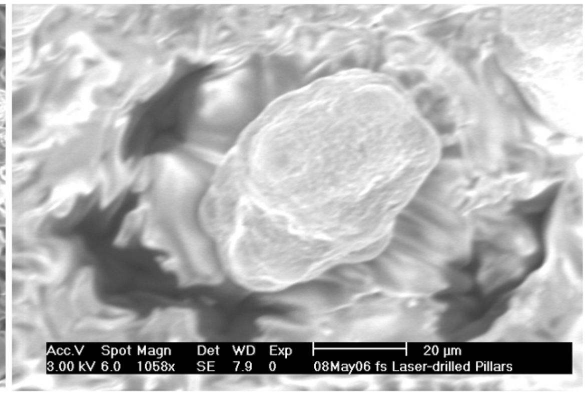

ALAC02.TIF

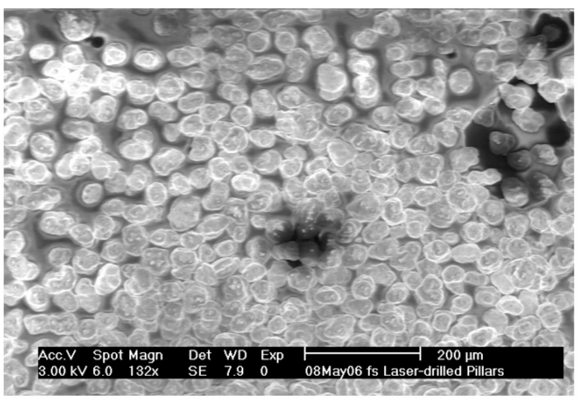

ALAC03.TIF

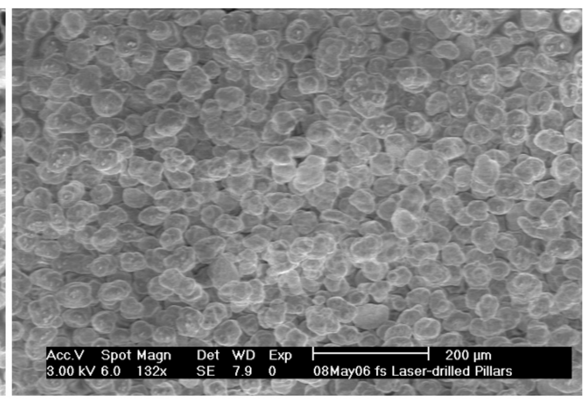

ALAC04.TIF

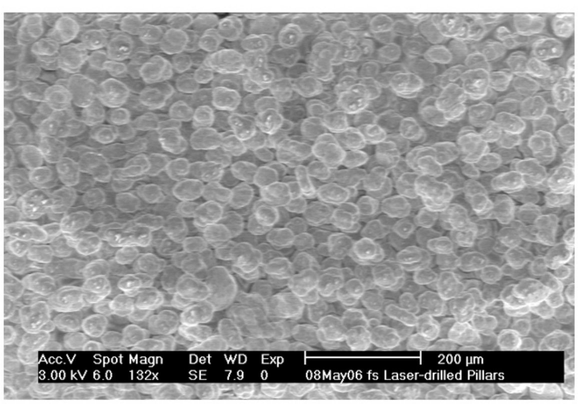

ALAC05.TIF

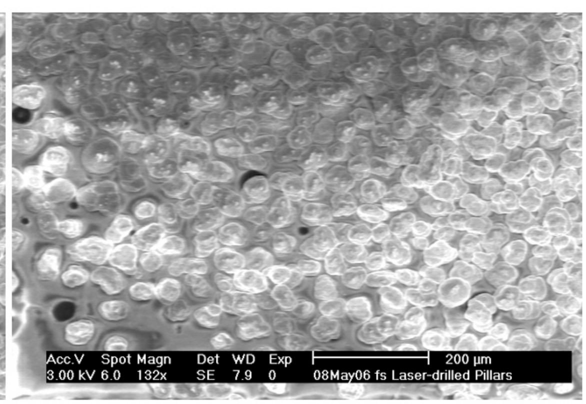

ALAC06.TIF

As-received aluminum acetate powders, unsputtered

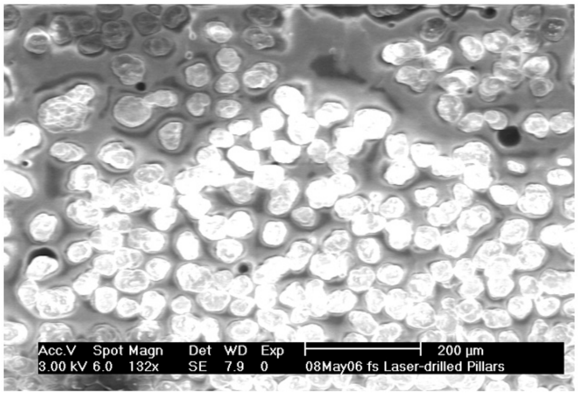

ALAC07.TIF

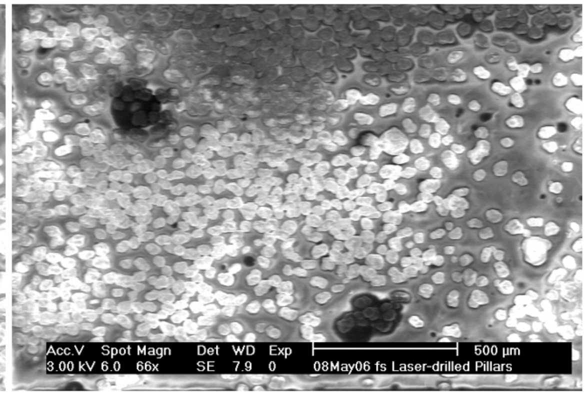

ALAC08.TIF

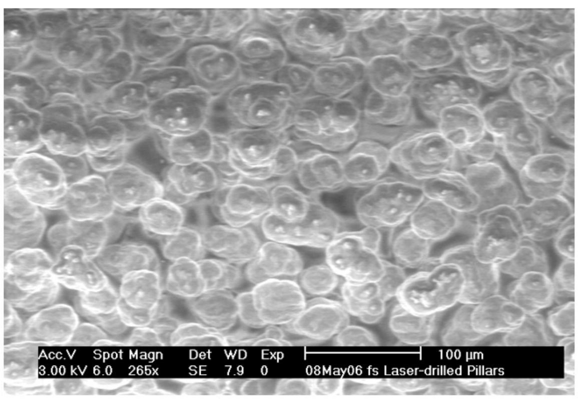

ALAC09.TIF

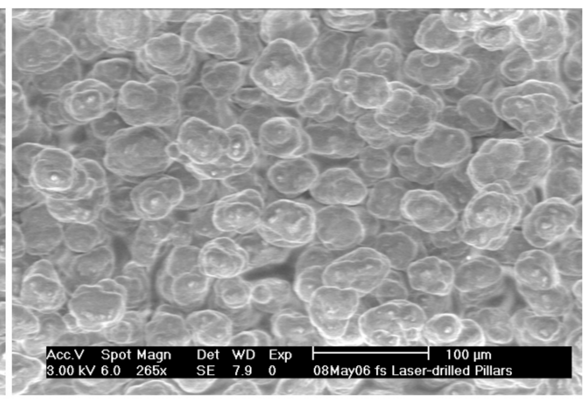

ALAC10.TIF

Aluminum acetate powders, sputtered

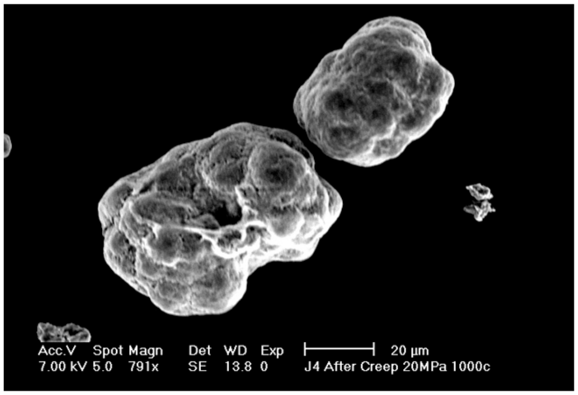

ALACA01.TIF

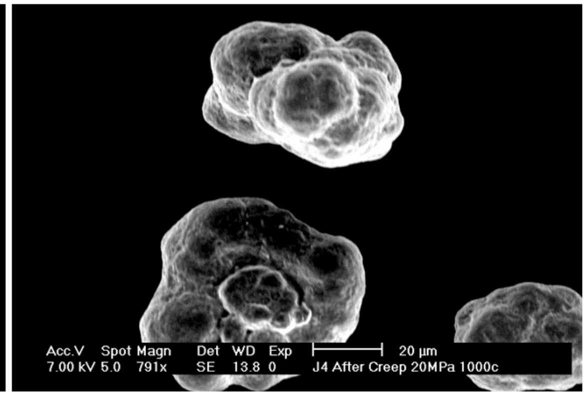

ALACA02.TIF

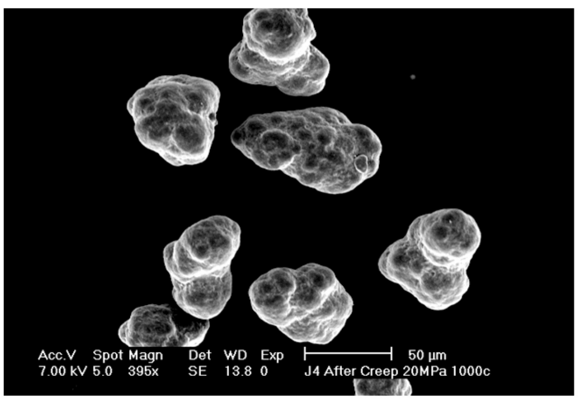

ALACA03.TIF

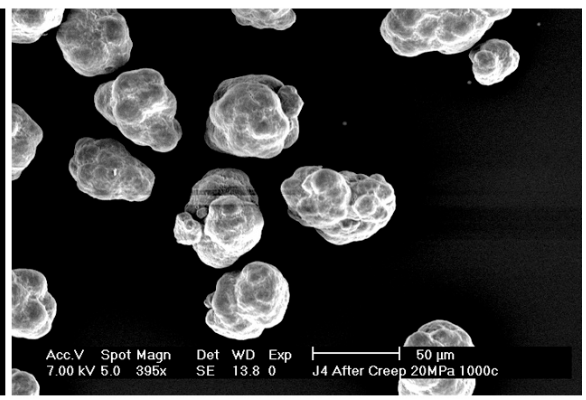

ALACA04.TIF

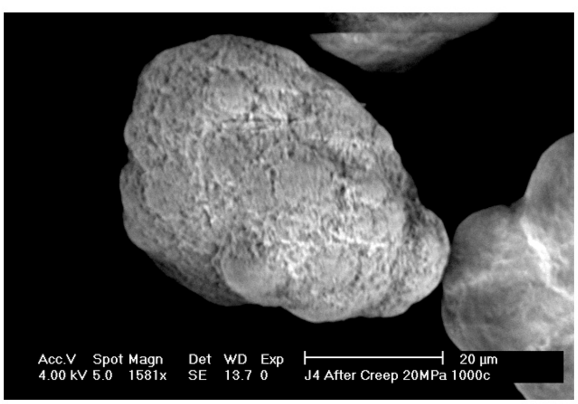

ALACA05.TIF

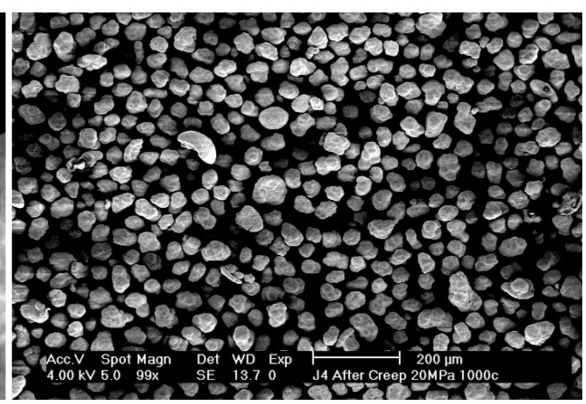

ALACA06.TIF

As-received palladium acetate, unsputtered

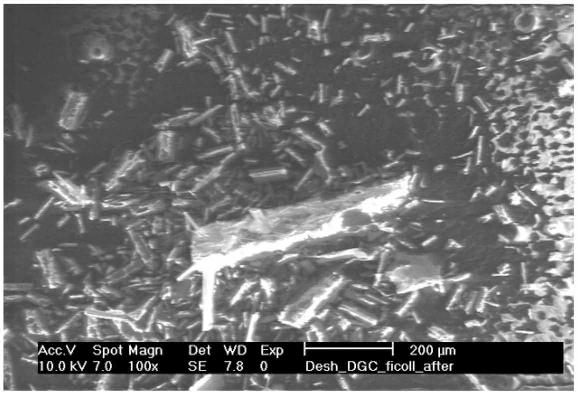

PDAC01.TIF

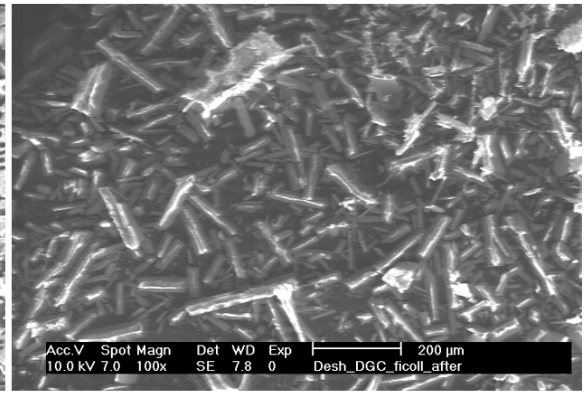

PDAC02.TIF

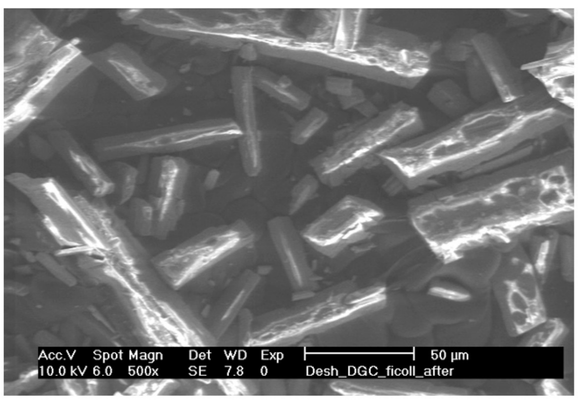

PDAC03.TIF

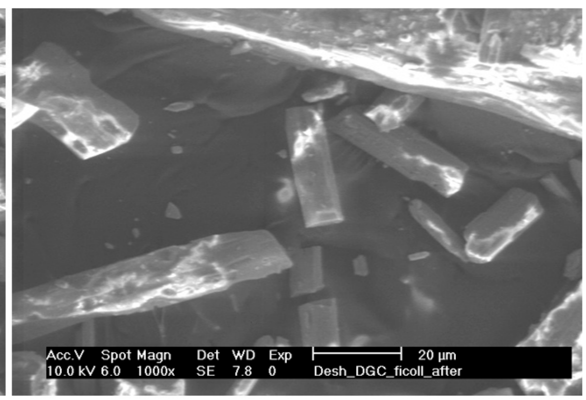

PDAC04.TIF

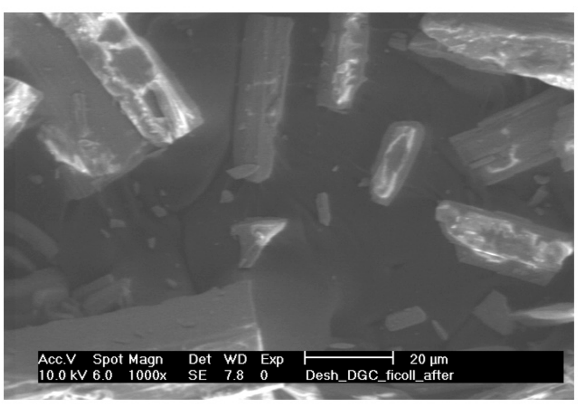

PDAC05.TIF

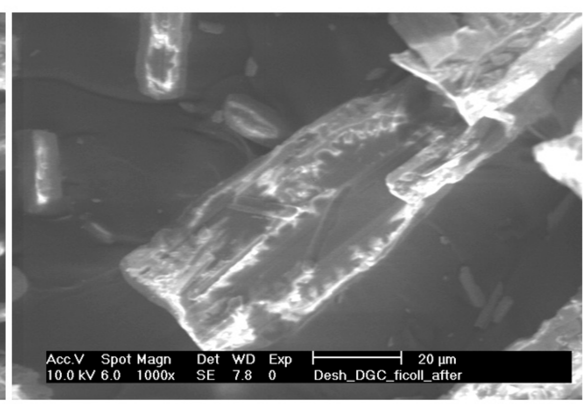

PDAC06.TIF

As-received palladium acetate, unsputtered

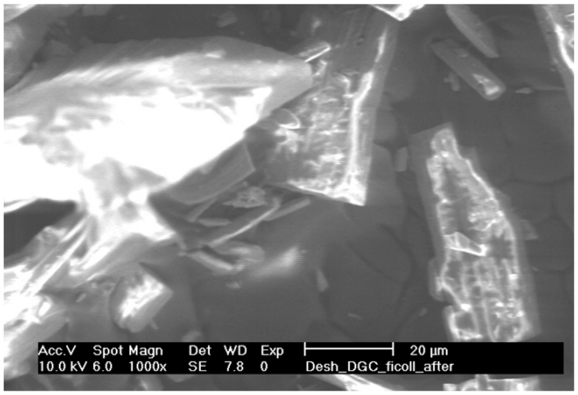

PDAC07.TIF

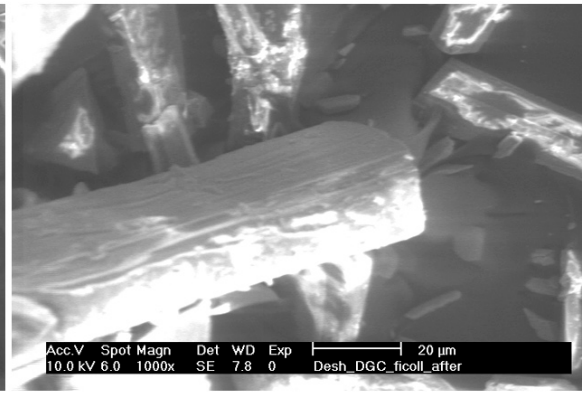

PDAC08.TIF

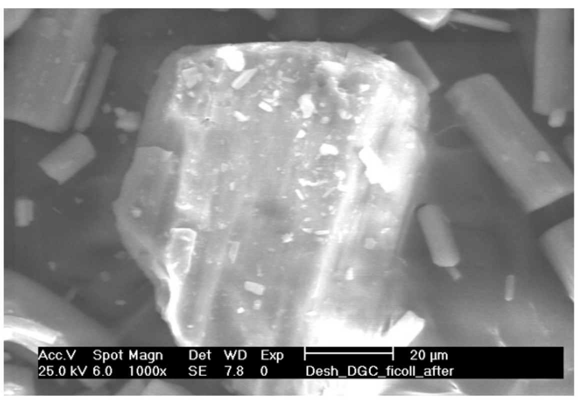

PDAC09.TIF

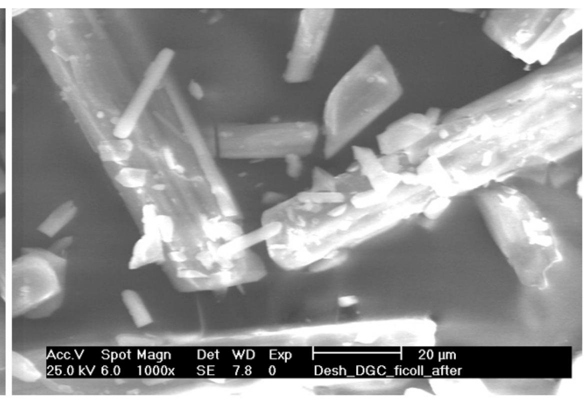

PDAC10.TIF

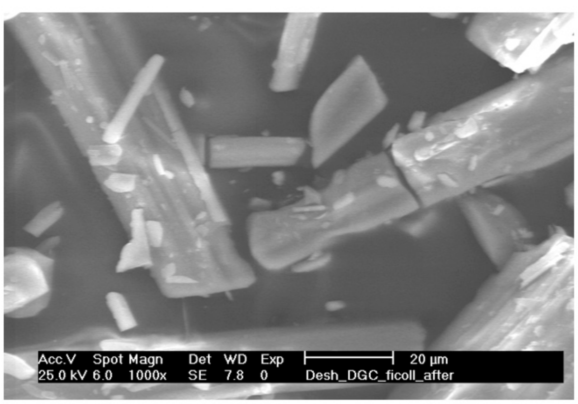

PDAC11.TIF

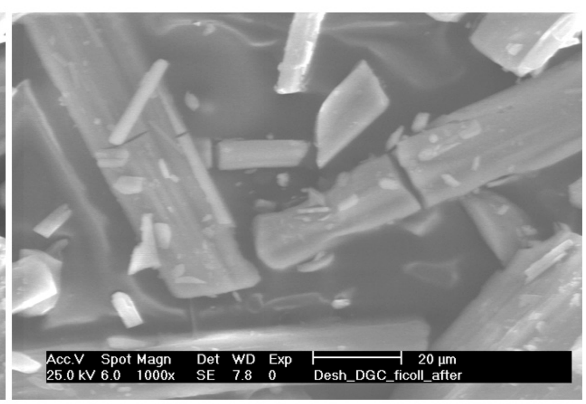

PDAC12.TIF

As-received palladium acetate, unsputtered

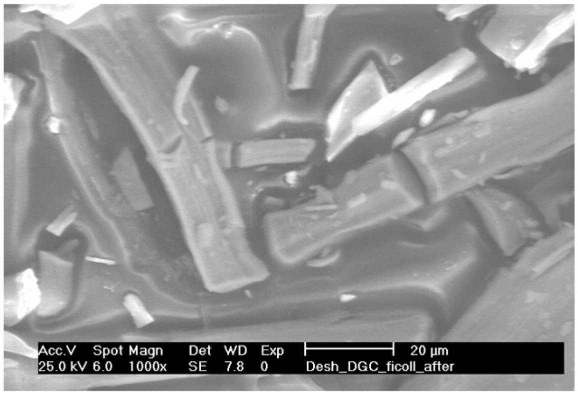

PDAC13.TIF

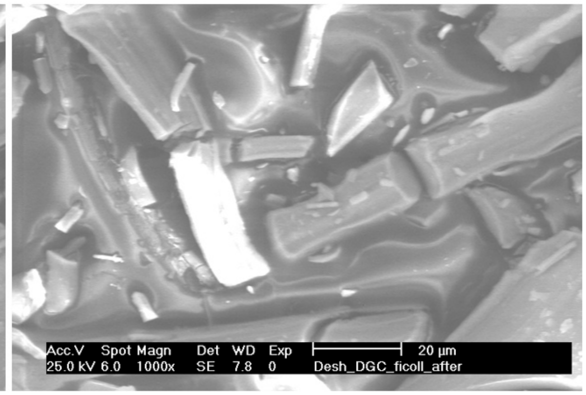

PDAC14.TIF

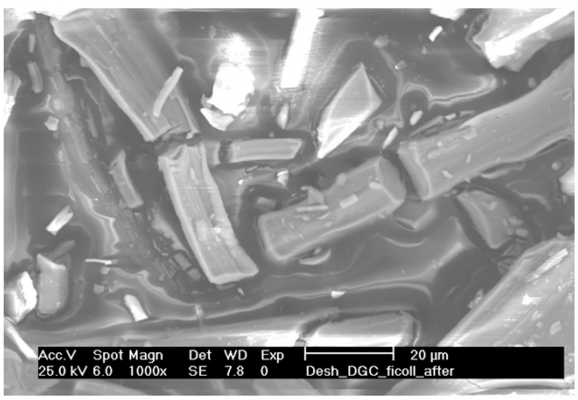

PDAC15.TIF

Palladium acetate, sputtered

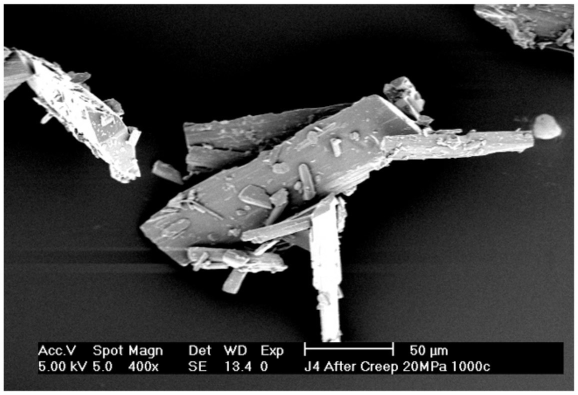

PDACA01.TIF

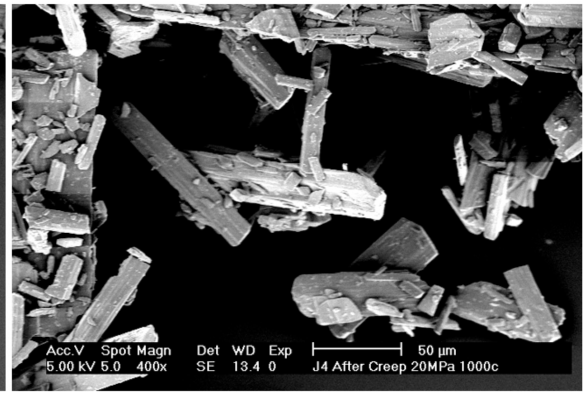

PDACA02.TIF

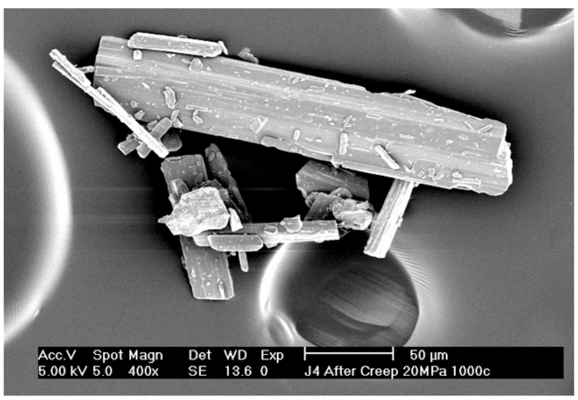

PDACA03.TIF

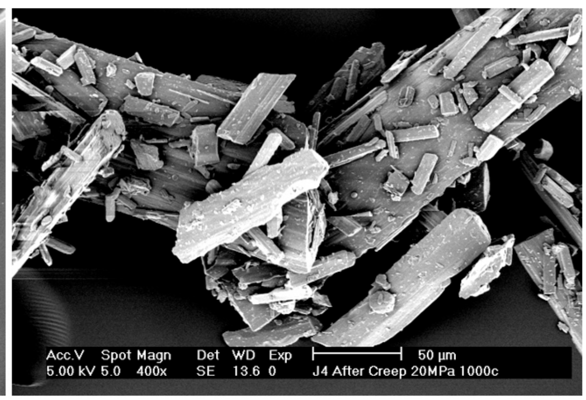

PDACA04.TIF

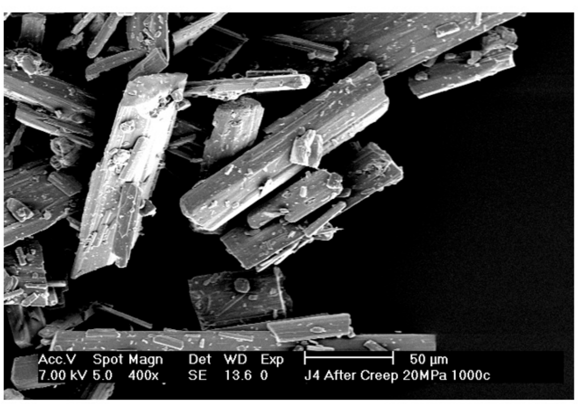

PDACA05.TIF

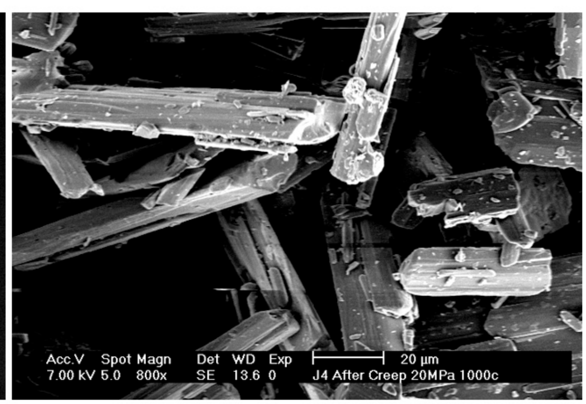

PDACA06.TIF

Copper acetate, sputtered

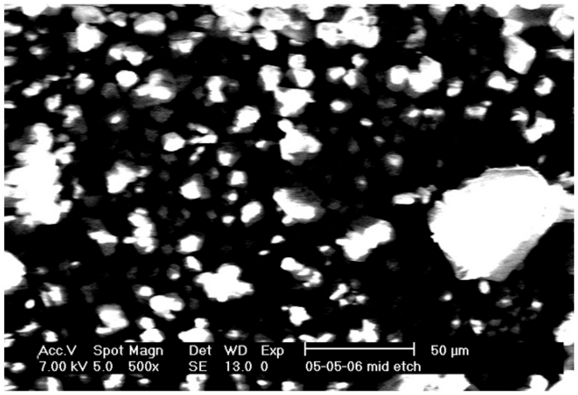

CUAC02.TIF

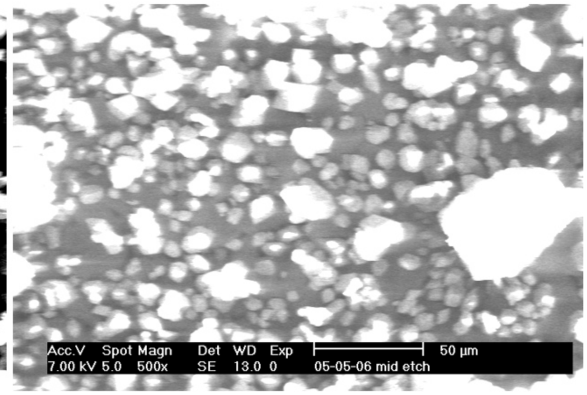

CUAC03.TIF

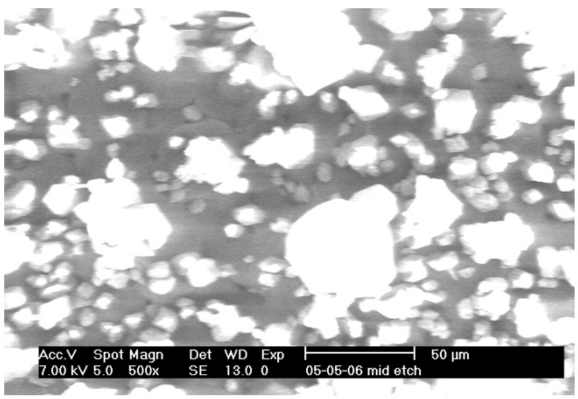

CUAC04.TIF

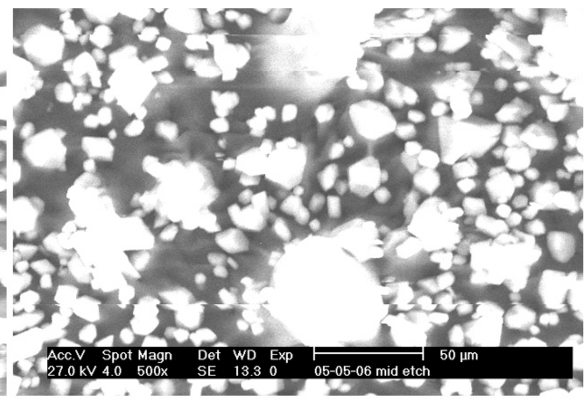

CUAC05.TIF

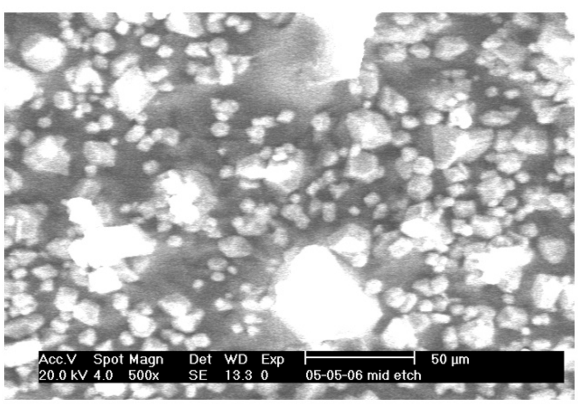

CUAC06.TIF

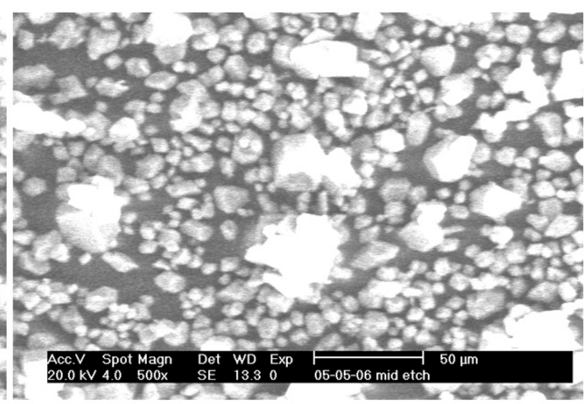

CUAC07.TIF

Copper acetate, sputtered

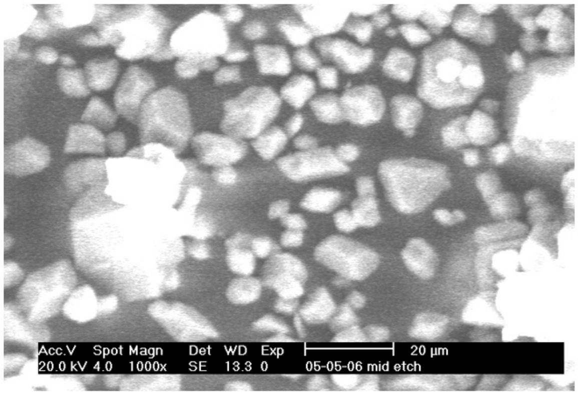

CUAC08.TIF

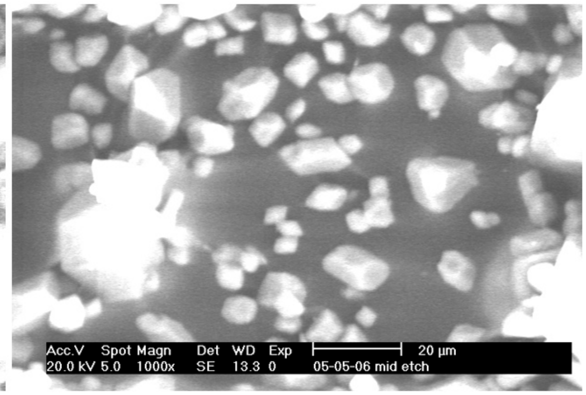

CUAC09.TIF

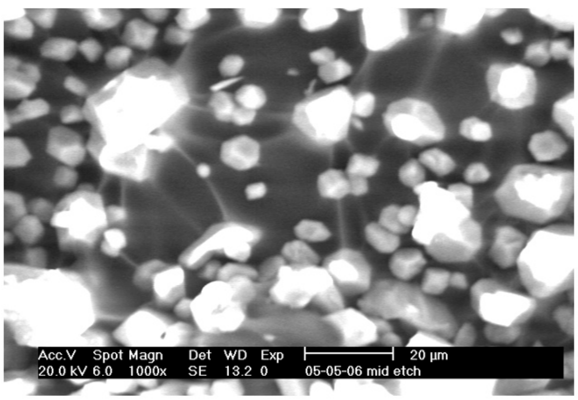

CUAC10.TIF

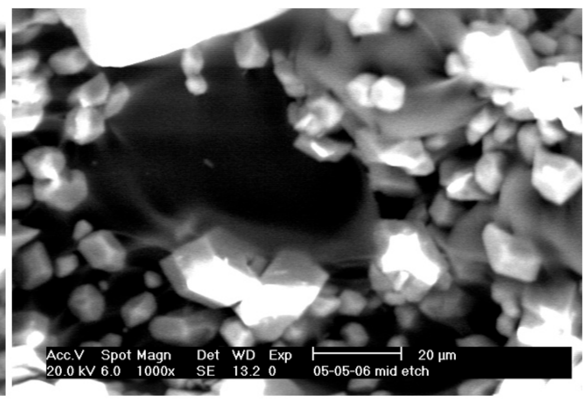

CUAC11.TIF

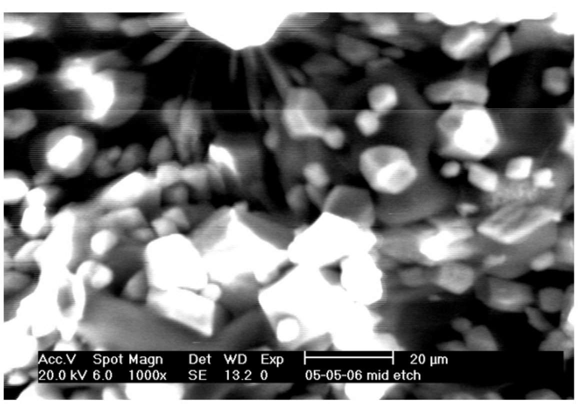

CUAC12.TIF

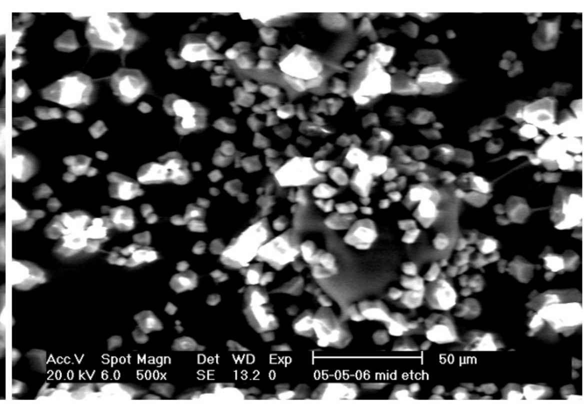

CUAC13.TIF

Copper acetate, sputtered

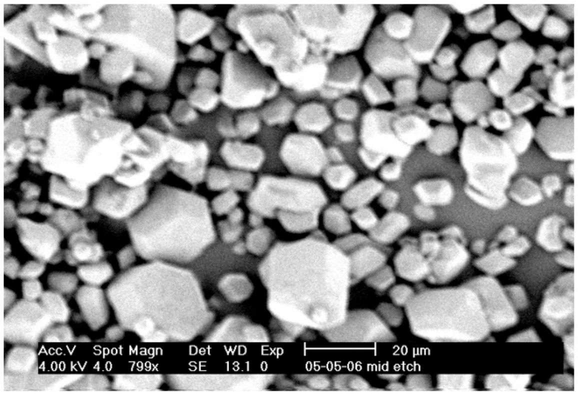

CUAC14.TIF

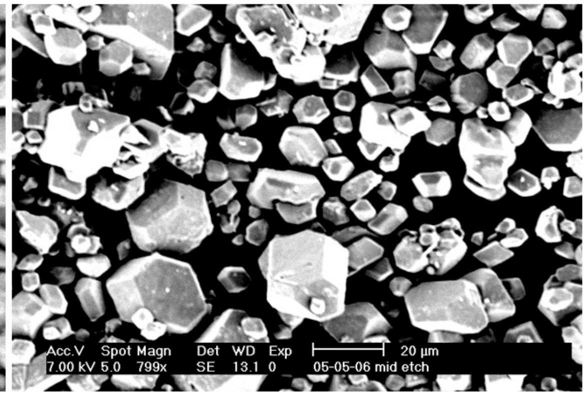

CUAC15.TIF

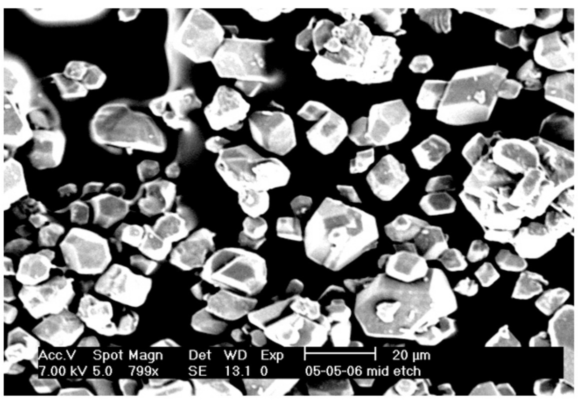

CUAC16.TIF

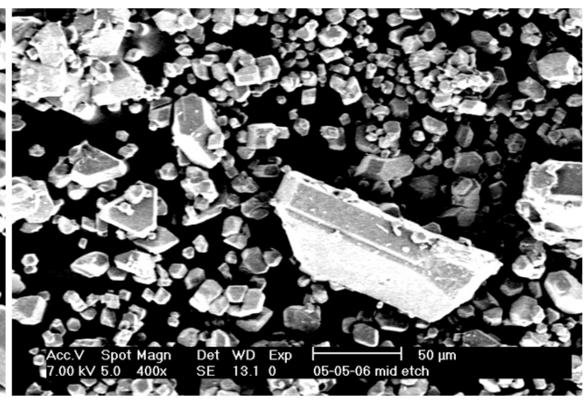

CUAC17.TIF

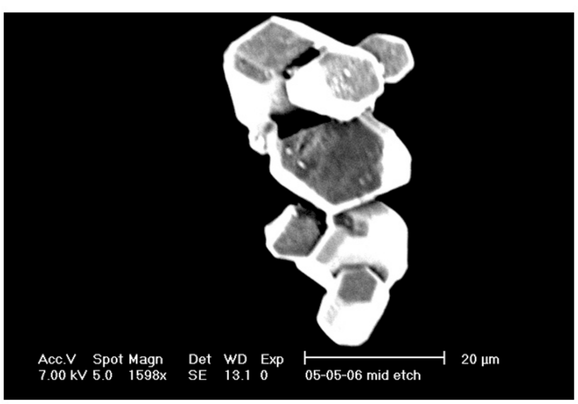

CUAC18.TIF

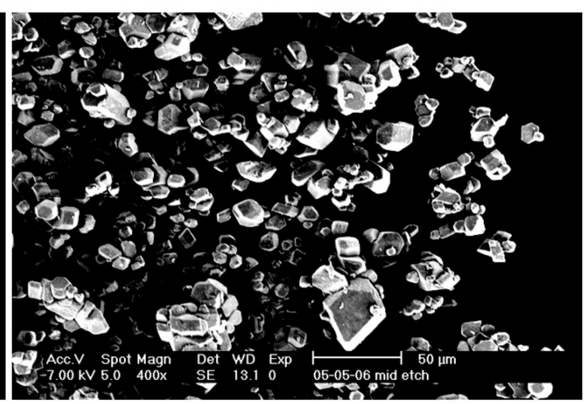

CUAC19.TIF

C.6.2 Sensor film SEM images

Sensor A

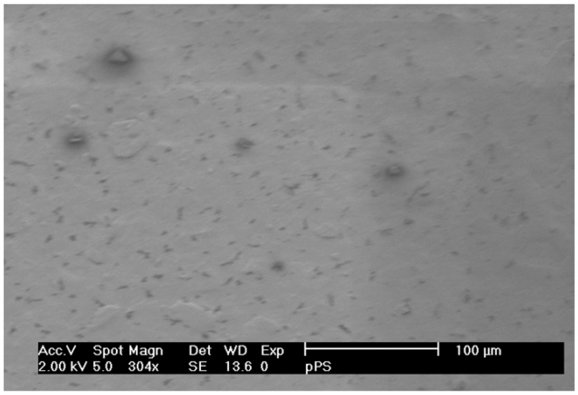

MSPSENA0.TIF

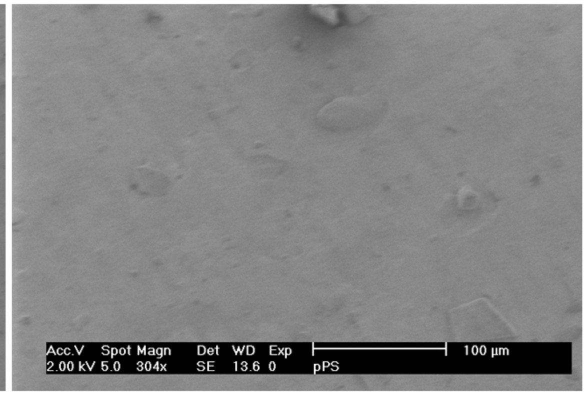

MSPSENA1.TIF

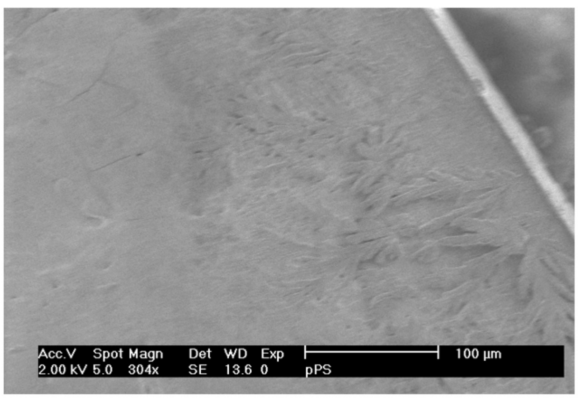

MSPSENA2.TIF

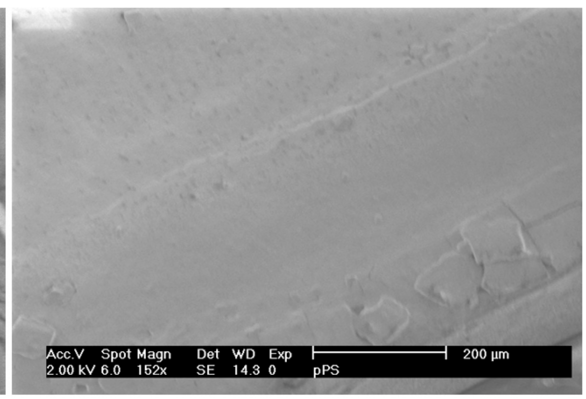

MSPSENA3.TIF

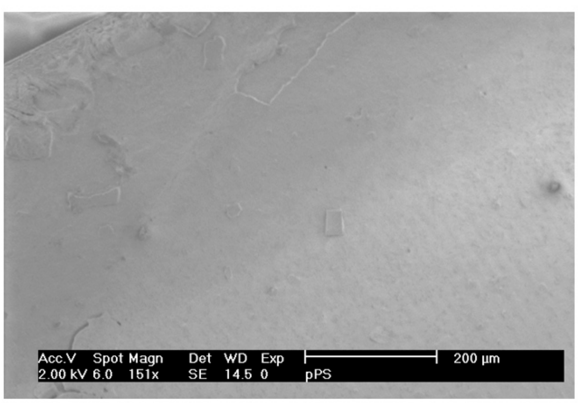

MSPSENA4.TIF

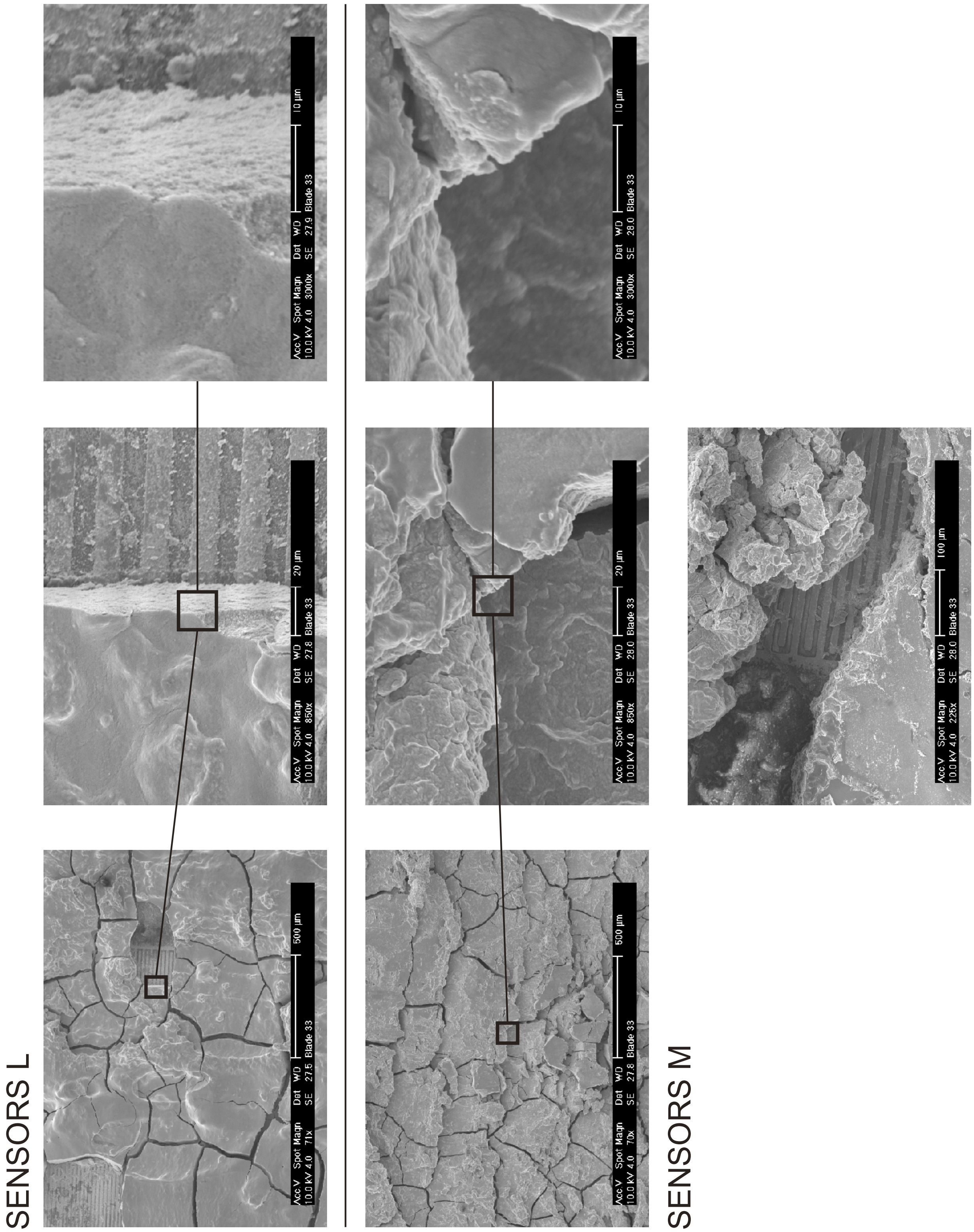
SENSORS L
Acc V Spot Magn Det WD 500 µm
10.0 kV 4.0 71x SE 27.6 Blade 33
Acc V Spot Magn Det WD 20 µm
10.0 kV 4.0 850x SE 27.8 Blade 33
Acc V Spot Magn Det WD 10 µm
10.0 kV 4.0 3300x SE 27.9 Blade 33
SENSORS M
Acc V Spot Magn Det WD 500 µm
10.0 kV 4.0 70x SE 27.8 Blade 33
Acc V Spot Magn Det WD 20 µm
10.0 kV 4.0 850x SE 28.0 Blade 33
Acc V Spot Magn Det WD 10 µm
10.0 kV 4.0 3300x SE 28.0 Blade 33
Acc V Spot Magn Det WD 100 µm
10.0 kV 4.0 225x SE 28.0 Blade 33

Pd-doped SnO_2 and SnO_2 dispersion mixture film

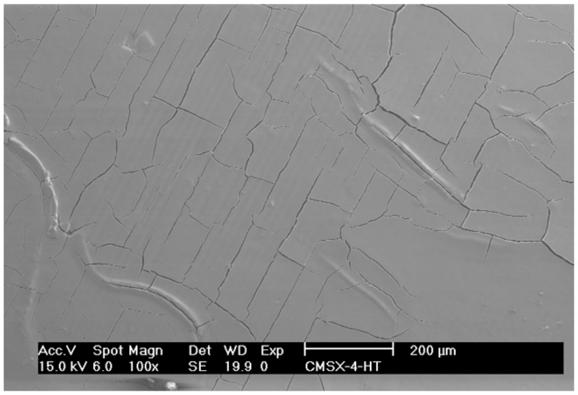

PDHYB01.TIF

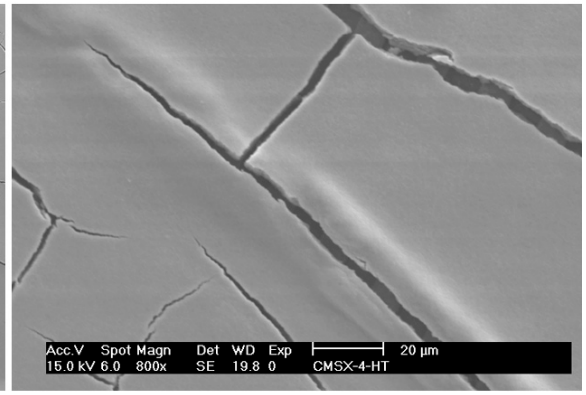

PDHYB03.TIF

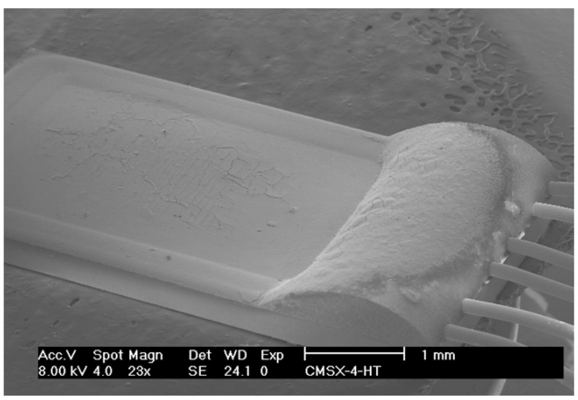

PDHYB04.TIF

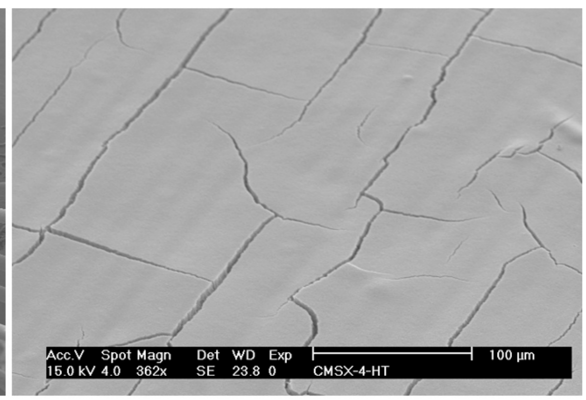

PDHYB05.TIF

Sensor ZR with 1 and 5 layers deposited

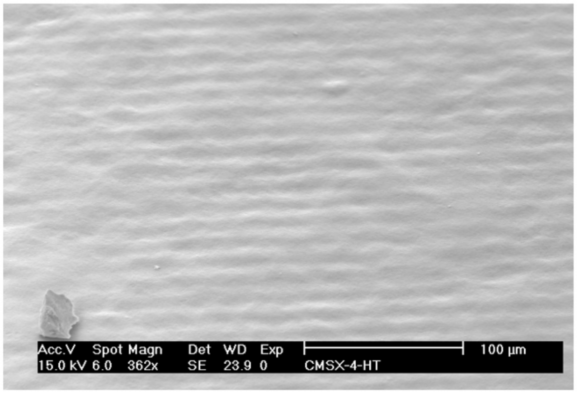

ZR_LAY1_01.TIF

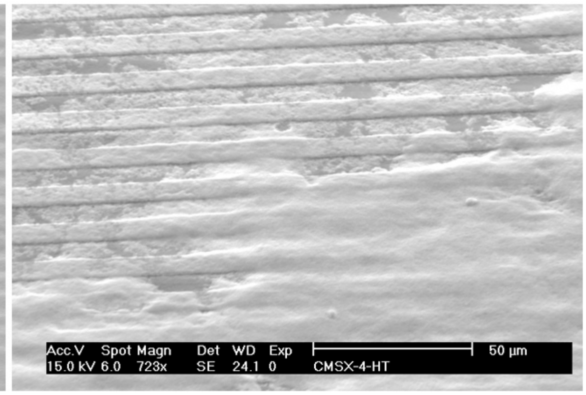

ZR_LAY1_02.TIF

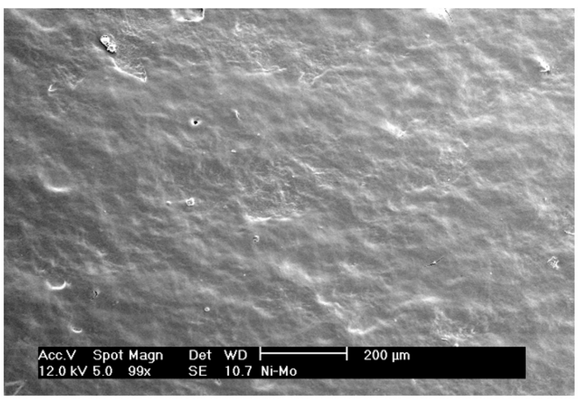

ZR_LAY5_01.tif

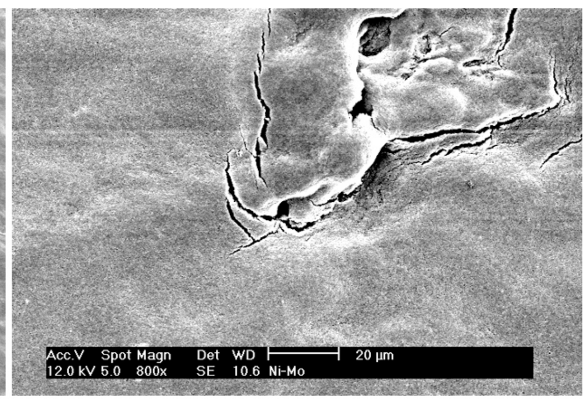

ZR_LAY5_02.tif

Sensor ZT with sputtered gold layer on SnO_2

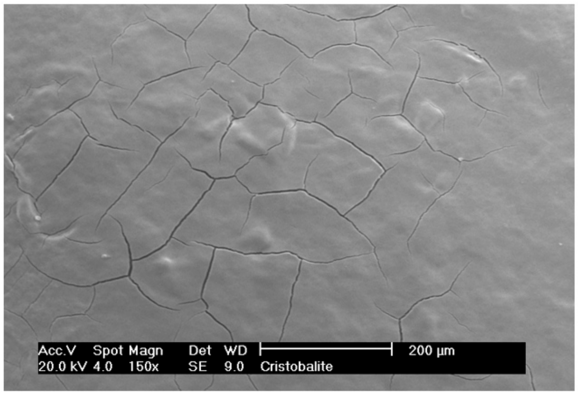

AUSPUT02.TIF

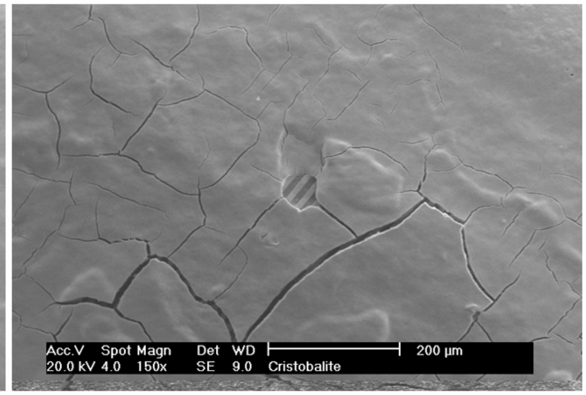

AUSPUT03.TIF

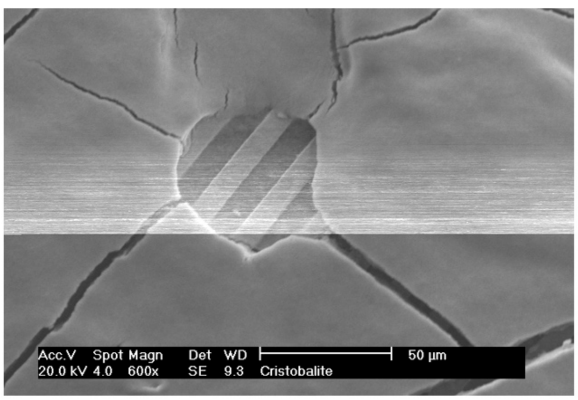

AUSPUT04.TIF

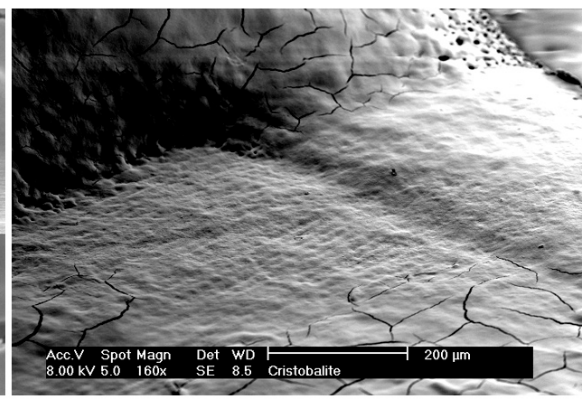

AUSPUT05.TIF

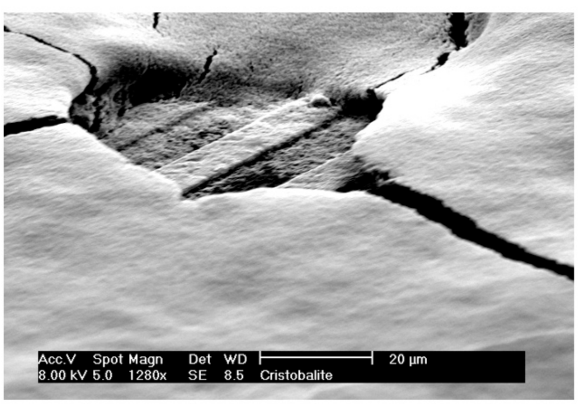

AUSPUT06.TIF

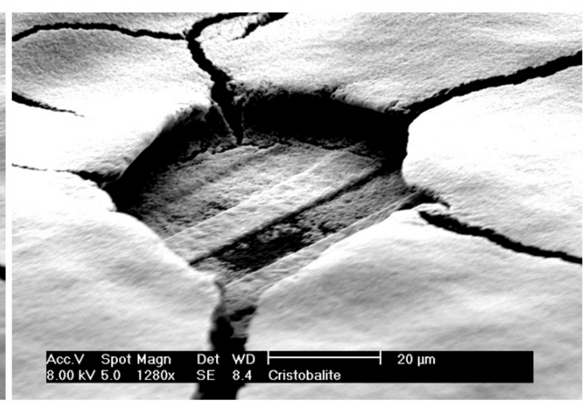

AUSPUT07.TIF

Sensor ZT with sputtered gold layer on SnO_2, with XEDS results

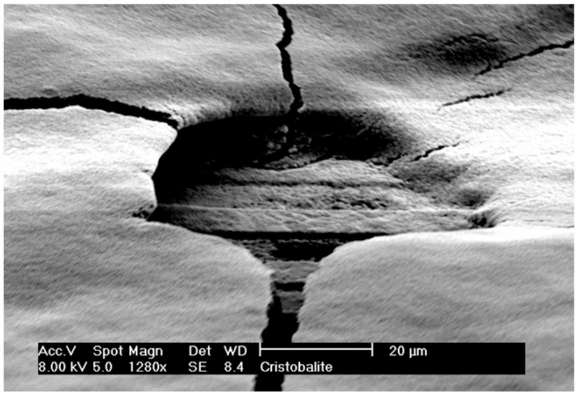

AUSPUT08.TIF

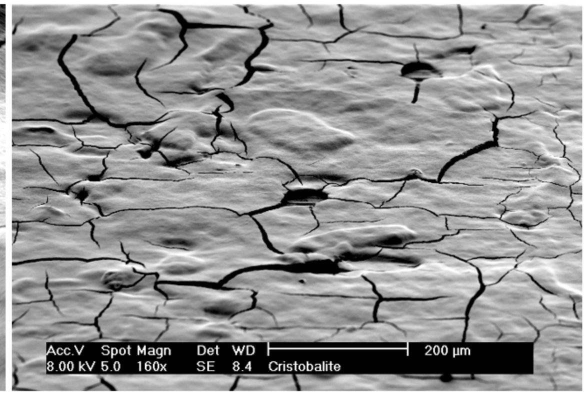

AUSPUT09.TIF

EDAX ZAF Quantification (Standardless)
Element Normalized
SEC Table : Default

Elem	Wt %	At %	K-Ratio	Z	A	F
O K	19.46	64.75	0.0327	1.2304	0.1365	1.0001
AuM	4.86	1.31	0.0385	0.8541	0.9267	1.0005
SnL	75.68	33.94	0.7001	0.9255	0.9996	1.0000
Total	100.00	100.00				

Element	Net Inte.	Backgrd	Inte. Error	P/B
O K	8.29	1.53	4.06	5.42
AuM	3.59	3.99	9.47	0.90
SnL	63.00	3.52	1.33	17.90

Picture 1.png

Sensor ZV with 5 layers and 5 hours sintering

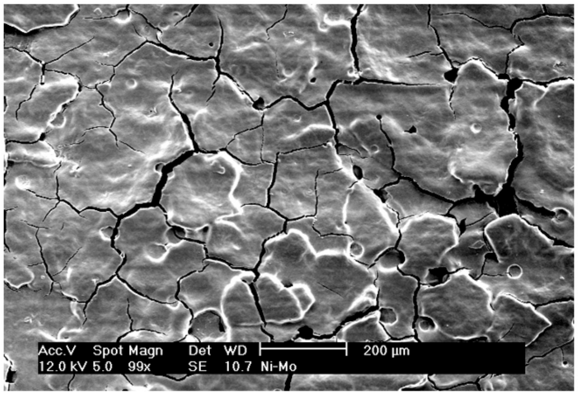

Szv01.tif

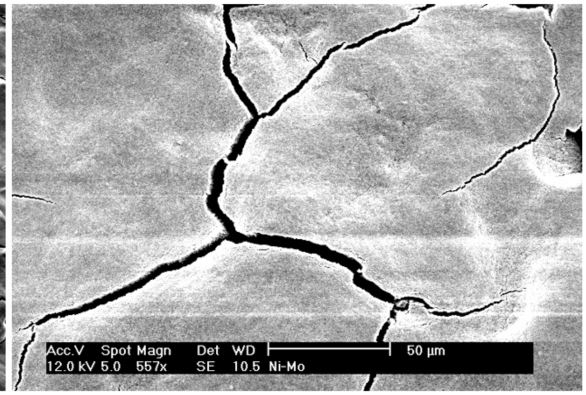

Szv02.tif

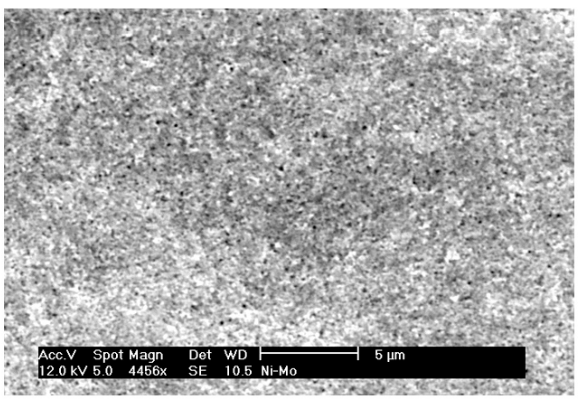

Szv03.tif

Sensor ZX with single layer of SnO_2 dispersion

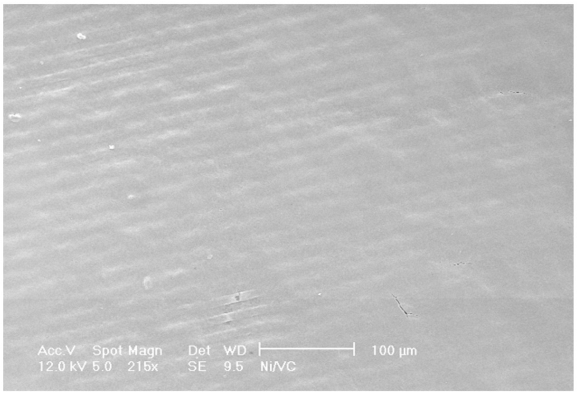

Sxly101.tif

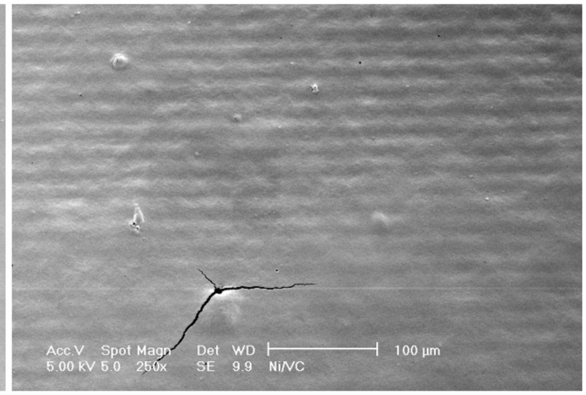

Sxly102.tif

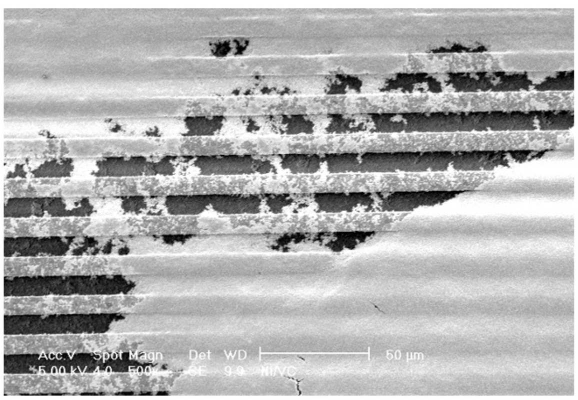

Sxly103.tif

BIBLIOGRAPHY

BIBLIOGRAPHY

[1] van Mol, A. M. B., Alcott, G. R. & Allendorf, M. D. Tin oxide precursor chemistry and its link to coating properties. *American Ceramic Society Bulletin* **84**, 37–41 (2005).

[2] Dinh, N. N., Bernard, M. C., Gof, A. H.-L., Stergiopoulos, T. & Falaras, P. Photoelectrochemical solar cells based on SnO_2 nanocrystalline films. *Comptes Rendus Chimie* **9**, 676–683 (2006).

[3] Batzill, M. & Diebold, U. The surface and materials science of tin oxide. *Progress in Surface Science* **79**, 47–154 (2005).

[4] Seiyama, T., Kato, A., Fujiishi, K. & Nagatani, M. A New Detector for Gaseous Components using Semiconductive Thin Films. *Analytical Chemistry* **34**, 1502 (1962).

[5] Malyshev, V. V. & Pislyakov, A. V. SnO_2-based thick-film-resistive sensor for H2S detection in the concentration range of 1-10 mg m-3. *Sensors and Actuators B: Chemical* **47**, 181–188 (1998).

[6] Devi, G. S., Manorama, S. & Rao, V. J. High sensitivity and selectivity of an SnO_2 sensor to H_2S at around 100 ^oC. *Sensors and Actuators B: Chemical* **28**, 31–37 (1995).

[7] Zhao, Y., Feng, Z. & Liang, Y. SnO_2 gas sensor films deposited by pulsed laser ablation. *Sensors and Actuators B: Chemical* **56**, 224–227 (1999).

[8] Shin, W., Matsumiya, M., Qiu, F., Izu, N. & Murayama, N. Thermoelectric gas sensor for detection of high hydrogen concentration. *Sensors and Actuators B: Chemical* **97**, 344–347 (2004).

[9] Bittencourt, C., Llobet, E., Ivanov, P., Correig, X., Vilanova, X., Brezmes, J., Hubalek, J., Malysz, K., Pireaux, J. J. & Calderer, J. Influence of the doping method on the sensitivity of Pt-doped screen-printed SnO_2 sensors. *Sensors and Actuators B: Chemical* **97**, 67–73 (2004).

[10] Brezmes, J., Llobet, E., Vilanova, X., Orts, J., Saiz, G. & Correig, X. Correlation between electronic nose signals and fruit quality indicators on shelf-life measurements with pinklady apples. *Sensors and Actuators B: Chemical* **80**, 41–50 (2001).

[11] Gardner, J. W., Shin, H. W. & Hines, E. L. An electronic nose system to diagnose illness. *Sensors and Actuators B: Chemical* **70**, 19–24 (2000).

[12] Ehrmann, S., Jungst, J., Goschnick, J. & Everhard, D. Application of a gas sensor microarray to human breath analysis. *Sensors and Actuators B: Chemical* **65**, 247–249 (2000).

[13] Ihokura, K. & Watson, J. *The Stannic Oxide Gas Sensor - Principles and Applications* (CRC Press, Boca Raton, Florida, 1994).

[14] Madler, L., Roessler, A., Pratsinis, S. E., Sahm, T., Gurlo, A., Barsan, N. & Weimar, U. Direct formation of highly porous gas-sensing films by in situ thermophoretic deposition of flame-made Pt/SnO_2 nanoparticles. *Sensors and Actuators B: Chemical* **114**, 283–295 (2006).

[15] Kennedy, M. K., Kruis, F. E., Fissan, H., Mehta, B. R., Stappert, S. & Dumpich, G. Tailored nanoparticle films from monosized tin oxide nanocrystals: Particle synthesis, film formation, and size-dependent gas-sensing properties. *Journal of Applied Physics* **93**, 551–560 (2003).

[16] Miller, T. A., Bakrania, S. D., Perez, C. & Wooldridge, M. S. *Nanostructured Tin Dioxide materials for Gas Sensor Applications*. Functional Nanomaterials (American Scientific Publishers, 2006), first edn.

[17] Yamazoe, N. New approaches for improving semiconductor gas sensors. *Sensors and Actuators B: Chemical* **5**, 7–19 (1991).

[18] Choe, Y.-S. New gas sensing mechanism for SnO_2 thin-film gas sensors fabricated by using dual ion beam sputtering. *Sensors and Actuators B: Chemical* **77**, 200–208 (2001).

[19] Ivanov, P., Llobet, E., Vilanova, X., Brezmes, J., Hubalek, J. & Correig, X. Development of high sensitivity ethanol gas sensors based on Pt-doped SnO_2 surfaces. *Sensors and Actuators B: Chemical* **99**, 201–206 (2004).

[20] Nicoletti, S., Dori, L., Cardinali, G. C. & Parisini, A. Gas sensors for air quality monitoring: realisation and characterisation of undoped and noble metal-doped SnO_2 thin sensing films deposited by the pulsed laser ablation. *Sensors and Actuators B: Chemical* **60**, 90–96 (1999).

[21] Wurzinger, O. & Reinhardt, G. CO-sensing properties of doped SnO_2 sensors in H_2-rich gases. *Sensors and Actuators B: Chemical* **103**, 104–110 (2004).

[22] Sung, J.-H., Lee, Y.-S., Lim, J.-W., Hong, Y.-H. & Lee, D.-D. Sensing characteristics of tin dioxide/gold sensor prepared by coprecipitation method. *Sensors and Actuators B: Chemical* **66**, 149–152 (2000).

[23] Heilig, A., Barsan, N., Weimar, U. & Gopel, W. Selectivity enhancement of SnO_2 gas sensors: simultaneous monitoring of resistances and temperatures. *Sensors and Actuators B: Chemical* **58**, 302–309 (1999).

[24] Ying, Z., Wan, Q., Song, Z. T. & Feng, S. L. Controlled synthesis of branched SnO_2 nanowhiskers. *Materials Letters* **59**, 1670–1672 (2005).

[25] Comini, E., Bianchi, S., Faglia, G., Ferroni, M., Vomiero, A. & Sberveglieri, G. Functional nanowires of tin oxide. *Applied Physics A-Materials Science & Processing* **89**, 73–76 (2007).

[26] Kolmakov, A., Zhang, Y. X., Cheng, G. S. & Moskovits, M. Detection of CO and O_2 using tin oxide nanowire sensors. *Advanced Materials* **15**, 997 (2003).

[27] Tresback, J. S., Vasiliev, A. L. & Padture, N. P. Engineered metal-oxide-metal heterojunction nanowires. *Journal of Materials Research* **20**, 2613–2617 (2005).

[28] Takada, T., Fukunaga, T. & Maekawa, T. New method for gas identification using a single semiconductor sensor. *Sensors and Actuators B: Chemical* **66**, 22–24 (2000).

[29] Licznerski, B. W., Nitsch, K., Teterycz, H., Sobanski, T. & Wisniewski, K. Characterisation of electrical parameters for multilayer SnO_2 gas sensors. *Sensors and Actuators B: Chemical* **103**, 69–75 (2004).

[30] Cavicchi, R. E., Walton, R. M., Aquino-Class, M., Allen, J. D. & Panchapakesan, B. Spin-on nanoparticle tin oxide for microhotplate gas sensors. *Sensors and Actuators B: Chemical* **77**, 145–154 (2001).

[31] Baik, N. S., Sakai, G., Miura, N. & Yamazoe, N. Hydrothermally treated sol solution of tin oxide for thin-film gas sensor. *Sensors and Actuators B: Chemical* **63**, 74–79 (2000).

[32] Sakai, G., Baik, N. S., Miura, N. & Yamazoe, N. Gas sensing properties of tin oxide thin films fabricated from hydrothermally treated nanoparticles: Dependence of CO and H_2 response on film thickness. *Sensors and Actuators B: Chemical* **77**, 116–121 (2001).

[33] Cukrov, L. M., McCormick, P. G., Galatsis, K. & Wlodarski, W. Gas sensing properties of nanosized tin oxide synthesised by mechanochemical processing. *Sensors and Actuators B: Chemical* **77**, 491–495 (2001).

[34] Min, B.-K. & Choi, S.-D. SnO_2 thin film gas sensor fabricated by ion beam deposition. *Sensors and Actuators B: Chemical* **98**, 239–246 (2004).

[35] Mandayo, G. G., Castano, E., Gracia, F. J., Cirera, A., Cornet, A. & Morante, J. R. Built-in active filter for an improved response to carbon monoxide combining thin- and thick-film technologies. *Sensors and Actuators B: Chemical* **87**, 88–94 (2002).

[36] Chowdhuri, A., Gupta, V. & Sreenivas, K. Enhanced catalytic activity of ultrathin CuO islands on SnO_2 films for fast response H_2S gas sensors. *IEEE Sensors Journal* **3**, 680–686 (2003).

[37] Kammler, H. K., Madler, L. & Pratsinis, S. E. Flame synthesis of nanoparticles. *Chemical Engineering & Technology* **24**, 583–596 (2001).

[38] Grass, R. N. & Stark, W. J. Flame spray synthesis under a non-oxidizing atmosphere: Preparation of metallic bismuth nanoparticles and nanocrystalline bulk bismuth metal. *Journal of Nanoparticle Research* **8**, 729–736 (2006).

[39] Vital, A., Angermann, A., Dittmann, R., Graule, T. & Topfer, J. Highly sinter-active (Mg-Cu)-Zn ferrite nanoparticles prepared by flame spray synthesis. *Acta Materialia* **55**, 1955–1964 (2007).

[40] Wal, R. L. V., Hall, L. J. & Berger, G. M. Optimization of flame synthesis for carbon nanotubes using supported catalyst. *Journal of Physical Chemistry B* **106**, 13122–13132 (2002).

[41] Salata, O. Applications of nanoparticles in biology and medicine. *Journal of Nanobiotechnology* **2**, 3 (2004).

[42] Rosner, D. E. Flame synthesis of valuable nanoparticles: Recent progress/current needs in areas of rate laws, population dynamics, and characterization. *Industrial & Engineering Chemistry Research* **44**, 6045–6055 (2005).

[43] Wegner, K. & Pratsinis, S. E. Gas-phase synthesis of nanoparticles: scale-up and design of flame reactors. *Powder Technology* **150**, 117–122 (2005).

[44] Miller, T. A., Bakrania, S. D., Perez, C. & Wooldridge, M. S. A new method for direct preparation of tin dioxide nanocomposite materials. *Journal of Materials Research* **20**, 2977–2987 (2005).

[45] Zhu, W. H. & Pratsinis, S. E. Synthesis of SiO_2 and SnO_2 particles in diffusion flame reactors. *AICHE Journal* **43**, 2657–2664 (1997).

[46] Nakazawa, S., Yokomori, T. & Mizomoto, M. Flame synthesis of carbon nanotubes in a wall stagnation flow. *Chemical Physics Letters* **403**, 158–162 (2005).

[47] Wal, R. L. V., Ticich, T. M. & Stephens, A. B. Can soot primary particle size be determined using laser-induced incandescence? *Combustion and Flame* **116**, 291–296 (1999).

[48] Hall, D. L., Wang, A. A., Joy, K. T., Miller, T. A. & Wooldridge, N. S. Combustion synthesis and characterization of nanocrystalline tin and tin oxide (SnOx, x=0-2) particles. *Journal of the American Ceramic Society* **87**, 2033–2041 (2004).

[49] Limaye, A. U. & Helble, J. J. Effect of precursor and solvent on morphology of zirconia nanoparticles produced by combustion aerosol synthesis. *Journal of the American Ceramic Society* **86**, 273–278 (2003).

[50] Pratsinis, S. E., Zhu, W. H. & Vemury, S. The role of gas mixing in flame synthesis of titania powders. *Powder Technology* **86**, 87–93 (1996).

[51] Vemury, S., Pratsinis, S. E. & Kibbey, L. Electrically controlled flame synthesis of nanophase TiO_2, SiO_2, and SnO_2 powders. *Journal of Materials Research* **12**, 1031–1042 (1997).

[52] Pratsinis, S. E. Flame aerosol synthesis of ceramic powders. *Progress in Energy and Combustion Science* **24**, 197–219 (1998).

[53] Gutsch, A., Muhlenweg, H. & Kramer, M. Tailor-made nanopartictes via gas-phase synthesis. *Small* **1**, 30–46 (2005).

[54] Wooldridge, M. S. Gas-phase combustion synthesis of particles. *Progress in Energy and Combustion Science* **24**, 63–87 (1998).

[55] Dima, A., Dima, O., Moldovan, C., Cobianu, C., Savaniu, C. & Zaharescu, M. Substrate influence on the response of sol-gel derived SnO_2 gas-sensors. *Thin Solid Films* **427**, 427–431 (2003).

[56] Guidi, V., Butturi, M. A., Carotta, M. C., Cavicchi, B., Ferroni, M., Malagu, C., Martinelli, G., Vincenzi, D., Sacerdoti, M. & Zen, M. Gas sensing through thick film technology. *Sensors and Actuators B: Chemical* **84**, 72–77 (2002).

[57] Mueller, R., Jossen, R., Kammler, H. K. & Pratsinis, S. E. Growth of zirconia particles made by flame spray pyrolysis. *AICHE Journal* **50**, 3085–3094 (2004).

[58] Miller, T. A., Bakrania, S. D., Perez, C. & Wooldridge, M. S. A new method for direct preparation of tin dioxide nanocomposite materials. *Journal of Materials Research* **20**, 2977–2987 (2005).

[59] Wang, A. An Experimental Investigation of the Satruation of Tetramethyl Tin Vapor/Argon Mixtures (2001).

[60] Miller, T. A. Combustion Synthesis of Metal/Metal Oxide Nanocomposite Materials (2005).

[61] Powder Diffraction File, compiled by JCPDS. International Centre for Diffraction Data, Swarthmore, PA (1990).

[62] Rasband, W. S. ImageJ U. S. National Institutes of Health, Bethesda, Maryland, USA, http://rsb.info.nih.gov/ij/, 1997-2007. .

[63] Bakrania, S. D., Miller, T. A., Perez, C. & Wooldridge, M. S. Combustion of multiphase reactants for the synthesis of nanocomposite materials. *Combustion and Flame* **148**, 76–87 (2007).

[64] *CRC Handbook of Chemistry and Physics* (CRC Press, New York, 2004), 85th edn.

[65] Gallagher, P. K. & Gross, M. E. The Thermal-Decomposition of Palladium Acetate. *Journal of Thermal Analysis* **31**, 1231–1241 (1986).

[66] Kristl, M. & Drofenik, M. Preparation of Au_2S_3 and nanocrystalline gold by sonochemical method. *Inorganic Chemistry Communications* **6**, 1419–1422 (2003).

[67] Jain, K., Pant, R. P. & Lakshmikumar, S. T. Effect of Ni doping on thick film SnO_2 gas sensor. *Sensors and Actuators B: Chemical* **113**, 823–829 (2006).

[68] Dreizin, E. Phase changes in metal combustion. *Progress in Energy and Combustion Science* **26**, 57 – 78 (2000).

[69] Dreizin, E. L. Effect of phase changes on metal-particle combustion processes. *Combustion Explosion and Shock Waves* **39**, 681–693 (2003).

[70] Bakrania, S. D., Perez, C. & Wooldridge, M. S. Methane-assisted combustion synthesis of nanocomposite tin dioxide materials. *Proceedings of the Combustion Institute* **31**, 1797–1804 (2007).

[71] Wostek-Wojciechowska, D., Jeszka, J. K., Uznanski, P., Amiens, C., Chaudret, B. & Lecante, P. Synthesis of gold nanoparticles in solid state by thermal decomposition of an organometallic precursor. *Materials Science-Poland* **22**, 407–413 (2004).

[72] Hamaoui, B. E., Zhi, L., Wu, J., Li, J., Lucas, N. T., Tomovic, Z., Kolb, U. & Mullen, K. Solid-state pyrolysis of polyphenylene-metal complexes: A facile approach toward carbon nanoparticles. *Advanced Functional Materials* **17**, 1179–1187 (2007).

[73] Hu1, M.-S., Chen, H.-L., Shen, C.-H., Hong, L.-S., Huang, B.-R., Chen, K.-H. & Chen, L.-C. Photosensitive gold-nanoparticle-embedded dielectric nanowires. *Nature Materials* **5**, 102–6 (2006).

[74] Pustovalov, V. K. . & Babenko, V. A. Optical properties of gold nanoparticles at laser radiation wavelengths for laser applications in nanotechnology and medicine. *Laser Physics Letters* **1**, 516–20 (2004).

[75] Pasquato, L., Pengo, P. & Scrimin, P. Functional gold nanoparticles for recognition and catalysis. *Journal of Materials Chemistry* **14**, 3481–3487 (2004).

[76] Haruta, M. Catalysis: Gold rush. *Nature* **437**, 1098–1099 (2005).

[77] Obaid, A., Alyoubi, A., Samarkandy, A., Al-Thabaiti, S., Al-Juaid, S., El-Bellihi, A. & Deifallah, E.-H. Kinetics of Thermal Decomposition of Copper(II) Acetate Monohydrate. *Journal of Thermal Analysis and Calorimetry* **61**, 985–994 (2000).

[78] Mahfouz, R., Alshehri, S., Monshi, M. & El-Salam, N. Isothermal decomposition of gamma-irradiated palladium acetate. *Radiat. Eff. Defects Solids (Switzerland)* **159**, 345 – 51 (2004).

[79] Zhang, J. Y. & Boyd, I. W. Photo-decomposition of thin palladium acetate films with 126 nm radiation. *Applied Physics A: Materials Science & Processing* **65**, 379–382 (1997).

[80] Saha, M., Banerjee, A., Halder, A. K., Mondal, J., Sen, A. & Maiti, H. S. Effect of alumina addition on methane sensitivity of tin dioxide thick films. *Sensors and Actuators B: Chemical* **79**, 192–195 (2001).

[81] Xiong, Y., Akhtar, M. K. & Pratsinis, S. E. Formation of Agglomerate Particles by Coagulation and Sintering: the Evolution of the Morphology of Aerosol-made Titania, Silica and Silica-Doped Titania Powders. *Journal of Aerosol Science* **24**, 301–313 (1993).

[82] Xing, Y., Koylu, U. O. & Rosner, D. E. Synthesis and restructuring of inorganic nano-particles in counterflow diffusion flames. *Combustion and Flame* **107**, 85–102 (1996).

[83] Zawadzki, A. G., Giunta, C. J. & Gordon, R. G. Kinetic Modeling of the Chemical Vapor-Deposition of Tin Oxide from Tetramethyltin and Oxygen. *Journal of Physical Chemistry* **96**, 5364–5379 (1992).

[84] Coblenz, W. S., Dynys, J. M., Cannon, R. M. & Coble, R. L. Initial stage solid state sintering models. A critical analysis and assessment. *Materials Science Research* **13**, 141 – 157 (1980).

[85] Leite, E. R., Cerri, J. A., Longo, E., Varela, J. A. & Paskocima, C. A. Sintering of ultrafine undoped SnO_2 powder. *Journal of the European Ceramic Society* **21**, 669–675 (2001).

[86] Arcidiacono, S., Bieri, N. R., Poulikakos, D. & Grigoropoulos, C. P. On the coalescence of gold nanoparticles. *International Journal of Multiphase Flow* **30**, 979–994 (2004).

[87] Egry, I., Lohoefer, G. & Jacobs, G. Surface-tension of liquid-metals - results from measurements on ground and in-space. *Physical Review Letters* **75**, 4043–4046 (1995).

[88] Cobianu, C. *et al.* A SnO_2 microsensor device for sub-ppm NO_2 detection. *Sensors and Actuators B: Chemical* **58**, 552–555 (1999).

[89] Epifani, M., Alvisi, M., Mirenghi, L., Leo, G., Siciliano, P. & Vasanelli, L. Sol-gel processing and characterization of pure and metal-doped SnO_2 thin films. *Journal of the American Ceramic Society* **84**, 48–54 (2001).

[90] Lee, S., Lee, G.-G., Kim, J. & Kang, S.-J. L. A novel process for fabrication of SnO_2-based thick film gas sensors. *Sensors and Actuators B: Chemical* **123**, 331–335 (2007).

[91] Vuong, D. D., Sakai, G., Shimanoe, K. & Yamazoe, N. Preparation of grain size-controlled tin oxide sols by hydrothermal treatment for thin film sensor application. *Sensors and Actuators B: Chemical* **103**, 386–391 (2004).

[92] Yasunaga, S., Sunahara, S. & Ihokura, K. Effects of tetraethyl orthosilicate binder on the characteristics of an SnO_2 ceramic-type semiconductor gas sensor. *Sensors and Actuators* **9**, 133–145 (1986).

[93] Watson, J., Ihokura, K. & Coles, G. S. V. The Tin Dioxide Gas Sensor. *Measurement Science & Technology* **4**, 711–719 (1993).

[94] Garje, A. D. & Aiyer, R. C. Electrical and gas-sensing properties of a thick film resistor of nanosized SnO_2 with variable percentage of permanent binder. *International Journal of Applied Ceramic Technology* **3**, 477–484 (2006).

[95] Becker, T., Ahlers, S., Bosch-v. Braunmuhl, C., Muller, G. & Kiesewetter, O. Gas sensing properties of thin- and thick-film tin-oxide materials. *Sensors and Actuators B: Chemical* **77**, 55–61 (2001).

[96] Karthigeyan, A., Gupta, R. P., Burgmair, M., Sharma, S. K. & Eisele, I. Influence of oxidation temperature, film thickness and substrate on NO_2 sensing of SnO_2 ultra thin films. *Sensors and Actuators B: Chemical* **87**, 321–330 (2002).

[97] Wang, S., Zhao, Y., Huang, J., Wang, Y., Kong, F., Wu, S., Zhang, S. & Huang, W. Preparation and CO gas-sensing behavior of Au-doped SnO_2 sensors. *Vacuum* **81**, 394–397 (2006).

[98] Safonova, O. V., Rumyantseva, M. N., Ryabova, L. I., Labeau, M., Delabouglise, G. & Gaskov, A. M. Effect of combined Pd and Cu doping on microstructure, electrical and gas sensor properties of nanocrystalline tin dioxide. *Materials Science And Engineering B-Solid State Materials For Advanced Technology* **85**, 43–49 (2001).

[99] McFarland, A. D., Haynes, C. L., Mirkin, C. A., Van Duyne, R. P. & Godwin, H. A. Color My Nanoworld. *Journal of Chemical Education* **81**, 544 (2004).